Project THEMIS
Technical Report No. 12

NUMERICAL SIMULATION OF WIND, TEMPERATURE, SHEAR STRESS AND TURBULENT ENERGY OVER NONHOMOGENEOUS TERRAIN

by

Chin-hua Huang

and

E. C. Nickerson

FLUID MECHANICS PROGRAM
ENGINEERING RESEARCH CENTER
COLLEGE OF ENGINEERING
COLORADO STATE UNIVERSITY
FORT COLLINS, COLORADO

Project THEMIS
Technical Report No. 12

NUMERICAL SIMULATION OF WIND, TEMPERATURE, SHEAR STRESS AND TURBULENT ENERGY OVER NONHOMOGENEOUS TERRAIN

by

Chin-hua Huang
and
E. C. Nickerson

Prepared under

Office of Naval Research

Contract No. N00014-68-A-0493-0001

Project No. NR 062-414/6-6-68(Code 438)

U.S. Department of Defense

Washington, D. C.

Fluid Dynamics and Diffusion Laboratory
College of Engineering
Colorado State University
Fort Collins, Colorado

March 1972

CER71-72CH-ECN23

ABSTRACT

NUMERICAL SIMULATION OF WIND, TEMPERATURE, SHEAR STRESS AND TURBULENT ENERGY OVER NONHOMOGENEOUS TERRAIN

Airflow in the atmospheric surface layer over nonhomogeneous surfaces with discontinuities in surface roughness and temperature is investigated by numerical techniques. A computational scheme is developed for solving the steady state two-dimensional boundary layer equations. Several theorems of convergence are proved. A successful numerical test, which has been compared to the exact solution, is achieved. Some iterative schemes, which have already enjoyed considerable success without theoretical support are here shown to be convergent.

The variations in pressure and buoyancy force associated with changes in surface roughness have been neglected by previous investigators whose work is included in the present study. The numerical results of velocity and shear stress are compared with wind tunnel and field data. The roughness and temperature discontinuities are shown to have an effect on the upstream as well as the downstream flow conditions.

Significant variations in the horizontal velocity, vertical velocity and shear stress profiles near the roughness discontinuity occurred between those cases neglecting and those retaining the pressure terms in the governing equations. The predicted physical quantities for diabatic conditions also show significant differences in those two cases; thus, the pressure terms should be retained in the governing equations.

No inflection point in the wind profile for neutral conditions has been observed in the mixing length model; however, it has been observed in both the turbulent energy model and the model presented in this study. The field and wind tunnel observations also confirm the presence of an inflection point. The inflection point is less visible in the presented model as compared with the turbulent energy model.

For a small change in surface roughness, the wind profiles simulated by the numerical method are in good agreement with wind tunnel data. The distribution of the surface shear stress predicted by the presented theory is in better agreement with Bradley's field data than previously existing theories.

A proposed mechanism of turbulent energy transfer is developed, based upon the results of numerical experiments that explain the distribution of shear stress, and, hence, the distribution of velocity profiles in the atmospheric surface layer. Two different theories, the mixing length theory and the turbulent energy theory, are modified, and examined in detail; a theory is developed to remove some weaknesses of previously existing theories.

TABLE OF CONTENTS

TABLE OF CONTENTS - (Continued)

TABLE OF CONTENTS - (Continued)

LIST OF TABLES

LIST OF FIGURES

LIST OF FIGURES (Continued)

LIST OF FIGURES (Continued)

LIST OF FIGURES (Continued)

LIST OF SYMBOLS

Symbol	Definition	Dimension
a_1	Empirical function defined as the ratio between shear stress and turbulent intensity	---
a_2	Empirical function defined in Eq. (2-13)	---
a_{ij}	Entries of a matrix	---
A(X)	A matrix operator	---
B	A matrix with known entries	---
c	Empirical function defined as the ratio between turbulent kinetic energy and shear stress	---
C, A_1, B_1	Constant	---
C^P	Order of a continuous Frechet derivative of g	---
C_p	Specific heat at constant pressure	$HM^{-1}\theta^{-1}$
C_v	Specific heat at constant volume	$HM^{-1}\theta^{-1}$
D(X)	A diagonal matrix	---
d_{ij}	Entries of a matrix	---
det[D(x)]	Determinant of matrix D(x)	---
D_g	An open subset of product space, $R^n \times R^n$	---
e	Error	---
E	Mass flux	$ML^{-2}T^{-1}$
E(x)	Strictly lower triangular matrix	---
f_i, f(x)	A system of nonlinear equations	---
f'	Frechet derivative of f	---
f'^{-1}	Inverse of Frechet derivative f'	---
f_p	Functional representation of Poisson's equation	---

LIST OF SYMBOLS - (Continued)

Symbol	Definition	Dimension
f_u	Functional representation of horizontal momentum equation	---
f_w	Functional representation of continuity equation	---
f_θ	Functional representation of thermal energy equation	---
F	A known function	---
F(x)	Strictly upper triangular matrix	---
g(x)	A system of nonlinear equations	---
g_x, g_y	Partial Frechet derivative of g with respect to x and y variables	---
g	Gravity	LT^{-2}
g*	Nondimensional gravity	---
g_x^{-1}	Inverse of Frechet derivative g_x	---
$g_{I,i}, g_{II,\omega,i}, g_{III,i}$	A system of nonlinear equations for the Jacobi-Newton Method, the "modified" Newton's Method and the nonlinear Gauss-Seidel method, respectively	---
h(x)	Height of the internal boundary layer	L
h_s	Mean height of roughness elements	L
$H \equiv g_x^{-1} gy$	H is defined as $-g_x^{-1} gy$	---
H'	Heat flux	$HL^{-2}T^{-1}$
k	von Karman constant	---
K_x	Horizontal eddy viscosity	L^2T^{-1}
K_z	Vertical eddy viscosity	L^2T^{-1}
K_h	Eddy conductivity	L^2T^{-1}
K_m	Eddy diffusivity for momentum	L^2T^{-1}
K_w	Eddy diffusivity for mass	L^2T^{-1}

LIST OF SYMBOLS - (Continued)

Symbol	Definition	Dimension
ℓ_o	A length scale of the self-preserving processes	L
$\ell_1, \ell_2, \ell_3, \ell_5, \ell'$	Length scales	L
ℓ_d	Diffusion length	L
ℓ_ε	Dissipation length	L
L	Monin-Obukhov length	L
$\mathcal{L}$	Dissipation length scale	L
L'	A length defined as $L\, K_h/K_m$	L
$m, M=-\ln \frac{z}{z_o}$	Roughness parameter	---
M	Matrix	---
N	Matrix	---
P	Pressure	$ML^{-1}T^{-2}$
P*	Nondimensional pressure	---
P_o	Pressure at reference state	$ML^{-1}T^{-2}$
$\tilde{p}$	Pressure deviation from reference state	$ML^{-1}T^{-2}$
$\overline{\tilde{p}}$	Mean value of $\tilde{p}$	$ML^{-1}T^{-2}$
p'	Fluctuation pressure from $\tilde{p}$	$ML^{-1}T^{-2}$
q_*	Frictional humidity	---
$\tilde{q}^2$	Twice value of turbulent kinetic energy	L^2T^{-2}
$\tilde{q}$	$= \sqrt{\overline{q^2}}$	L/T
R	Gas constant	$L^2T^{-2}\theta^{-1}$
R^n	A real n-dimensional space	---
Re	Reynolds number	---
R_f	Flux Richardson number	---
Ri	Richardson number	---

LIST OF SYMBOLS - (Continued)

Symbol	Definition	Dimension
S	An open neighborhood of a point $x^* \epsilon R^n$	---
SXS	Product space belongs to D_g	---
S'	Boundary	---
S_o	A measure of the change of the surface stress	---
T	Temperature	θ
T_o	Temperature at reference state	θ
$\tilde{T}$	Temperature deviation from reference state	θ
$\bar{\tilde{T}}$	Mean value of $\tilde{T}$	θ
T'	Fluctuation temperature from $\tilde{T}$	θ
$\bar{u},\bar{v},\bar{w}$	Mean velocity components in x, y, z directions	L/T
$\bar{u}^*,\bar{v}^*,\bar{w}^*$	Nondimensional velocity in x, y, z directions	L/T
$\bar{u}_h$	Horizontal mean velocity at the edge of internal boundary	L/T
u_*	Frictional velocity	L/T
u_{*_o}	Frictional velocity upwind of the roughness discontinuity	L/T
u_{*_1}	Frictional velocity downwind of the roughness discontinuity	L/T
u',v',w'	Velocity fluctuations in x, y, z directions	L/T
u_i'	Components of velocity fluctuation in i direction where $u_1'=u'$, $u_2'=v'$, $u_3'=w'$	L/T
x,y,z	Distance along longitudinal, lateral and vertical direction	L

Symbol	Definition	Dimension
x^*	A solution of a system of nonlinear equations	---
x_o	Initial vector	---
x_1, x_2, x_3	Corresponding to x, y, and z, respectively	L
z_o	Roughness length upwind of the roughness discontinuity	L
z_1	Roughness length downwind of the roughness discontinuity	L
α, α'	Constant	---
α_h	A ratio defined as K_h/K_m	---
α_q	A ratio defined as K_w/K_m	---
β_u, β_t, β	Constant	---
δ	Boundary layer thickness	L
δ_{ij}	Kronecker delta	---
ε	Energy dissipation per unit mass	L^2T^{-3}
ε	Belong to	---
ζ	Nondimensional horizontal distance	---
$\zeta' = \frac{z}{L}$	Nondimensional height defined as z/L	---
η	Nondimensional vertical distance	---
$\overline{\theta}$	Mean potential temperature	θ
θ'	Fluctuation of potential temperature	θ
$\overline{\theta}^*$	Nondimensional mean potential temperature	---
θ_*	Frictional potential temperature	θ
κ	Thermal conductivity	$HL^{-1}T^{-1}\theta^{-1}$
Λ	Dissipation length scale	L
λ	An eigenvalue of the matrix $H_{II,\omega}$	---

LIST OF SYMBOLS - (Continued)

Symbol	Definition	Dimension
μ	Dynamic coefficient of molecular viscosity	$ML^{-1}T^{-1}$
μ_i	An eigenvalue of the Jacobi matrix B	---
ν	Kinematic coefficient of molecular viscosity	L^2T^{-1}
ρ	Density of air	ML^{-3}
ρ_o	Density of air at reference state	ML^{-3}
$\tilde{\rho}$	Density of air deviation from reference state	ML^{-3}
$\overline{\tilde{\rho}}$	Mean value of $\tilde{\rho}$	ML^{-3}
ρ'	Fluctuation pressure from $\tilde{\rho}$	ML^{-3}
$\rho(H)$	Spectral radius of H	---
σ	Area	L^2
τ	Kinematic horizontal shear stress	L^2T^{-2}
τ_x, τ_y	Kinematic shear stress in x, y direction	L^2T^{-2}
τ^*	Nondimensional shear stress	---
ϕ, ϕ_m	Nondimensional wind shear	---
Φ	Defined as ϕ^{-2}	---
χ	Pressure gradient normal to boundary	$ML^{-2}T^{-2}$
ω, ω_p	Relaxation factor	---
$\omega_u, \omega_w, \omega_\theta$		
ω_{opt}	Optimum relaxation factor	---
∇^2	Laplace operator	L^{-2}

Chapter I

INTRODUCTION

1.1 General Remarks

The airflow over homogeneous terrain in the atmospheric surface layer has been the subject of extensive studies in the past few decades. The so-called "constant flux layer" near the earth's surface in the homogeneous plane, considering mean physical quantities and turbulent characteristics, is well understood. The airflow over a flat plate has long interested fluid dynamicists who have successfully simulated this flow in the wind tunnel.

Although the airflow over homogeneous terrain has been extensively studied, the airflow over a complex surface with abrupt changes in temperature and roughness occurs more often in nature. In fact, it is extremely difficult to find a perfectly homogeneous terrain on the earth's surface; for all practical purposes, it is usually assumed that there is an infinite upstream fetch over a homogeneous surface. The study of airflow over complex surfaces under various stability conditions is of great interest, because of its relation to evaporation from crop fields or from lakes, to the diffusion of air pollutants in urban areas, to lake and sea breezes and because of its interaction with the general circulation. The atmospheric motions are influenced by the underlying surface, which is the source of heat and moisture fluxs. Since the large-scale and meso-scale considerations of the air motion depend on the micrometeorological conditions, the study of dynamic micrometeorology should prove to be very rewarding.

In order to improve the predictability of wind, temperature, water vapor and air pollutants in the atmospheric boundary layer, more physical insight into the mechanism of turbulent transports is required. Unfortunately, field measurements are inadequate both in quality and accuracy. Because of the numerous uncontrollable factors involved in the atmospheric surface layer, it is quite difficult to interpret the resulting measurements. One promising method of attacking this problem and of interpreting the transfer mechanism of turbulent energy, heat, and momentum is through the use of a high-speed computer to solve the governing equations for the flow by a numerical technique.

1.2 Statement of the Problem

The physical problem considered is the air flow moving over a surface with an abrupt change in surface roughness and temperature. Since many previous workers dealt with neutral conditions and disregarded the influence of roughness discontinuities on the upstream flow, we will incorporate this effect into our model and also extend the model to diabatic conditions.

Since certain terms in the governing equations are difficult to incorporate into the internal boundary-layer models, it is felt that a generalized mathematical model can most easily be realized through a numerical simulation. Such simulations should lead to a deeper and broader physical insight into the problem.

Therefore, the purpose of our study is to integrate a closed set of nonlinear equations of motion by numerical techniques. The objectives in this study are the following:

(1) Develop a theory of airflow over inhomogeneous terrain in order to avoid some weaknesses of previous theories and to improve the

predictability of the mean flow, temperature, shear stress, and turbulent energy in the atmospheric surface layer.

(2) To propose a mechanism of turbulent energy transport in order to explain the distribution of shear stresses and hence, the distribution of wind profiles.

(3) Develop a numerical scheme with theoretical support, which should be applicable to three-dimensional boundary layer flow.

(4) Retain the pressure and buoyancy terms in the governing equations in order to examine the buoyancy and pressure effects on the flow, and the effect of the roughness discontinuity on the upwind flow.

(5) To compare the results among various theories, and the results predicted by various theories with those of wind tunnel and field measurements.

(6) To answer why the k-theory model works so well in predicting the mean flow field in light of a newly developed theory.

(7) To examine the applicability of the traditional concept of the internal boundary layer.

1.3 Historical Background

Phillips, as early as in 1956, found by analyzing synoptic charts, that the surface wind blows much stronger over smooth terrain than over rough terrain. Phillips (1956), Mintz (1958) and many others have set up two-parameter models for the study of atmospheric general circulation, including friction and heating terms in the atmospheric surface layer. Numerical studies of the sea breeze with the assumptions of constant heat flux and momentum flux in the surface boundary layer have been carried out by Fisher (1961) and many others. The successful numerical investigations of the general circulation and meso-scale circulation all

depend upon the ability to incorporate the dynamic aspects of airflow influenced by complex surfaces. The vertical distribution of velocity and shear stress profiles are modified when the flow moves from one type of roughness and temperature to a new surface with a different roughness and temperature. The modified airflow in turn will affect the local transfer rates of heat and moisture.

In the early stages of research, almost all reliable experiments were performed in wind tunnels (Jacobs, 1939) or in closed hydraulic channels (Nikuradse, 1933; Tani, 1958). Recently, Yeh and Nickerson (1970) have successfully simulated the mean flow field and turbulent characteristic of the atmospheric boundary layer flow downstream from a roughness discontinuity. Field observations of mean flow encountering abrupt changes in surface roughness have been obtained by Lettau (1962) and Bradley (1968). Data obtained from wind tunnel and field observations are still inadequate to construct a general mathematical model. It is felt that only through numerical experiments combined with experimental data, either obtained from the field or the wind tunnel, can a generalized mathematical model be deduced and the mechanisms involved be understood.

The concept of the "internal boundary layer" was first introduced by Elliott (1958) and subsequently modified by Panofsky and Townsend (1964) and Townsend (1965a, 1965b). Numerical models without a prior assumption about an "internal boundary layer" have been constructed by Nickerson (1968), Onishi and Estoque (1968) and Taylor (1969). Almost all theories deal with neutral conditions and employ mixing length hypothesis, The main drawback of the mixing length model is that it disregards the upstream history of an air parcel. Bradshaw, et al

(1967) have successfully solved this problem by replacing the mixing length with a turbulent energy equation. Following the work of Bradshaw et al.(1967), Peterson (1969) applied this idea to the atmospheric turbulent boundary layer. Although reasonable mean meteorological variables and shear stress have been obtained by this model, some problems arise. The turbulent energy was assumed to be linearly correlated with the shear stress and they considered the turbulent energy equation as if it were an equation for the Reynolds shear stress. It turns out, however, that they used the wrong equation for the Reynolds shear stress. Considering the unsound mathematical background of these models, one might ask why the mixing length model and the Bradshaw model work so well. We will return to this question later and attempt to answer it in light of a new theory developed in this thesis.

Many investigators assume the existence of an "internal boundary layer," which means that when a turbulent flow encounters a sudden change in surface roughness, the effect of this change is not felt immediately through the turbulent boundary layer, but is diffused outwards as the flow moves downstream. However, there is definite evidence that when the flow encounters a sudden change in surface roughness, the effects are immediately felt not only downstream but upstream as well. The upstream effects of roughness discontinuity have been numerically studied by both Wagner (1966) and Onishi and Estoque (1968). Wagner considered the unsteady flow problem, while Onishi and Estoque solved the problem of two-dimensional flow moving from one type of roughness to another.

The effects of roughness discontinuity have been observed by Stearn and Lettau (1964), who carried out field experiments in and

around a group of discarded Christmas trees planted on frozen Lake Mendota.

The entire flow field imbedded in the planetary boundary layer can be classically divided into three regions as shown in Figure 1-1. The flow in each region has a different structure. Region I is an equilibrium boundary layer, where the velocity profiles have similar shape. In this region, there is no inertial acceleration, and a constant shear stress exists. A large number of theoretical and experimental studies have been carried out in the past few decades in this region. However, the assumption of an equilibrium flow in the planetary boundary layer is an over simplification. The pioneering work was carried out by Prandtl and von Karman (see Schlichting, 1968), who determined that a logarithmic velocity profile exists in this region. Region II is a transition region ($0 < x < x_1$). In this region, the new surface will cause the flow to change from its equilibrium condition. The acceleration or deceleration of the flow depends on whether the new surface is respectively smoother or rougher than the upstream surface. The change of mean physical quantities and the characteristics of turbulence are initially restricted to a shallow layer near the surface, which gradually diffuses outward, as the flow advances downstream. This shallow layer grows thicker as air progresses downstream; such a layer is called an "internal boundary layer." The flow outside this layer has not been affected by the underlying surface. Region III is a new equilibrium boundary layer. The internal boundary layer will deepen as the flow progresses downstream. Thus, if the fetch is long enough, it is possible to assume that beyond a certain distance x_1 in the downstream direction, the flow will eventually reestablish a new equilibrium with the underlying

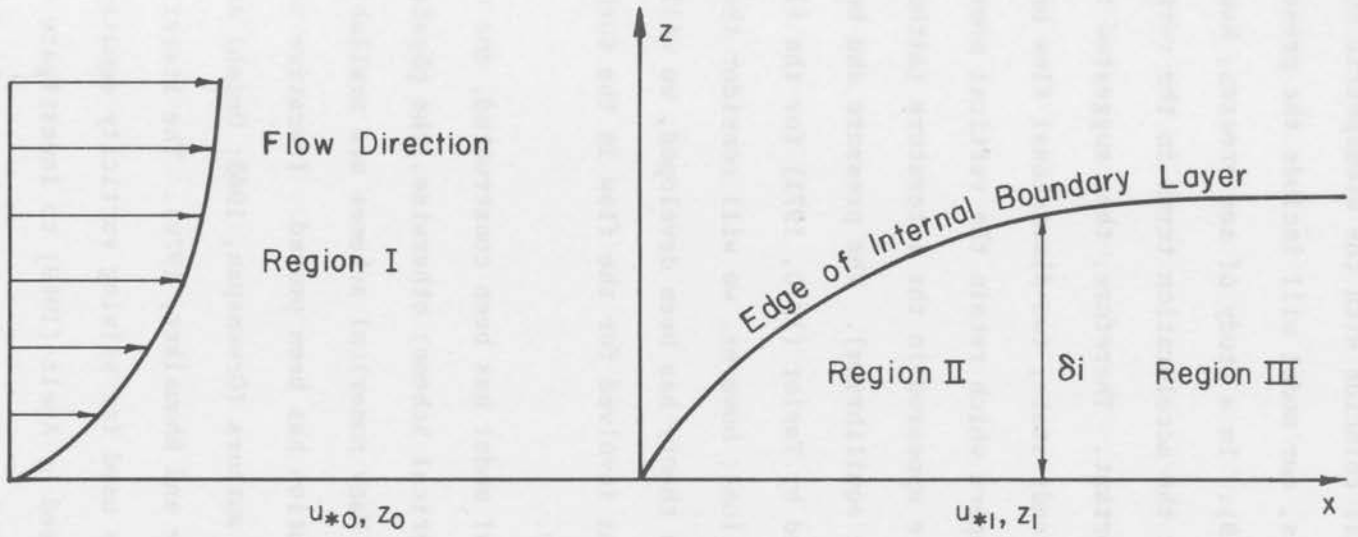

Figure 1-1 Regions of flow downstream with an abrupt change in surface roughness

surface. Finally, the internal boundary layer will cover the entire depth of the atmospheric boundary layer, and the thickness of the internal boundary layer will coincide with the atmospheric boundary layer.

For neutral conditions, our model will include the pressure term neglected by Peterson (1969). In a study of sea breezes, Neuman and Mahrer, (1971) showed that the acceleration terms in the vertical momentum equation are important. Therefore, they suggested that these terms be retained. For steady state, two-dimensional flow under diabatic conditions, no papers which retain the vertical momentum equation in the system have appeared in the literature (although most writers assume hydrostatic equilibrium). The pressure and buoyancy effects have been neglected by Taylor (1970, 1971) for the flow under stable and unstable conditions; however, we will consider these effects in our model. After a new theory has been developed, we will investigate the various mechanisms involved for the flow in the turbulent atmospheric boundary layer.

After the mathematical model has been constructed, one needs to search for a relevant numerical scheme; otherwise, the physical problems will still be unsettled. Many numerical schemes are available; however, no convergence to the solution has been proved. Iterative schemes have been developed by several authors (Greenspan, 1968; Onishi and Estoque, 1968; Apelt, 1969; Estoque and Bhumalker, 1970). The iterative scheme developed by Greenspan was used for solving vorticity equations, and a similar scheme has been used by Apelt (1969) to investigate the problem of cavity flow. The iterative scheme developed by Onishi and Estoque

(1968), and Estoque and Bhumalker (1970) for solving the primitive equations has also enjoyed considerable success; however, no proof of convergence has been made, since Estoque and Bhumalker (1970) justified his results only numerically.

We will develop an iterative scheme for solving a system of non-linear partial differential equations and prove several convergence theorems. Under certain hypotheses, the scheme will converge to the solution.

Chapter II

THEORETICAL BACKGROUND

2.1 Analytical Model

The fully developed turbulent airflow blowing steadily from one region to another region with different surface roughness was first considered by Elliott (1958). He assumed that far upstream the turbulent flow is in equilibrium with the underlying surface and that the air in the transition region immediately adjusts to the new surface,. The depth of the layer influenced by the underlying surface grows with downstream distance from the roughness discontinuity. The lower boundary layer of small vertical extent where the effects of the new surface roughness are felt was called the "internal boundary layer" by Elliott. Under the assumption of the conservation of momentum for steady state flow, he needed only the equations of continuity and horizontal momentum without pressure gradient force to close the system.

Applying the von Karman integral technique, Elliott obtained an analytical expression for the height of the internal boundary layer:

$$\frac{d}{dx}\int_{z_1}^{h(x)} \bar{u}^2 dx - \bar{u}_h \frac{d}{dx}\int_{z_1}^{h(x)} \bar{u} dz = u_{*o}^2 - u_{*1}^2 \qquad (2\text{-}1)$$

where $h(x)$ is the height of the internal boundary layer, $\bar{u}_h$ is the velocity at the edge of the internal boundary layer, and u_{*o} and u_{*1} are the surface frictional velocities upstream and downstream respectively. The quantities u_{*o} and u_{*1} are assumed to be

functions of the downstream distance x only. z_1 is the downstream roughness length; k the von Karman constant which is equal to 0.4.

The momentum equation (2-1) has been obtained by assuming constant shear stress within the internal boundary layer and zero pressure gradient. Equation (2-1) simply states the conservation of momentum, i.e., the loss of momentum by advection, must also be equal to the net gain of momentum by frictional velocity. The mean flow inside the internal boundary layer is described by

$$\overline{u} = \frac{u_{*1}(x)}{k} \ln \frac{z}{z_1} . \qquad (2\text{-}2)$$

In Elliott's model, it was assumed that the shear stress is independent of height inside the internal boundary layer; outside the internal boundary layer, the flow has the same shear stress as the upstream fluid. Therefore, a discontinuity in shear stress appears at the edge of the internal boundary layer. Since the wind profile is continuous across the edge of the internal boundary layer and the air does not feel the influence of the surface roughness, the acceleration of air is negligible. The negligible acceleration of air at the edge of the internal boundary layer contradicts the existence of the shear stress discontinuity, which implies the maximum acceleration of air at that same point. The assumption of constant shear stress inside the internal boundary layer would imply that the air is either not accelerating or not decelerating. However, the opposite is true, for when the air moves over a new surface, it will either accelerate or decelerate. Since the acceleration or deceleration of air is usually negligible near the edge of the internal boundary layer, the velocity

profile is continuous; hence, the shear stress distribution should also be continuous.

Since the constant local shear stress assumed by Elliott inside the internal boundary layer is unrealistic, several authors have made an attempt to improve Elliott's model by introducing various forms for the shear stress distribution in the internal boundary layer. Panofsky and Townsend (1964) avoided the unrealistic distribution of shear stress used in Elliott's model; they assumed that the distribution of shear stress varies with height in the internal boundary layer. The shear stress distribution was assumed to take the form

$$u_* = u_{*o} \left[(1-S_o) + S_o \frac{z}{d}\right] \tag{2-3}$$

and

$$S_o = \frac{\ln z_1/z_o}{\ln \frac{h(x)}{z_o} - 1} = \frac{(u_{*o} - u_{*1})}{u_{*o}} , \tag{2-4}$$

where S_o is a measure of the change of the surface stress, which is a function of downstream distance.

Taylor (1967) constructed a model based upon the von Karman - Pohlhausen technique using a higher order polynomial to fit the vertical distribution of frictional velocity:

$$u_{*1} = u_{*o} \left\{(1-S_o) + S_o\left[10 \left(\frac{z}{h}\right)^3 + 15 \left(\frac{z}{h}\right)^4 + 6 \left(\frac{z}{h}\right)^5\right]\right\} . \tag{2-5}$$

All three theories (Elliott, 1958; Panofsky and Townsend, 1964; and Taylor, 1967) are basically similar; they consider mathematical

simplifications which lead to an approximate solution. The main differences between their theories lie in the manner in which they prescribe the vertical distribution of frictional velocity; however, the mean velocity profiles downstream from the roughness continuity predicted by all three theories do not differ significantly. This indicates that the change of the mean horizontal velocity is insensitive to the distribution of shear stress. The three predicted results for the growth of the internal boundary layer thickness also differ. Taylor (1969) found that his model was less accurate in predicting the distribution of shear stress in an internal boundary layer than Panofsky and Townsend's model.

Townsend (1965a, 1965b) tried to generalize the previous works and introduced the self-preserving turbulent flow. For the flow over an abrupt change in surface roughness, Townsend postulated that the flow is self-preserving, which means that distributions of each quantity have the same form at all distances from the point of transition; they differ only in common scales of velocity and length. Townsend (1965a) proposed a self-preserving flow having the shear stress distribution of the form:

$$\tau = u_1^2 + \tau_s \, F\left(\frac{z}{\ell_o}\right) = u_1^2 + (u_o^2 - u_1^2) \, F\left(\frac{z}{\ell_o}\right) \quad , \qquad (2\text{-}6)$$

where $u_o^2 - u_1^2$ is a velocity scale, and ℓ_o is a length scale of the self-preserving process. Using the mixing length transfer relation, the distribution function $F(\frac{z}{\ell_o})$, a universal function, has been derived and has the exponential form

$$F\left(\frac{z}{\ell_o}\right) = e^{-\frac{z}{\ell_o}} \quad . \tag{2-7}$$

2.2 Numerical Models

2.2.1 Mixing length theory - The methods advanced by Elliott, Panofsky and Townsend, and Taylor are applicable only to a restricted class of flow. The theories postulate the vertical distributions of frictional velocity and then deduce the horizontal component of the mean velocity. On the other hand, numerical simulation without a prior assumption about the internal boundary layer can avoid some of the difficulties encountered by the similarity methods; it can also apply to any class of flow. Therefore, it should lead to a deeper and broader insight into the dynamic processes of the flow than an over-simplified analytical method.

The steady state, two-dimensional, incompressible fluid moving over horizontal terrain with an abrupt change in surface roughness has been investigated by several workers (Nickerson, 1968, Onishi and Estoque, 1968; Taylor, 1969, 1970 and 1971) using numerical techniques. The models were based on the steady state, two-dimensional turbulent boundary layer equations with the mixing-length assumption. The turbulent boundary layer equations and the equation of continuity may be written as

$$\bar{u}\frac{\partial \bar{u}}{\partial x} + \bar{w}\frac{\partial \bar{u}}{\partial z} = -\frac{1}{\bar{\rho}}\frac{\partial P}{\partial x} + \frac{\partial}{\partial x}\left(K_x \frac{\partial \bar{u}}{\partial x}\right) + \frac{\partial}{\partial z}\left(K_z \frac{\partial \bar{u}}{\partial z}\right) \tag{2-8}$$

$$\bar{u}\frac{\partial \bar{w}}{\partial x} + \bar{w}\frac{\partial \bar{w}}{\partial z} = -\frac{1}{\bar{\rho}}\frac{\partial P}{\partial z} - g + \frac{\partial}{\partial x}\left(K_x \frac{\partial \bar{w}}{\partial x}\right) + \frac{\partial}{\partial z}\left(K_z \frac{\partial \bar{w}}{\partial z}\right) \tag{2-9}$$

$$\frac{\partial \bar{u}}{\partial x} + \frac{\partial \bar{w}}{\partial z} = 0 \quad , \tag{2-10}$$

in which a Cartesian coordinate system has been used. The x-axis is the horizontal direction parallel to plane of mean wind, while the z-axis is normal to the x-axis pointing in the vertical direction. $\bar{u}$ and $\bar{w}$ are the mean velocity components corresponding to x and z. $\bar{\rho}$ is the mean density of air; P, the pressure; K_x the horizontal eddy viscosity; and K_z, the vertical eddy viscosity.

Nickerson (1968) reduced the system of equations (2-8), (2-9), and (2-10) to parabolic equations (2-8) and (2-10) without considering the pressure effect, horizontal diffusion terms or the vertical momentum equation. Townsend (1965) compared his own results with Elliott (1958) and Panofsky and Townsend (1964); he found that the forms of eddy exchange coefficient used by the previous workers are relatively unimportant. Based on Townsend's findings, Nickerson assumed that the exchange coefficient K_z is a linear function of height away from the wall; it does not vary in the downwind direction. He solved the system of equations (2-8) and (2-10) by the Dufort-Frankel Scheme, marching according to the direction of flow. Taylor (1969) used the same system of equations as in Nickerson's model. However, he considered the eddy exchange coefficient as depending not only on the height but also on the vertical wind shear; this consideration is essentially the mixing length hypothesis for the exchange coefficient. Taylor reduced the nonlinear system of equations to ordinary differential equations, and solved the system of equations by the standard method of Runge-Kutta. Since all of the above researchers solved the system of parabolic

equations, no upstream effects of roughness discontinuity can be found in their results.

Onishi and Estoque (1968) did not consider the horizontal diffusion terms. They solved the system of equations by an iterative method. No theoretical support for the convergence has been given. However, they included the pressure terms in their model, thus retaining the vertical momentum equation. The pressure terms included in the system of equations cannot be computed by the marching scheme used by the previous workers, which can be obtained only through the Poisson equation by an iterative technique. The roughness discontinuity, which perturbs the oncoming flow, also perturbs the pressure field. The change in pressure will result in the change of the flow's momentum which in turn will affect the flow upstream.

Taylor (1970) considered the approaching flows under unstable conditions with a step change both in heat flux (or temperature), and surface roughness. In order to investigate the flow under unstable conditions, he included, in addition to the momentum and continuity equations an energy equation written in terms of temperature rather than potential temperature. The closure he chose is the mixing length assumption, using the formula for nondimensional wind shear developed by Businger-Dyer (unpublished). The vertical momentum equation has not been considered in the set of equations; the buoyancy term and pressure term have been ignored in his numerical experiment. Despite these shortcomings, he was able to obtain a distribution of shear stress profiles which is quite different from the profiles obtained under neutral conditions. For slightly stable conditions, Taylor (1971) also included the equation for water vapor in his model. He made an

attempt to compare his numerical results with field measurements (Rider, et. al., 1963). However, his results are far from conclusive due to the uncertainty and incompleteness of the field measurements. As in the case of unstable conditions, he was again able to demonstrate that exchange coefficients and shear stress profiles change significantly when compared with those of neutral conditions.

2.2.2 Turbulent energy model - At the present time, the calculation of the flow in the turbulent boundary layer usually employs the mixing length assumption to close the system, which provides the first approximation for the turbulent boundary layer problem. The mixing length hypothesis states that the shear stress is a local property, which is related to the mean velocity gradient and the distance from the wall. Since the mixing length hypothesis disregards the past history of the flow behavior in the boundary layer, Dryden (1947) proposed that the shear stress is closely related to the turbulent kinetic energy. Based on the evidence that the turbulent kinetic energy is positively correlated with the shear stress, Bradshaw et al, (1967), following Townsend (1961), used the turbulent kinetic energy equation to generalize the mixing length theory, thus taking the past history of turbulent characteristics into account. The turbulent energy equation (Hinze, 1968) for two-dimensional steady state can be written as

$$\underbrace{\bar{u}\frac{\partial}{\partial x}\left(\frac{\overline{q^2}}{2}\right)}_{\text{horizontal advection}} + \underbrace{\bar{w}\frac{\partial}{\partial z}\left(\frac{\overline{q^2}}{2}\right)}_{\text{vertical advection}} = \underbrace{-\overline{u'w'}\frac{\partial \bar{u}}{\partial z}}_{\text{production}} - \underbrace{\frac{\partial}{\partial z}\left[\overline{w'\left(\frac{p'}{\rho}+\frac{q^2}{2}\right)}\right]}_{\text{diffusion}} - \underbrace{\varepsilon}_{\text{dissipation}}, \quad (2\text{-}11)$$

In the above equation, the viscous and normal stress terms have been neglected. ε is the dissipation of turbulent kinetic energy

by the action of molecular viscosity, and P' is the fluctuating component of the static pressure. A bar over a symbol denotes the time average. The resultant fluctuating velocity is

$$\overline{q^2} = \overline{u'^2} + \overline{v'^2} + \overline{w'^2} \quad . \tag{2-12}$$

Consideration of the system of equations which includes the horizontal momentum equation, the equation of continuity and the turbulent kinetic energy equation does not close the system, since there are more unknown than the number of equations in the system. Therefore, more information is needed in order to close the system of equations. Some empirical functions must be introduced to make the system closed; this is precisely what has been done by Townsend (1956, 1961), Bradshaw et al. (1967) and McDonald (1968) in two-dimensional incompressible viscous flow. The empirical functions are introduced by modeling the diffusion, and dissipation terms in the turbulent kinetic energy equation. In the mixing length theory, one assumption is enough, while in this model three empirical functions are required. They are

$$\text{(i)} \quad (-\overline{u'w'}) = a_1 \frac{\overline{q^2}}{2}$$

$$\text{(ii)} \quad \overline{w' \left(\frac{P'}{\rho} + \frac{q^2}{2}\right)} = \tau_{max}^{\frac{1}{2}} \cdot \tau \cdot a_2 \left(\frac{z}{\delta}\right)$$

$$\text{(iii)} \quad \varepsilon = \frac{\tau^{3/2}}{\ell \left(\frac{z}{\delta}\right)} \quad , \tag{2-13}$$

where δ is the boundary layer thickness, a_1 is the ratio between the shear stress and the turbulent intensity, a_2 is another turbulent parameter. ℓ is the dissipation length and $\varepsilon = \nu\overline{(\partial u_i'/\partial x_j)^2}$ is the dissipation. The diffusion coefficient a_2 and the dissipation length ℓ are assumed to be universal functions of z/δ. The first relation (i) states that the magnitude of the shear stress is proportional to the turbulent intensity. The second relation (ii) expresses the diffusion term as a function of the local shear stress and the maximum shear stress at a particular station. The third relation (iii) implies that the dissipative eddies are approximately isotropic. By substituting the above three empirical functions into the turbulent kinetic energy equation, one obtains the following dynamic equation for turbulent shear stress:

$$\frac{\bar{u}}{a_1}\frac{\partial \tau}{\partial x} + \frac{\bar{w}}{a_1}\frac{\partial \tau}{\partial z} = \tau\frac{\partial \bar{u}}{\partial z} - \tau_{max}^{1/2}\frac{\partial}{\partial z}(a_2\tau) - \frac{\tau^{3/2}}{\ell} \quad . \tag{2-14}$$

Since the shear stress is related to the scale of mixing length, the above equation is a generalized mixing length equation. Omitting the convective terms and diffusion term in (2-14), equation (2-14) is reduced to the mixing length equation hypothesized by Prandtl (1925), if one chooses the dissipation length to be equal to kz, where k is the von Kármán constant. Thus, the inclusion of the advective and diffusive terms in the turbulent energy equation generalizes the mixing length equation; the upstream effect on the mixing length has been taken into consideration in this model. Although more information is available from the turbulent energy model, one has to pay a higher price by obtaining three empirical functions.

The two-dimensional turbulent energy model developed by Bradshaw et al. (1967) has been shown to be very successful in calculating turbulent boundary layer flow. They determined the shear stress from the turbulent kinetic energy equation with the aid of three empirical functions. This concept of modeling has been extended to the atmospheric boundary layer by Peterson (1969), who assumed that the process for the diffusion of the turbulence energy is the same as that of momentum; the dissipation scale ℓ is chosen to be equal to kz, where k is the von Kármán constant. This means that under equilibrium conditions, dissipation is equal to production. Monin (1959) has argued that the dissipation length $\ell = kz$ is probably also valid for non-equilibrium conditions with accelerating or decelerating flow. Furthermore, Peterson assumed that a_1, relating shear stress to turbulent energy, is equal to 0.16. He stated that the value is close to the value of $a_1 = 0.15$ used by Bradshaw et al., and suggested that the constant a_1 is a universal function. Actually the value of a_1 chosen by Bradshaw is 0.3 which is twice as large as that used by Peterson (1969). The latter reduced the equation (2-14) to a parabolic equation rather than a hyperbolic equation (Bradshaw et al., 1967). His results indicate that a "kink" appears in the predicted velocity profile; the nondimensional wind shear is either less than or greater than unity depending on whether the flow is accelerating or decelerating. The predicted non-dimensional wind shear, which is assumed to be equal to unity for neutral conditions in mixing length theory, seems in very close agreement with the observations.

Chapter III

WIND AND TEMPERATURE PROFILES IN THE SURFACE LAYER

3.1 Atmospheric Boundary Layer

In the earth's atmosphere, the layer of fluid which is influenced by the combined action of Coriolis force, the thermal stratification and surface friction is called the atmospheric boundary layer. Thus the atmospheric boundary layer is a turbulent boundary layer with density stratification in a rotating coordinate system. Within the atmospheric boundary layer, there are two distinct layers (Figure 3-1): one is called the "Ekman layer", the other is the "surface layer." The thickness of the Ekman layer can be determined by the equation $H' = C\, V_{gr}/f'$, where V_{gr} is the gradient wind velocity at the upper boundary of the layer, $f' = 2\Omega\sin\phi'$ is the Coriolis parameter, Ω is the angular velocity of the earth, ϕ' is the latitude, and C is a nondimensional factor.

The thickness of the Ekman layer usually extends to about 1 km with $V_{gr} = 10$ m/sec and $f' = 10^{-4}$ sec^{-1}; this is approximately one order of magnitude less than the effective thickness of the earth's atmosphere, 10 km. The wind direction changes with height in order to maintain a balance between the Coriolis, pressure gradient, and frictional forces, and the vertical turbulent flux decreases with height. The thickness of the surface layer extends up to about 50 meters over homogeneous terrain. The wind direction is considered to be constant; the variations in shear stress and vertical momentum flux are negligible. The Coriolis force is not important in the surface layer.

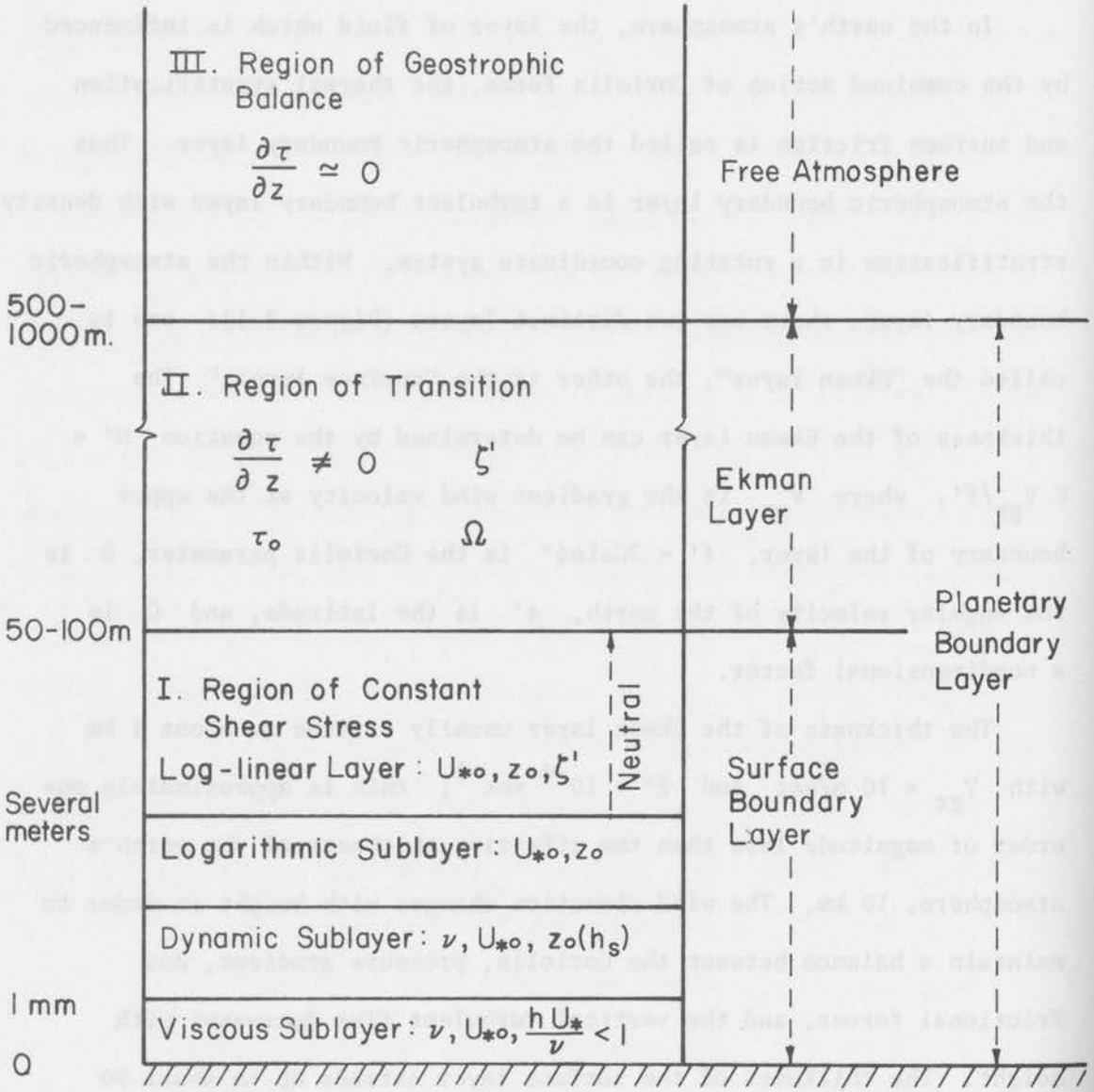

Figure 3-1 Schematic diagram of atmospheric boundary layer

In their numerical modeling of the atmosphere, meteorologists have become increasingly concerned with the interaction between the atmosphere and the underlying surface. The surface of the earth supplies the heat and water vapor to the atmosphere; it also extracts momentum from the atmosphere by the friction of the earth. Therefore, the atmospheric motion will be modified by changes in surface roughness. Hence, this study will be primarily restricted to a consideration of the air in the nonhomogeneous surface layer.

In the homogeneous surface layer, the shear stress is approximately constant,

$$\tau_x + \nu \frac{\partial \bar{u}}{\partial z} \doteq u_*^2$$

$$\tau_y + \nu \frac{\partial \bar{v}}{\partial z} \doteq 0 \quad . \tag{3-1}$$

This surface layer corresponds to the wall region of the turbulent boundary layer in a nonrotating coordinate system with thermal stratification. As one approaches the surface of the earth, the effect of thermal stratification on turbulence becomes less important, and finally its effect vanishes. The layer in which the influence of density stratification can be neglected is called "the sublayer."

In the lower part of the layer near the earth's surface, the structure of the turbulent flow is determined by the three constant parameters, ν, u_* and the roughness parameter represented by z_o or h_s, where h_s is the mean height of roughness. This layer is called "the dynamic sublayer" (Monin, 1970), since in this layer, the characteristics of turbulence are determined by the dynamic factors

ν, u_* and z_o. The underlying surface can be divided into two distinct surfaces: one is dynamically smooth; the other is dynamically rough. The criteria used to separate these two kinds of surfaces depend on the ratio $h_s u_*/\nu$.

If $h_s u_*/\nu$ is less than unity, the underlying surface is called dynamically smooth; on the other hand, if the ratio $h_s u_*/\nu$ is much larger than unity, the underlying surface is called dynamically rough. In the case of a dynamically smooth surface, the dynamic sublayer is not influenced by the roughness elements; the important scaling parameters in this case are ν and u_*. The Reynolds shear stress is negligible compared to the viscous stresses; this layer is called "the viscous sublayer." The thickness of the viscous sublayer in the atmospheric boundary layer is about one millimeter. In the viscous sublayer, equation (3-1) reduces to

$$\nu \frac{\partial \bar{u}}{\partial z} \doteq u_*^2 \,. \tag{3-2}$$

Hence the mean velocity profile is a linear function of height:

$$\bar{u} = \frac{u_*^2}{\nu} z \,. \tag{3-3}$$

This equation is valid for the height $z \leq 5 \frac{\nu}{u_*}$. In the case of a dynamically rough surface, the viscous sublayer is almost nonexistent. When the flow passes through the roughness elements, vortices are generated. This type of surface is more frequently observed in the atmospheric boundary layer.

For $z >> \nu/u_*$, h_s, the dynamic parameter of the dynamic sublayer depends primarily on the frictional velocity u_*, and very little on molecular viscosity of air ν. Thus from dimensional analysis, the resulting equation for the mean velocity gradient is

$$\frac{\partial \bar{u}}{\partial z} = \frac{u_*}{kz} \quad . \tag{3-4}$$

Integrating equation (3-4), we obtain the logarithmic wind profile:

$$\bar{u} = \frac{u_*}{k} \ln \frac{z}{z_o} \quad . \tag{3-5}$$

This equation represents the mean velocity profile in the upper part of the dynamic sublayer, and indicates the dynamic interaction between the underlying surface and the air above. The equation is valid for height $z >> h_s$. If the ratio of z/h_s is not significantly larger than unity, then the effect of the roughness elements will appear in (3-5). The thickness of the dynamic sublayer depends on the thermal stratification. It would be deeper for air approaching neutral conditions. For adiabatic conditions, the thickness of the dynamic sublayer occupies the entire surface layer. The roughness parameter z_o of the logarithmic sublayer depends on the distribution of the height, the size and the shape of the roughness elements of the underlying surface. The roughness parameter z_o usually does not depend on the wind speed. However, it may depend on the wind speed, when the grass is bent by the action of shear stress. The corresponding height of z_o for h_s is shown in Table 1 (Priestly, 1959; Laikhtman, 1961; and Lettau, 1967).

TABLE 1 ROUGHNESS PARAMETER z_o CORRESPONDING TO HEIGHT h_s

	z_o(cm)	h_s(cm)
Smooth Snow	0.001	
Deserts	0.03	
Mowed Grass	0.2-0.7	1.5-3.0
High Grass	9.3-3.7	60-70
Shrubs and Trees	10	
Forests	50-100	1000
Cities	100	

When the height h_s is relatively high, as in the case of high vegetation, the above logarithmic wind profile must be modified to:

$$\bar{u} = \frac{u_*}{k} \ln \frac{z-d}{z_o} , \tag{3-6}$$

where d is the zero plane displacement. The roughness parameter z_o usually lies between $h_s/2$ and h_s.

As with the definition of eddy viscosity, one can also define the eddy conductivity for heat K_h and the eddy diffusivity for mass K_w, and write

$$H = - \rho C_p K_h \frac{\partial \bar{\Theta}}{\partial z} \tag{3-7}$$

$$E = - \rho K_w \frac{\partial \bar{q}}{\partial z} . \tag{3-8}$$

The presence of water vapor and heat in the dynamic sublayer does not change the characteristics of turbulence; therefore, one can consider water vapor and heat as passive substances in the layer. The effect of buoyancy force can also be neglected in the dynamic sublayer. As with frictional velocity, we can define two scales, "frictional temperature" and "frictional humidity" as

$$\Theta_* = - \frac{H}{k\rho_o C_p u_*} \tag{3-9}$$

$$q_* = - \frac{E}{k\rho_o u_*} . \tag{3-10}$$

Since heat flux and water vapor flux are positive upward if distributions of temperature and humidity decrease with height; Θ_* and q_* are negative for upward transport of heat and moisture.

In the logarithmic sublayer, all statistical properties are determined by three constant parameters u_*, Θ_* and q_*. With the definitions of heat flux, water vapor flux, frictional temperature and frictional humidity, we obtain

$$\frac{\partial \overline{\Theta}}{\partial z} = \frac{\Theta_*}{\alpha_h z} \tag{3-11}$$

$$\frac{\partial \overline{q}}{\partial z} = \frac{q_*}{\alpha_q z} \tag{3-12}$$

where

$$\alpha_h = K_h / K_m$$

$$\alpha_q = K_w / K_m .$$

From (3-11) and (3-12), we can obtain logarithmic equations for mean potential temperature and humidity profiles:

$$\overline{\Theta}(z) - \overline{\Theta}(z_o) = \frac{\Theta_*}{\alpha_h} \ln \frac{z}{z_o} \tag{3-13}$$

$$\overline{q}(z) - q(z_o) = \frac{q_*}{\alpha_q} \ln \frac{z}{z_o} \tag{3-14}$$

The above equations are similar to the mean velocity profile in the dynamic sublayer (3-5).

3.2 The Monin-Obukhov Similarity Theory

Above the logarithmic sublayer, the buoyancy force cannot be neglected. The heat and humidity become active in this region. Monin and Obukhov (1954) attempted to generalize the wind, temperature and humidity profiles in the surface layer to diabatic conditions. They postulated that in order for similar profiles to exist in the surface layer, the relevant scaling parameters must be u_*, $H/C_p\rho_o$, E/ρ_o and g/T. The length L depends on the stability, which is defined as

$$L = - \frac{u_*^3 C_p \rho_o T}{kgH} \tag{3-13}$$

and the sign for L is

$$L = \begin{cases} \text{negative for unstable conditions} \\ \infty \quad \text{for neutral conditions} \\ \text{positive for stable conditions.} \end{cases}$$

The velocity scale is u_*, which in turn can be used to determine the temperature and humidity scales θ_* and q_* through (3-9) and (3-10). According to the similarity hypothesis advanced by Monin and Obukhov (1954), the nondimensional wind and temperature should be universal functions of the nondimensional height $\zeta' = z/L$:

$$\frac{kz}{u_*} \frac{\partial \bar{u}}{\partial z} = \phi(\zeta') \tag{3-14}$$

$$\frac{z}{\theta_*} \frac{\partial \bar{\theta}}{\partial z} = \frac{\phi(\zeta')}{\alpha_h(\zeta')} \quad , \tag{3-15}$$

where $\phi(\zeta')$ is a universal function, depending only on stability ζ'.

The nondimensional wind shear ϕ can be expressed in terms of the eddy viscosity defined by $K_m = u_*^2/\frac{\partial \bar{u}}{\partial z}$ as

$$\phi(\zeta') = \frac{kzu_*}{K_m(z)} \quad . \tag{3-16}$$

In an analogous manner, we obtain the nondimensional lapse rate $\phi(\zeta')/\alpha_h(\zeta')$ as given by

$$\frac{\phi(\zeta')}{\alpha_h(\zeta')} = \frac{kzu_*}{K_h(z)} \quad . \tag{3-17}$$

From the definition of L, ϕ, K_m, K_h and Ri, one can show that the gradient Richardson number is equivalent to the nondimensional height $\zeta' = z/L$, given by

$$\frac{z}{L} = \phi(\zeta') \frac{K_h}{K_m} R_f = \phi(\zeta') \, Ri \quad . \tag{3-18}$$

By integrating (3-14) and (3-15), we obtain the universal functions for momentum and heat respectively:

$$\bar{u}(z_1) - \bar{u}(z_2) = \frac{u_*}{k} [f(\frac{z_1}{L}) - f(\frac{z_2}{L})] \tag{3-19}$$

$$\bar{\Theta}(z_1) - \bar{\Theta}(z_2) = \Theta_* [f_t(\frac{z_1}{L}) - f_t(\frac{z_2}{L})] . \tag{3-20}$$

For the flow in neutral stratification, $L \to \infty$, $\phi(0) = 1$ and $\zeta' \to 0$, equation (3-19) reduces to the logarithmic velocity law (3-5). The universal functions in (3-19) and (3-20) can be written as

$$f(\zeta') = \ln \zeta' + \text{const} \quad \text{for } |\zeta|' << 1 \tag{3-21}$$

$$f_t(\zeta') = \frac{1}{\alpha_h} \ln\zeta' + \text{const} \quad \text{for } |\zeta'| << 1 \ . \tag{3-22}$$

The logarithmic laws (3-21) and (3-22) also hold for $z \to 0$ and for L as a fixed constant, which implies that the dynamic sublayer does exist as the height approaches zero.

If we expand the nondimensional wind shear ϕ in a Taylor's series in (3-14) and (3-15), after integrating (3-14) and (3-15) for the case $|\zeta'| \lesssim 1$, and retaining only the linear terms of Taylor's series, we obtain universal functions of the log-linear law for wind and temperature profiles:

$$f(\zeta') \doteq \ln\zeta' + \beta_u\zeta' + \text{const} \quad \text{for } |\zeta'| \lesssim 1 \tag{3-22}$$

$$f_t(\zeta') \doteq \frac{1}{\alpha_h} \ln\zeta' + \beta_t\zeta' + \text{const} \quad \text{for } |\zeta'| \lesssim 1 \ . \tag{3-23}$$

For very strong instability, since the temperature profile is independent of u_*, Obukhov (1946) and Monin (1950) showed that the universal function for temperature profile is possible only for $f_t(\zeta') \sim \zeta'^{-1/3}$. Thus the universal functions for wind and temperature profiles for very unstable cases are:

$$f(\zeta') = C\,\zeta'^{-1/3} + \text{const} \quad \zeta' << -1 \tag{3-24}$$

$$f_t(\zeta') = \frac{C}{\alpha_h} \zeta'^{-1/3} + \text{const} \quad \zeta' << -1 \tag{3-25}$$

where C is some constant.

For very strong stability, the universal functions for wind and temperature profiles (Monin 1970) are

$$f(\zeta') \doteq \frac{1}{R_o} \zeta' + \text{const} \quad \zeta' >> 1 \tag{3-26}$$

$$f_t(\zeta') \doteq \frac{1}{\alpha_h R_o} \zeta' + \text{const} \quad \zeta' >> 1 \ . \tag{3-27}$$

where R_o is a finite limit on R_f.

The theoretical predictions advanced by Monin and Obukhov (1954) agree very well with experimental data. Table 2 is a summary of the constants α_h, β_u, β_t and C for various stability conditions.

The nondimensional wind shear has been introduced in (3-14). In addition, since the vertical heat flux is rarely available, the most frequently measured quantities are temperature and mean wind velocity. When these quantities are given, following Panofsky (1964), we define,

$$L' = \frac{u_* \frac{\partial \bar{u}}{\partial z} T}{kg \frac{\partial \bar{\theta}}{\partial z}} \ . \tag{3-28}$$

Then L' is related to the Monin-Obukhov stability length L by

$$L' = L \frac{K_h}{K_m} \ . \tag{3-29}$$

The ratio K_h/K_m depends only on the Richardson number.

TABLE 2 A SUMMARY OF THE CONSTANTS α_h, β_u, β_t, FOR VARIOUS AUTHORS AND STABILITY CONDITIONS

Authors	Stability	ζ'	$\alpha_h = K_h/K_m$	β_u	β_t	C
Pandolfo (1966)	Unstable		ϕ_m^{-1}			
Charnock (1967)	Strong Instability	-4.5	3.5			
Zilitinkevich and Chalikov (1968)	Stable	0∿0.4	0.83	9.9	10.4	
	Unstable	-1.2∿0		1.4	2.0	
	Free Convection		0.87			1.25
Laykhtman & Ponomareva (1969)	Stable	0∿0.10	0.8			
	Unstable	-0.8∿ -0.3	$3.2\lvert\zeta'\rvert^{0.35}$			
	Unstable	<-0.8	3.0			
Businger et al (1971)	Stable		$\frac{1.0+4.7\zeta'}{0.74+4.7\zeta'} \simeq 1.2$			
	Unstable		$\frac{1.35(1-9\zeta')^{\frac{1}{2}}}{(1.0-15\zeta')^{\frac{1}{4}}}$			

By the definitions of the nondimensional wind shear and stability length L', we have

$$\frac{kz}{u_*}\frac{\partial \bar{u}}{\partial z} = \phi(\frac{z}{L}) = \phi(\frac{z}{L'}) \quad . \tag{3-30}$$

For a small value of z/L', (3-30) becomes

$$\frac{ku}{u_*}\frac{\partial \bar{u}}{\partial z} = 1 + \beta' \frac{z}{L'} \quad . \tag{3-31}$$

where β' is a constant. Thus the velocity profile is

$$\bar{u} = \frac{u_*}{k} [\ln \frac{z}{z_o} + \beta' \frac{z}{L'}] \quad . \tag{3-32}$$

The values of β' are listed in Table 3.

The values of nondimensional wind shear obtained by various researchers are shown in Table 4.

For a nearly neutrally stratified airflow, most investigators agree that the ratio K_h/K_m is nearly unity. Thus, the temperature profile is given as

$$\bar{\Theta}(z) - \bar{\Theta}_o(z_o) = \Theta_* [\ln \frac{z}{z_o} + \beta' \frac{z}{L'}] \quad . \tag{3-33}$$

Analogous to equation (3-18), the relation between the gradient Richardson number and z/L' is given by

$$Ri = \frac{\frac{z}{L'}}{\phi(\frac{z}{L'})} \quad . \tag{3-34}$$

TABLE 3 THE VALUE OF β' FOR VARIOUS AUTHORS AND STABILITY CONDITIONS

Author	Stability	β'
Deacon (1962)	Unstable	4
Panofsky et al. (1960)	Unstable	4.5
Taylor (1960)	Unstable	6
Monin and Obukhov (1954)	Unstable	0.6
	Stable	0.6
McVehil (1964)	Stable	7
Plate and Lin (1966)	Unstable	2
	Stable	7

TABLE 4 THE VALUE OF NONDIMENSIONAL WIND SHEAR FOR VARIOUS RESEARCHERS AND STABILITY CONDITIONS

Authors	Unstable ϕ_m	Constant	Range
Holzman (1943)	$(1-\gamma Ri)^{-\frac{1}{2}}$	$\gamma = 8.2$	
Monteith (1957)	$(1-\gamma Ri)^{-\frac{1}{2}}$	$\gamma \simeq 10$	
KEYPS	$(1-\gamma Ri)^{-\frac{1}{4}}$	$\gamma = 18$	$0 < Ri$ to free convection
Webb (1970)	$1 + \gamma \frac{z}{L}$	$\gamma = 4.5$	
Businger-Dyer	$(1-\gamma \frac{z}{L})^{-\frac{1}{4}}$	$\gamma = 15$	

Authors	Stable ϕ_m	Constant	Range
McVehil (1964)	$1 + \alpha \frac{z}{L}$	$\alpha = 7$	$0 < Ri < 0.12 \sim 0.14$
Webb (1970)	$1 + \alpha \frac{z}{L}$	$\alpha = 5.2$	
Oke (1970)	$(1- \alpha Ri)^{-1}$	$\alpha = 5.0$	$0 < Ri < R_{crit} \sim 0.1$
Businger et al (1971)	$1 + \alpha \frac{z}{L}$	$\alpha = 4.7$	$0 < \frac{z}{L} < \sim 1.2$

Authors	Strong Stable ϕ_m	Constant	Range
Webb (1970)	$1 + \alpha$	$\alpha = 5.2$	$1 \leq \frac{z}{L}$

For log-linear law, $\phi = 1 + \beta' z/L'$, thus equation (3-34) becomes

$$Ri = \frac{\frac{z}{L'}}{1+\beta' \frac{z}{L'}} \qquad (3\text{-}35)$$

Due to large variations in observed profiles under stably stratified conditions, the inversion profiles cannot be fitted to the KEYPS equation by a single curve. The results obtained by Taylor (1960) and Takeuchi (1961) showed that the Monin-Obukhov similarity wind profiles are applicable even under stable conditions; however, they did not define the range of applicability. The analysis of McVehil (1964) establishes the range of applicability of the Richardson number for which the Monin-Obukhov log-linear law is valid. Following Monin-Obukhov's similarity argument for small values of z/L, and expanding ϕ in Taylor series, after retaining only the linear term, one finds:

$$\phi = 1 + \alpha \frac{z}{L}$$

$$= \frac{1}{1 - \alpha R_f} \quad . \qquad (3\text{-}35)$$

The second equality has been obtained from the definition of L and R_f, where α is some constant. Equation (3-35) is valid for stable as well as unstable conditions. However, it is only valid for very small values of z/L in unstable cases. Under stable conditions, such restrictions are not necessarily required. The equation is applicable to large values of z/L as suggested by Taylor (1960). A mean value of six has been obtained by Taylor (1960) and Takeuchi

(1961). This would imply a critical Richardson number of 1/6, which agrees quite well with the theoretical result of 1/7 (Ellison, 1957). If we introduce the quantities L' and α' as before, the Monin-Obukhov log-linear law becomes

$$\phi = \frac{1}{1-\alpha' Ri} \tag{3-35}$$

The above nondimensional wind shear is valid for Ri less than 0.1 with $\alpha' = 7$, and for cases where the Richardson number does not exceed 1/7. The value of $Ri = 1/7$ represents the critical Richardson number. The results obtained by McVehil agree with Deacon's conclusions (1949), that the critical Richardson number was about 0.15.

Data have been obtained from three sets of observations: the O'Neill, Nebraska data of 1953; (Lettau and Davidson, 1957) and of 1956 (Barad, 1958) and Antarctic Profiles (Dalrymple, 1961; McVehil 1964). The analysis of these data suggests that the ratio of K_h/K_m is less than unity under stable stratification. If we define the ratio of the buoyancy term and the production term in the turbulent energy equation, we obtain

$$R_f = \frac{K_h}{K_m} \cdot Ri \quad . \tag{3-37}$$

Where R_f is the flux Richardson number, and the ratio K_h/K_m also depends on the gradient Richardson number. Pandolfo (1966) suggested that the ratio of eddy conductivity to eddy diffusivity is uniquely related to the nondimensional wind shear under unstable conditions. This relation is expressed by

$$\phi = \frac{K_m}{K_h} \quad . \tag{3-38}$$

Therefore the flux Richardson number in an unstable atmosphere becomes

$$R_f = \phi^{-1} Ri = (1 - \gamma Ri)^{\frac{1}{4}} Ri \quad , \tag{3-39}$$

where $$\phi = (1.0 - 18\ Ri)^{-\frac{1}{4}} \quad \text{for} \quad Ri < 0 \ . \tag{3-40}$$

By definition of various quantities, z/L, ϕ and R_f and with the aid of (3-38) suggested by Pandolfo, it is easy to show that

$$z/L = Ri \quad . \tag{3-41}$$

The stability parameter z/L is equal to Ri. Since L is nearly constant in the lower atmospheric boundary layer, this indicates that the Richardson number is a function of height.

From the definition of nondimensional wind shear and the ratio of K_m/K_h postulated by Pandolfo (1966), the eddy diffusivity and the eddy conductivity may be written as

$$K_m = k^2 z^2 \Phi \frac{\partial \bar{u}}{\partial z} \tag{3-41}$$

$$K_h = k^2 z^2 \Phi^{3/2} \tag{3-42}$$

for unstable conditions,

where $\Phi = \phi^{-2}$

$$\phi = (1.0 - 18\ Ri)^{-\frac{1}{4}} \quad \text{for} \quad Ri < 0 \quad . \tag{3-43}$$

Most authors agree that the ratio of the eddy diffusivity to the eddy conductivity is nearly equal to unity for stable conditions. Hence, the eddy conductivity is the same as the eddy diffusivity for stable conditions, and

$$K_m = k^2 z^2 \Phi \frac{\partial \bar{u}}{\partial z} \tag{3-44}$$

$$K_h = k^2 z^2 \Phi \frac{\partial \bar{u}}{\partial z}$$

for stable conditions,

where $\Phi = \phi^{-2}$

$$\phi = (1.0\text{-}7\ Ri)^{-1} \quad \text{for} \quad 0 < Ri < 0.1. \tag{3-46}$$

3.3 Modeling the Surface Layer

Conventional approaches to numerical general circulation modeling usually employ the traditional mixing length theory (Smagorinsky et al. 1965; Miyakoda et al., 1969), although the Monin-Obukhov similarity theory has long been known to offer remarkable success in representing wind and temperature profiles in the constant flux layer. Surprisingly, the similarity theory has only been adopted recently (Delsol, et al., 1971), presumably because other physical and mathematical treatments were mainly concerned with other aspects of the problem. With the advance

of more complex mathematical models, perhaps the time has come to consider the modeling of the surface boundary layer. Some of the theories of the surface boundary layer have already been described in some detail. We will now summarize those results along with some theories which have not previously been mentioned.

(1) the mixing length theory:

(i) The Prandtl mixing length theory is:

$$K_m = \ell^2 \frac{\partial \bar{u}}{\partial z} \quad \text{for} \quad z_o \leq z \leq z_t \ , \tag{3-47}$$

where z_o is the roughness parameter, and z_t is the height of the constant flux layer. The mixing length ℓ is given by

$$\ell = kz \ ,$$

where

$$k = 0.4.$$

(ii) The Clayton theory (not yet published) includes both the unstable and stable cases.

For the unstable case, the eddy coefficient for the momentum is

$$K_m = \ell^2 \left|\frac{\partial \bar{u}}{\partial z}\right| (1-\alpha S^*) \ ; \tag{3-47}$$

and for the stable case,

$$K_m = \ell^2 \frac{\partial \bar{u}}{\partial z} (1+\alpha S^*) \ , \tag{3-48}$$

where $\alpha = 18,$

$$S^* = \frac{(g\ell)^{\frac{1}{2}} \frac{\partial \bar{\theta}}{\partial z}}{\bar{\theta} \left(\frac{\partial \bar{u}}{\partial z}\right)}$$

(2) the similarity theory:

A number of the similarity theories are based on the Monin-Obukhov similarity theory (Lumley and Panofsky, 1964; Monin and Yaglom, 1966). The formulations of these theories are shown in the following.

(i) The Monin-Obukhov similarity theory (1954), from dimensional analysis in the constant flux layer, states that:

$$\frac{\bar{u}(z) - \bar{u}(z_o)}{u_*} = f\left(\frac{z}{L}\right) - f\left(\frac{z_o}{L}\right) , \qquad (3\text{-}49)$$

where L is the Monin-Obukhov length, f is a universal function to be determined empirically, and u_* is the friction velocity.

(ii) The Businger-Dyer theory for the nondimensional wind in unstable conditions, is

$$\phi = \left(1 - \gamma \frac{z}{L}\right)^p$$

where γ is the Businger-Dyer constant, and

$\gamma = 16.0$ and $p = -0.25$, and (Paulson, 1967)

$\gamma = 15.0$ and $p = -0.275$, and (Dyer, to be published).

(iii) The KEPYS theory is as follows.

For unstable conditions, the nondimensional wind shear is given by:

$$\phi_m = (1 - \gamma' Ri)^{-\frac{1}{4}} \quad , \tag{3-51}$$

where $\gamma' = 18$ (Panofsky et al., 1960).

Pandolfo (1966) has shown that

$$\frac{z}{L} = Ri(z),$$

therefore, equation (3-51) becomes

$$\phi_m = (1 - \gamma' \frac{z}{L})^{-\frac{1}{4}} \quad . \tag{3-53}$$

Equation (3-53) is very close to the Businger-Dyer formula.

(iv) The Yamamoto and Shimanuki theory (1966) follows.

The formula for ϕ_m proposed by Yamamoto and Shimanuki is an improvement over the KEYPS equation.

For unstable conditions, they find

$$\phi_m^4 - |\zeta^*| \phi_m^3 - 2\phi_m^2 + 1 = 0 \quad ,$$

where $\zeta^* = - \frac{az}{L}$ and $a = 15$ is a constant.

For stable conditions, the relation

$$\phi_m^4 - |\zeta^*|^{1-2p} \phi_m^3 - 2\phi_m^2 + 1 = 0 \quad ,$$

holds, where $p = 1/6$.

(v) The McVehil theory (1964) is another similarity theory. For stable conditions,

$$\phi_m = 1 + \alpha \frac{z}{L} \quad ,$$

where α is an empirical constant. With some modification formula is also suggested by others (Paulson; 1967, Webb, 1970), where α is an empirical constant and

$$\alpha = \begin{cases} 7 & \text{(McVehil, 1964)} \\ 7.5 & \text{(Paulson, 1967)} \\ 5p & p = 1 \quad \text{for} \quad \frac{z}{L} \leq 1 \\ & p = \frac{L}{z} \quad \text{for} \quad 1 < \frac{z}{L} < 6 \quad \text{(Webb, 1970)} \\ 4.7 & \text{(Businger et al., 1971).} \end{cases}$$

(vi) The Clarke theory (1970) is still another. The non-dimensional wind shear is expressed as

$$\phi_m = \{(1 + 5p \frac{z}{L})^{-1} + 0.079 \frac{z}{L}\}^{-1} \quad . \qquad (3\text{-}55)$$

This is an interpolation formula using a z^{-2} profile at a great height and a Webb profile close to the surface.

It is customary to treat the atmospheric surface layer as the constant flux layer in numerical modeling in previous theories, thus, no dynamic modeling of the surface boundary layer has ever been made. Since previous theories are only valid for flow over homogeneous terrain, we will need to develop a theory that has no such limitation. The model developed in Chapter IV possesses internal mathematical

consistency and is without a priori assumptions, as are necessary in previous theories.

3.4 Effects of Roughness and Various Stabilities on Wind Profiles

The observed wind profiles in the field and wind tunnel, which reveal the effects of surface roughness, will be presented in this section. The wind profiles under various stability conditions with constant fluxes are theoretically derived. The results show the influence of various stabilities on wind profiles.

The requirement necessary for the application of Reynolds law in modeling the atmospheric boundary layer cannot be met in the wind tunnel; however, the Reynolds number appears not to be an essential parameter for the atmospheric boundary layer. It is known from Nikuradse's experiments (1933) that flow may be independent of the Reynolds number, and it may depend only on the roughness and turbulence. Therefore, the modeled flow must be turbulent, similar to that of the natural wind.

Simulation of atmospheric shear flows by wind tunnels has been discussed by a number of investigators (see Cermak et al., 1966) and can be clearly seen in Figure 3-2. Wind profiles from wind tunnels and from the natural environment are shown in Figure 3-2, (Jensen, 1958). The figure is used to demonstrate that natural wind over rough surface can be simulated by a wind tunnel. The profile at Hojer represents flow over a smooth surface, while the profiles at Frerslev, Alberteland and Nasgard represent observations over cultivated fields. The wind profile for the area over the central part of Copenhagen is also shown in Figure 3-2. Wind profiles simulated by a wind tunnel are

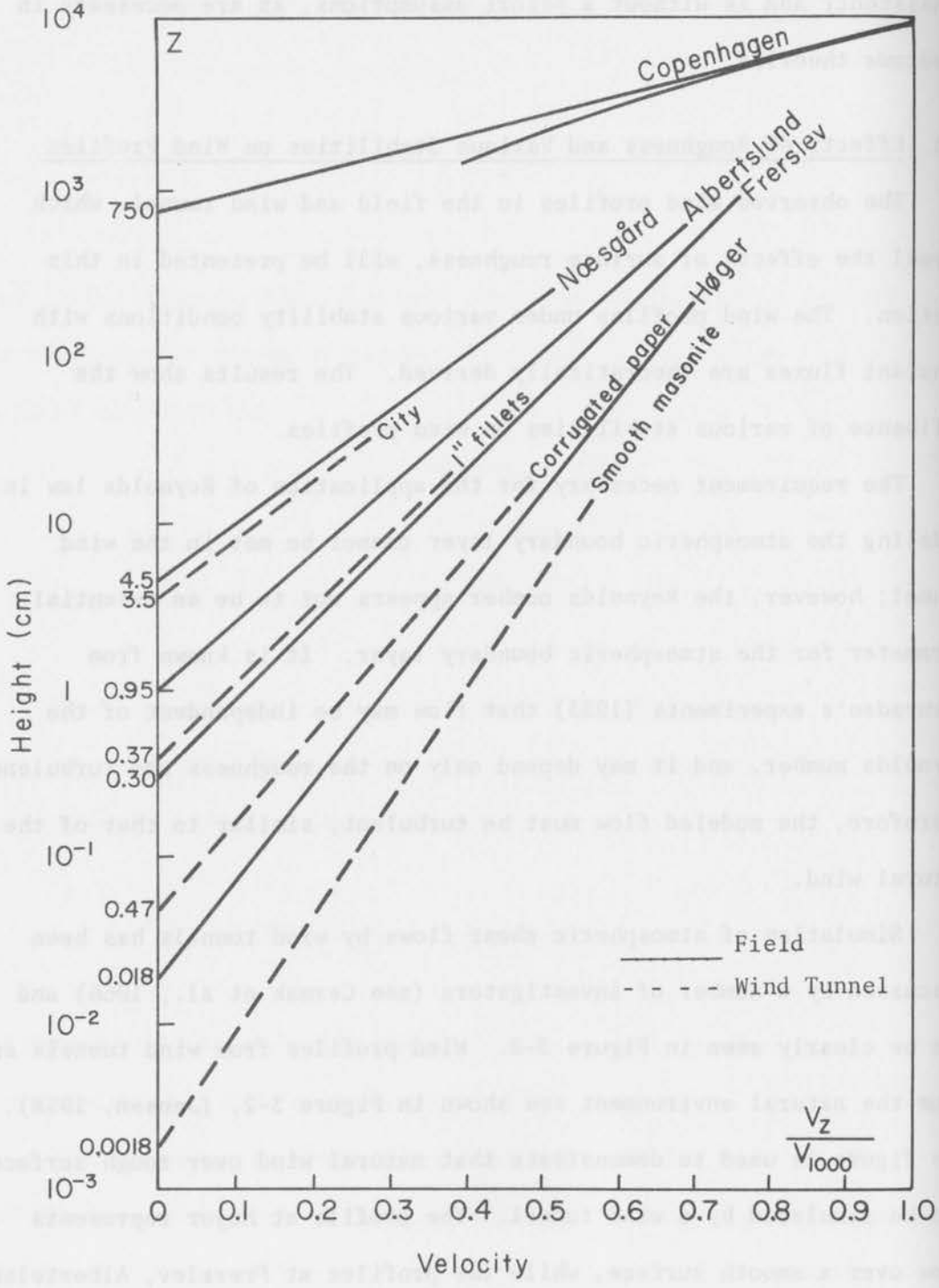

Figure 3-2 Velocity profiles over various terrains in the field and wind tunnel. The abscissa is the velocity normalized by the velocity at a height of 100 meters; the ordinate is the height above the surface on a logarithmic scale (from Jensen, 1958)

different surfaces covered with masonite sheets, corrugated paper, fillets and models of houses. Figure 3-2 shows the effects of the surface roughness on the flow that can be simulated in a wind tunnel.

The velocity profile is modified by the surface roughness, therefore, roughness parameters z_o are important parameters in controlling the flow field. The influence of various surface roughnesses on the wind profile is shown in Figure 3-2. For homogeneous terrain, the wind profile essentially follows a logarithmic law under neutral stratification. Figure 3-2 shows that the wind profiles in the atmospheric boundary layer can be simulated by a wind tunnel. For the flow from smooth to rough transition, or from rough to smooth, the wind profile somewhere between the two wind profiles in equilibrium with the underlying surfaces can be qualitatively inferred from Figure 3-2.

The nondimensional wind shear in a constant flux layer is

$$\frac{kz\,\frac{\partial \bar{u}}{\partial z}}{u_{*o}} = \left(1 - \gamma\,\frac{z}{L}\right)^{-\frac{1}{4}} \tag{3-56}$$

from equation (3-53). If velocity and length are scaled with respect to u_{*o}/k and z_o, respectively, we obtain the nondimensional equation (3-56) as

$$\frac{\partial \bar{u}}{\partial z} = \frac{(1 + \beta z)^{-\frac{1}{4}}}{z} \quad , \tag{3-57}$$

where $\beta = -\frac{\alpha}{L}$.

Integrating equation (3-57) we get

$$\bar{u}(z) = \int_1^z \frac{1}{z\,(1 + \beta z)^{-\frac{1}{4}}}\,dz \quad , \tag{3-58}$$

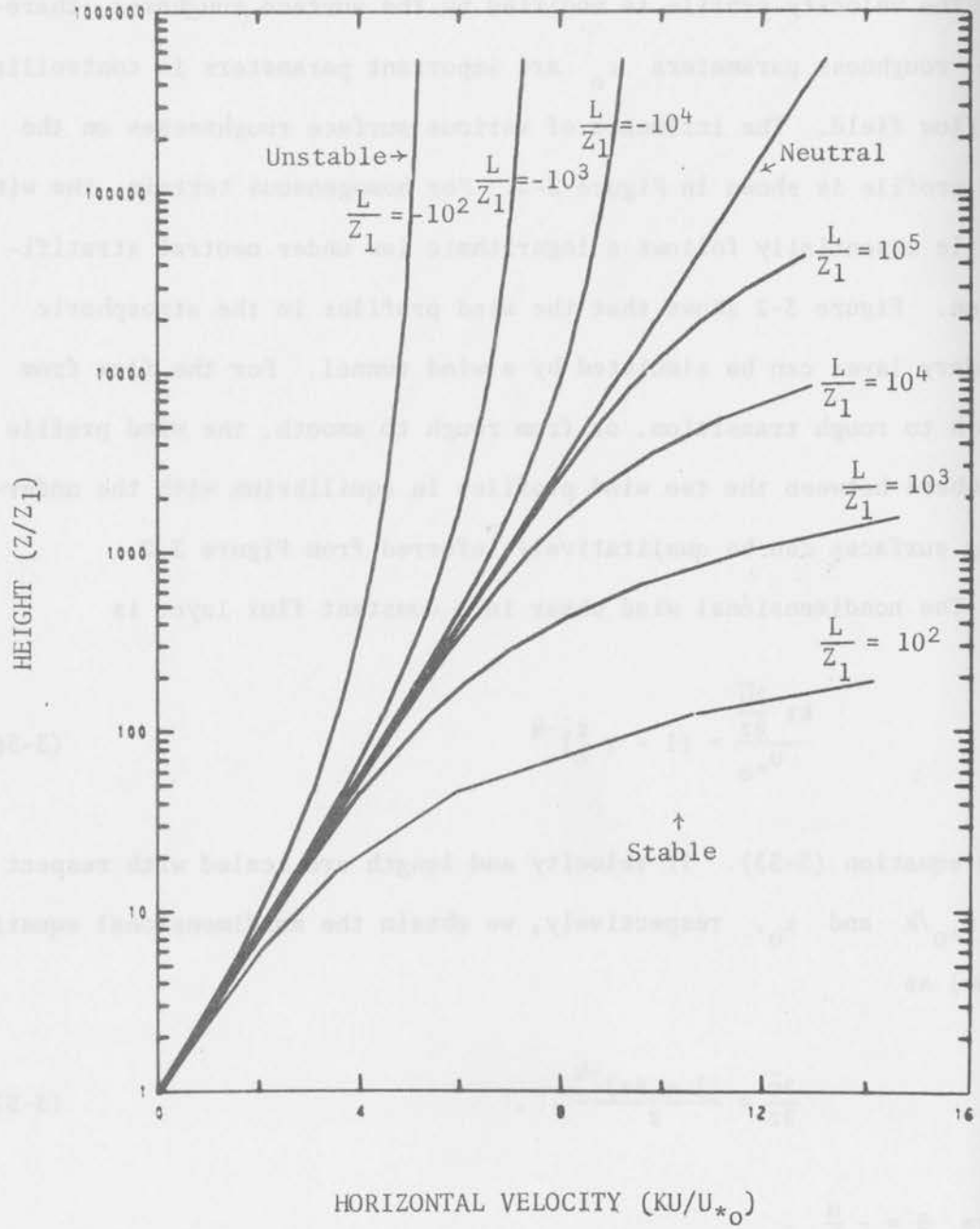

Figure 3-3 Velocity profiles for various stability conditions

and we obtain the velocity profile as

$$\bar{u}(z) = \ln \frac{[(1 + \beta z)^{\frac{1}{4}} - 1][(1 + \beta)^{\frac{1}{4}} + 1]}{[(1 + \beta z)^{\frac{1}{4}} + 1][(1 + \beta)^{\frac{1}{4}} - 1]}$$

$$+ 2 \tan^{-1}(1 + \beta z)^{\frac{1}{4}} - 2 \tan^{-1}(1 + \beta) \quad . \qquad (3\text{-}60)$$

The nondimensional log-linear wind profile for stable conditions can be obtained from the Webb profile; after integrating Equation (3-59) we have

$$\bar{u}(z) = \ln z + \beta(z-1) \quad , \qquad (3\text{-}61)$$

where $\beta = \frac{r}{L}$ and $r = 5.2$ (Webb, 1970).

The wind profiles from equations (3-60) and (3-61) are plotted in Figure 3-3; the figure indicates the effects of various instabilities.

Chapter IV

THEORETICAL DEVELOPMENT

The conventional approach to closing the system of equations describing turbulent flow is to use the mixing length assumption. The mixing length hypothesis has long been popular in solving boundary layer problems, and has worked well in many engineering and atmospheric problems. An alternative approach to the boundary layer flow has been considered by several authors in recent years. Turbulent energy closure has been investigated by Glushko (1965); Bradshaw et al. (1967); Bechwith and Bushnell (1968); Mellor and Herring (1968, 1970), for the calculation of boundary layer development in fluid mechanics; and Bradshaw et al., who use three empirical functions to relate the turbulent intensity, diffusion and dissipation to the shear stress profile. Mellor and Herring (1968) define length scales relating shear stress and dissipation to turbulent kinetic energy and assume that the transport of kinetic energy is the same as that of momentum. These concepts by Bradshaw et al., have been utilized to investigate the flow in the atmospheric surface layer by Peterson (1969). He chose two empirical functions and one assumption similar to Bradshaw's three empirical functions. The first function which relates the turbulent intensity to the shear stress is a constant of 0.16. Bradshaw et al., however, use a constant of 0.30. The second function which relates the dissipation to the shear stress is equal to the mixing length kz, where k is a von Kármán "constant". Under equilibrium conditions, the dissipation is equal to $\tau^{3/2}/kz$, where τ is the shear stress. Although Monin (1959) argued that this

relation is also valid even under non-equilibrium conditions, there is no adequate quantity of data, to support his claim. It is not clear whether Monin's claim holds true in accelerating or decelerating flows. Donaldson et al., (1968) and Mellor and Herring (1970) made an attempt to close the system consisting of the momentum equation, the equation of continuity, and either the double velocity correlations or turbulent energy equation by introducing several length scales.

We now will seek a fundamental framework for the model theory. The aim is to try to choose length scales in order to close the system of equations. If unknown terms have maximum correlation with known quantities, then these unknown variables can be replaced by the known quantities. Thus, the assumptions based on empirical facts must be used to reduce the number of unknown variables. This reduction will serve as a foundation for the further refinement and future work. Although turbulent energy closure is more complicated and requires more empirical functions, it can provide more information about the turbulent quantities which cannot be obtained from the heuristic model of mixing length. These turbulent quantities can be used in comparison with the experimental data.

A set of basic equations is needed in order to obtain a complete set of equations. To obtain such results and proceed with the study in the following sections we will first derive the basic equations and then the equations for the turbulent quantities.

4.1 Equation of State

The equation of state for an ideal gas which relates pressure to the density and temperature is

$$P = \rho RT \quad , \tag{4-1}$$

where the values of pressure, density and temperature are denoted by P, ρ and T, respectively. R is a gas constant and equal to $C_p - C_v$ for an ideal gas, where C_p is specific heat at constant pressure and C_v is specific heat at constant volume.

A reference state will be defined in which the temperature distribution is a function of height; the effects of viscosity, heat conduction and radiation are considered to be negligible. The values of pressure, density and temperature will be denoted by P_o, ρ_o and T_o, respectively. The pressure in the reference state obeys the hydrostatic relation

$$\frac{\partial P_o}{\partial z} = - \rho_o g \quad , \tag{4-2}$$

and the equation of state for the reference atmosphere will be

$$P_o = \rho_o R T_o \quad . \tag{4-3}$$

The instantaneous values of pressure, density and temperature will be expressed as

$$\begin{aligned} P &= P_o + \tilde{P} \\ \rho &= \rho_o + \tilde{\rho} \\ T &= T_o + \tilde{T} \end{aligned} \tag{4-4}$$

where the tilde represents the departure of a quantity from the reference state. To a high degree of approximation, the product of the perturbed quantities can be neglected. The perturbed quantities of pressure, density, and temperature are related as

$$\frac{\tilde{P}}{P_o} = \frac{\tilde{\rho}}{\rho_o} + \frac{\tilde{T}}{T_o} \tag{4-5}$$

A scale analysis by Dutton and Fichtl (1969) shows that if the vertical pressure gradient term has the same order of magnitude as the buoyancy term, then

$$\frac{\tilde{P}}{P_o} \sim (\frac{\tilde{\rho}}{\rho_o}) \frac{L_w}{H_\alpha} , \tag{4-6}$$

where L_w is the vertical scale and H_α is the scale height defined by

$$H_\alpha^{-1} = - \frac{1}{\rho_o} \frac{\partial \rho_o}{\partial z} . \tag{4-7}$$

We will assume that the perturbed quantity of density, $\tilde{\rho}$, is much smaller compared to the reference density, ρ_o. Thus,

$$|\frac{\rho}{\rho_o}| << 1. \tag{4-8}$$

In the shallow convective atmosphere, L_w/H_α is also smaller than unity. Therefore, the relative pressure variation in (4-5) can be ignored as compared to the relative density variation for the shallow convective atmosphere, Equation (4-5) can be approximated as

$$\frac{\tilde{\rho}}{\rho_o} + \frac{\tilde{T}}{T_o} = 0 \quad . \tag{4-9}$$

4.2 Equation of Continuity

The equation of continuity is

$$\frac{\partial \rho}{\partial t} + \frac{\partial \rho u_i}{\partial x_i} = 0 \quad , \tag{4-10}$$

which may be expanded in the form

$$\frac{\partial \rho}{\partial t} + u_i \frac{\partial \rho}{\partial x_i} = - \rho_o \left(1 + \frac{\tilde{\rho}}{\rho_o}\right) \frac{\partial u_i}{\partial x_i} \quad . \tag{4-11}$$

The condition in (4-8) allows us to neglect the relative density variation $\tilde{\rho}/\rho_o$ term as compared with unity on the right side of (4-11). Equation (4-11) becomes

$$\frac{\partial \rho}{\partial t} + u_i \frac{\partial \rho}{\partial x_i} = - \rho_o \frac{\partial u_i}{\partial x_i} \quad . \tag{4-12}$$

According to the scale analysis of convection for compressible flow derived by Dutton and Fichtl (1969), the technique of Fourier analysis can be used to define certain scales. Dutton and Fichtl, furthermore, made the assumptions that the order of magnitude of the pressure gradient is the same as the buoyancy force, and the pressure and buoyancy terms are out of phase. With such assumptions and definitions of scales, they concluded that in a deep convective case the depth scale, L_w, for the fluid is permitted to be the same

order of magnitude as the scale height, H_α, in the atmosphere. For a deep convective case the relevant equation of continuity may be of the form

$$\frac{\partial \rho_o u_i}{\partial x_i} = 0 \quad . \tag{4-13}$$

This equation is useful in studying the gravity wave in the atmosphere, since a vertical scale of several kilometers is allowed. The equation of continuity for deep convection (4-13) reduces to

$$\rho_o \frac{\partial u_i}{\partial x_i} + w \frac{\partial \rho_o}{\partial z} = 0 \quad . \tag{4-14}$$

For a case of shallow convection, the vertical scale is much less than the scale height. Therefore, the last term in (4-14) may be eliminated, and equation (4-14) becomes

$$\frac{\partial u_i}{\partial x_i} = 0 \quad . \tag{4-15}$$

For a shallow convective atmosphere with a low Mach number, the approximate equation of continuity permits us to treat the compressible medium as incompressible. The vertical scale validated in the shallow convection is less than about half a kilometer. Another important consequence is that relatively high frequencies are permitted. As the vertical scale approaches the horizontal scale, the magnitude of the vertical velocity becomes the same as the horizontal velocity.

4.3 Equations of Motion

The Navier-Stokes equations of instantaneous motion of a compressible, viscous, diffusive and nonhomogeneous fluid which is subjected to a uniform body force in a Newtonian medium and in a nonrotation system (Jeffreys, 1931), are

$$\rho \frac{\partial u_i}{\partial t} + u_j \frac{\partial u_i}{\partial x_j} = - \rho g \delta_{3i} + \frac{\partial}{\partial x_K} \cdot$$

$$\{-(P + \frac{2}{3} \mu \frac{\partial u_j}{\partial x_j}) \delta_{ik}\} + \frac{\partial}{\partial x_K} \{\mu (\frac{\partial u_i}{\partial x_K} + \frac{\partial u_k}{\partial x_i})\} \quad . \qquad (4\text{-}16)$$

All tensor components refer to a right-handed Cartesian coordinate system, x_i $(i = 1, 2, 3)$ denotes as follows,

$$x_1 = x, \quad x_2 = y, \quad x_3 = z \quad .$$

z is in the vertical direction, while x and y axis are in the horizontal direction. δ_{ij} is the Kronecker delta, μ is the coefficient of molecular viscosity, P is the static pressure at any point in the fluid and is a mean value of the normal stresses exerted through the orthogonal axes meeting at the point. The value of P should be invariant under rotation of a coordinate system. Equations (4-16) express the conservation of momentum. We are mainly considering the fluid motion at a very low Mach number and assume that the dynamic coefficient of viscosity, $\mu = \rho\nu$, does not depend on the temperature. In addition, temperature variations permitted in the fluid must be small compared to the temperature in the reference state.

By substituting the perturbations equations (4-4) into the Navier-Stokes equations (4-16) and writing the non-viscous, non-inertial acceleration terms in the vertical direction, one obtains

$$-\frac{1}{\rho}\frac{\partial P}{\partial z} - g = -\left(1 - \frac{\tilde{\rho}}{\rho_o}\right)\frac{1}{\rho_o}\frac{\partial \tilde{P}}{\partial z} - \frac{\tilde{\rho}}{\rho_o}\, g \quad , \tag{4-17}$$

where the higher order terms of the relative density perturbation have been ignored. In order that the product of perturbation quantities in (4-17) can be neglected, it is required that

$$\left|\frac{\tilde{\rho}}{\rho_o}\right| << 1 \quad . \tag{4-18}$$

Thus, we can write (4-17) as

$$-\frac{1}{\rho}\frac{\partial P}{\partial z} - g = -\frac{1}{\rho_o}\frac{\partial \tilde{P}}{\partial z} + \frac{\tilde{T}}{T_o}\, g \quad . \tag{4-19}$$

After substituting (4-19) into the Navier-Stokes equation (4-16), and making use of the continuity equation, we obtain

$$\frac{\partial u_i}{\partial t} + u_j\frac{\partial u_i}{\partial x_j} = -\frac{1}{\rho_o}\frac{\partial \tilde{P}}{\partial x_i} + \frac{\tilde{T}}{T_o}\, g\, \delta_{3i} + \nu\frac{\partial^2 u_i}{\partial x_k \partial x_k} \quad . \tag{4-20}$$

where ν is the kinematic viscosity and assumed constant for a low Mach number.

Equation (4-20) essentially contains Boussinesq's approximations (Spiegel and Veronis, 1960), which states that the variations in

density result primarily from thermal effects, not pressure, and that in the equations for the rate of change of momentum and mass, the variations of density may be neglected, except when they are associated with the gravitational acceleration in the buoyancy term.

4.4 Equations of Mean Velocity Field

We will now consider a mean flow in a turbulent boundary layer. This flow is in the surface layer, and the depth of the fluid is less than a few tens of meters. It will be assumed that the turbulent motion of flow can be separated into mean flow and superimposed eddy motion. Thus, the instantaneous components of turbulent motion will be denoted as

$$u_i = \bar{u}_i + u'_i \qquad (i = 1, 2, 3) \quad . \tag{4-21}$$

The instantaneous values of pressure and temperature can also be expressed as

$$\begin{aligned} \tilde{P} &= \bar{\tilde{P}} + P' \\ \tilde{T} &= \bar{\tilde{T}} + T' \quad , \end{aligned} \tag{4-22}$$

where the overbar at the top of a symbol denotes the mean value of a physical quantity with respect to time averaged at a fixed point in space. Following Osborne Reynolds, an assumed significant mean value can be taken, which implies that the time interval is short enough and that the turbulent fluctuations are so rapid that the change in the mean value can be ignored. Taking the mean value and applying the

Reynolds' rule: if A and B are dependent variables, and S (of any of x_i (i = 1,2,3) and t) an independent variable, then $\overline{AB} = \overline{A}\ \overline{B}$, and $\overline{\partial A}/\partial X = \partial\overline{A}/\partial S$ (Goldstein, 1965). Reynolds' principles can be applied to the physical quantities so that

$$\overline{u_i'} = 0\ ,\quad \overline{\rho'} = 0,\quad \overline{T'} = 0,\quad \overline{P'} = 0\ . \tag{4-23}$$

If we substitute $\overline{u_i} + u_i'$ for u_i into the momentum equation (4-20) and equation of continuity (4-15), and use Reynolds' principles, we obtain,

$$\frac{\partial \overline{u}_i}{\partial t} + \frac{\partial u_i'}{\partial t} + \overline{u}_j \frac{\partial \overline{u}_i}{\partial x_j} + u_j' \frac{\partial \overline{u}_i}{\partial x_j} + \overline{u}_j \frac{\partial u_i'}{\partial x_j} + u_j' \frac{\partial u_i'}{\partial x_j}$$

$$= -\frac{1}{\rho_o}\frac{\partial \tilde{\overline{p}}}{\partial x_i} - \frac{1}{\rho_o}\frac{\partial p'}{\partial x_i} + \frac{\tilde{\overline{T}}}{T_o} g\,\delta_{3i} + \frac{T'}{T_o} g\,\delta_{3i}$$

$$+ \nu\left(\frac{\partial^2 \overline{u}_i}{\partial x_j \partial x_j} + \frac{\partial^2 u_i'}{\partial x_j \partial x_j}\right) \tag{4-24}$$

$$\frac{\partial \overline{u}_i}{\partial x_i} + \frac{\partial u_i'}{\partial x_i} = 0\ . \tag{4-25}$$

Taking the average value of (4-24) and (4-25), we obtain the equations for mean motion and the continuity equation for the mean flow, respectively. They are expressed as:

$$\frac{\partial \bar{u}_i}{\partial t} + \bar{u}_k \frac{\partial \bar{u}_i}{\partial x_k} = - \frac{1}{\rho_o} \frac{\partial \tilde{P}}{\partial x_i} + \frac{\tilde{T}}{T_o} g \delta_{3i}$$

$$+ \frac{\partial}{\partial x_k} \{ - \overline{u_k' u_i'} + \nu \frac{\partial \bar{u}_i}{\partial x_k} \} \qquad (4\text{-}26)$$

$$\frac{\partial \bar{u}_i}{\partial x_i} = 0 \quad . \qquad (4\text{-}27)$$

If we subtract (4-27) from (4-25), we have $\partial u_i'/\partial x_i = 0$. Because $\partial u_i'/\partial x_i = 0$, equation (4-26) can be obtained. The equations of mean motion assume the same form as (4-20) of the instantaneous motion, except the terms called Reynolds stresses, $- \rho_o \overline{u_k' u_i'}$.

4.5 The Turbulent Energy Equation

Owing to the presence of viscosity, the turbulent motion in the atmosphere will dissipate into heat if there is no continuous supply of energy for the maintenance of the turbulent motions. Consequently, these motions will decay with time. How the flow changes its pattern, and the relation between the velocity fluctuations during decay can be investigated by describing the double velocity correlations. Subtracting (4-26) from (4-24) and (4-27) from (4-25), the equations of turbulent motion and the equation of continuity for u_i' are expressed respectively as

$$\frac{\partial u_i'}{\partial t} + \bar{u}_k \frac{\partial u_i'}{\partial x_k} = - \frac{1}{\rho_o} \frac{\partial P'}{\partial x_i} + \frac{T'}{T_o} g \delta_{3i}$$

$$- u_k' \frac{\partial \bar{u}_i}{\partial x_k} - u_k' \frac{\partial u_i'}{\partial x_k} + \overline{u_k' \frac{\partial u_i'}{\partial x_k}}$$

$$+ \nu \frac{\partial^2 u_i'}{\partial x_k \partial x_k} \qquad (4\text{-}28)$$

$$\frac{\partial u_i'}{\partial x_i} = 0 \quad . \tag{4-29}$$

To obtain the equations of motion for the stresses $\overline{u_i'u_j'}$, the moment of (4-28) with u_j' is added to another moment of (4-28) after interchanging the indices. The result is

$$\frac{\partial \overline{u_i'u_j'}}{\partial t} + \bar{u}_k \frac{\partial \overline{u_i'u_j'}}{\partial x_k} = - \overline{u_k'u_j'} \frac{\partial \bar{u}_i}{\partial x_k} - \overline{u_k'u_i'} \frac{\partial \bar{u}_j}{\partial x_k}$$

$$- \frac{1}{\rho_o} \overline{u_j' \frac{\partial P'}{\partial x_i}} - \frac{1}{\rho_o} \overline{u_i' \frac{\partial P'}{\partial x_j}}$$

$$+ \frac{\overline{u_j'T'}}{T_o} g \delta_{3j} + \frac{\overline{u_i'T'}}{T_o} g \delta_{3i}$$

$$+ \frac{\partial}{\partial x_k} \overline{u_k'u_i'u_j'}$$

$$+ \nu \overline{u_j' \frac{\partial^2 u_i'}{\partial x_k \partial x_k}} + \nu \overline{u_i' \frac{\partial^2 u_j'}{\partial x_k \partial x_k}} \quad . \tag{4-30}$$

The resulting equation (4-30) describes the relation between the turbulence motions. If we contract (4-30), we obtain the turbulence energy equation. Equation (4-30) can also be written in the following form,

$$\frac{\partial \overline{u_i'u_j'}}{\partial t} + \bar{u}_k \frac{\partial \overline{u_i'u_j'}}{\partial x_k} = - \overline{u_k'u_j'} \frac{\partial \bar{u}_i}{\partial x_k} - \overline{u_k'u_i'} \frac{\partial \bar{u}_j}{\partial x_k}$$

$$- \frac{\partial}{\partial x_i} \left(\overline{u_j' \frac{P'}{\rho_o}}\right) - \frac{\partial}{\partial x_j} \left(\overline{u_i' \frac{P'}{\rho_o}}\right)$$

$$+ \overline{\frac{P' \frac{\partial u_j'}{\partial x_i}}} + \overline{\frac{P' \frac{\partial u_i'}{\partial x_j}}}$$

$$+ \frac{\overline{u_j'T'}}{T_o} g \delta_{3j} + \frac{\overline{u_i'T'}}{T_o} g \delta_{3i}$$

$$+ \frac{\partial}{\partial x_k} (\overline{u_k' u_i' u_j'})$$

$$+ \frac{\partial}{\partial x_k} \left(\overline{u_j' \nu \frac{\partial u_j'}{\partial x_k}}\right) + \frac{\partial}{\partial x_k} \left(\overline{u_i' \nu \frac{\partial u_j'}{\partial x_k}}\right)$$

$$- 2 \nu \overline{\frac{\partial u_i'}{\partial x_k} \frac{\partial u_j'}{\partial x_k}} . \qquad (4\text{-}31)$$

If we contract (4-31), we obtain the turbulent energy equation,

$$\frac{\partial}{\partial t} \left(\frac{\overline{q^2}}{2}\right) + \bar{u}_k \frac{\partial}{\partial x_k} \left(\frac{\overline{q^2}}{2}\right) = - \overline{u_k' u_i'} \frac{\partial \bar{u}_i}{\partial x_k} + \frac{\overline{u_i'T'}}{T_o} g \delta_{3i}$$

I II III IV

$$+ \frac{\partial}{\partial x_k} \left(\overline{u_k' \frac{q^2}{2}} - \overline{u_k' \frac{P'}{\rho_o}} + \frac{\partial}{\partial x_k} \left(\frac{\overline{q^2}}{2}\right)\right)$$

V VI VII

$$- \nu \overline{\left(\frac{\partial u_i'}{\partial x_k}\right)\left(\frac{\partial u_i'}{\partial x_k}\right)} . \qquad (4\text{-}32)$$

VIII

The turbulent energy equation states: the change of turbulent kinetic energy per unit mass of fluid (i.e., the local rate of change term, (I), and advection term, (II)) is equal to the sum of the production terms: the transformation of energy through interaction of Reynolds stress and wind shear to mean motion (III), the production of turbulent energy due to buoyancy forces (IV), the convective diffusion of turbulent energy (V) and turbulent pressure (VI) by turbulence, the turbulent energy transport by viscous shear stresses of the turbulent motion (VII), and dissipation by the turbulent motion (VIII). The dissipation term (VIII) is positive definite; it always extracts the turbulent energy from the fluid. The production term (III) usually is positive; however, a small region of negative production in the case of wall jets has been observed.

4.6 Equations of Double Velocity Fluctuation

Considering the index i as fixed, and taking the moment of (4-28) by u_i', the turbulent energy equations for each velocity component are obtained:

$$\frac{\partial}{\partial t}\left(\frac{\overline{u_i'^2}}{2}\right) = -\overline{u_i'u_j'}\,\frac{\partial \bar{u}_i}{\partial x_j} + \frac{\overline{u_i'T'}}{T_o}\,g\,\delta_{3i}$$

$$- \bar{u}_k \frac{\partial}{\partial x_k}\left(\frac{\overline{u_i'^2}}{2}\right) - \nu\,\overline{\left(\frac{\partial u_i'}{\partial x_j} + \frac{\partial u_j'}{\partial x_i}\right)\frac{\partial u_i'}{\partial x_j}} - \frac{1}{\rho_o}\,\overline{u_i'\frac{\partial P'}{\partial x_i}}$$

$$+ \frac{\partial}{\partial x_j}\left(-\left(\frac{\overline{u_i'^2}}{2}\right)u_j' + \nu\,\frac{\partial}{\partial x_j}\left(\frac{\overline{q^2}}{2}\right) + \nu\,\frac{\partial}{\partial x_i}\left(\overline{u_i'u_j'}\right)\right), \quad (4\text{-}33)$$

where no summation is taken in the equation over index i. These are the equations for the mean square of the longitudinal, the

normal and lateral component. A similar interpretation used in the turbulent energy equation can also apply to these equations. The second term from the last represents the diffusion of energy down the gradient by the viscous action. The last term represents the conduction of energy by the pressure gradient force (Mellor and Herring 1970). The terms inside the bracket only symbolize the transport of energy from one place to another and not the destruction or creation of energy.

4.7 Energy Equations

For the derivation of the equations of motion, we assumed that momentum was conserved. Subsequently, we derived the momentum equations for the mean motion and equations for the double velocity correlation. Similarly, the conservation of entropy results in the equation

$$\frac{\partial \bar{T}}{\partial t} + \bar{u}_k \frac{\partial \bar{T}}{\partial x_k} = \frac{\partial}{\partial x_k} \left(\kappa \frac{\partial \bar{T}}{\partial x_k} - \overline{u_k' T'} \right) . \qquad (4\text{-}34)$$

where κ is thermal conductivity. The last term represents heat transferred by eddy motion associated with temperature fluctuations. Other terms are analogous to the mean momentum equation.

An equation for the transport of heat by eddy motion, represented by the last term of (4-34), can be expressed as

$$\frac{\partial \overline{u_i' T'}}{\partial t} + \bar{u}_k \frac{\partial \overline{u_i' T'}}{\partial x_k} = - \overline{u_i' u_k'} \frac{\partial \bar{T}}{\partial x_k} - \overline{u_k' T'} \frac{\partial \bar{u}_i}{\partial x_k}$$

$$- \frac{\partial}{\partial x_k} \overline{(u_i' u_k' T')}$$

$$- \kappa \overline{u_i' \frac{\partial^2 T'}{\partial x_k \partial x_k}} - \overline{T' \frac{\partial^2 u_i'}{\partial x_k \partial x_k}}$$

$$- \frac{1}{\rho_o} \overline{T' \frac{\partial P'}{\partial x_i}} + g \frac{\overline{T'^2}}{T_o} \delta_{3i} \qquad (4\text{-}35)$$

An equation for the temperature variance, the last term in (4-35), can be written as

$$\frac{\partial}{\partial t} \left(\frac{\overline{T'^2}}{2}\right) + \bar{u}_k \frac{\partial}{\partial x_k} \left(\frac{\overline{T'^2}}{2}\right) = - \overline{u_k' T'} \frac{\partial \bar{T}}{\partial x_k} - \overline{u_k' \frac{\partial}{\partial x_k} \left(\frac{T'^2}{2}\right)} + \overline{\kappa T' \frac{\partial^2 T'}{\partial x_k \partial x_k}} \; . \qquad (4\text{-}36)$$

The closure of the system of equations (4-26), (4-27), (4-31), (4-33), (4-34), (4-35), and (4-36) can be achieved in principle, if some length scales are provided (Donaldson et al., 1968). Length scales relate the unknown quantities to the known quantities by invariant modeling, which is based on the conventional assumption that the flow of a physical quantity is transported down a gradient. A specific simple model describing atmospheric flow, devoid of convective terms, has been used to demonstrate this idea (Donaldson et al., 1968).

In order to use the double velocity equation (4-31) or turbulent energy equation (4-32) as a closure, one should relate production, triple velocity correlation, diffusion, and dissipation terms to the known quantities, as in the following section. The fundamental framework of this approach is proposed by Prandtl (1945) and Rotta (1951). Turbulent energy closure has not been developed enough to receive the general agreement acknowledged of the mixing length

closure. Turbulent energy closure, however, does provide some insight into the dynamic process of turbulent flow and makes future research promising and attractive.

Dissipation Term ε: - From experimental evidence and dimensional reasoning (Rotta, 1962), the dissipation term is related to the turbulent energy as

$$\varepsilon = C \frac{(\overline{q^2})^{3/2}}{\ell_o} \tag{4-37}$$

Let $\Lambda = \frac{\ell_o}{C}$ be another length scale, where ℓ_o is an appropriate length scale which depends on large eddies and is independent of viscosity except near the wall. The length scale ℓ_o is comparable with Prantl's mixing length. The dimensionless constant C depends on the structure of the large eddy motion. Equation (4-37) has long been recognized by most workers. It was found experimentally that dissipation is related to the three halves power of the turbulent energy in wake, jet and in homogeneous turbulence for large Reynolds number flows. Since this length scale is determined by the large eddies, the viscous dissipation terms in (4-31) become

$$2\nu \overline{\frac{\partial u_i' \partial u_j'}{\partial x_k \partial x_k}} = \frac{2}{3} \varepsilon \delta_{ij} \quad . \tag{4-38}$$

Pressure - Velocity Correlation - The important hypothesis for pressure-velocity terms was derived by Rotta (1951). In one of his works he discusses the physical basis for the term $\overline{P' \partial u_i'}/\rho_o \partial x_j$. He maintains that under contraction these terms must vanish. Since the terms are zero in the total turbulent energy equation, they represent

a net energy flow between component energies. Rotta also postulates that the pressure-velocity correlation is related to the shear stress, thus,

$$\overline{\frac{p'}{\rho_o}\frac{\partial u_i'}{\partial x_j}} = -\frac{1}{6}\frac{\sqrt{\overline{q^2}}}{\ell_1}\left(\overline{u_i'u_j'} - \frac{\delta_{ij}}{3}\overline{q^2}\right) . \tag{4-39}$$

Mellor and Herring (1970) also make a traditional assumption that the flow of pressure fluctuations is down a gradient, i.e.,

$$\overline{p'u_i'} = \frac{\sqrt{\overline{q^2}}\,\ell_2}{3}\frac{\partial \overline{q^2}}{\partial x_i} , \tag{4-40}$$

where the scales ℓ_1 and ℓ_2 are to be determined.

Triple Velocity Correlation - The flux of a physical quantity down the gradient will be assumed in obtaining expressions for the triple velocity terms,

$$\overline{u_i'u_j'u_k'} = \sqrt{\overline{q^2}}\,\ell_3\left(\frac{\overline{\partial u_i'u_k'}}{\partial x_i} + \frac{\overline{\partial u_i'u_k'}}{\partial x_j} + \frac{\overline{\partial u_i'u_j'}}{\partial x_k}\right) , \tag{4-41}$$

which is analogous to viscous diffusion.

Viscous Diffusion Terms - Viscous diffusion terms are simple to deal with and are transferable into flux form.

$$\overline{\left(u_j' \nu \frac{\partial u_i'}{\partial x_k}\right)} + \overline{\left(u_j' \nu \frac{\partial u_j'}{\partial x_k}\right)}$$

$$= \nu \frac{\overline{\partial u_i'u_j'}}{\partial x_k} \tag{4-42}$$

The molecular diffusion term can be neglected as compared with the eddy diffusion term except in the immediate vicinity of the boundary.

If we substitute equations (4-37), (4-38), (4-39), (4-40), (4-41), (4-42) into (4-31) the equation for the double velocity correlation is derived:

$$\frac{\overline{Du_i'u_j'}}{Dt} = \frac{\partial}{\partial x_k}\left[(\nu + \sqrt{\overline{q^2}}\ell_3)\left(\frac{\overline{\partial u_j'u_k'}}{\partial x_i} + \frac{\overline{\partial u_i'u_k'}}{\partial x_j} + \frac{\sqrt{\overline{q^2}}\ell_2}{2}\cdot\right.\right.$$

$$\left.\left.(\delta_{ki}\frac{\overline{\partial q^2}}{\partial x_i} + \delta_{ki}\frac{\overline{\partial q^2}}{\partial x_j})\right]\right.$$

$$- \overline{u_k'u_i'}\frac{\partial \bar{u}_j}{\partial x_k} - \overline{u_k'u_j'}\frac{\partial \bar{u}_i}{\partial x_k} - \frac{1}{3}\sqrt{\frac{\overline{q^2}}{\ell_1}}\left(\overline{u_i'u_j'} - \frac{\delta_{ij}}{3}\overline{q^2}\right) - \frac{2}{3}\left(\frac{\overline{q^2}}{\Lambda}\right)^{\frac{3}{2}}\delta_{ij}$$

$$+ \frac{\overline{u_j'T'}}{T_o} g\,\delta_{3j} + \frac{\overline{u_i'T'}}{T_o} g\,\delta_{3i} \cdot \qquad (4\text{-}43)$$

Equation (4-43) contains four equations. By contraction (4-43) we obtain the turbulent energy equation,

$$\frac{D}{Dt}\left(\frac{\overline{q^2}}{2}\right) = \frac{\partial}{\partial x_k}\left[(\nu + \sqrt{\overline{q^2}}\ell_3)\left(\frac{\partial}{\partial x_k}\left(\frac{\overline{q^2}}{2}\right) + \frac{\overline{\partial u_i'u_k'}}{\partial x_i}\right) + \sqrt{\overline{q^2}}\,\ell_2\frac{\partial}{\partial x_k}\left(\frac{\overline{q^2}}{2}\right)\right]$$

$$- \overline{u_k'u_i'}\frac{\partial \bar{u}_i}{\partial x_k} - \left(\frac{\overline{q^2}}{\Lambda}\right)^{3/2} - \frac{\overline{u_i'T'}}{T_o} g\,\delta_{3i} \cdot \qquad (4\text{-}44)$$

An equation similar to (4-44) has been obtained by Mellor and Herring (1970) under neutral conditions. Equations (4-43) or (4-44) combined with (4-26), (4-27), (4-33), (4-34), (4-35), and (4-36) form a closure, provided that the length scales are specified.

Chapter V

NUMERICAL MODELS

In the following sections, the two-dimensional boundary layer flow is considered. A numerical procedure is developed which may be extended in a straight forward manner to the three-dimensional case. The flow in the atmospheric surface layer which encounters an abrupt change in surface roughness under various stability conditions will be investigated. Flow under neutral condition has been investigated by Nickerson (1968) and Taylor (1969), and the pressure effects and the effects of the roughness discontinuity on the upstream velocity profile have been considered by Onishi and Estoque (1968). Flow under stable and unstable stratifications has also been investigated by Taylor (1970; 1971); for those investigations he used the Runga-Kutta method to solve a system of nonlinear parabolic equations. Taylor, however, did not consider the buoyancy and pressure effects because the Runga-Kutta method is only capable of solving parabolic equations and is not applicable to elliptic equations. Also, the pressure term can only be obtained by solving Poisson's equation; so for our purposes the marching technique of the Runga-Kutta method cannot be applied in this study.

In the model developed for this study, we include the buoyancy and pressure terms and can therefore include the buoyancy and pressure effects on the upstream flow which effects were neglected by Taylor (1970, 1971). We use the "modified" Newton's method to integrate the system of equations by an iterative technique. The pressure and buoyancy terms in the momentum equations, neglected by Peterson (1969),

together with a closure scheme that makes use of the turbulent kinetic energy equation will also be considered. Finally, a theory is developed to avoid some inappropriate assumptions of the previous models.

5.1 Mixing Length Model

The mixing length model is particularly simple and widely used in atmospheric science and engineering. The model has predominated for the past decades in the study of atmospheric flow, although it is independent of past history of turbulent motion. The two-dimensional equations of motion, the continuity equation, and the energy equation for the mean flow and the mixing length hypothesis constitute a closed set of equations, which can be written respectively as

$$\bar{u}\frac{\partial \bar{u}}{\partial x} + \bar{w}\frac{\partial \bar{u}}{\partial z} = -\frac{1}{\rho_o}\frac{\partial \tilde{P}}{\partial x} + \frac{\partial}{\partial z}\left(-\overline{w'u'}\right) \tag{5-1}$$

$$\bar{u}\frac{\partial \bar{w}}{\partial x} + \bar{w}\frac{\partial \bar{w}}{\partial z} = -\frac{1}{\rho_o}\frac{\partial \tilde{P}}{\partial z} + \frac{\tilde{\Theta}}{\Theta_o}\,g + \frac{\partial}{\partial z}\left(-\overline{w'^2}\right) \tag{5-2}$$

$$\frac{\partial \bar{u}}{\partial x} + \frac{\partial \bar{w}}{\partial z} = 0 \tag{5-3}$$

$$\bar{u}\frac{\partial \bar{\Theta}}{\partial x} + \bar{w}\frac{\partial \bar{\Theta}}{\partial z} = \frac{\partial}{\partial z}\left(-\overline{\Theta'w'}\right) . \tag{5-4}$$

To close this incomplete set of equations, the double correlations are related to the mean flow fields; we define

$$-\overline{u'w'} = K_m\frac{\partial \bar{u}}{\partial z} \tag{5-5}$$

$$-\overline{w'w'} = K_m\frac{\partial \bar{w}}{\partial z} \tag{5-6}$$

$$-\overline{\Theta'w'} = K_h\frac{\partial \bar{\Theta}}{\partial z} , \tag{5-7}$$

where K_m and K_h are coefficients of turbulent diffusion for momentum and heat, respectively. Mean potential temperature is $\bar{\Theta}$, K_m represents eddy diffusivity and K_h represents eddy conductivity. Equations (5-1), (5-2), (5-3), and (5-4) with (5-5), (5-6), (5-7) consist of four equations with four unknowns. Thus, the system is closed by using mean flow fields.

The eddy diffusivity for various stability conditions is defined by

$$K_m = k^2 z^2 \Phi \frac{\partial \bar{u}}{\partial z} \quad , \tag{5-7}$$

where Φ depends on stability, and is equal to unity for neutral conditions. For unstable air, the KEPY equation for Φ and for stable air, the McVehil's equation for Φ will be used:

$$\begin{aligned} \Phi &= (1-18Ri)^{\frac{1}{2}} \quad >1 \quad \text{for unstable} \quad Ri < 0 \\ &= 1 \qquad\qquad\qquad\qquad\quad Ri = 0 \\ &= (1-7Ri)^2 \quad <1 \qquad\quad 0 < Ri < 0.14 \quad . \end{aligned} \tag{5-8}$$

Pandolfo (1966) has suggested that the turbulent Prandtl number depends on the stability and is related to the nondimensional wind shear, ϕ, for an unstable case as

$$\frac{K_m}{K_h} = \phi \quad , \tag{5-9}$$

where the nondimensional wind shear is defined as

$$\phi = \frac{kz}{\tau^{\frac{1}{2}}} \frac{\partial \bar{u}}{\partial z} \quad , \tag{5-10}$$

and is a function of the Richardson number.

If we cross differentiate (5-1) and (5-2) with x and z, and add the resultant equations, the result is,

$$\left(\bar{u} \frac{\partial}{\partial x} + \bar{w} \frac{\partial}{\partial z}\right)\left(\frac{\partial \bar{u}}{\partial x} + \frac{\partial \bar{w}}{\partial z}\right) + \left\{\left(\frac{\partial \bar{u}}{\partial x}\right)^2 + 2 \frac{\partial \bar{w}}{\partial x} \frac{\partial \bar{u}}{\partial z} + \left(\frac{\partial \bar{w}}{\partial z}\right)^2\right\}$$

$$= - \left(\frac{\partial^2}{\partial x^2} + \frac{\partial^2}{\partial z^2}\right) \frac{\bar{\tilde{p}}}{\rho_o} + \frac{\partial}{\partial z} \left\{\frac{\partial}{\partial z}\left(K_m \frac{\partial \bar{u}}{\partial z}\right) + \frac{\partial}{\partial z}\left(K_m \frac{\partial \bar{w}}{\partial z}\right)\right\}$$

$$+ \frac{g}{\Theta_o} \frac{\partial \bar{\tilde{\theta}}}{\partial z} \quad . \tag{5-11}$$

Using the equation of continuity (5-3), equation (5-11) can be reduced to

$$\frac{\partial^2}{\partial x^2}\left(\frac{\bar{\tilde{p}}}{\rho_o}\right) + \frac{\partial^2}{\partial z^2}\left(\frac{\bar{\tilde{p}}}{\rho_o}\right) = \frac{\partial}{\partial z} \left\{\frac{\partial K_m}{\partial x} \frac{\partial \bar{u}}{\partial z} + \frac{\partial K_m}{\partial z} \frac{\partial \bar{w}}{\partial z}\right\}$$

$$- 2 \left\{\frac{\partial \bar{w}}{\partial x} \frac{\partial \bar{u}}{\partial z} + \left(\frac{\partial \bar{u}}{\partial z}\right)^2\right\}$$

$$+ \frac{g}{\Theta_o} \frac{\partial \bar{\tilde{\theta}}}{\partial z} \quad . \tag{5-12}$$

We will consider the boundary conditions (Figure 5-1) in the following section.

(i) Lower boundary conditions at $z = z_i$ - The parameter z_i is a local roughness parameter. Non-slip conditions at the surface $z = z_i$ will be assumed. The lower boundary conditions, therefore, can be specified as

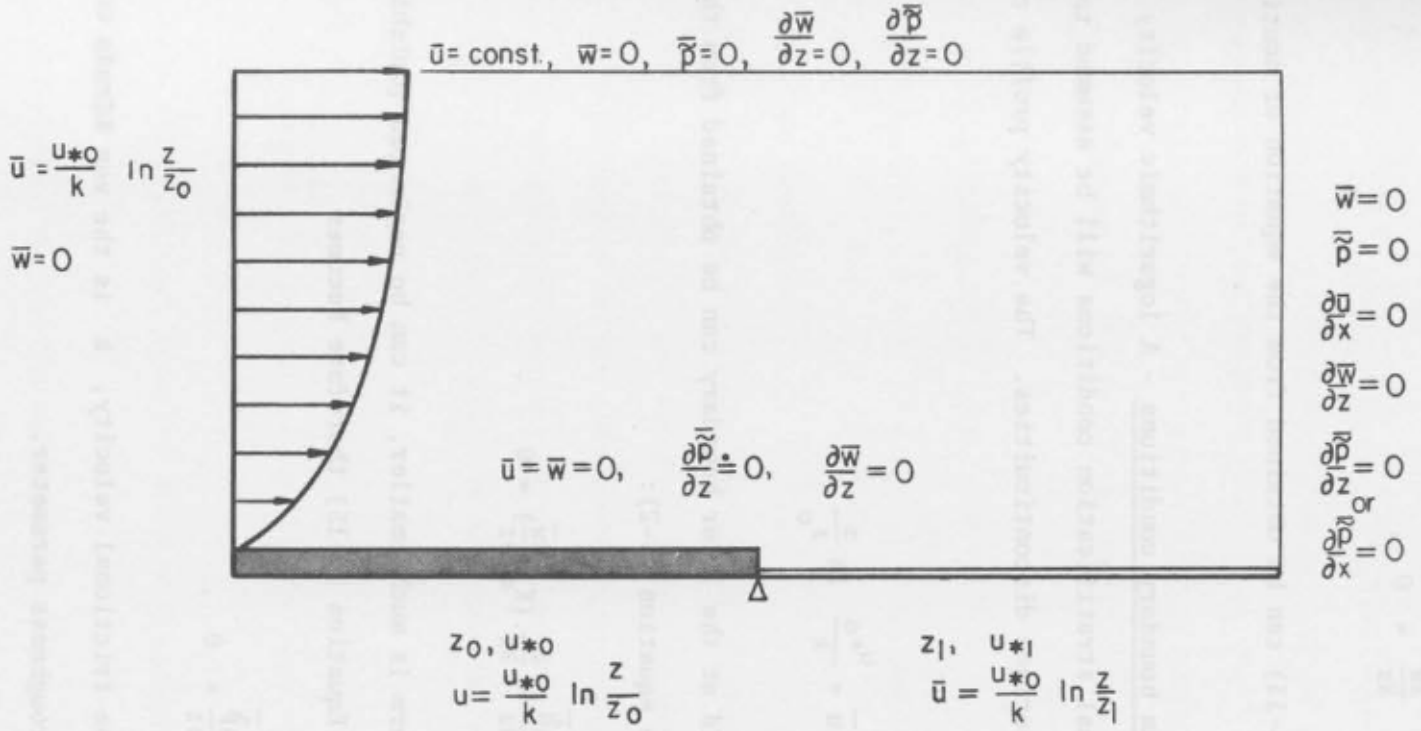

Figure 5-1 Schematic diagram of boundary conditions

$$\bar{u} = \bar{w} = 0$$

$$\frac{\partial \bar{w}}{\partial z} = 0 \quad , \tag{5-13}$$

where equation (5-13) can be obtained from the equation of continuity (5-3).

(ii) Upstream boundary conditions - A logarithmic velocity profile for neutral thermal stratification conditions will be assumed to exist upstream of any surface discontinuities. The velocity profile can be expressed as

$$\bar{u} = \frac{u_{*o}}{k} \ln \frac{z}{z_o} \quad . \tag{5-14}$$

The pressure field at the lower boundary can be obtained from the vertical momentum equation (5-2):

$$-\frac{1}{\rho_o} \frac{\partial \bar{P}}{\partial z} + \frac{\partial}{\partial z} \left(K_m \frac{\partial \bar{w}}{\partial z}\right) = 0 \quad . \tag{5-15}$$

Since the last term is much smaller, it can be neglected (Onishi and Estoque, 1968). Equation (5-15) therefore becomes

$$-\frac{1}{\rho_o} \frac{\partial \bar{P}}{\partial z} = 0 \quad ,$$

where u_{*o} is the frictional velocity, k is the von Kármán constant and z_o is the roughness parameter.

(iii) Downstream boundary conditions - For neutral conditions we assume that the hydrostatic condition holds and there is no pressure

perturbation. The horizontal velocity gradient and vertical velocity gradient are zero:

$$\overline{w} = 0, \quad \overline{\mathcal{P}} = 0, \quad \frac{\partial \overline{u}}{\partial x} = 0, \quad \frac{\partial \overline{w}}{\partial z} = 0, \quad \frac{\partial \overline{\mathcal{P}}}{\partial z} = 0 \quad .$$

For diabatic conditions, we assume

$$\frac{\partial \overline{\mathcal{P}}}{\partial x} = 0 \text{ , instead of } \overline{\mathcal{P}} = 0 \text{ at the downstream boundary.}$$

(iv) Upper boundary conditions - For simplicity, we assume

$$\overline{u} = \text{constant}, \quad \overline{w} = 0, \quad \overline{\mathcal{P}} = 0, \quad \frac{\partial \overline{w}}{\partial z} = 0, \quad \text{and} \quad \frac{\partial \overline{\mathcal{P}}}{\partial z} = 0$$

for all stability conditions.

The roughness of the underlying surface of airflow will be characterized by introducing the local roughness parameter, z_i, to describe the wind profile in the atmospheric boundary layer. The horizontal mean velocity and vertical mean velocity are all zero at $z = z_i$; thus, the wind profile close to the boundary can be described as

$$\overline{u} = \frac{u_*(x,z)}{k} \ln \frac{z}{z_i}$$

where u_* is the frictional velocity which will generally vary with position.

We will consider the airflow moving from a rough surface to a smooth surface or vice versa or the air encountering a step change in surface temperature. The upstream and downstream roughness and

frictional velocity will be denoted by roughness parameters z_o, u_{*o} and z_1, u_{*1}, respectively. If we assume that the airflow encounters a step change in the surface roughness, a surface of discontinuity at the junction of two different roughnesses will exist. Physically, this cannot occur in nature. The surface roughness must change in a continuous fashion, even though it may change very rapidly. Since we do not have adequate experimental data to illustrate the degree of roughness change near the surface of discontinuity, the degree of change is not known. Here, however, we will assume that near the surface of discontinuity the roughness varies approximately linear with distance.

For convenience, the variables in equations (5-1), (5-2), (5-3), and (5-4) are nondimensionalized with respect to u_{*o}, Θ_o and z_1 as follows:

$$\overline{u}^* = \frac{k\overline{u}}{u_{*o}}$$

$$\overline{w}^* = \frac{k\overline{w}}{u_{*o}}$$

$$\overline{\Theta}^* = \frac{\overline{\Theta}}{\Theta_o} \qquad (5\text{-}16)$$

$$\Theta' = \frac{\overline{\gamma_\Theta}}{\Theta_o}$$

$$p^* = \frac{k^2}{u_{*o}^2}\,\frac{p}{\rho_o}$$

$$g^* = \frac{k^2 z_1}{u_{*o}^2}\,g$$

$$g = 980 \text{ cm/sec}^2$$

$$\eta = \frac{x}{z_1}$$

$$\zeta = \ln \frac{z}{z_1} \quad .$$

These equations then take the form, after dropping the star over each symbol,

$$\bar{u} \frac{\partial \bar{u}}{\partial \eta} + \bar{w} e^{-\zeta} \frac{\partial \bar{u}}{\partial \zeta} = - \frac{\partial P}{\partial \eta} + k^2 e^{-\zeta} \frac{\partial}{\partial \zeta} (K_m \frac{\partial \bar{u}}{\partial \zeta}) \qquad (5\text{-}17)$$

$$\bar{u} \frac{\partial \bar{w}}{\partial \eta} + \bar{w} e^{-\zeta} \frac{\partial \bar{w}}{\partial \zeta} = - e^{-\zeta} \frac{\partial P}{\partial \zeta} + \Theta' g + k^2 e^{-\zeta} \frac{\partial}{\partial \zeta} (K_m \frac{\partial \bar{w}}{\partial \zeta}) \qquad (5\text{-}18)$$

$$\frac{\partial \bar{u}}{\partial \eta} + e^{-\zeta} \frac{\partial \bar{w}}{\partial \zeta} = 0$$

$$\frac{\partial^2}{\partial \zeta} \frac{\bar{u}}{\partial \eta} + e^{-\zeta} [\frac{\partial^2 \bar{w}}{\partial \zeta^2} - \frac{\partial \bar{w}}{\partial \zeta}] = 0 \qquad (5\text{-}19)$$

$$\bar{u} \frac{\partial \bar{\Theta}}{\partial \zeta} + \bar{w} e^{-\zeta} \frac{\partial \bar{\Theta}}{\partial \zeta} = k^2 e^{-\zeta} \frac{\partial}{\partial \zeta} (K_h \frac{\partial \bar{\Theta}}{\partial \zeta}) \quad , \qquad (5\text{-}20)$$

A variable grid length system consisting of 28 points in the horizontal and 29 points in the vertical has been used for the numerical integration of the governing equations. The logarithmic and hyperbolic sine functions are used to specify the grid spacing in the vertical and horizontal directions, respectively; the range of the nondimensional distance in the horizontal direction is of the order of $-10^5 \leq x \leq 10^6$ and in the vertical direction of the order of $z \leq 10^6$. This grid system

therefore provides for maximum resolution at the surface ($z = z_o$) and in the immediate vicinity of the roughness discontinuity ($x = 0$), while still providing a sufficiently large total area.

To investigate the velocity and temperature profiles in the surface boundary layer, plausible assumptions about the eddy viscosity and eddy conductivity coefficients must be introduced. The mixing length assumptions are the simplest of many choices. For all atmospheric conditions, the form of the eddy viscosity and eddy conductivity coefficients can be assumed as follows:

$$K_m = \Phi \frac{\partial \overline{u}}{\partial \zeta}$$

$$K_h = \phi K_m,$$

where Φ and ϕ are universal functions, uniquely determined by the stability.

The upstream boundary conditions are

$$\overline{w} = 0$$

$$\overline{u} = \zeta + m,$$

where

$$m = - \ln \frac{z_o}{z_1} .$$

The nondimensionalized Poisson's equation for pressure can be written as

$$\frac{\partial^2 P}{\partial \eta^2} + b^2 \left\{ \frac{\partial^2 P}{\partial \zeta^2} - \frac{\partial P}{\partial \zeta} \right\} \tag{5-21}$$

$$= k^2 b \frac{\partial}{\partial \zeta} \left\{ b \frac{\partial K_m^*}{\partial \eta} \frac{\partial \bar{u}}{\partial \zeta} \right\} + k^2 b^3 \frac{\partial K_m^*}{\partial \zeta} \left\{ \frac{\partial^2 \bar{w}}{\partial \zeta^2} - \frac{\partial \bar{w}}{\partial \zeta} \right\}$$

$$+ k^2 b^3 \frac{\partial \bar{w}}{\partial \zeta} \left\{ \frac{\partial^2 K_m^*}{\partial \zeta^2} - \frac{\partial K_m^*}{\partial \zeta} \right\} - 2 \left\{ b \left(\frac{\partial \bar{u}}{\partial \zeta}\right)\left(\frac{\partial \bar{w}}{\partial \eta}\right) + \left(\frac{\partial \bar{u}}{\partial \eta}\right)^2 \right\}$$

$$+ g\, b \frac{\partial \bar{\Theta}}{\partial \zeta} ,$$

where

$$K_m = \Phi \left| \frac{\partial \bar{u}}{\partial \zeta} \right| , \quad K_m^* = b^{-1} K_m ,$$

$$b = e^{-\zeta} .$$

5.2 Turbulent Energy Model

Bradshaw et al. (1967) have postulated that the shear stress is closely related to turbulent kinetic energy. The transport of the turbulent energy is governed by the turbulent energy equation (the turbulent energy has its past history as well as local properties). Dryden (1946) maintained that the shear stress cannot be uniquely determined by the gradient of mean velocity at a fixed point in space alone. In view of the close relation between the shear stress and the turbulent kinetic energy, Bradshaw et al. (1967) have proposed an alternate approach, correlating shear stress with other parameters that describe the turbulent structure. The assumptions were made, Bradshaw et al. (1967), that the turbulent kinetic energy and the dissipation and diffusion of the turbulent kinetic energy are related to the shear stress profile. The same idea has been applied to the atmospheric

boundary layer (Peterson, 1969). We, however, will retain the pressure effects in momentum equations in our model.

We will consider the turbulent kinetic energy closure with particular emphasis on motions in the atmospheric boundary layer. The turbulent energy equation (4-32) for the two-dimensional, steady, compressible mean flow, outside the viscous sublayer is

$$\bar{u}\frac{\partial}{\partial x}\left(\frac{\overline{q^2}}{2}\right) + \bar{w}\frac{\partial}{\partial z}\left(\frac{\overline{q^2}}{2}\right) = -\overline{u'w'}\frac{\partial \bar{u}}{\partial z} - \frac{\partial}{\partial z}\left(\overline{p'w'} + \overline{w'\frac{q^2}{2}}\right) - \varepsilon$$

$$- \frac{\overline{\theta'w'}}{\theta_o} g\,\delta_{3i} \quad , \tag{5-22}$$

where ε is a dissipation term and is defined as

$$\varepsilon = \nu\,\overline{\left(\frac{\partial u_i'}{\partial x_j}\right)^2} \quad . \tag{5-23}$$

Equation (5-22), together with equations (5-17), (5-18), and (5-19), does not form a closed set. Additional assumptions are thus required so that the equations can be written in terms of the dependent variables $\bar{u}$, $\bar{w}$, τ, and $\bar{\tilde{p}}$ for neutral conditions. A proportionality between shear stress and turbulent kinetic energy has been proposed by Bradshaw et al. (1967), with the constant of proportionality being equal to 0.3. On the other hand, Peterson selected a value of 0.16. Although Peterson (1969) suggested that the empirical function relating shear stress to turbulent energy is a universal constant, his suggestion is based on the two empirical constants, 0.16 (Peterson, 1969) and 0.15 (Bradshaw et al., 1967). Careful examination, reveals a mistake made by Peterson; the empirical constants differ by about a factor of two.

Following Townsend (1956), both Peterson (1969) and Bradshaw et al., (1967) assumed that the shear stress is proportional to the turbulent energy, as

$$\tau = \left(\frac{a_1}{2}\right) \overline{q^2} = a_1 \left(\frac{\overline{q^2}}{2}\right) , \tag{5-24}$$

where

$$a_1 = \begin{cases} 0.34 \text{ (Rose, 1966)} \\ 0.3 \text{ (Bradshaw et al., 1967)} \\ 0.16 \text{ (Peterson, 1970)} \\ 0.25 \text{ (Hinze, 1968)} \\ 0.25 \text{ (Present)} . \end{cases}$$

From equations (4-37), and (5-23), the dissipation term can be correlated with the shear stress by

$$\varepsilon = \frac{\left(\overline{q^2}\right)^{3/2}}{\Lambda} = \frac{\tau^{3/2}}{\mathcal{L}} \tag{5-25}$$

where $\mathcal{L} = \left(\frac{a_1}{2}\right)^{3/2} \Lambda$. This relation is assumed by Bradshaw et al., (1967), where $\mathcal{L}$ is a dimensional length scale. This length scale is most important, because in the turbulent boundary layer the magnitude of dissipation is usually much larger than advection or diffusion. For equilibrium flow conditions, the dissipation is equal to $\frac{\tau^{3/2}}{kz}$. If the flow is not in equilibrium, Monin (1959) suggests that this relation is still valid. Therefore, the length scale $\mathcal{L}$ is equal to the mixing length. Peterson (1969) as well as Mellor and Herring (1968) further assumed that the transport of turbulent kinetic energy by the action of turbulent motion is proportional to the gradient of mean turbulent kinetic energy and that the mechanism for the transport

of the turbulent kinetic energy is the same as the transport of momentum. The function of the diffusion term is to smooth out the shear stress profile without changing its basic shape. The diffusion term in the turbulent energy equation can be expressed as

$$\overline{P'w'} + \overline{w' \left(\frac{q^2}{2}\right)} = - K_m \frac{\partial}{\partial z} \left(\frac{\overline{q^2}}{2}\right) \quad , \tag{5-26}$$

where

$$K_m = \frac{\tau}{\frac{\partial \bar{u}}{\partial z}} \quad . \tag{5-27}$$

By substituting (5-24), (5-25), (5-26) and (5-27) into (5-22) for neutral atmospheric stability, equation (5-22) becomes

$$\bar{u} \frac{\partial}{\partial x} \left(\frac{\tau}{a_1}\right) + \bar{w} \frac{\partial}{\partial z} \left(\frac{\tau}{a_1}\right) = \tau \frac{\partial \bar{u}}{\partial z} + \frac{\partial}{\partial z} \left(K_m \frac{\partial}{\partial z} \left(\frac{\tau}{a_1}\right)\right) - \frac{\tau^{3/2}}{kz} \tag{5-28}$$

If the shear stress in (5-27) is substituted into (5-28), we obtain the generalized mixing length equation, with additional terms representing advection and diffusion. Equation (5-28) with horizontal and vertical momentum equations and the equation of continuity form a closed set of four equations with four unknowns, $\bar{u}$, $\bar{w}$, $\bar{\tilde{P}}$, and τ. The boundary conditions are the same as for the mixing length model.

We will nondimensionalize equation (5-28). The characteristic velocity and length scale for nondimensionalizing the velocity and distance were defined in equation (5-16). Nondimensional shear stress will be defined here as

$$\tau^* = \frac{\tau}{\tau_o} \quad , \tag{5-29}$$

where τ_o is the upstream shear stress. With this definition, the generalized mixing length equation (5-28) can be rewritten as

$$\bar{u} \frac{\partial}{\partial \eta} \left(\frac{\tau}{a_1}\right) + \bar{w} e^{-\zeta} \frac{\partial}{\partial \zeta} \left(\frac{\tau}{a_1}\right) = \tau e^{-\zeta} \frac{\partial \bar{u}}{\partial \zeta} + e^{-\zeta} \frac{\partial}{\partial \zeta} \left[K_m \frac{\partial \tau}{\partial \zeta}\right]$$

$$- \tau^{3/2} e^{-\zeta} \quad . \tag{5-30}$$

In this equation it is understood that every dependent and independent variable is nondimensional. All empirical functions previously discussed in this section can in principle be measured. Although highly accurate measurements cannot be obtained, a first approximation can be provided Refinement can be achieved by comparing the numerical calculated results of the turbulent boundary development with experimental results.

Along the same line as Bradshaw's model, a phenomenological model is proposed by Nee and Kovasznay (1969), who artificially create a dynamic equation for the eddy viscosity analogous to Bradshaw's shear stress equation. Both models can be considered as a transformation from the turbulent energy equation to the shear stress equation or the eddy viscosity equation; however, the physical grounds behind these models are rather unclear.

Let us assume that

$$\overline{q^2} = A_1 K_m \left|\frac{\partial \bar{u}}{\partial z}\right| \quad , \quad \text{and}$$

$$\frac{\varepsilon}{(\frac{\partial \bar{u}}{\partial z})} = f(K_m, \ell) = B_1 \frac{K_m^2}{\ell^2} \quad ,$$

where A_1 and B_1 are universal constants, and $(\partial\bar{u}/\partial z)$ is also a constant. In addition, $\varepsilon/(\partial\bar{u}/\partial z)$ is assumed a universal function depending on K_m and a length scale ℓ. If we further assume that the diffusion of turbulent energy is the same as the transport of momentum, and substitute the above two equations into the turbulent energy equation, we obtain

$$\bar{u} \frac{\partial K_m}{\partial x} + \bar{w} \frac{\partial K_m}{\partial z} = A_1 K_m \frac{\partial \bar{u}}{\partial z} + \frac{\partial}{\partial z} (K_m \frac{\partial K_m}{\partial z}) - B_1 \frac{K_m^2}{\ell^2} \quad .$$

This equation is proposed by Nee and Kovasznay (1969) and formed a closure together with horizontal momentum equation and equation of continuity for the study of quasi-parallel turbulent shear flows.

5.3 A Theory

It is extremely difficult at this stage to consider the complete set of equations developed in the previous chapter. An alternative approach is to consider equations (4-43) and (4-44) for the boundary layer approximation. The usual boundary layer approximation to equations (4-43) and (4-44) for mean turbulent kinetic energy per unit mass and for shear stress, respectively, are:

$$\bar{u} \frac{\partial}{\partial x} (\frac{\overline{q^2}}{2}) + \bar{w} \frac{\partial}{\partial z} (\frac{\overline{q^2}}{2}) = - \overline{u'w'} \frac{\partial \bar{u}}{\partial z}$$

$$+ \frac{\partial}{\partial z} [(\tilde{q}\ell_2 + \frac{5}{3}\nu + \frac{5}{3}\tilde{q}\ell_3) \frac{\partial}{\partial z} (\frac{\overline{q^2}}{2})$$

$$- \frac{\overline{(q^2)}^{3/2}}{\Lambda} - \frac{\overline{u'_i \theta'}}{\theta_o} g \delta_{3i} \qquad (5\text{-}31)$$

$$- \overline{u'w'} = \tilde{q} \ell_1 \frac{\partial \bar{u}}{\partial z} , \qquad (5\text{-}32)$$

where $\tilde{q} = \sqrt{\overline{q^2}}$. The last equation (5-32) also can be obtained directly by dimensional argument. From the mixing length theory, we know that the Reynolds shear stress is a function of the scale length and velocity gradient in the vertical direction; from the turbulent energy theory, we also know that it is positively correlated with turbulent kinetic energy. Therefore, the relevant parameters for the Reynolds shear stress inferred from the mixing length theory and the turbulent energy theory are one length scale, shear velocity gradient and turbulent kinetic energy. The Reynolds shear stress can be expressed in the functional form as

$$-\overline{u'w'} = f \left(\ell_1', \frac{\partial \bar{u}}{\partial z}, \tilde{q}\right) . \qquad (5\text{-}33)$$

From dimensional analysis of equation (5-33), we obtain

$$-\overline{u'w'} = \tilde{q} \ell_1 \frac{\partial \bar{u}}{\partial z} ,$$

which is the same form as (5-32), where a nondimensional constant associated with f has been absorbed into ℓ_1. This form of Reynolds shear stress has also been formulated theoretically by Mellor and Herring (1970) from another point of view for the study of turbulent boundary layer development in the wind tunnel under neutral conditions.

Equations (5-31) and (5-32) with the two momentum equations and the equation of continuity and the thermal energy equation form a closed set of boundary layer equations, provided that the length scales are specified. These equations are very attractive from a computational point of view; they provide a sound mathematical background.

The mathematical model developed by Bradshaw et al. (1967) used experimental evidence and hypothesized that the mean turbulent kinetic energy is proportional to the shear stress profile. The shear stress then can be predicted by the turbulent energy equation. However, the turbulent energy equation is independent of the shear stress transport equation, since the contraction of the double velocity correlation equation will result in the turbulent energy equation. The assumptions by Bradshaw et al. (1967), therefore, are made relative to inappropriate terms in the wrong equation.

For nearly isotropic turbulence, Mellor and Herring (1970) argued that some assumptions should be made about the diffusion and dissipation terms. The Reynolds shear stress equation should result in a form similar to conventional Newtonian or Boussinesq relationships. If we define a nondimensional tensor a_{ij} that departs from isotropy as

$$\overline{u_i' u_j'} = (\delta_{ij} + a_{ij}) \frac{\overline{q^2}}{3} \tag{5-34}$$

where $a_{ij} = 0$, and if we substitute (5-34) into (4-31), we obtain an approximate equation,

$$-\overline{u_i' u_j'} + \frac{\delta_{ij}}{3} \overline{q^2} = \tilde{q} \ell_1 \left(\frac{\partial \bar{u}_j}{\partial x_i} + \frac{\partial \bar{u}_i}{\partial x_j}\right) . \tag{5-35}$$

For two-dimensional turbulent boundary layer flow, equation (5-35) becomes

$$-\overline{u'w'} = \tilde{q}\, \ell_1 \frac{\partial \bar{u}}{\partial z} \quad . \tag{5-36}$$

We now assume that the transport of heat and momentum are analogous. We can, therefore, postulate that

$$-\overline{\Theta'w'} = \tilde{q}\, \ell_5 \frac{\partial \bar{\Theta}}{\partial z} \quad , \tag{5-37}$$

where $\ell_5 = \ell_1 \phi$, and ϕ is a universal function depending only on stability, and equal to the nondimensional wind shear.

Substituting (5-36), and (5-37) into (5-31) we obtain

$$\bar{u} \frac{\partial}{\partial x} \left(\frac{\overline{q^2}}{2}\right) + \bar{w} \frac{\partial}{\partial z} \left(\frac{\overline{q^2}}{2}\right) = \tilde{q}\, \ell_1 \left(\frac{\partial \bar{u}}{\partial z}\right)^2$$

$$+ \frac{\partial}{\partial z} \left[\tilde{q}\, \ell_2 + \frac{5}{3}\nu + \frac{5}{3}\tilde{q}\, \ell_3\right] \frac{\partial}{\partial z} \left(\frac{\overline{q^2}}{2}\right)$$

$$- \frac{1}{\ell_\varepsilon} \left(\frac{\overline{q^2}}{2}\right)^{3/2} - \tilde{q}\, \ell_5 \frac{g}{\Theta_o} \frac{\partial \bar{\Theta}}{\partial z} \quad , \tag{5-38}$$

where $\ell_\varepsilon = \Lambda\, 2^{-3/2}$.

According to the experience gained by Bradshaw et al. (1967), well inside the turbulent boundary layer a gradient-diffusion form representing transport processes exists. Peterson (1969) also assumed the gradient form for the vertical flux of turbulent energy. Mellor and Herring (1970) carried out a numerical integration of the boundary

layer equations. In comparison with the experimental results, they found that

$$\ell_2 + \frac{5}{3}\ \ell_3 = (1 \pm 0.1)\ \ell_1 \quad . \tag{5-39}$$

Thus, in the atmospheric turbulent boundary layer, equation (5-38) can be approximated as

$$\bar{u}\frac{\partial}{\partial x}\left(\frac{\overline{q^2}}{2}\right) + \bar{w}\frac{\partial}{\partial z}\left(\frac{\overline{q^2}}{2}\right) = \tilde{q}\,\ell_1\left(\frac{\partial \bar{u}}{\partial z}\right)^2 + \frac{\partial}{\partial z}\left[\tilde{q}\,\ell_1\frac{\partial}{\partial z}\left(\frac{\overline{q^2}}{2}\right)\right] - \frac{1}{\ell_\varepsilon}\left(\frac{\overline{q^2}}{2}\right)^{3/2} - \tilde{q}\,\ell_5\frac{g}{\Theta_o}\frac{\partial \bar{\Theta}}{\partial z} \tag{5-40}$$

As a first approximation, we postulate the length scales ℓ_1, ℓ_5 and ℓ_ε to be universal functions. The length scale ℓ_ε in equation (5-40) is comparable to the mixing length. For the flow in the adiabatic condition and in equilibrium, and from equation (5-40), we know that the dissipation of turbulent energy is equal to the production of turbulent energy, and from the direct consequence of the logarithmic velocity profile, we obtain

$$\frac{\left(\frac{q^2}{2}\right)^{3/2}}{\ell_\varepsilon} = \frac{\tau^{3/2}}{kz} \tag{5-41}$$

From field observation, for air over a relatively homogeneous terrain, Cramer and Record (1969) show that the ratio of turbulent energy to the shear stress is a constant with an approximate value of

4.0 for averaging times of 1.2 minutes at heights of 40 and 16 meters. Experimental information by Hinze (1968) also confirms the results, which shows that the turbulent kinetic energy is, indeed, uniform in a constant stress layer. Such results suggest that the length scale is a universal function. Using this relation we arrive at

$$\ell_\varepsilon = 3.2\ z\ , \tag{5-42}$$

where $(\frac{\overline{q^2}}{2})/\tau = c = 4.0$.

In the constant shear stress layer, the distribution of the mean velocity profile follows the logarithmic law for an adiabatic condition. By the definition of shear stress and the universal relation between shear stress and turbulent kinetic energy in neutral equilibrium flow, the following expression for the length scale ℓ_1 is obtained:

$$\ell_1 = \frac{1}{\sqrt{2c}}\ kz\ . \tag{5-43}$$

Combining equation (5-32) with equation (5-40), neglecting the advection terms and diffusion term, we obtain

$$-\overline{u'w'} = k^2 z^2 \frac{\partial \bar{u}}{\partial z} \frac{\partial \bar{u}}{\partial z}\ .$$

This is essentially the mixing length hypotheses for shear stress. Thus, the k-theory model may be considered as an approximation to the presented theory.

Table 5 is a summary of various length scales used by different authors.

The constants associated with length scales ℓ_ε, ℓ_d, and ℓ_1 will be referred to as dissipation, diffusion and eddy viscosity

TABLE 5 THE VALUE OF LENGTH SCALES ℓ_ε, ℓ_d, AND ℓ_1 FOR VARIOUS AUTHORS

Authors	ℓ_ε	ℓ_d	ℓ_1
Weighardt (1945)	2.22z	0.107z	0.158z
Glusko (1965)	3.2z	0.095z	0.141z
Spalding (1967)	3.2z	0.083z	0.141z
Mellor and Herring (1970)	4.24z	0.16z	0.16z
Present	3.2z	0.141z	0.141z

constants, respectively. The constants suggested by Weighart (1945) are based on the data obtained from the decay of isotropic turbulence for his dissipation length. His diffusion constant is based on data from the turbulent energy distribution near the center line of ducts and the eddy viscosity constant on the velocity profile near the wall. Glushko (1965) obtained his eddy viscosity constant based on data summarized by Hinze (1968). The dissipation and diffusion constants were obtained by carrying out the numerical experiment to solve a set of two-dimensional turbulent boundary layer equations, including the turbulent energy equation, the momentum equation and the equation of continuity, for obtaining the best correlations with the experimental data of mean velocity and turbulent energy distribution. Mellor and Herring (1968) postulated the constants obtained by adjusting the results of the numerical experiment to the best fit with the mean velocity and turbulent energy profiles measured by Klebanoff (1955) under the condition of constant pressure. With the scale lengths ℓ_ε, ℓ_d, ℓ_1 and ℓ_5 specified, the set of equations containing two momentum equations, equations of continuity, thermal energy equations, turbulent energy equations and equation for Reynolds shear stress form a closed system. In principle, we can solve this set of equations for flow with density stratification; however, for the primary investigation we will consider the flow under neutral conditions only, since the length scales under neutral condition may or may not be applicable to the diabatic conditions.

Chapter VI

ITERATIVE METHODS OF NONLINEAR EQUATIONS

One of the most useful numerical techniques for solving a system of nonlinear equations is Newton's method. Many articles dealing with the modification and convergence of Newton's method have been published since the fundamental paper of Kantorovich (1949) appeared. Recently, several authors have considered iterative methods consisting of a combination of Jacobi, Gauss-Seidel and Newton's iterative methods for solving a system of nonlinear equations. Some iterative schemes (Greenspan, 1968; Onishi and Estoque, 1968; Apelt, 1969; and Estoque and Bhumalker, 1970) and many other similar to Newton's method have enjoyed considerable success without theoretical explanation. Our intention here is not to review iterative methods exhaustively, since many excellent books dealing with these subjects are already available (Ames, 1965, 1969; Forsythe and Wason, 1960; Fox, 1962). We will develop a numerical scheme based on a modification of Newton's method. Several theorems considering the convergence of iterative methods will be proved. A numerical test, which will be compared to the exact solution for arbitrary initial guess, is carried out.

Theorems and definition which are utilized for the proof of other theorems in the text are given in Appendix A.

6.1 Iterative Processes

For solving a system of nonlinear equations by iterative processes, we will consider the real twice continuously differentiable n nonlinear equations with n unknowns:

$$f_i\ (x_1,\ x_2,\ldots x_n) = 0 \quad i = 1,\ldots n \tag{6-1}$$

in vector notation or in vector representation as

$$f(x) = A(x)x - B = 0\ , \tag{6-2}$$

where the operator $A(x)$ is nonlinear, and B is a matrix with known entries. Based on the results of linear theory, a more general difference equation (Ortega and Rochoff, 1966) can be used to describe equations (6-1) and (6-2):

$$g(x^{n+1},\ x^n) = 0 \quad n = 0,\ 1,\ 2,\ldots, \tag{6-3}$$

where g is a nonlinear mapping from an open subset, D_g, of product space, $R^n \times R^n$ into R^n, and where R^n is a real n-dimensional space. The function g is nonlinear in both x^{n+1} and x^n. Here g_x and g_y are the partial Fréchet derivatives of g with respect to the first and second vector variables. The g_x^{-1} is the inverse of the Fréchet derivative defined on x. H is defined as $-g_x^{-1}\ g_y$ evaluated at a solution $(x^*,\ x^*)$. We denote a continuous Fréchet derivative of g with order p for $x \in S$ by $g \in c^p(S \times S)$, where $S \times S \subset D_g$.

In the discussion of the asymptotic rate of convergence of the Grauss-Seidel type iterative processes and its application (Ortega and Rochoff, 1966), the magnitude of the spectral radius is not known a priori. The solution, x^*, however, is required to be known before numerical evaluation of the spectral radius.

The purpose of this section is to remove the a priori assumption about the spectral radius. By using matrix properties, it can be shown that the spectral radius of the magnification matrix is less than unity, if some restrictions are imposed on the Fréchet derivative of f. Many of the partial differential equations arising in fluid mechanics, meteorology and physics satisfy those restrictions on f'. We will, however, consider the following types of nonlinear difference equations (Ortega and Rockoff, 1966),

I. The Jacobi-Newton Method,

$$g_{I,i}(x^{n+1}, x^n) = \frac{\partial f_i}{\partial x_i}(x^n)\,[x^{n+1} - x^n] + f_i(x^n) = 0$$

$$i = 1,\ldots N$$

$$n = 0, 1,\ldots \quad .$$

II. The "modified" Newton's Method,

$$g_{II,\omega,i,}(x^{n+1}\ x^n) = \frac{\partial f_i}{\partial x_i}(x^{n,i})\,[x_i^{n+1} - x_i^n] + \omega f_i\,(x^{n,i}) = 0$$

$$i = 1,\ldots N$$

$$n = 0, 1.... \ ,$$

where $x^{(n,i)} = (x_1^{n+1},\ldots, x_{i-1}^{n+1}, x_i^n \ldots, x_N^n)$.

III. The nonlinear Gauss-Seidel Method,

$$g_{III,i}(x^{n+1}, x^n) = f_i\,(x_1^{n+1},\ldots,x_i^{n+1}, x_{i+1}^n,\ldots,x_N^n) \ ,$$

$$i = 1,....N$$

$$n = 0, 1..... \quad .$$

6.2 Theorems of Convergence

The following theorems of convergence will be considered.

Theorem I. Let $f(x) = 0$ or $g(x,y) = 0$ be a system of nonlinear equations. Assume that the Fréchet derivative of f at x has a regular splitting of the matrix, $f'(x)$, and the inverse of the Fréchet derivative, $[f'(x)]^{-1}$, exists and is non-negative. Let S be an open neighborhood of a point, $x^* \in R^n$. Assume that $g \in c^1(S \times S)$, g_x^{-1} is defined and continuous on $S \times S$, and $f(x^*) = 0$ or $g(x^*, x^*) = 0$.

We define

$$H = - \frac{g_y(x^*,x^*)}{g_x(x^*,x^*)} \quad , \tag{6-4}$$

denoting the matrices, $[g_x(x^*,x^*)]^{-1} \; g_y(x^*,x^*)$, for g_I, $g_{II,\omega}$ and g_{III} by H_I, $H_{II,\omega}$ and H_{III}, respectively.

For each ω in the range $0 < \omega \leq 1$, there exists a neighborhood S of x^* such that the sequence $\{x^i, i = 1,2,3,\ldots\}$ converges to the solution x^* for the Jacobi-Newton method, the nonlinear Gauss-Siedel method and the "modified" Newton method, if the successive overrelaxation factor, ω, is in the range $0 < \omega \leq 1$.

Proof:

Since the Fréchet derivative of $f(x)$ has a regular splitting of the matrix $f'(x)$, it may be expressed:

$$f'(x) = D(x) - B(x) \qquad x \in S \tag{6-5}$$

and $D(x)$ or $B(x) = E(x) + F(x) \geq 0$, $D(x)$ is a diagonal matrix, and $E(X)$ and $F(X)$ are strictly lower triangular and strictly upper

triangular n x n matrices, respectively. From equations (6-4) and (6-5), one can easily show that,

$$H_I = \frac{E(x^*) + F(x^*)}{D(x^*)} \tag{6-6}$$

$$H_{II,\omega} = \frac{[(1-\omega)\ D(x^*) + \omega\ F(x^*)]}{[D(x^*) - \omega\ E(x^*)]} \quad \text{for} \quad 0 < \omega \leq 1 \tag{6-7}$$

$$H_{III} = \frac{F(x^*)}{[D(x^*) - E(x^*)]} \quad . \tag{6-8}$$

All iterative methods considered can be described by the following choices,

$$M = D \qquad N = E + F$$

$$M = D - E \qquad N = F$$

$$M = \frac{1}{\omega}(D - \omega E), \quad N = \frac{1}{\omega}(\omega F + (1-\omega)D) \qquad \omega \neq 0 \ . \tag{6-9}$$

We now consider some special properties of the matrices M and N in equation (6-9). We note that D is a positive and diagonally dominant matrix, and either F or E+F is a non-negative matrix from equation (6-5) by hypothesis. It is obvious that for $0 < \omega \leq 1$ the different splittings of M and N in equation (6-9) possess the common properties of the inverse of M, $M^{-1} \geq 0$ and $N \geq 0$.

By hypothesis, we know the inverse of the Fréchet derivative, $F'(x^*)^{-1} \geq 0$, and from the above results we know $M^{-1} \geq 0$ and $N \geq 0$; therefore $M^{-1}N \geq 0$ results. With the aid of the Perron-Frobenous

theory of non-negative matrices (Th. 2.7 Varga, 1962), we can determine the spectral radius $\rho(M^{-1}N)$ of $M^{-1}N$ (pp. 89, Varga, 1962) as shown to be

$$\rho(M^{-1}N) = \frac{\rho\,(f'^{-1}N)}{1+\rho\,(f'^{-1}N)} < 1 \quad . \tag{6-10}$$

Because the matrices $M^{-1}N$ and $f'^{-1}N$ are non-negative matrices, the associated eigenvalue ρ's of the matrices $M^{-1}N$ and $f'^{-1}N$ are necessarily non-negative. Obviously $\rho(f'^{-1}N)/[1 + \rho(f'^{-1}N)]$ is a monotone function of $\rho(f'^{-1}N)$. Since $\rho(f'^{-1}N)$ is non-negative, it is obvious that $\rho(M^{-1}N) < 1$; thus, the matrix $M^{-1}N$ is convergent. As a consequence of Theorem 3 (Ortega and Rockoff, 1966), there exists a neighborhood S of x^*. The iterative methods of I, II, and III are all, consequently, convergent.

A similar proof of Theorem 1 is independently given by (Ortega and Rheinholdt, 1970).

Theorem 2. Let $f(x) = 0$ or $g(x,y) = 0$ be a system of nonlinear equations. Assume that the Fréchet derivative of f at x has a regular splitting of the matrix $f'(x)$. Let S be an open neighborhood of a point $x^* \in R^n$ and assume that $g \in c^1(S \times S)$, g_x^{-1} is defined and continuous on $S \times S$ and $f(x^*) = 0$ or $g(x^*, x^*) = 0$.

In addition, let the matrix D be the diagonal matrix whose diagonal entries d_{ii} are defined as

$$d_{ii} = \frac{1}{a_{ii}} \qquad 1 \leq i \leq n \tag{6-11}$$

If $f' = (a_{ij})$ is a real $n \times n$ matrix with $a_{ij} \leq 0$ for all $i \neq j$, and $a_{ij} > 0$ for all $i = j$, and the matrix $B = I - Df'$ is non-negative and convergent, then all methods considered in Theorem 1 are convergent for any initial vector, $x_o \in S$.

Proof: From all hypothesis given and on the basis of Theorem 3.10 (Varga, 1962), it can be shown that f' is non-singular and the inverse of the Fréchet derivative $f^{-1} \geq 0$. Since $f^{-1} \geq 0$ and by hypotheses f' has a regular splitting of matrix f', all the conditions satisfy theorem 1. As a consequence of theorem 1, all iterative methods considered in theorem 1 are convergent.

The considerations of the irreducibility of matrix B is given in theorem 3. If matrix B is irreducible, it can be shown that the inverse of the Fréchet derivative of f is strictly greater than zero. The proof is similar to those already given.

Theorem 3: Let $f(x) = 0$ or $g(x,y) = 0$ be a system of nonlinear equations. Assume that the Fréchet derivative of f at x has a regular splitting of the matrix $f'(x)$. Let S be an open neighborhood of a point $x^* \in R^n$ and assume that $g \in c^1(S \times S)$, that g_x^{-1} is defined and continuous on $S \times S$ and that $f(x^*) = 0$ or $g(x^*,x^*) = 0$. In addition, let the matrix D be the diagonal matrix whose diagonal entries are defined in equation (6-11). If the matrix $B = I - D^{-1}f'$ is non-negative, irreducible, and convergent, then all methods considered in theorem 1 are convergent.

Proof: the proof of theorem 3 follows from theorem 1 and theorem 3.11 (Varga, 1962).

Theorem 4. Let $f(x)$ or $g(x,y) = 0$ be a system of nonlinear equations and assume that the Fréchet derivative $f'(x) = (a_{ij}(x))$ is

a real, irreducibly diagonally dominant $n \times n$ matrix with $a_{ij} \leq 0$ for all $i \neq j$, and $a_{ii} > 0$ for all $1 \leq i \leq n$. Let S be an open neighborhood of a point, $x^* \in R^n$, and assume that $g \in c^1(S \times S)$ and g_x^{-1} are defined and continuous on $S \times S$ and $f(x^*) = 0$ or $g(x^*, x^*) = 0$. All methods considered in theorem 1, then, are convergent for any initial vector $x_o \in S$.

Proof: By hypotheses the Fréchet derivative $f'(x)$ is a real, irreducible, diagonally dominant $n \times n$ matrix with positive diagonal entries and non-negative off-diagonal entries; thus, the Fréchet derivative, $f'(x)$, has a regular splitting of the matrix $f'(x)$. By corollary (pp. 85, Varga, 1962) we know that the inverse of the Fréchet derivative, $f'(x)$ is non-negative, i.e.,

$$[f'(x)]^{-1} > 0. \tag{6-12}$$

Since $\det [D(x)] \neq 0$, $x \in S$, g_x^{-1} exists for each g_I, $g_{II\omega}$, and g_{III} owing to non-vanishing determinant of the diagonal matrix and is continuous on $S \times S$. As a consequence of these results and using theorem 1, the Jacobi-Newton method, the nonlinear Gauss-Siedel method and the "modified" Newton's method for $0 < \omega \leq 1$ are convergent.

Theorem 5. If $f'(x) = (a_{ij})$ is a real, symmetric and non-singular $n \times n$ irreducible matrix, where $a_{ij} \leq 0$ for all $i \neq j$ and $f'(x)$ is positive definite, then all iterative methods considered are convergent for $x_o \in S$.

Proof: Since $f'(x)$ has non-positive off-diagonal entries and is definite, the diagonal entries of f' are positive real numbers. These results imply that M is nonsingular with $M^{-1} \geq 0$; hence,

the Fréchet derivative of $f(x)$ has a regular splitting of the $n \times n$ matrix. The above hypotheses also imply that the inverse of the Fréchet derivative of f is positive by Corollary 2 (Vargas, pp. 85, 1962). Following the theorem 1, therefore, all iterative methods considered are convergent.

Theorem 6. If $f'(x) = I-B$, where $B = L + U$ is a non-negative irreducible, and convergent $n \times n$ matrix, and L and U are strictly lower and upper triangular matrices, respectively, then, the successive overrelaxation matrix, $H_{II.\omega}$ is convergent for all $0 < \omega \leq 1$. Moreover if $0 < \omega_1 < \omega_2 \leq 1$, then:

$$0 < \rho\,(H_{II,\omega_2}) < \rho\,(H_{II,\omega_1}) < 1 \qquad 0 < \omega_1 < \omega_2 \leq 1$$

$$0 < \rho\,(H_{II,1}) < \rho(H_I) \quad .$$

Proof: The proof of theorem 6 is similar to linear theory (Vargas, 1962, pp. 92).

In addition, by the Stein-Rosenberg theorem, we have

$$0 < \rho\,(H_{II,1}) < \rho\,(H_I) \quad .$$

From the above we know that the Gauss-Seidel method is convergent faster than the other two methods if any initial vector $x^0 \in S$. However, under the conditions imposed on f', the under relaxation methods may improve the global convergence.

Theorem 7: Let $f'(x) = D(x) - E(x) - E^*(x)$ be an $n \times n$ Hermitian matrix, where D is Hermitian and positive definite, and

$D - \omega E$ is nonsingular for $0 \leq \omega \leq 2$, then $\rho(H_\omega) < 1$, if $f'(x)$ is positive definite and $0 < \omega < 2$.

Proof: We derive these results by replacing A by $f'(x)$ in theorem 3.6 (p. 77, Varga, 1962).

Theorem 8: Let the Fréchet derivative of f be a consistently ordered 2-cyclic matrix with non singular diagonal entries of f', and assume that f' is irreducible, diagonally dominant and symmetric, and $f' = D - E - F$, $D \geq 0$, $E + F \geq 0$. Let the eigenvalues of the associated Jacobi matrix B be real and non-negative, with $0 \leq \rho(B) < 1$ and let an open neighborhood of a point $x^* \in R^n$. Assume that $g \in c^1(S \times S)$ and g_x^{-1} is defined and continuous on $S \times S$ and $g(x^*, x^*) = 0$.

There, then, exists a neighborhood S of x^* such that the sequence $\{x^n, n = 0,1,\ldots.\} \subset S$ converges to x^* for the "modified" Newton's method with $0 < \omega < 2$.

Proof: By the above hypothesis and theory developed by Young (1954) for a system of linear equations, the "modified" Newton's method for a point of successive overrelaxation which satisfies Th. 4.4 (p. 111, Varga, 1962) is convergent for each $0 < \omega < 2$.

As in the linear problem, the following fundamental relationship holds for the nonlinear problem (Theorem 4.3, Varga, 1962),

$$(\lambda + \omega - 1)^2 = \lambda \omega^2 \mu_i^2 \qquad (6\text{-}13)$$

for some i, $1 \leq i \leq r$. Where μ_i is an eigenvalue of the Jacobi matrix B, λ is an eigenvalue of the matrix $H_{II,\omega}$. The relationship in equation (6-13) holds between the eigenvalues μ_i of H_I and the

eigenvalue of $H_{II,\omega}$. We denote the optimum value of the successive overrelaxation factor, ω by W_{opt}, which minimizes the spectral radius of $\rho(H_{II,\omega})$. The optimum relaxation factor W_{opt}, then, is given by:

$$W_{opt} = \frac{2}{1 + \sqrt{1 - \rho^2(H_I)}} \quad . \tag{6-14}$$

Virtually all of the theories developed by Young (1954) for linear equations is also applicable to nonlinear equations, if matrix A is replaced by Fréchet derivative f' .

6.3 Numerical Test

A numerical example, which satisfies all conditions in Theorem 4, is given in the following. We will consider a system of two nonlinear equations with two unknowns,

$$f_1(x,y) = 0 \tag{6-15}$$

$$f_2(x,y) = 0 \quad . \tag{6-16}$$

The algorithm for the "modified" Newton's formula for the system (6-15) and (6-16), then, takes the following form,

$$x^{n+1} = x^{(n)} - \omega \frac{f_1(x^{(n)}, y^{(n)})}{\frac{\partial f_1(x^{(n)}, y^{(n)})}{\partial x}} \tag{6-17}$$

$$y^{n+1} = y^{(n)} - \omega \frac{f_2\,(x^{(n+1)},\, y^{(n)})}{\frac{\partial f_2\,(x^{(n+1)},\, y^{(n)})}{\partial y}} \tag{6-18}$$

where n is the number of iteration and ω is a relaxation factor. Note that the result of the newly calculated value of $x^{(n+1)}$ in equation (6-17) is used to get $y^{(n+1)}$ in equation (6-18). The numerical example we consider is

$$f_1(x,y) = x^2 + 2x - 3y - 5 = 0 \tag{6-19}$$

$$f_2(x,y) = y^2 + y - 2x + 2 = 0 \quad . \tag{6-20}$$

The exact solution of the system of equations (6-19) and (6-20) is:

$$x^* = 2.0$$

$$y^* = 1.0 \ , \quad \text{and}$$

the Fréchet derivative of $f(x)$ is:

$$f'(x,y) = \begin{pmatrix} 2x + 2 & -3 \\ -2 & 2y + 1 \end{pmatrix} . \tag{6-21}$$

If we choose an initial guess for x and y such that

$$x_o = 0.6$$

$$y_o = 0.6 \quad ,$$

then,

$$f'(x,y) = \begin{pmatrix} 3.2 & -3 \\ -2 & 2.2 \end{pmatrix} .$$

By virtue of equation (6-21) the algorithm of the "modified" Newton's method from equations (6-17), (6-18), (6-19), and (6-20) takes the following form,

$$x^{(n+1)} = x^{(n)} - \omega \frac{x^{(n)^2} + 2x^{(n)} - 3y^{(n)} - 5}{2x^{(n)} + 2} \qquad (6\text{-}21)$$

$$y^{(n+1)} = y^{(n)} - \omega \frac{-2x^{(n+1)} + y^{(n)^2} + y^{(n)} + 2}{2y^{(n)} + 1} \quad . \qquad (6\text{-}22)$$

The numerical processes for integrating the system of equations (6-21) and (6-22) follow. We choose some initial values for x^o, y^o, and the relaxation factor, ω, the latter is set equal to 0.5. From (6-21), we obtain $x^{(1)}$, and inserting $x^{(1)}$ and y^o into (6-22), we have $y^{(1)}$. Then we calculate $x^{(2)}$ and $y^{(2)}$ in (6-21) and (6-22) from $x^{(1)}$ and $y^{(1)}$, and the cycle for calculating $x^{(r)}$ and $y^{(r)}$ from (6-21) and (6-22) is repeated until the predetermined criteria for the error is satisfied. For a convergence test of

$||x^{(n+1)} - x^{(n)}|| \leq 10^{-6}$, the number of iterations and the initial guess for the starting values of x^o and y^o are tabulated in Table 6.

TABLE 6 THE NUMBER OF ITERATIONS, THE RELAXATION FACTOR, ω_o , AND THE INITIAL GUESS FOR THE STARTING VALUES OF x^o AND y^o

Initial value		Relaxation factor	Number of iterations
x^o	y^o	ω	
0.0	0.0	0.5	50
0.6	0.6	0.5	48
1.5	0.6	0.5	47
2.5	1.5	0.5	47
10.0	10.5	0.5	57
Exact Solution			
$x^* = 2.0$	$y^* = 1.0$		

Chapter VII

THE FINITE DIFFERENCE METHOD

The momentum equations (5-17) and (5-18), the equation of continuity (5-19) and the thermal energy equation (5-20) may form a closure, provided that the eddy diffusivity and eddy conductivity are specified. We can solve the set of nonlinear partial differential equations by using the iterative technique of the "modified" Newton's method. The mixing length model, which relates the exchange coefficients to the mean flow fields, is simpler and uses fewer empirical constants; therefore, it will be used for closure of the nonlinear partial differential equations.

The finite differences for the pressure field, (Poisson's equation). Equation (5-21), the momentum equation (5-17), the thermal energy equation (5-20) and the equation of continuity (5-19) are written in the following sections. The grid system is shown in Figure 7-1. The unbalanced spacing is used for finite difference equations.

7.1 Poisson's Equation

The finite differences for the pressure field in equation (5-21) are

$$\frac{2}{\Delta\eta(i) + \Delta\eta(i+1)} \left[\frac{P(i+1,j) - P(i,j)}{\Delta\eta(i+1)} - \frac{P(i,j) - P(i-1,j)}{\Delta\eta(i)}\right]$$

$$+ b^2(j) \left\{\frac{2}{\Delta\zeta(i) + \Delta\zeta(j+1)} \left[\frac{P(i,j+1) - P(i,j)}{\Delta\zeta(j+1)} - \frac{P(i,j) - P(i,j-1)}{\Delta\zeta(j)}\right]\right.$$

$$\left. - \frac{P(i,j) - P(i,j-1)}{\Delta\zeta(j)}\right\}$$

$$= k^2 b(j) \frac{2}{\Delta\zeta(j) + \Delta\zeta(j+1)} \left\{ \frac{1}{\Delta\eta(i) + \Delta\eta(i+1)} \left(K_m(i+1,j+1) - K_m(i-1,j+1) \right) \right.$$

$$\frac{\bar{u}(i,j+1) - \bar{u}(i,j)}{\Delta\zeta(j+1)} - \frac{1}{\Delta\eta(i) + \Delta\eta(i+1)} \cdot$$

$$\left. \left(K_m(i+1,j) - K_m(i-1,j) \right) \frac{\bar{u}(i,j) - \bar{u}(i,j-1)}{\Delta\zeta(j)} \right\}$$

$$+ k^2 b^3(j) \frac{2}{\Delta\zeta(j) + \Delta\zeta(j+1)} \left(K_m^*(i,j+1) - K_m^*(i,j) \right) \cdot$$

$$\left\{ \frac{2}{\Delta\zeta(j) + \Delta\zeta(j+1)} \left[\frac{1}{\Delta\zeta(j+1)} \left(\bar{w}(i,j+1) - \bar{w}(i,j) \right) - \frac{1}{\Delta\zeta(j)} \left(\bar{w}(i,j) \right. \right. \right.$$

$$\left. \left. \left. -\bar{w}(i,j-1) \right) \right] - \frac{1}{\Delta\zeta(j) + \Delta\zeta(j+1)} \left(\bar{w}(i,j+1) - \bar{w}(i,j-1) \right) \right\}$$

$$-2 \left\{ b(j) \left[\frac{\bar{u}(i,j+1) - \bar{u}(i,j-1)}{\Delta\zeta(j) + \Delta\zeta(j+1)} \right] \left[\frac{\bar{w}(i+1,j) - \bar{w}(i-1,j)}{\Delta\eta(i) + \Delta\eta(i+1)} \right] \right.$$

$$\left. + \left[\frac{\bar{u}(i+1,j) - \bar{u}(i-1,j)}{\Delta\eta(i) + \Delta\eta(i+1)} \right]^2 \right\} + g\, b(j) \left[\frac{\bar{\theta}(i,j+1) - \bar{\theta}(i,j-1)}{\Delta\zeta(j) + \Delta\zeta(j+1)} \right] \quad (7\text{-}1)$$

7.2 Momentum Equation and the Energy Equation

For the flow with $\bar{u}(i,j) \geq 0$ and $\bar{w}(i,j) \leq 0$. We use the upwind difference for the advective term. The upwind difference has stabilizing effects, which have long been known to meteorologists. The finite difference analogous to equation (5-17) is

$$\bar{u}(i,j)\left[\frac{\bar{u}(i,j)-\bar{u}(i-1,j)}{\Delta\eta(i)}\right]+\bar{w}(i,j)\,e^{-\zeta j}\left[\frac{\bar{u}(i,j+1)-\bar{u}(i,j)}{\Delta\zeta}\right]$$

$$+\frac{P(i+1,j)-P(i-1,j)}{\Delta\eta(i)+\Delta\eta(i+1)}-k^2\,e^{-\zeta j}\,\frac{2}{\Delta\zeta(j)+\Delta\zeta(j+1)}\cdot$$

$$\left\{K_m(i,j+1)\left[\frac{\bar{u}(i,j+1)-\bar{u}(i,j)}{\Delta\zeta(j+1)}\right]-K_m(i,j)\left[\frac{\bar{u}(i,j)-\bar{u}(i,j-1)}{\Delta\zeta(j)}\right]\right\}=0\quad. \tag{7-2}$$

Rearrangement of equation (7-2) results in the following functional representation,

$$f_{u(i,j)}\left[\bar{u}^{(n+1)}_{(i-1,j)},\ \bar{u}^{(n+1)}_{(i,j-1)},\ \bar{u}^{(n)}_{(i,j)},\ \bar{u}^{(n)}_{(i+1,j)},\ \bar{u}^{(n)}_{(i,j+1)}\right]=0\quad. \tag{7-3}$$

Employing central differences to the eddy diffusivity and eddy conductivity in the above equation, we have:

$$K_m^{n+1}=\phi^n\,\frac{\bar{u}^n(i,j+1)-\bar{u}^{n+1}(i,j-1)}{\Delta\zeta(j)+\Delta\zeta(j+1)} \tag{7-4}$$

$$K_h^{n+1}=(\phi^n)^{-1}\,K_m^{(n+1)}\quad, \tag{7-5}$$

where $\phi^n=(1-18R^n_{(i,j)})^{-\frac{1}{4}}$

$$Ri^n_{(i,j)}=-\frac{g[\bar{\theta}^n(i,j+1)-\bar{\theta}^{n+1}(i,j-1)]}{e^{-\zeta j}\,\frac{[\bar{u}^n(i,j+1)-\bar{u}^{n+1}(i,j-1)]}{[\Delta\zeta(j)+\Delta\zeta(j+1)]}} \tag{7-6}$$

$$\Phi^n=(\phi^n)^{-2}\quad. \tag{7-7}$$

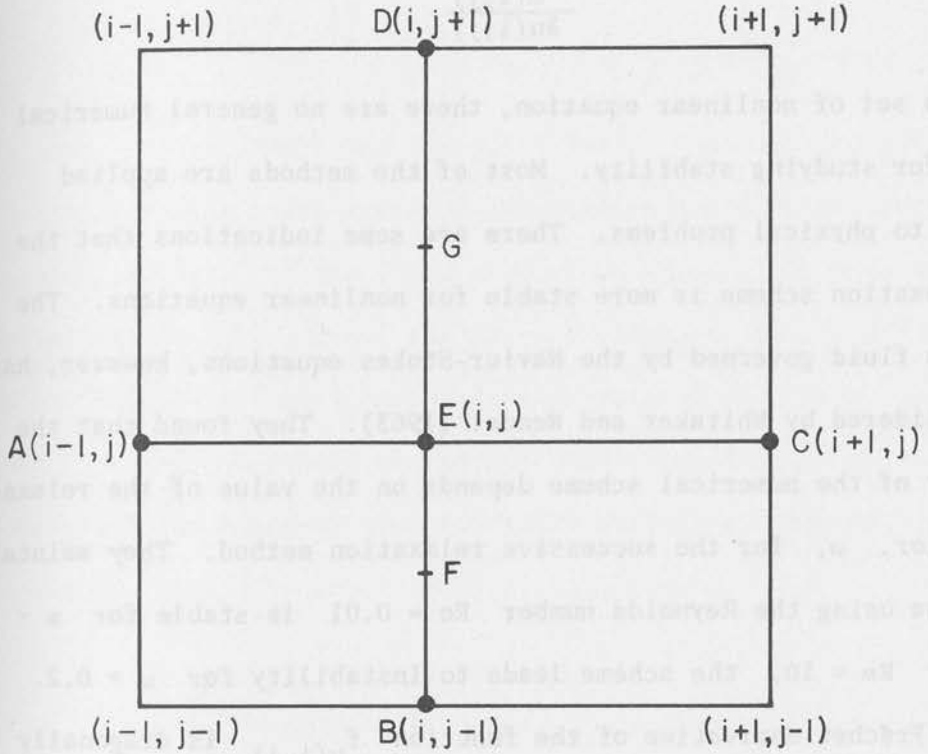

$\Delta\eta(i) = AE$ $\qquad F = \frac{1}{2} BE$

$\Delta\eta(i+1) = EC$ $\qquad G = \frac{1}{2} ED$

$\Delta\zeta(j) = BE$ $\qquad K(i,j) = K_m$ at point F

$\Delta\zeta(j+1) = ED$ $\qquad K(i,j+1) = K_m$ at point G

Figure 7-1 Grid system used in numerical integration

The numerical scheme, we use, is the "modified" Newton's method:

$$\bar{u}^{(n+1)}_{(i,j)} = \bar{u}^{(n)}_{(i,j)} - \omega_u \frac{f_{u(i,j)}}{\frac{\partial f_{u(i,j)}}{\partial u(i,j)}} \quad . \tag{7-8}$$

In a set of nonlinear equation, there are no general numerical methods for studying stability. Most of the methods are applied directly to physical problems. There are some indications that the underrelaxation scheme is more stable for nonlinear equations. The Newtonian fluid governed by the Navier-Stokes equations, however, has been considered by Whitaker and Wendel (1963). They found that the stability of the numerical scheme depends on the value of the relaxation factor, ω, for the successive relaxation method. They maintain the scheme using the Reynolds number $Re = 0.01$ is stable for $\omega < 0.4$; for $Re = 10$, the scheme leads to instability for $\omega > 0.2$.

The Fréchet derivative of the function $f_{u(i,j)}$ is diagonally dominant, and the determinant of $\partial f_u(i,j)/\partial u(i,j)$ is nonsingular. We also assume that the function $f_{u(i,j)}$ is continuous and that a solution exists. Furthermore, we choose the relaxation factor ω_u with a range $0 < \omega_u \leq 1$. The optimum value of ω_u is based on numerical experiments. Thus the set of nonlinear equations satisfy all conditions given in Theorem 4. For any arbitrary initial guess for the starting value $u_{o(i,j)}$, the sequence $\{u^n_{(i,j)}\}$ converges to a unique solution $u^*_{(i,j)}$.

Since the energy equation (5-20) has the same form as the momentum equation, the finite difference representation can be made analogous to the momentum equation. We will, therefore, not present the finite difference analog of the energy equation here.

7.3 Equation of Continuity

The continuity equation in the form

$$\frac{\partial \bar{w}}{\partial z} = - \frac{\partial \bar{u}}{\partial x} \tag{7-9}$$

has been used by Onishi and Estoque (1968). Although the vertical velocities at the lower and upper boundaries may both be zero, the numerical integral of the right side of equation (7-9) will not necessarily vanish. Onishi and Estoque attempted to avoid those difficulties by introducing any arbitrary function, $f(z)$, in such a way that the constraint of the continuity equation (7-9) will assure that the boundary conditions are satisfied. Equation (7-9) after introducing the above constraints, becomes:

$$\frac{\partial \bar{w}}{\partial z} = f(z) - \frac{\partial \bar{u}}{\partial x} \quad . \tag{7-10}$$

Upon integrating from the bottom to the top of a column of air, equation (7-10) maintins its equality. Although constraints preserve equality in equation (7-10), for the two-point boundary problem, there are an infinite number of choices for the function $f(z)$. The vertical velocity, $\bar{w}$, therefore, may have infinite solutions, depending on the choice of function $f(x)$. The artificial function $f(z)$ can be discarded, if the continuity equation in the form of the second order partial differential equation has been used such that

$$\frac{\partial^2 \bar{w}}{\partial z^2} = - \frac{\partial^2 \bar{u}}{\partial z \partial x} \quad . \tag{7-11}$$

This equation automatically meets the boundary conditions and preserves equality. The finite difference form of equation (7-11) can be written:

$$\frac{1}{[\Delta\zeta(j) + \Delta\zeta(j+1)]\quad[\Delta\eta(i) + \Delta\eta(i+1)]}\left[\bar{u}(i+1,j+1) - \bar{u}(i-1,j+1)\right.$$

$$\left. - \bar{u}(i+1,j-1) + \bar{u}(i-1,j-1)\right] \quad + e^{-\zeta j} \quad \left\{\frac{1}{\Delta\zeta(j) + \Delta\zeta(j+1)}\right.$$

$$\left[\frac{\bar{w}(i,j+1) - \bar{w}(i,j)}{\Delta\zeta(j+1)} - \frac{\bar{w}(i,j) - \bar{w}(i,j-1)}{\Delta\zeta(j)}\right]$$

$$\left. - \frac{\bar{w}(i,j+1) - \bar{w}(i,j-1)}{\Delta\zeta(j) + \Delta\zeta(j+1)}\right\} = 0 \quad . \tag{7-12}$$

The finite difference equations for the pressure equation (7-1), the thermal equation (5-20) and the equation of continuity (7-11) can be written analogous to equation (7-8), respectively:

$$p_{(i,j)}^{(n+1)} = p_{(i,j)}^{(n)} - \omega_p \left(\frac{f_{p(i,j)}}{\frac{\partial f_{p(i,j)}}{\partial p(i,j)}}\right) \tag{7-13}$$

$$\bar{\theta}_{(i,j)}^{(n+1)} = \bar{\theta}_{(i,j)}^{(n)} - \omega_\theta \frac{f_{\theta(i,j)}}{\frac{f_{\theta(i,j)}}{\partial\theta_{(i,j)}}} \tag{7-14}$$

$$\bar{w}_{(i,j)}^{(n+1)} = \bar{w}_{(i,j)}^{(n)} - \omega_w \frac{f_{w(i,j)}}{\frac{\partial f_{w(i,j)}}{\partial w(i,j)}} \tag{7-15}$$

Equations (7-8) and (7-13) can be reduced to the same system of equations as that of Onishi and Estoques' model (1968), if we make

$\omega_u = \omega_p = 1$ and linearize the functions f_u and f_p. The system of nonlinear equations (7-8), (7-13), (7-14), and (7-15) with (7-4) and (7-5) form a closure. We have solved this set of equations by using a CDC 6400 computer.

7.4 Boundary Conditions

The general discussion for Poisson's equation of the first and second kind along the boundaries are outlined in this section. In the numerical integration of Poisson's equation, the finite-difference equation should be made consistent with the boundary conditions.

7.4.1 Boundary conditions of the first kind (Dirchlet Conditions - Poisson's equation can be written as

$$\nabla^2 P = F(x,z); \tag{7-16}$$

with the Dirchlet boundary conditions, such that P is constant along the boundary, where F is a known function. The finite difference form of this equation may be written in the form

$$P_{(i-1,j)} + P_{(i,j-1)} + P_{(i+1,j)} + P_{(i,j+1)} - 4P_{(i,j)} - F_{(i,j)} = 0 \tag{7-17}$$

where P is a fixed constant along the boundaries, the linear equation (7-16) converges to give the solution by means of the Jacobi iterative method (see Smith, 1965).

The error vector is expressed as

$$|e^{n+1}| = \rho \; | \; e^{(n)}|$$

where n is the index of iteration and ρ is the spectral radius of the iteration matrix. Then the spectral radius, ρ, for the Jacobi iteration corresponding to equation (7-17) can be shown to be

$$\rho(J) = \frac{1}{2}\left(\cos\frac{\Pi}{P} + \cos\frac{\Pi}{q}\right) , \tag{7-18}$$

where P and q are the number of grid points in the x and z directions, respectively. The spectral radius for the Gauss-Seidel iteration is:

$$\rho(G) = \{\rho(J)^2\} , \tag{7-19}$$

that is, the Gauss-Seidel method converges twice as fast as the Jacobi method. The systems of linear equation (7-16) can be represented by a matrix that is symmetrical, positive definite and consistently ordered.

Young (1949) shows that the system converges to the solution with the relaxation factor,

$$\omega = \frac{2}{1 + [1-\rho(G)^2]} . \tag{7-20}$$

The rate of convergence of the successive overrelaxation method developed by Young (1949) is considerably faster than the Jacobi and Gauss-Seidel method. The rate of convergence depends on the value of the relaxation factor, ω .

7.4.2 Boundary conditions of the second kind (Neuman conditions) - Poisson's equation with boundary conditions of the second kind or Neuman conditions, is represented by:

$$\nabla^2 P = F \quad , \tag{7-21}$$

where P is any physical variable not necessarily representing pressure and F is a known function with certain Neuman boundary conditions such that

$$\frac{\partial P}{\partial n} = \chi(x,z) \tag{7-22}$$

along the boundaries. Here n is the coordinate normal to the boundary, and χ is the known function along the boundary. We integrate the governing equation (7-21) over the entire domain, and with the aid of Gauss' divergence theorem, derive:

$$\iint F \, d\sigma = \iint \nabla^2 P d\sigma = \int \frac{\partial P}{\partial n} \, dS' \quad . \tag{7-23}$$

The following equation results,

$$\iint F \, d\sigma = \int \chi dS' \quad , \tag{7-24}$$

where σ is the area and S' is the boundary. The boundary condition in equation (7-22) will then be written:

$$P_{i,2} - P_{i,1} = \chi_{i,1\frac{1}{2}} \quad \Delta\sigma \qquad i = 2,3..... M-1 \tag{7-25}$$

Substituting equation (7-25) into the finite difference form of equation (7-21) we have:

$$P_{(i-1,2)} + P_{(i,1)} + P_{(i+1,2)} + P_{(i,3)} - 4P_{(i,2)} - F_{(i,2)} = 0 \; ;$$

therefore,

$$P_{(i-1,2)} + P_{(i+1,2)} + P_{(i,3)} - 3P_{(i,2)} - F_{(i,2)} - \chi_{(i,1\frac{1}{2})} \cdot \Delta\sigma = 0 \ . \tag{7-26}$$

The equation for the pressure, (7-1), can be easily expressed similar to equation (7-26) for the grid points near the boundaries.

7.5 Numerical Processes

We employ the "modified" Newton's method of optimum displacement by point to solve the system of equations (7-8), (7-13), (7-14), and (7-15). The method is applied to each point from the bottom to the top of the air column. We then, survey each column from left to right in the same direction as the flow. The finite difference equations are used only for flow moving from rough to smooth surface with heating. With this information we are prepared to begin solving the set of equations.

(i) Initially, we set $P^{(o)} = 0$ and $\bar{w}^{(o)} = 0$ for all grid points. The potential temperature has an upstream boundary value $\bar{\theta} = 1.0$. We also make an arbitrary initial approximation for the horizontal velocity field $\bar{u}^{(o)}$. With the horizontal velocity, $\bar{u}^{(o)}$, we can compute $K_m^{(o)}$ and $K_h^{(o)}$ from equations (7-4) and (7-5), respectively.

(ii) Next, using equation (7-13), we calculate $P^{(1)}$ from the known values $\bar{u}^{(o)}$, $\bar{w}^{(o)}$, $\bar{\theta}^{(o)}$, $K_m^{(o)}$, $K_h^{(o)}$ available from step (i) by successive iteration of the "modified" Newton's method. We calculate $P^{(1)}$ at each grid point as soon as the new iterative values of $P^{(1)}$ are available, and we utilize this new iterative value $P^{(1)}$ for the calculation of $P^{(1)}$ in the next grid point.

(iii) The values $\bar{u}^{(o)}$, $\bar{w}^{(o)}$, $\bar{\theta}^{(o)}$, $p^{(1)}$, $K_m^{(o)}$ and $K_h^{(o)}$ have been obtained from steps (i) and (ii), which are used for the calculation of $\bar{u}^{(1)}$ from equation (7-8). We use $\bar{u}^{(1)}$ available from the previous calculation to compute $K_m^{(1)}$ and $K_h^{(1)}$ at the same grid point, then we proceed to compute $\bar{\theta}^{(1)}$ from equation (7-14) and $\bar{w}^{(1)}$ from equation (7-15). We scan each point in the entire flow field and then go to the next step.

(iv) The final iterative values obtained from (iii) are reset as initial conditions, and we set them equal to $\bar{u}^{(1)}$, $\bar{w}^{(1)}$, $p^{(1)}$, $\bar{\theta}^{(1)}$, $K_m^{(1)}$, $K_h^{(1)}$. We repeat the processes from steps (i) to (iii) to obtain $\bar{u}^{(2)}$, $\bar{w}^{(2)}$, $p^{(2)}$, $\bar{\theta}^{(2)}$, $K_m^{(2)}$ and $K_h^{(2)}$. The cycles from (i) to (iv) are repeated to compute $\bar{u}^{(n)}$, $\bar{w}^{(n)}$, $p^{(n)}$, $\bar{\theta}^{(n)}$ $K_m^{(n)}$, $K_h^{(n)}$ as n increases until we obtain the prescribed degree of convergent solution giving the balance in velocity fields and the temperature and pressure field.

A similar numerical technique described in this chapter is also applicable to the turbulent energy and turbulent-Newtonian models; therefore, the finite differences of these models will not be given.

Chapter VIII

RESULTS AND DISCUSSION

The results of numerical integration for various models are presented in the following sections. We have considered the abrupt change of surface roughness and temperature, and the effects of non-homogeneous surface on the upstream flow. The thermal response to characteristics of the turbulence regime has also been examined. Also, numerical results have been compared with wind tunnel measurements and field observations. Turbulent kinetic energy usage to close the system of equations has been investigated and various terms in the turbulent energy equation have been calculated. The alternative models, other than k-theory, i.e., the turbulent energy model and turbulent energy - Newtonian model, are integrated numerically in this study.

8.1 Airflow From Rough to Smooth Transition Under Neutral Conditions --k-Theory

The airflow moving from one type of surface roughness to a new surface under neutral stratification has been investigated in detail. Such flow has been considered by several authors; however, almost all of them have not considered the influence of roughness discontinuity on the upstream flow. Furthermore, the problem is far from settled; many phenomena still remain to be explained. The abrupt change in surface roughness serves to perturb the approaching flow, and thus, the effects of a roughness discontinuity on the upstream flow may appear. In our model, the equation of continuity is written in the form of a second order partial differential equation. The solution of that equation automatically satisfies the boundary conditions and preserves equality

at any location between the vertical velocity and vertical integral of the horizontal divergence. We also compare the distribution of wind profiles with wind tunnel measurements and the distribution of surface shear stress with data obtained from field observations.

8.1.1 Retaining pressure terms: Case 1 - Airflow passing from rough surface to smooth surface with a relative roughness ratio of $m \simeq 5.0$ has been considered in Case 1. The pressure terms in our model have been retained. The velocity profiles at various distances from roughness discontinuity are shown in Figure 8.1.1. The wind profile of the fully developed turbulent flow far from the discontinuity of surface roughness in the upstream location is shown by Curve 1 in Figure 8.1.1. The flow is in equilibrium with the underlying surface characterized by the roughness parameter, z_o, and, it is assumed, follows the logarithmic wind profile. The velocity profile in Curve 2 at a nondimensional distance of $x = -8.0 \times 10^2$ is still located in the upstream position, and the accelerated wind velocity is caused by the pressure gradient force. This upstream effect has also observed by Wagner (1966) and Onishi and Estoque (1968).

Downstream of the roughness discontinuity, the air readjusts to the new surface of relatively smooth terrain. As a result of this smooth surface and less surface friction, the air accelerates, as shown at Curves 3 and 4. As the air gradually readjusts to its new surface, it begins to slow down and gradually reestablishes a new equilibrium wind profile with the underlying surface, as seen at Curve 5 in Figure 8.1.1.

Distribution of the pressure field is shown in Figure 8.1.2. The motion of the air has been perturbed by the presence of roughness discontinuity; therefore, fluctuations in pressure are observed. The maximum value of negative pressure located near the roughness discontinuity has the effect of accelerating the air ahead of the surface discontinuity. This effect has been shown in Figure 8.1.1 at Curve 2. Although the air in the rear part of the surface discontinuity is decelerated by the pressure gradient force, the pressure effects are mainly felt near the surface of roughness discontinuity and the air is still accelerating forward.

The vertical velocity field is shown in Figure 8.1.3. After the air passes over the surface of roughness discontinuity, downward motion of the air is induced due to the acceleration of the air. Such motion is required to satisfy the equation of continuity. The downward motion of air supplies the downward flux of horizontal momentum to the surface and as the air progresses downstream the airflow gradually regains its equilibrium conditions. The maximum downward motion is found above the surface discontinuity. Since the air is continuously accelerating in the upper portion of the flow but slowing down in the downstream direction and reestablishing its equilibrium conditions near the surface, the downward motion reduces its strength with downstream distance in the lower part of the boundary layer. The flux of horizontal momentum in the upper part of the flow field continuously feeds momentum to the air below by eddy motions, maintaining the field of downward motion. In the atmosphere, the air in the lower layer moves much slower than the air above it; hence, the region of maximum acceleration shifts upward while air moves in a downstream

direction, and the axis of maximum downward motion tilts upward and extends toward the downstream direction, as in Figure 8.1.3.

The shear stress profiles are shown in Figure 8.1.4. The lower part of the shear stress profile in Curve 2 is increasing as a result of the effect of the pressure gradient force. The shear stress profile decreasing with height at Curve 2 results from the combined effect of the pressure gradient force and downward motion that produces a region of maximum acceleration corresponding to the minimum shear stress at Curve 2. The distribution of the shear stress profile, which varies with height, is shown in subsequent curves of 2, 3, 4 and 5 in Figure 8.1.4 at various distances from the surface of roughness discontinuity. The thickness of the constant shear stress layer, however, becomes deeper as the fetch becomes longer. This is due to the flux of momentum that is continuously supplied to the lower part of the surface layer, and can be seen by comparing curves 3 with 4 and curves 4 with 5 in Figure 8.1.4.

The surface stress is shown in Figure 8.1.5. The normalized shear stress is equal to unity in the upstream far from the surface discontinuity. The shear stress, then, continuously increases toward the roughness discontinuity by the action of dynamic pressure induced by surface discontinuity. The shear stress reaches a maximum value before the abrupt change of surface roughness; then, it suddenly drops toward a minimum value. Downstream of the roughness discontinuity, the flux of horizontal momentum is continuously supplied to the surface by the action of downward and eddy motions. The surface shear stress, therefore, increases with downstream distance. After the air attains a relatively long fetch, due to a decrease in momentum flux from above,

the downward motion gradually vanishes and the surface shear stress reaches an asymptotic constant, as shown in Figure 8.1.5.

8.1.2 Neglecting pressure terms: Case 2 - In this case, all conditions are the same as in case 8.1.1, except that the pressure is omitted. The wind profiles are shown in Figure 8.1.6. For a relatively long fetch, the wind profiles in this case are virtually the same as Case 1, which includes pressure terms. This comparison can be seen in Curves 4 and 5 in Figure 8.1.1 and in Figure 8.1.6. However, owing to the presence of pressure in Case 1, the main difference between the velocity profiles in Case 1 and Case 2 is observed near the roughness discontinuity. In front of the roughness discontinuity, the air which has been pushed forward by the pressure gradient force, is accelerating near the earth's surface; compare Curve 2 in Figure 8.1.1 and Figure 8.1.6. To the rear of the roughness discontinuity, the air is decelerated by the pressure gradient force, as seen by comparing Curve 3 in Figure 8.1.1 to Curve 3 in Figure 8.1.6. The field of vertical velocity is shown in Figure 8.1.7.

The region of maximum downward motion is located far above the surface of discontinuity in Case 2; however, if the pressure terms are included in the momentum equations, the region of maximum downward motion is found near the surface of roughness discontinuity, as indicated in Figure 8.1.3. The magnitude of downward motion will be overestimated, if the pressure terms are not included in the system of equations as can be seen by comparing the vertical velocity fields in Figure 8.1.7 and Figure 8.1.3. The maximum value of downward motion in Case 2 is about six times larger than the value in Case 1. The shear stress profiles in the cases with and without pressure

effects are shown in Figure 8.1.4 and Figure 8.1.8, respectively. Again, the main differences of shear stress profiles in both cases, 1 and 2, occur near the roughness discontinuity in response to the pressure gradient force.

In front of the roughness discontinuity, the air is accelerating in Case 1; therefore, the magnitude of the shear stress is larger in Case 1 than that of Case 2, as indicated by Figure 8.1.4 and Figure 8.1.8. Curve 3 in Figure 8.1.4 and Figure 8.1.8 indicates that in Case 1 the air has been pushed back by pressure gradient force, and in Case 2, the air is accelerating as a result of compensation of downward motion. The slope of the shear stress profile in Case 1, therefore, is steeper than that of Case 2, and its magnitude is also smaller. The difference in shear stress is a result of the different velocity profiles in Case 1 and Case 2. The surface shear stress without the presence of the pressure field is shown in Figure 8.1.9. The main difference between Case 1 and Case 2 is the distribution of surface shear stress near the roughness discontinuity. In Case 1 the surface shear stress is larger in front of the roughness discontinuity and smaller in the rear than the stress in Case 2; these results are in response to the pressure field.

8.2 Airflow in Transition From Smooth to Rough Under Neutral Conditions --k-Theory

The results of airflow moving from smooth to rough terrain with $m \simeq -5$ and with abrupt change in surface roughness with and without pressure terms is shown in the following sections for Case 1 and Case 2, respectively.

8.2.1 Retaining pressure terms: Case 1 - The velocity profiles for Case 1 are shown in Figure 8.2.1. Curve 1 represents the horizontal mean velocity profile in the upstream location, where air is not affected by the roughness discontinuity. The effect of roughness discontinuity on the upstream flow is shown at Curve 2 of Figure 8.2.1. Curve 2 is at an upstream location with a nondimensional distance of $x = -1.1 \times 10^2$. After the change of surface roughness, the flow is modified by the friction of the rough surface, as shown by Curves 3, 4 and 5 in Figure 8.2.1. The pressure field is shown in Figure 8.2.2, which indicates that the air near the roughness discontinuity is first decelerating, then accelerating and finally again decelerating in response to the pressure field.

The field of vertical motion is shown in Figure 8.2.3. The maximum region of upward motion is located above the roughness discontinuity. Similar distributions of the vertical velocity field have appeared in the numerical integration of a set of unsteady equations by Wagner (1966), as shown in Figure 8.2.3a and in the field observations of Stearns and Lettau (1964) as shown in Figure 8.2.3b. Figure 8.2.3a and Figure 8.2.3b show the pattern of vertical velocity fields obtained by Wagner (1966), and Stearns and Lettau (1964), respectively. Their results indicate the influence of the roughness discontinuity on the upstream flow.

The distribution of shear stress profiles is shown in Figure 8.2.4. The change of the profiles is relatively sharp compared with the flow from rough to smooth transition. This phenomenon indicates that over relatively rough terrain, the air adjusts to the underlying surface more rapidly than over smooth terrain. The small effect of

the roughness discontinuity on the stress profile in the upstream location is also shown at Curve 2 in Figure 8.2.4.

The distribution of surface shear stress is shown in Figure 8.2.5. In front of the roughness discontinuity, the surface shear stress slightly decreases and then suddenly increases as the air moves over a rough surface. After the surface shear stress reaches its peak value, it decreases abruptly and then gradually decreases in magnitude to an asymptotic value. Similar distribution of the surface shear stress has been obtained by Yeh and Nickerson (1970), as shown in Figure 8.2.5a.

8.2.2 Neglecting pressure terms: Case 2 - The horizontal mean velocity profiles at various locations are shown in Figure 8.2.6. Since pressure terms have been excluded from this model, the velocity profile at Curve 2 in Figure 8.2.6 almost keeps its upstream value. No significant change in velocity profiles, as revealed by comparison of Curves 3, 4 and 5 in Case 1 and Case 2, has been observed. If the pressure terms are not included in the set of equations, the vertical velocity field will be overestimated, as shown in comparison of Figure 8.2.7 to Figure 8.2.3. The distribution of shear stress is shown in Figure 8.2.8. Without pressure terms there is no effect of roughness discontinuity on the shear stress at an upstream location, as shown at Curve 2 in Figure 8.2.8. The distribution of shear stress and surface shear stress (Figure 8.2.9) is similar to those profiles with the pressure force, as in Case 1.

8.3 Airflow in Transition from Rough to Smooth Under Unstable Conditions--k-Theory

The air flowing from a rough to smooth surface with $m \simeq 5$ and over a heated surface of nondimensional potential temperature 1.05 is

considered. Since the effects of surface roughness are dominant, the flow is essentially similar to the flow in Case 1, section 8.1. The velocity at Curve 2 in Figure 8.3.1 is slightly greater than the case without heating, as shown at Curve 2 in Figure 8.1.1. This is in response to thermal effects and the pressure force. The velocity indicated by Curve 5 in Figure 8.3.1 is significantly larger than the case with neutral conditions, as shown at Curve 5 in Figure 8.1.1. This effect is therefore a response to the surface heating.

The pressure field is shown in Figure 8.3.2, where the pressure gradient force is slightly larger than that of the case with neutral conditions shown in Figure 8.1.2. Owing to a slightly large pressure gradient force, the air will accelerate a little faster than air under neutral conditions in front of a roughness discontinuity. Air with surface heating will decelerate more than air without surface heating in the rear of the roughness discontinuity. The special phenomenon of the pressure field in Figure 8.3.2 is that there is a positive region of pressure field in the upper right hand side. Which is produced by surface heating. This positive pressure field created by heating has not been observed in the case with neutral stratification. The positive pressure force will result in a slight retardation of the airflow.

The field of vertical velocity in this case is similar to the case without heating. These results indicate that roughness is the dominant factor. Since the surface of the earth has been heated, however, the increase in momentum will result in an increasing downward motion near the earth's surface, as seen in Figure 8.3.3.

The shear stress, shown in Figure 8.3.4 increases as a result of the heating of the earth's surface as comparing Curve 2 in Figure 8.1.4 and Figure 8.3.4. The distribution of surface shear stress, shown in Figure 8.3.5, is increasing slightly faster as the air approaches the roughness discontinuity and then drops at a slightly faster rate than airflow without heating. At $x = 1.8 \times 10^6$ in Figure 8.3.5, the surface shear stress is increasing at a faster rate than airflow with neutral stratification.

8.4 Airflow Over Step Change in Surface Temperature with no Change in Surface Roughness--k-Theory

In order to isolate the thermal effects from the effects of roughness on flow, we will consider air moving over an abrupt change in surface potential temperature and over constant surface roughness.

8.4.1 Retaining pressure terms: Case 1 - The pressure terms are included in this case. The wind profiles are shown in Figure 8.4.1. Curve 1 represents the wind profile in the far upstream station. Without pressure effects, the flow will accelerate; however due to the presence of the pressure force the flow approaching the temperature discontinuity decelerates. After the flow passes over the point of temperature discontinuity, it will accelerate near the earth's surface and the air in the upper layer will decelerate because of the induced upward vertical motion of the heated surface of the earth.

The distribution of potential temperature is shown in Figure 8.4.2. The potential temperature continuously increases as the air progresses in the downstream direction. The pattern of the pressure field shown in Figure 8.4.3, resembles the flow in transition from smooth to rough

encountering the roughness discontinuity. The pattern of the field of vertical motion shown in Figure 8.4.4 also resembles the flow in transition from smooth to rough. The region of maximum upward motion is displaced upward above the temperature discontinuity; however, near the earth's surface, some small downward motion is induced by the increasing momentum near the earth's surface.

The distribution of shear stress is shown in Figure 8.4.5. In the lower layer as the air approaches the point of temperature discontinuity, the shear stress continuously decreases in response to the pressure field. After the air passes over the temperature discontinuity, the shear stress gradually increases. The increase of shear stress in the lower atmospheric surface layer is a result of transfer of shear stress or turbulent energy from above, since the maximum region of shear stress is produced near the edge of the internal boundary layer by thermal effects. The maximum value in a shear stress profile moves upward as the air progresses in a downstream direction.

The surface shear stress is shown in Figure 8.4.6. Before the temperature discontinuity, the surface shear stress decreases in response to the negative pressure force; however, after the temperature discontinuity, the surface shear stress increases, and the heated air near the earth's surface accelerates, because the turbulent energy or shear stress produced by thermal effects is transferred downward from above.

8.4.2 Neglecting pressure terms: Case 2 - By heating the earth's surface in the absence of a pressure force, the mean horizontal wind accelerates as the air moves in the downwind direction, as shown in

Figure 8.4.7. No retarded flow has been observed under these circumstances which is in contrary to what occurs in Case 1 of this section. The potential temperature profiles are shown in Figure 8.4.8. No significant change in potential temperature profiles has been observed by a comparison of the profiles in Figure 8.4.8 to Figure 8.4.2. The pattern of vertical velocity is shown in Figure 8.4.9. The field of vertical motion in Case 2 is only similar to Case 1 in the lower part of the atmospheric surface layer. It can be seen, however, by comparing Figure 8.4.4 to Figure 8.4.9 that the field is quite distinct in these two cases. There is an intense region of upward motion above the temperature discontinuity in Case 1.

The shear stress profiles in Case 1 and Case 2 (Figure 8.4.10) are quite different. Without pressure effect, there is no decrease in shear stress as the air advances downwind direction. Because there is no induced upward motion in Case 2, the shear stress profiles are sharper than those of Case 1 in Figure 8.4.5 near the edge of the internal boundary layer. For $x < o$ the surface shear stress in Case 2 remains unchanged instead of decreasing as in Case 1; for $x > o$ the surface shear stress increases as in Case 1. Figure 8.4.11 shows the distribution of surface shear stress. The surface shear stress is not monotonously decreasing; the distribution is quite distinct from that of Case 2 (Figure 8.4.6).

8.5 Airflow in Transition from Rough to Smooth Under Neutral Conditions --Turbulent Energy Model

8.5.1 Retaining pressure terms: Case 1 - Here we will consider the airflow from rough to smooth terrain with a roughness parameter

of $m \simeq 5$. In this case, we assume that the distribution of shear stress is proportional to the turbulent kinetic energy, this assumption is based on experimental work. We also assume that the transport of turbulent energy is the same as the transport of momentum and the dissipation length scale is related to the scale of mixing length. It has been assumed by one researcher that the equilibrium velocity profile in the upstream position can be used to compute the shear velocity gradient for the vertical advective term in the turbulent energy equation (Peterson, 1969); however, no such assumption has been made in our model. We then integrate the set of equations in the model to obtain numerical results.

The velocity profiles obtained by this model, are shown in Figure 8.5.1. Since in this model the magnitude of the pressure gradient force is larger in the upstream region, the air moves faster, as shown at Curve 2 in this case, than at Curve 2 in Figure 8.1.1 which is based on the mixing length model. The air after passing through the roughness discontinuity moves much faster, as indicated in Curves 3, 4 and 5, than that predicted by the simplest model of mixing length. These results can be anticipated, because the mixing length model does not take the history of a particle into consideration. On the other hand, the turbulent kinetic energy model does include the advective terms and diffusion term. At a downstream station, therefore, the air parcel at a fixed point inherits part of the momentum flux or turbulent energy coming from the upstream region by the advection of the medium, and also gains part of its energy by the processes of diffusion from the air above, possessing a relatively large amount of turbulent energy or momentum flux.

The wind profile of Curve 5 shows a distinct feature that is absent from the mixing length model. There is a "kink" in the upper region of the profile, which is not observed by the mixing length model. The "kink" in wind profiles is produced by fast moving air in the lower region of the surface layer. A limited amount of experimental work confirms the existence of the "kink" in the wind profile as shown in Bradley's data in Figures 8.5.1a and 8.5.1b, and Yeh and Nickerson's data in Figure 8.5.1c.

Figure 8.5.2 shows the pressure field for the turbulent energy model. The pressure gradient force is slightly larger in the turbulent energy model than in the mixing length models. The pattern of vertical motion as shown in Figure 8.5.3 is similar to the case obtained by the mixing length model, as shown in Figure 8.1.3.

The shear stress profiles at various locations are shown in Figure 8.5.4. Curve 2 indicates that the shear stress in the upstream station at nondimensional distance of $x = -8.0 \times 10^2$ is increased by the action of the dynamic pressure force; the magnitude of the shear stress is greater than unity. The shear stress at Curve 2 in Figure 8.5.4 is greater than unity, while the shear stress at Curve 2 in Figure 8.1.4 of k-theory may be less than unity. The shear stress profiles appear to be much steeper above the constant shear stress layer than that of k-theory, as indicated by Curves 3, 4 and 5 in Figure 8.5.4.

The "kink" in the wind profile, as shown in Curve 5 in Figure 8.5.1, appears in response to the combined action of diffusion and advection of turbulent kinetic energy, and can be explained by the distribution of shear stress profile. Due to the advection and diffusion of the turbulent kinetic energy, the surface shear stress also shows a

much larger value than that of the mixing length model, as indicated in Figure 8.5.5. The magnitude of the surface shear stress increases at a much faster rate than that of the mixing length model after the air passes through the roughness discontinuity. For the rough-smooth transitions, the inflection point at the wind profile is less visible in Peterson's model. It can, however, be clearly detected in Curve 5 in Figure 8.5.1 of our model. This difference between our model and Peterson's model may be due to the following differences: since in our model we have included the pressure terms in our equations, we also use the vertical momentum equation; our choice of the constant of proportionality which relates the shear stress to turbulent kinetic energy is 0.25, a value larger than the value 0.16 used by Peterson. Furthermore, Peterson does not directly solve the exact form of the horizontal momentum equation; the vertical advective term is approximated by using the logarithmic wind profile in the upstream location.

Figure 8.5.6 shows the nondimensional wind shear ϕ versus the distance from the roughness discontinuity. Curve 2 is at an upstream location, which reveals that the roughness discontinuity has an effect on the upstream flow. The nondimensional wind shear is usually assumed to be equal to unity under neutral stratification. However ϕ may not be equal to unity for airflow over inhomogeneous terrain under neutral conditions. All of the nondimensional wind shear ϕ shown in Figure 8.5.6 are less than unity. Initially the gains of the turbulent kinetic energy immediately after the change of roughness are fairly small. As the fetch increases, however, the air continuously gains turbulent kinetic energy, leading to continuously smaller values of nondimensional wind shear profiles, as shown in Curves 3 and 4. The

minimum value of the nondimensional wind shear is displaced toward much higher levels, as the air moves over a fairly long fetch in the downstream direction. Initially the turbulent energy adjusts slowly to new surface conditions, however, after some distance, the turbulent energy will continually adjust itself to new surface conditions. The nondimensional wind shear, therefore, will shift toward the upstream value of unity, and the air will gradually reestablish its equilibrium with surface conditions.

The nondimensional wind shear less than unity is also observed by Busch and Panofsky (1968), who analyzed the data obtained from the measurement at Round Hill near South Dartmouth in Massachusetts by Record and Cramer (1966) for the period 1960 to 1963. They used two towers, as shown in Figure 8.5.7: One is located at a rough surface covered by open fields, bushes and woods, and during the above mentioned period data were collected under the conditions of the mean westerly wind; the other tower is located in a smooth area covered by grass 40 miles north of the shoreline of Buzzard Bay. Mean wind directions during the experiments varied from south through west to north. The grass trimmed to a length of 5 to 10 centimeters, covers a radius of about 100 meters to the west and north around the tower, T_1. The north and east of tower T_2 are covered by a wooded area, which is about 300 meters away from tower T_1. Tower T_2 is installed about 900 meters to the north-west of tower T_1. The site area is covered with brush of an average height of 1.5 meters. The surrounding area of tower T_2, except in the west, is covered by scattered woods with an average height of about 8 meters.

Busch and Panofsky (1968) analyzed the data for the non-dimensional wind shear measured at Round Hill Station, as shown in Figure 8.5.8. For unstable conditions, the solid line represents the best fit by the KEYP equation for the data obtained by Swinbank; for stable conditions, the line is based on McVehil's formula. For tower T_2, Swinbank's curve fits the Round Hill observational data well; however, the data in tower T_1 show a systematic lower value of about one half of the value at tower T_2. This difference can be explained in that tower T_2 is influenced by a relative homogeneous, rough terrain and the turbulence there has adjusted to the surface conditions. When air reaches tower T_1, however, the area is relatively smooth, and the air accelerates and the intensity of the turbulence decreases. Since the air parcels coming from upstream carry with them relatively high turbulent energy, and since the velocity adjusts rapidly to the underlying terrain, the nondimensional wind shear at tower T_1 is only half the value at tower T_2.

Evidence of the nondimensional wind shear that is not equal to unity under neutral conditions is also indicated in the wind tunnel experiments (Yeh and Nickerson, 1970). Yeh and Nickerson investigated the flow in transition from a smooth to rough surface with the upwind and downwind parameters $z_o = 4.08 \times 10^{-4}$ in and $z_1 = 3.06 \times 10^{-2}$ in, respectively. From analysis of their data, we find that the non-dimensional wind shear is greater than unity, as in Figure 8.5.9. This implies that the flow is not in equilibrium with the new surface.

8.5.2 Turbulent energy budget - The various terms in the turbulent energy equation are shown in Figures 8.5.10 and 8.5.11, 8.5.12 and 8.5.13 for different locations. In these figures, Curve 1 represents

the horizontal advection term; Curve 2, vertical advection terms; Curve 3, the production term; Curve 4, the diffusion term; and Curve 5, the dissipation term.

The various terms in the turbulent energy equation at upstream station $x = -4.4 \times 10^{-5}$ are shown in Figure 8.5.10. The production term is equal to the dissipation term, and other terms are negligibly small. The production and dissipation of turbulent energy are the same, which implies that the nondimensional wind shear is equal to unity, and the velocity profile follows the logarithmic law. Figure 8.5.11 at station $x = 2.7 \times 10^{4}$ shows that the turbulent energy at almost any level is continuously decreasing. The high turbulent energy is diffused downward: as a result, in the lower level, the turbulent energy increases by diffusion; in the higher level, the turbulent energy decreases, since part of its turbulent energy has been transported to the lower level. In Figure 8.5.12 at $x = 4.4 \times 10^{5}$, the air gains turbulent energy in the lower layer by processes of diffusion and loses turbulent energy in the higher layer by the action of turbulent diffusion and dissipation exceeding production.

The maximum difference between the production and dissipation of turbulent energy gradually moves upward, as can be seen by comparing Curves 3 and 5 in Figure 8.5.11 and Figure 8.5.12. In the lower layer the air continuously restores its equilibrium with the underlying surface; therefore, this difference between dissipation and production gradually vanishes. In Figure 8.5.13 at $x = 1.8 \times 10^{6}$, the decrease of turbulent energy for a given parcel of air becomes smaller, as shown at Curves 1 and 2, and the magnitude of positive and negative diffusion terms for different regions also decrease. The flow attempts

to restore its new equilibrium with the underlying surface, since the difference between the production term and the dissipation term decreases, as shown in Curves 3 and 5. Since nondimensional wind shear is equivalent to the ratio of the production of turbulent energy to the dissipation of turbulent energy in the turbulent energy model, the distribution of the nondimensional wind shear ϕ and the location of minimum value of ϕ can be easily inferred by comparing Curve 5 representing the dissipation term with Curve 3 representing the production term in the same Figures 8.5.10, 8.5.11, 8.5.12 and 8.5.13.

For rough to smooth transition, the air accelerates, and hence the nondimensional wind shear is less than unity. This phenomenon was explained by Busch and Panofsky (1968), who suggested that the turbulent energy of a given parcel of air decreases since dissipation far exceeds production. However, the statement is only true when there is no other mechanism involved. If the turbulent energy of a given parcel of air is continuously decreasing, ϕ may be greater than unity. In view of the increase of surface shear stress after the change of surface discontinuity and the relative increase of the surface shear stress in the turbulent energy model as compared to the mixing length model, the explanation is only partially correct. In the turbulent energy model the nondimensional wind shear is equal to the ratio of the production term to the dissipation term. Since the dissipation of turbulent energy exceeds the production of turbulent energy, ϕ is less than unity for air in transition from a rough to smooth surface.

An interpretation of the value of ϕ, which is less than unity, may be considered from another point of view. Since the turbulent

energy is assumed to be proportional to u_*^2 in the turbulent energy model, the friction velocity and turbulent energy still maintain some portion of their upstream value by the processes of advection and diffusion, and the velocity profile adjusts itself more rapidly to the underlying surface.

8.5.3 Neglecting pressure terms: Case 2 - In this case, all conditions are the same as in Case 1 in section 8.5.1, except the pressure terms are excluded. The distribution of horizontal velocity, vertical velocity, shear stress, surface shear stress, and non-dimensional wind shear are shown in Figures 8.5.14, 8.5.15, 8.5.16, 8.5.17, and 8.5.18, respectively. Comparison of Case 1 with Case 2 in this section is similar to the argument pertaining to the comparison of Case 1 and Case 2 in section 8.1. As expected, the main difference in Case 1, and Case 2 in section 8.5 is in the physical variables near the point of roughness discontinuity. Curve 3 in Figure 8.5.18 in comparison with Curve 3 in Figure 8.5.6, reveals that the nondimensional wind shear where there is zero pressure gradient is smaller than the nondimensional wind shear where there is a pressure gradient force. This result implies that the dissipation of turbulent energy in the case with zero pressure gradient may be larger than dissipation in the case with pressure force in the lower layer of an air column or the production of turbulent energy in Case 2 may be larger than that of Case 1.

8.6 A Theory--The Turbulent Energy--Newtonian Model

The flow conditions in this section are the same as in section 8.5. The numerical results of integrating a closed set of equations in the turbulent energy - Newtonian Model are presented in this section for

the flow with step change in surface roughness under neutral conditions. Physical quantities of the model that are similar in this section and in the previous sections will not be discussed here.

8.6.1 Retaining pressure terms: Case 1 - The wind profiles in this case are shown in Figure 8.6.1. The inflection point is visible in Curve 5, but the curvature is smaller than in Section 8.5.1. The pressure and vertical velocity fields are shown in Figure 8.6.2 and Figure 8.6.3, respectively. The general features of the pressure and vertical velocity fields are not significantly different in this case and the case in Section 8.5. The distribution of the shear stress is shown in Figure 8.6.4. The shape of Curve 2 in this case is quite different from the curve presented in Section 8.5 (Figure 8.5.4). In general, the magnitude of the shear stress is slightly smaller in this case than the shear stress in Section 8.5 (Figure 8.5.4). The surface shear stress is shown in Figure 8.6.5. The difference between this model and the turbulent energy model is that after the air flows over the roughness discontinuity, the surface shear approaches an asymptotic value faster than it does in the case in Figure 8.5.5. The non-dimensional wind shear is shown in Figure 8.6.6.

The nondimensional wind shear in the turbulent energy model has been assumed equal to the ratio of production to dissipation. That is, however, inconsistent with the definition of nondimensional wind shear. The nondimensional wind shear assumed in the turbulent energy model is true only if the dissipation is assumed equal to $\tau^{3/2}/kz$. In the present model, no such assumption about ϕ has been made. The value of the nondimensional wind shear, as shown in Figure 8.6.6, is larger than that predicted by the turbulent energy model. If we

would not have assumed the nondimensional wind shear in the turbulent energy model to be equal to unity below the nondimensional vertical height of $z < 500$, the calculated surface shear stress would be unrealistic. In the present case, we assume that the logarithmic law is only valid in a very shallow layer ($z < 10$ for $x > 0$) near the earth's surface. The predicted surface shear stress is in better agreement with field data than existing theories, (Figure 8.8.5).

The turbulent energy in this case is shown in Figure 8.6.7. The turbulent energy model assumes that the turbulent energy is linearly correlated to the shear stress. Such an assumption implies that by obtaining the turbulent energy, the shear stress can automatically be derived. This assumption, however, is invalid. For example, no shear is present in the flow in the grid generated turbulence along a moving wall (Uzkan and Reynolds, 1967). By inspection of the numerical results obtained by the turbulent energy - Newtonian Model, the assumed relation between turbulent energy and shear stress in the turbulent energy model does not hold in general. This result was also confirmed by Yeh and Nickerson (1970). Each term in the turbulent energy equation at various locations is shown in Figures 8.6.8, 8.6.9, 8.6.10 and 8.6.11. The general shapes are the same in this case and in the case predicted by the turbulent energy model. They, however, differ in detail. The difference between the production and dissipation is smaller in the present case than in the case predicted by the turbulent energy model. Such a comparison implies that the air in this case restores its equilibrium near the earth's surface faster than that predicted by the turbulent energy model.

8.6.2 Neglecting pressure terms: Case 2 - The predicted physical quantities in Case 1 and Case 2 have similar distributions, they differ near the roughness discontinuity. The wind profiles are shown in Figure 8.6.12. The vertical velocity is shown in Figure 8.6.13, the shear stress profiles in Figure 8.6.14, the surface shear stress in Figure 8.6.15, the nondimensional wind shear in Figure 8.6.16, and the turbulent energy profiles in Figure 8.6.17. Each term in the turbulent energy equation at various locations is subsequently shown in Figures 8.6.18, 8.6.19, 8.6.20 and 8.6.21.

8.6.3 Mechanism of turbulent energy transfer - The mechanism of turbulent energy transfer is capable of explaining the behaviors of shear stress profiles and, hence, the velocity profiles. Based on the previous analysis of various terms in the turbulent energy equation, we will propose the mechanism of turbulent energy transfer in a column of air. For a steady state, two-dimensional turbulent boundary layer flow, there is no local rate of change of turbulent energy; the various terms, namely horizontal advection, vertical advection, production, diffusion and dissipation terms, are in balance. There exists two distinct layers in a column of air: one is near the surface of the earth; the other is above the first layer, as shown in Figure 8.6.22. In the lower layer the difference between production and dissipation of turbulent energy is relatively small; the downward motion results in an increase of turbulent energy, and the diffusion of turbulent energy also contributes to the net gain of turbulent energy. As a result, the outgoing turbulent energy by horizontal advection in the layer is larger than the incoming turbulent energy by horizontal advection in the same layer. On the other hand, in the

upper layer, the dissipation exceeds the production; however, the downward motion still contributes to the gain of the turbulent energy. The diffusion of turbulent energy reverses its sign and becomes a negative contribution to the turbulent energy. Consequently, the outgoing turbulent energy by horizontal advection is less than the incoming turbulent energy by horizontal advection. Such a turbulent transfer mechanism can be used to explain the change of shear stress profiles in Figure 8.6.4. In the lower layer the outgoing turbulent energy by horizontal advection increases, which results in an increase in the shear stress, as shown in the sequences of Curves 3, 4 and 5. In the upper layer the outgoing turbulence by horizontal advection decreases, which results in a reduction of the magnitude of the shear stress, as shown in the curves. The acceleration of a given air parcel can be observed from the slope of the shear stress profile. Since the acceleration of a given parcel of air depends on the vertical gradient of shear stress, the distribution of wind profile can be explained from the distribution of shear stress.

8.6.4 Growth of internal boundary layer - The variation of the internal boundary thickness with distance from the roughness discontinuity ($m \simeq 5$) for various theories, i.e., the k-theory, Bradshaw's (or Peterson) theory and the present theory is shown in Figure 8.6.23. The concept of an internal boundary layer which postulates the growth of the internal boundary beginning right at the roughness discontinuity is not applicable. The growth of the internal boundary layer begins upstream of the discontinuity at a nondimensional distance of the order 10^4, this result is further confirmed in wind tunnel experiments (Yeh and Nickerson, 1970). The height of the interface defined in this

study is that where the slope of the shear stress profile at a location intersects the shear stress profile at the upstream location, or where the value of nondimensional shear stress difference, $\tau - \tau_{*_o}$ is less than 0.1.

The growth of the internal boundary layer predicted by the k-theory in this study for smooth to rough transition as shown in Figure 8.6.23 further confirms the 0.8 power law predicted by previous workers (Elliott, 1958; Panofsky and Townsend, 1964; Taylor, 1969; Peterson, 1969). However, for rough to smooth transition, the growth of the internal boundary layer predicted by various models indicates that the rate of growth follows the 0.7 power as shown in Figure 8.6.23 rather than the 0.8 power, since the boundary adjustment is more slow in the case with rough to smooth transition than the case with smooth to rough transition. Although various theories predict the same rate of the growth of the internal boundary layer for rough to smooth transition, the heights of the interface predicted by various models are different as shown in Figure 8.6.23. The k-theory model predicts a rather high height of the interface, while the Bradshaw-Peterson model gives a rather low height of the interface. The height of the interface predicted by various models is approximately one tenth the downstream fetch for nondimensional distances larger than 10^4.

8.7 Comparison of Numerical Results with Wind Tunnel Measurements

The numerical integration of the mixing length model under a neutral condition is compared with experimental data measured from the wind tunnel, as shown in Figure 8.7.1 (Yeh and Nickerson, 1970). The flow Yeh and Nickerson consider is in transition from smooth to rough. For the case with a small change in surface roughness, the upstream

and downstream roughness parameters are $z_o = 1.4 \times 10^{-4}$ in and $z_1 = 7.0 \times 10^{-4}$ in, respectively, and the upstream surface friction velocity is $u_{*_o} = 1.17$ fps. In numerical integration, the pressure terms are retained in the governing equations. The velocity profiles obtained by numerical computations are in agreement with experimental data up to about $x = 6$ in obtained by Yeh and Nickerson (1970). For a large change in surface roughness, the distribution of the surface shear stress qualitatively agrees with experimental data, as can be seen by comparing Figure 8.2.5 with Figure 8.2.5a.

In the numerical model with pressure terms and without pressure terms in the governing equations, no significant change in the predicted wind profiles have been observed for the flow with a small change in surface roughness, the large discrepancy between the experimental data and numerical results exists near the roughness discontinuity. Further experimental investigations are required to eliminate the discrepancy.

8.8 Comparison of Surface Shear Stress with Various Theories

Despite the simplicity of mixing length model, the predicted value of surface shear stress agrees with the analytical models advanced by Elliott (1959), Panofsky and Townsend (1964), as well as with field data obtained by Bradley (1968). For air moving from a rough to a smooth surface, Curve 1 in Figure 8.8.1 illustrates present numerical results. Such results compare well with the theories of Elliott, Panofsky and Townsend. Curve 2 and 3, in which we have assumed that the nondimensional wind shear prescribed as a function of downstream distance is less than unity, fit the field data much better. This may

be considered equivalent to taking the past history of air parcels into account. Ignoring the past history of air parcels is the shortcoming of the mixing length model. For the air flowing from rough to smooth surface as seen in Figure 8.8.1, both the mixing length model and analytical models lead to an under prediction of the surface shear stress.

For the air flowing from smooth to rough terrain, the surface shear stress predicted by the mixing length model and analytical models (Elliott, 1959; Panofsky and Townsend, 1964) agrees with experimental results (Figure 8.8.2). Distribution of surface drag similar to the data of Bradley have been obtained in wind tunnel for the flow from a smooth surface to a canopy consisting of model trees as shown in Fig. 8.8.3 (Meroney, 1968). The surface shear stress is overestimated by previous models in this case, while the values of the surface shear stress are underestimated as compared to previous models of the air from rough to smooth terrain. This can be explained in that these models did not have the advection and diffusion terms for turbulent energy in their models. Including these terms in the turbulent energy model does predict the surface shear stress better than other models as shown in Figure 8.8.4, if the particular adjust merits in the model has been made. Curve 1 in Figure 8.8.4 gives the predicted surface shear stress distribution which agrees well with the experimental data. The significant difference between the turbulent energy model and the mixing length model or analytical models is that immediately after the air passes the roughness discontinuity, the surface shear stress predicted by the turbulent energy model rises at a much faster rate than the shear stress of previous models. The surface shear stress

predicted by the turbulent energy - Newtonian Model, shown in Figure 8.8.5, is in better agreement with field data than other existing theories.

Chapter IX

SUMMARY AND CONCLUSIONS

In this study, the mixing length and turbulent energy models have been used to describe air flowing either from a rough to smooth transition or from a smooth to rough transition under different stability conditions in the atmospheric boundary layer. The models describe the adjustment of the flow to the nonhomogeneous surface with abrupt change in surface roughness and temperature, with the flow at right angles to the line of roughness discontinuity. No hydrostatic assumption has been made about the flow, although the pressure terms and buoyancy force are retained in the governing equations. The flow in the far upwind location is in equilibrium with the underlying surface. The presented theory does not assume that the shear stress is proportional to the turbulent energy as the turbulent energy model does, since this relation does not hold, in general, for flow not in equilibrium. The turbulent energy equation has been retained, however; the scale lengths in the equation have been postulated, and are based on experimental analyses and theoretical considerations. The theory describes the flow governed by horizontal momentum, vertical momentum, continuity, turbulent energy equations, and a similarity form of shear stress that depends on turbulence, one scale length and velocity gradient. In the theory the processes of the diffusion of turbulent energy is postulated to have the same mechanism as the transport of momentum. The flow problem has been simulated by a high speed computer, the CDC 6400 at Colorado State University.

The mean horizontal, mean vertical velocity field, pressure field, shear stress, nondimensional wind shear and turbulent energy in the atmospheric surface layer have been predicted by a numerical technique. The following conclusions can be drawn from the analyses of the present investigations. The conclusions are numbered in accordance with the objectives stated in the introduction.

(1) The presented theory is not based on a priori assumption about the distribution of wind and shear stress profiles, but rather on empirical hypotheses deduced from theoretical and physical considerations and from the analyses of experimental work. None of the other existing theories has the ability to predict both turbulent energy and shear stress profiles, in which the prediction of one variable does not imply that we have the other. The predicted physical quantities agree with the available experimental data better than any previous model to date. The development of the present model, indicates that further research to investigate more complicated and complete models ought to prove rewarding.

(2) In relatively rough terrain, the air adjusts to the underlying surface more rapidly than in smooth terrain.

(3) For air flowing from a rough to smooth terrain, the dissipation of turbulent energy exceeds the production of turbulent energy for the flow downstream.

(4) Based on the analysis of the numerical results, a mechanism of turbulent energy transfer is proposed. It can be used to explain the distribution of shear stress profiles and, in turn, the distribution of wind profiles. There are two regimes of turbulent energy transfer in a column of air; for a rough to smooth transition, one

regime is in the lower layer, where the horizontal export of turbulent energy exceeds the horizontal import of turbulent energy; the second regime is in the upper layer, where the horizontal import of turbulent energy exceeds the horizontal export of turbulent energy.

(5) Some numerical schemes have already shown remarkable success without theoretical support. In this investigation we have proved several theorems of convergence, which can be used to show that certain numerical schemes are convergent.

(6) A "modified" Newton's method is used to solve the system of nonlinear equations, thus describing the flow in the atmospheric turbulent boundary layer, by an iterative process.

(7) The equation of continuity has been put in the form of a second order partial differential equation that automatically satisfies the boundary conditions at any moment. Thus, instability arising from the continuity equation has been avoided.

(8) In the turbulent energy model developed by Peterson (1969), the vertical wind shear in the vertical advection term of the horizontal momentum equation has been approximated by using the logarithmic wind profile in the upwind location. In solving the turbulent energy model, we have used the exact difference equations, and the pressure terms neglected by Peterson are thus included.

(9) The wind profiles, the vertical velocity field and the shear stress profiles near the roughness discontinuity depend very much upon whether or not the pressure terms are retained or neglected in the governing equations.

(10) Neglecting the pressure terms in the governing equations results in overestimating the value of vertical motion for the flow

either from a rough to smooth transition or from a smooth to rough transition under neutral condition. The maximum region of vertical motion in both cases is displaced upward from the origin of the roughness discontinuity, if the pressure terms are ignored.

(11) The effects of roughness discontinuity on the upwind flow have been observed in both the numerical models and field data. These effects can be seen from the wind profiles, vertical velocity field and shear stress profiles.

(12) The nondimensional wind shears become different near the roughness discontinuity, depending on whether the pressure terms in the governing equations are retained or neglected.

(13) The distribution of the predicted quantities are quite different in neutral and unstable cases. For unstable stratification, the zone of maximum turbulent energy is located near the edge of internal boundary layer.

(14) No inflection point in the wind profiles under neutral condition has been observed in the model of k-theory, but it has been observed in both the turbulent energy and turbulent energy-Newtonian models. However, the inflection point is less visible in the turbulent energy-Newtonian model.

(15) For a small change in surface roughness, the wind profiles simulated by the numerical method are in very good agreement with the data obtained in a wind tunnel and in the field. Thus, the flow from one terrain to a new terrain can be simulated by a wind tunnel. The distribution of surface shear stress simulated by numerical technique is in qualitative agreement with the data measured in a wind tunnel for a large change in surface roughness; however, the large discrepancy

in wind profiles obtained by the numerical model and measured in a wind tunnel exists near the roughness discontinuity. More experimentation is required to determine the influence of the roughness parameter on the flow near the roughness discontinuity.

(16) Nondimensional wind shear is an important parameter in understanding the properties of turbulence and wind profiles in the atmospheric surface layer. The k-theory implies that the nondimensional wind shear is equal to unity, disregarding accelerating or decelerating flow. Both theories, i.e., the turbulent energy model and the turbulent energy-Newtonian model, predict that the nondimensional wind shear is less than unity for accelerating flow. The field data collected at Round Hill Station and in a wind tunnel also confirm that nondimensional wind shear is not equal to unity for the accelerating or decelerating air.

(17) The distribution of surface shear stress predicted by various numerical models is in good agreement with analytical models and field data. The distribution of surface shear stress predicted by the presented theory is in excellent agreement with field data, since the theory takes into account the past history of a given air parcel and the characteristics of turbulence.

(18) All theories agree rather well in predicting the mean wind far downstream of roughness discontinuity, except near the edge of internal boundary layer, where wind profiles predicted by various models differ considerably. A discrepancy in predicting the physical quantities by various models exists near the roughness discontinuity.

(19) For most conditions, the dissipation and production terms in the turbulent energy equation are usually larger than other terms. Therefore, the k-theory model may be regarded as an approximation to the presented model and hence, in predicting the mean flow field, the k-theory model is relatively insensitive to the particular forms of shear stress used by previous researchers. However, when the dissipation of turbulent energy far exceeds the production of turbulent energy, the k-theory may not apply so well.

(20) In view of the improved predicted surface shear stress of the presented theory, the mixing length model in the fully developed turbulent boundary layer is not applicable in the transitory region. Wind tunnel observations also confirm this result.

(21) In view of the region of maximum absolute value of vertical motion located above the roughness discontinuity and the effects of this discontinuity on the upstream flow under various stability conditions, the traditional concept of the internal boundary layer introduced by Elliott (1958) is not applicable.

(22) The growth of the internal boundary layer does not begin right at the roughness discontinuity, but rather some distance upstream. The growth of the internal boundary for smooth to rough transitions follows the 0.8 power law, however for rough to smooth transitions, it follows the 0.7 power. The heights of the interface predicted by various models are different. The height of the interface predicted by the k-theory is higher than that of other theories, the height of the interface predicted by the present theory lies between that of the k-theory and that of the Bradshaw-Peterson theory.

REFERENCES

REFERENCES

Ames, W. F., 1965: *Nonlinear partial differential equations in engineering.* Academic Press.

———, 1969: *Numerical methods for partial differential equations.* Barnes and Noble, Inc. 291 pp.

Apelt, C. J., 1969: *The lecture note distributed in summer school.* Colorado State University.

Barad, M. L., 1959: Analysis of diffusion studies at O'Neill. *Advances in Geophysics,* 6, 389.

Beckwith, I. E., and D. M. Bashnell, 1968: *Calculation of mean and fluctuating properties of the incompressible turbulent boundary layer.* Proceedings Computation of Turbulent Boundary Layers, Vol. I-1968 AFOSR-IFP Stanford Conference, Stanford Univ. Mech. Engineering Dept.

Bradley, E. F., 1968: A micrometeorological study of velocity profiles and surface drag in the region modified by a change in surface roughness. *Quart. J. Roy. Meteor. Soc.,* 94, 361-379.

Bradshaw, P., D. H. Ferriss, and N. P. Atwell, 1967: Calculation of boundary-layer development using the turbulent energy equation. *J. Fluid Mech.,* 28, 593-616.

Busch, N. E. and H. A. Panofsky, 1968: Recent spectra of atmospheric turbulence. *Quart. J. Roy. Meteor. Soc.* 94, 132-148.

Businger, J. A., J. C. Wyngard, Y. Gzumi and E. F. Bradley, 1971: Flux-profile relationships in the atmospheric surface layer. *J. Atmos. Sci.* 28, 2. 181-189.

Cermak, J. E., V. A. Sandborn, E. J. Plate, G. J. Binder, H. Chuang, R. N. Meroney and S. Ito, 1966: *Similarity between meteorological wind tunnel flows and atmospheric motions.* CER-JEC-VAS-EJP-GJB-HC-RNM-SI17.

Charnock, H., 1967: Flux gradient relations near the ground in unstable conditions. *Quart. J. Roy. Meteor. Soc.,* 93, 97-100.

Clarke, R. H., 1970: *Recommended methods for the treatment of the boundary layer in numerical models.* Australian Meteorological Magazine. Vol. 18, No. 2, 51-71.

Cramer, H. E., et al., 1966: *Round Hill turbulence measurements.* Technical Report to U.S. Army Electronics Command, Grant No. DA-AMC-28-043-65-G10, December 1960, Dept. of Meteor., Mass. Inst. of Tech.

_____, and F. A. Record, 1969: *Properties of turbulent energy spectra and cospectra in the atmospheric surface layer.* U.S. Army Electronics Command, Atmospheric Technical Report ECOM-64-G1-F. Sciences Laboratory, Research Division, Fort Huachuca, Arizona. 95 pp.

Dalrymple, P. C., 1961: *Tech. Rep. ES-2,* Quartermaster Res. Center, Natick, Mass.

Deacon, E. L., 1949: Vertical diffusion in the lowest layers of the atmosphere. *Quart. J. Roy. Meteor. Soc.,* 75, 89-103.

Deacon, E. L., 1962: Aerodynamic roughness of the sea. *J. Geophys. Research,* 67, p. 3167.

Delsol, F., K. Miyakoda and R. H. Clarke, 1971: Parameterized processes in the surface boundary layer of an atmospheric circulation model. *Quart. J. Roy. Meteor. Soc.* 97, 181-208.

Dryden, H. L., 1947: *Some recent contributions to the study of transition and turbulent boundary layer.* Nat. Adv. Comm. Aero. Wash. Tech. Note. No. 1168, 32 p.

Dutton, J. A., and G. H. Fichtl, 1969: Approximate equations of motion for gases and liquids. *J. of Atm. Sci.,* 26, 241-254.

Donaldson, C. duP. and H. Rosenbaum, 1968: *Calculation of the turbulent shear flows through closure of the Reynolds equations by invariant modeling.* ARAP Rept. No. 127.

Ellison, T. H., 1957: Turbulent transport of heat and momentum from a rough plane. *J. Fluid Mech.* 2, 456-466.

Elliott, W. P., 1958: The growth of the atmospheric internal boundary layer. *Trans. Amer. Geophys. Union* 39, 1048-1054.

Estoque, M. A., 1962: A sea breeze as a function of prevailing synoptic situation. *J. Atmos. Sci.* 19, 244-250.

_____, and E. M. Bhumalker, 1970: A method for solving the planetary boundary-layer equations. *Boundary-Layer Meteor.* 1, 169-194.

Fisher, Edwin L., 1961: A theoretical study of the sea breeze. *J. Meteor.* 18, 216-233.

Forsythe, G., and W. Wasow, 1960: *Finite difference methods for partial differential equations.* Wiley and Sons, New York.

Fox, L., 1962: *Numerical solution of ordinary and partial differential equations.* London, Pergamon Press.

Glushko, C. S., 1965: *Turbulent boundary layer on a flat plate in an incompressible fluid.* Acad. Nauk, U.S.S.R., S. Mekhan, No. 4, 13. (Translation, NASA TT-F-10,080).

Goldstein, S., (ed.), 1965: *Modern development in fluid dynamics.* Dover Publications, Inc., Vol. II.

Greenspan, D., 1968: *Lectures on the numerical solutions of linear, singular and nonlinear differential equation.* Prentice-Hall, Inc., Englewood Cliffs, New Jersey, 186 pp.

Hinze, J. O., 1968: *Turbulence.* McGraw Hill, New York.

Holzman, B., 1943: The influence of stability on evaporation. *Ann. N.Y. Acad. Sci.* 44, 13-18.

Jacob, W., 1939: Umformung eines turbulenten geschwindigkeits-profiles. *Z angew. Math. Mech.*19, 87-100, (Trans. Variation in velocity profile with change in surface roughness. N.A.C.A., Tech. Mem. No. 951).

Jeffreys, H., 1931: *Cartesian Tensors,* Cambridge University Press.

Jensen, Martin, 1958: The model-law for phenomena in natural wind. *Ingenioren-international edition,* 2, 4, 121-128.

Kantorovich, L. V., 1949: On Neuton's method. *Trudy Mat. Inst. Steklov.* 28, 105-144.

Klebanoff, P. S., 1955: Characteristics of turbulence in a boundary layer with zero pressure gradient. *NACA Rept.* 1247.

Kovasznay, Leslie S. G., 1970: The turbulent boundary layer. *Annual Review of Fluid Mechanics.* Vol. 2, 95-112. Ed. Van Dyke M., Vincenti, W. G. and Wehausen, J. V.

Laykhtman, D. L., and S. M. Ponomareva, 1969: On the ratio of the turbulent transfer coefficients for heat and momentum in the surface layer of the atmosphere. *Izv. Atmos. and Ocean Phys.* 5, 12.

Lettau, H. H., and B. Davidson, 1957: *Exploring the atmosphere's first mile.* Pergamon Press, New York.

____, 1962: *Studies of the three-dimensional structure of the planetary boundary layer.* Annual Report DA36-039-SC-80282, U.S. Army Electronic Proving Ground.

____, 1967: In the collection and processing of field data. *Interscience,* New York, 3-40.

Lumley, J. L., and H. A. Panofsky, 1964: The structure of atmospheric turbulence. *Interscience, New York,* 239 pp.

McDonald, H. 1968: The departure from equilibrium of turbulent boundary layers. *Aero. Quart.* 19, 1.

McVehil, G. E., 1964: Wind and temperature profiles near the ground in stable stratification. *Quart. J. Roy. Meteor. Soc.* 90, 136-146.

Mellor, G. L., and H. J. Herring, 1968: *Two methods of calculating turbulent boundary layer behavior based on numerical solutions of the equations of motion. I. Mean Velocity Field Method; II. Mean Turbulent Field Method.* Proceedings - Computation of Turbulent Boundary Layers, Vol. I, 1968 AFOSR-IFP-Stanford Conference, Stanford Univ. Engr. Dept.

_____, 1970: *A study of turbulent boundary layer, Part II, Mean turbulent field closure.* Department of Aerospace and Mechanical Sciences, Report No. 914, 1-45.

Meroney, R. N., 1968: Characteristics of wind and turbulence in and above model forests. *J. Appl. Meteor.* 7, 780-788.

Mintz, Y., 1958: Design of some numerical general circulation experiments. *Bull. Res. Council of Israel* 7G, 67-114.

Miyakoda, K., J. Smagorinsky, R. F. Stickler and G. D. Hembree, 1969: Experimental extended predictions with a nine-level hemispheric model. *Mon. Weath. Rev.*, 97, pp. 1-76.

Monin, A. S., 1950: Inform. Bull. Chief Adminstr. *Hydrometeorol.* Serv., No. 1, 13-27.

_____, 1959: Smoke propagation in the surface layer of the atmosphere. *Adv. in Geophys.* 6, Academic Press, New York, 331-343.

_____, A. M. Obukhov, 1954: Basic regularity in turbulent mixing in the surface layer of the atmosphere. *Trudy Geophys. Inst. ANSSSR,* No. 24, 163.

_____, 1970: *The atmospheric boundary layer.* Annual Review of Fluid Mechanics, 2, Annual Reviews, Inc., California Ed. Van Dyke M., Vincenti, W. G. and J. V. Wehausen.

____, and Y. M. Yaglom, 1966: *Statistical hydromechanics,* Part 1: The mechanics of turbulence. Translation U.S. Dept. of Commerce, Joint Publications Research Service, No. 37, 763 Washington, D.C., 605 pp.

Monteith, J. L., 1957: Dew. *Quart. J. Roy. Meteor. Soc.* 83, 322-341.

Nee, V. W., and L. S. G. Kovasznay, 1969: Simple phenomenological theory of turbulent shear flows. *Phys. Fluids* 12:3, 473-484.

Neuman, J., and Y. Mahrer, 1971: A theoretical study of the land and sea breeze circulation. *J. of Atm. Sci.* 28, 532-542.

Nickerson, E. C., 1968: Boundary layer adjustment as an initial value problem. *J. Atmos. Sci.* 25, 207-213.

Nikuradse, J., 1933: Stromungsgesetze in rauken rohren. *Forsch. Arb. Ing. - Wes.* 361, also NACA TM 1292 (1950).

Obukhov, A. M., 1946: Turbulence in an atmosphere with inhomogeneous temperature. *Tr. Inst. Teor. Geofiz. Akad. Nauk S.S.S.R.*, 1, 95-115.

Oke, T. R., 1970: Turbulent transport near the ground in stable conditions. *J. Applied Meteor.* 9:5, 778-786.

Onishi, G., and M. A. Estoque, 1968: Numerical study on atmospheric boundary layer flow over inhomogeneous terrain. *J. Met. Soc. of Japan* 46, 280-286.

Ortega, J. M., and W. C. Rheinbolt, 1970: *Iterative solution of nonlinear equations in several variables*. Academic Press, Inc., 572 pp.

____, and M. L. Rockoff, 1966: Nonlinear difference equations and Gauss-Seidel type iterative methods. *J. SIAM Numer. Anal.*, Vol. 3, No. 3, 497-513.

Panofsky, H. A., A. K. Blackadar and G. E. McVehil, 1960: The diabatic wind profile. *Quart. J. Roy. Meteor. Soc.* 86, 390-398; 87, 597.

_____, and A. A. Townsend, 1964: Change of terrain roughness and the wind profile. *Quart. J. Meteor. Soc.* 90, 147-155.

Pandolfo, J. P., 1966: Wind and temperature for constant flux boundary layers in lapse conditions with a variable eddy conductivity to eddy viscosity ratio. *J. Atmos. Sci.* 23, 495-502.

Paulson, C. A., 1967: *Profiles of wind speed, temperature and humidity over the sea.* Ph.D. thesis, Univ. of Washington.

Plate, E. J. and C. W. Lin, 1966: *Investigations of the thermally stratified boundary layer.* Fluid Mechanics Papers, No. 5, Colorado State University.

Peterson, E. W., 1969: Modification of mean flow and turbulent energy by change in surface roughness under conditions of neutral stability. *Quart. J. Roy. Meteor. Soc.* 90, 561-576

Phillips, N. A., 1956: The general circulation of the atmosphere: a numerical experiment. *Quart. J. Roy. Meteor. Soc.* 82, 123-164.

Prandtl, L., 1925: Uber die ausgebildete turbulenz. *Z. Angew. Math. Mech.* 5, 136; Also, 1926, Proceedings of the 2nd International Congress of Applied Mechanics, Zurich.

_____, 1945: Über ein neues formelsystem für die ausgebildete turbulenz. *Nachnichten der Akad. Wiss. Göttingen Mathphys.* 6.

Priestley, C. H. B., 1959: *Turbulent transfer in the lower atmosphere.* University of Chicago Press, 130 pp.

Record, F. A., and H. E. Cramer, 1966: Turbulent energy dissipation rates and exchange processes above a nonhomogeneous surface. *Quart. J. Roy. Meteor. Soc.* 92, 519-532.

Rider, N. E., J. R. Philip, and E. F. Bradley, 1963: The horizontal transport of heat and moisture - a micrometeorological study. *Quart. J. Roy. Meteoro. Soc.* 89, 506-531.

Rose, W. G., 1966: Results of an attempt to generate a homogeneous turbulent shear flow. *J. Fluid Mech.* 25, 97-120.

Rotta, J. C., 1951: Stratische theorie nichthomogener turbulenz. *Z. Physik* 129, 547-572, and 131, 51-77.

_____, 1962: *Turbulence boundary layers in incompressible flow.* Progress in Aeronautical Sciences, Vol. 2, Pergamon Press.

Schlichting, H., 1968: *Boundary layer theory.* 6th ed. McGraw-Hill Book Company, Inc., New York.

Smagorinsky, J., S. Manabe and J. L. Hollaway, Jr., 1965: Numerical results from a nine-level general circulation model of the atmosphere. *Mon. Weath. Rev.*, 93, 727-768.

Smith, G. D., 1965: *Numerical solution of partial differential equations.* Oxford University Press.

Spiegel, E. A., and G. Veronis, 1960: On the Boussinesq approximation for a compressible fluid. *The Astrophysical J.* 131, 442-447.

Stearns, C. R., and H. H. Lettau, 1963: *Two wind-profile measurement experiments in airflow over the ice of Lake Mendota.* Annual Rept., Univ. of Wisconsin, Dept. of Meteor., 115 pp.

Takeuchi, K., 1961: On the structure of the turbulent field in the surface boundary layer. *J. Meteor. Soc. of Japan,* Ser. II, 39, 346-367.

Tani, I., 1958: *Experimental investigation of flow separation over a step.* In Görtler, H., ed., Boundary Layer Research Symposium at Freiburg, 26-29, August 1957, Springer Verlag, Berlin/Göttingen.

Taylor, R. J., 1960: Similarity theory in the relation between fluxes and gradients in the lower atmosphere. *Quart. J. Roy. Meteor. Soc.* 86, 67.

Taylor, P. A., 1967: *On turbulent wall flows above a change in surface roughness.* Ph. D. dissertation, Univ. of Bristol, Canada.

_____, 1969: On wind and shear-stress profiles above a change in surface roughness. *Quart. J. Roy. Meteor. Soc.* 95, 77-91.

_____, 1970: A numerical model of airflow above change in surface heat flux, temperature, and roughness for neutral and unstable conditions. *J. Boundary Layer Meteor.* 1, 18-39.

_____, 1971: *Airflow above changes in surface heat flux, temperature and roughness: an extension to include the stable case.* Boundary-Layer Meteorology, Vol. 1, No. 4, 474-497.

Townsend, A. A., 1956: *The structure of turbulent shear flow.* Cambridge University Press.

_____, A. A., 1961: Equilibrium layers and wall turbulence. *J. Fluid Mech.* 11, 97-120.

_____, 1965a: Self-preserving flow inside a turbulent boundary layer. *J. Fluid Mech.* 22, 773-797.

_____, 1965b: The response of a turbulent boundary layer to abrupt changes in surface conditions. *J. Fluid Mech.*, 22, 799-822.

Uzkan, T. and W. C. Reynolds, 1967: A shear-free turbulent boundary layer. *J. Fluid Mech.* 28:4, 803-821.

Varga, Richard S., 1962: *Matrix Iterative Analysis.* Prentice-Hall, Inc., Englewood Cliffs, New Jersey, 322 pp.

Wagner, N. K., 1966: *A two-dimensional, time dependent numerical model of atmospheric boundary layer flow over inhomogeneous terrain. Theoretical studies of the atmospheric boundary layer.* Final Report to U.S. Army Electronic Research and Development Activity, Hawaii Institute of Geophysics, Univ. of Hawaii, 1-80.

Webb, E. K., 1970: Profile relationships: the log-linear range, and extension to strong stability. *Quart. J. Roy. Meteor. Soc.* 96, 67-90.

Whitaker, S., and M. M. Wendel, 1963: Numerical solution of the equations of motion for flow around objects in channels at low Reynolds numbers. *Appl. Sci. Res.* 12, 91-104.

Wieghardt, K., 1945: *Addendum to Prandtl (1945).*

Yamamoto, G., and A. Shimanuki, 1964: The determination of lateral diffusivity in diabatic conditions near the ground from diffusion experiments. *J. of the Atmospheric Sciences* 21, 187-196.

_____, 1966: Turbulent transfer in diabatic conditions. *J. Meteor. Soc. Japan*, Vol. 44, No. 6, 301-307.

Yeh, F. F., and E. C. Nickerson, 1970: *Airflow over roughness discontinuity*. Technical Rept. No. 8. Project Themis. Fluid Dynamics and Diffusion Laboratory, College of Engineering, Colorado State Univ., Ft. Collins, Colo.

Young, D., 1954: Iterative methods for solving partial differential equations of elliptic type. *Trans. Amer. Math. Soc.* 76, 92-111.

Zilitinkevich, S. S., and D. V. Chalikov, 1968: Determining the universal wind-velocity and temperature profiles in the atmospheric boundary-layer. *Izv. Akad. Nauk. S.S.S.R., Atmos. and Ocean Phys.*, 4, 294-302.

APPENDIX A

APPENDIX A

The definition and theorems in the text of Matrix Iterative Analysis (Varga, 1962), and the theorem of convergence developed by Ortega and Rockoff (1966) are following:

DEFINITION 3.5. For $n \times n$ real matrices A, M, and N, $A = M - N$ is a regular splitting of the matrix A if M is nonsingular with $M^{-1} \geq 0$, and $N \geq 0$.

THEOREM 3.3. (Stein and Rosenberg). Let the Jacobi matrix $B \equiv L + U$ be a non-negative $n \times n$ matrix with zero diagonal entries, and let L_1 be the Gauss-Seidel matrix, the special case $\omega = 1$ of (3.39). Then, one and only one of the following mutually exclusive relations is valid:

1. $\rho(B) = \rho(L_1) = 0$.
2. $0 < \rho(L_1) < \rho(B) < 1$.
3. $1 = \rho(B) = \rho(L_1)$.
4. $1 < \rho(B) < \rho(L_1)$.

Thus, the Jacobi matrix B and the Gauss-Seidel matrix L_1 are either both convergent, or both divergent.

THEOREM 3.6. Let $A = D - E - E^*$ be an $n \times n$ Hermitian matrix, where D is Hermitian and positive definite, and $D - \omega E$ is non-singular for $0 \leq \omega \leq 2$. Then, $\rho(L_\omega) < 1$ if and only if A is positive definite and $0 < \omega < 2$.

THEOREM 3.10. If $A = (a_{i,j})$ is a real $n \times n$ matrix with $a_{i,j} \leq 0$ for all $i \neq j$, then the following are equivalent:

1. A is nonsingular, and $A^{-1} \geq 0$.

2. The diagonal entries of A are positive real numbers,

and letting D be the diagonal matrix whose diagonal entries $d_{i,i}$ are defined as

$$d_{i,i} = 1/a_{i,i}, \qquad 1 \leq i \leq n,$$

then the matrix $B = I - DA$ is non-negative and convergent.

THEOREM 3.11. If $A = (a_{i,j})$ is a real $n \times n$ matrix with $a_{i,j} \leq 0$ for all $i \neq j$, then the following are equivalent:

1. A is nonsingular, and $A^{-1} > 0$.

2. The diagonal entries of A are positive real numbers.

If D is the diagonal matrix defined by (3.66), then the matrix $B = I - DA$ is non-negative, irreducible, and convergent.

COROLLARY 1. If $A = (a_{i,j})$ is a real, irreducibly diagonally dominant $n \times n$ matrix with $a_{i,j} \leq 0$ for all $i \neq j$, and $a_{i,i} > 0$ for all $1 \leq i \leq n$, then $A^{-1} > 0$.

COROLLARY 2. If $A = (a_{i,j})$ is a real, symmetric and nonsingular $n \times n$ irreducible matrix, where $a_{i,j} \leq 0$ for all $i \neq j$, then $A^{-1} > 0$ if and only if A is positive definite.

THEOREM 3.13. If $A = M - N$ is a regular splitting of the matrix A and $A^{-1} \geq 0$, then

$$\rho(M^{-1}N) = \frac{\rho(A^{-1}N)}{1 + \rho(A^{-1}N)} < 1.$$

Thus, the matrix $M^{-1}N$ is convergent, and the iterative method of (3.70) converges for any initial vector $x^{(0)}$.

THEOREM 4.4 Let the matrix A be a consistently ordered p-cyclic matrix, with nonsingular diagonal submatrices $A_{i,i}$, $1 \leq i \leq N$. If all the eigenvalues of the pth power of the associated block Jacobi matrix B are real and non-negative, and $0 \leq \rho(B) < 1$, then with ω_b defined in (4.26),

1. $\rho(L_{\omega_b}) = (\omega_b - 1)(p - 1)$;

2. $\rho(L_{\omega}) > \rho(L_{\omega_b})$ for all $\omega \neq \omega_b$.

Moreover, the block successive overrelaxation matrix L_{ω} is convergent for all ω with $0 < \omega < p/(p - 1)$.

THEOREM 3.0. Let S' be an open neighborhood of a point $x^* \in R''$. Assume that $g \in C^1(S' \times S')$, g_x^{-1} is defined and continuous on $S' \times S'$ and

1. $g(x^*,x^*) = 0$. Define
$$H \equiv -[g_x(x^*,x^*)]^{-1} g_y(x^*,x^*),$$

2. that suppose that $\rho(H) \equiv \lambda < 1$. Then there exists a neighborhood S of x^* such that $g \in F(S;x^*)$.

where g is defined to belong to the class of functions $F(s;x^*)$ if for each initial vector $x^{(0)} \in S$, the difference equation has a unique solution $\{x^{(k)}, k = 0,1,\ldots\} \subset S$ which converges to x^*.

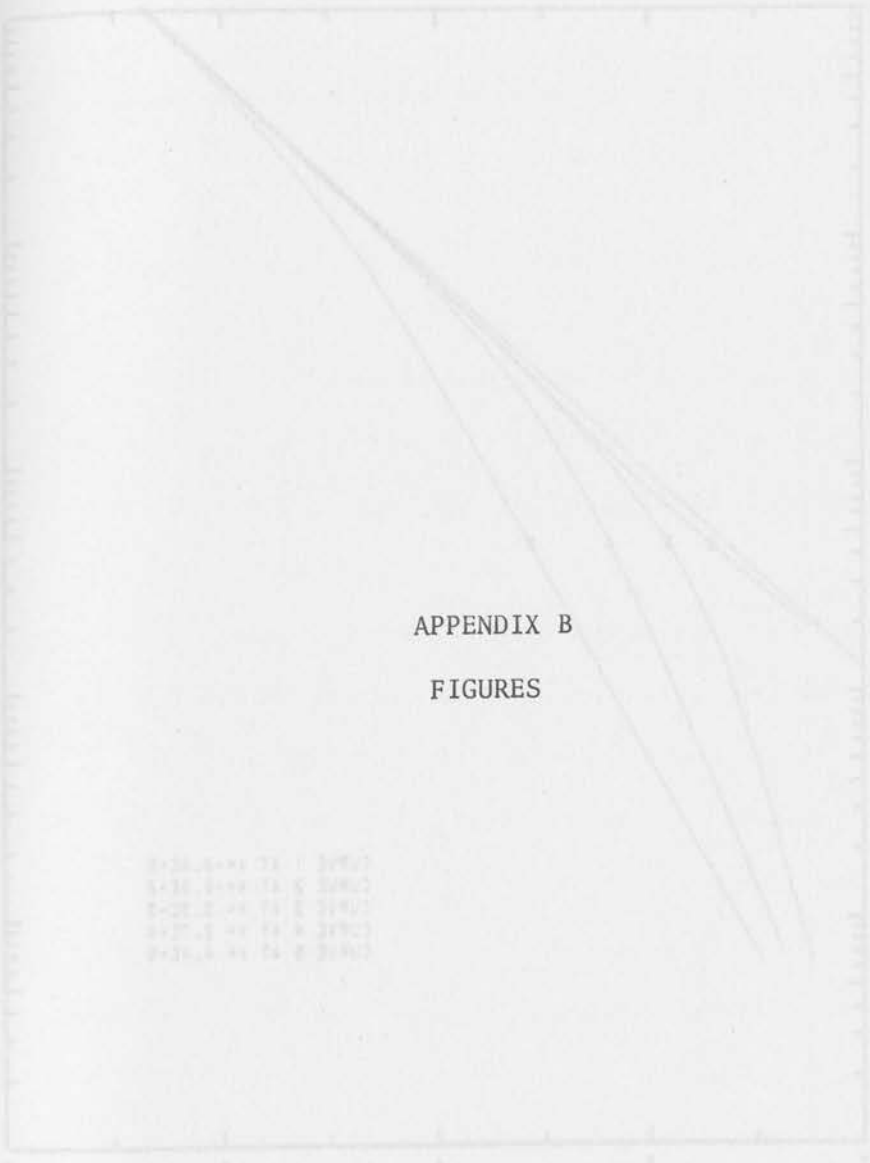

APPENDIX B

FIGURES

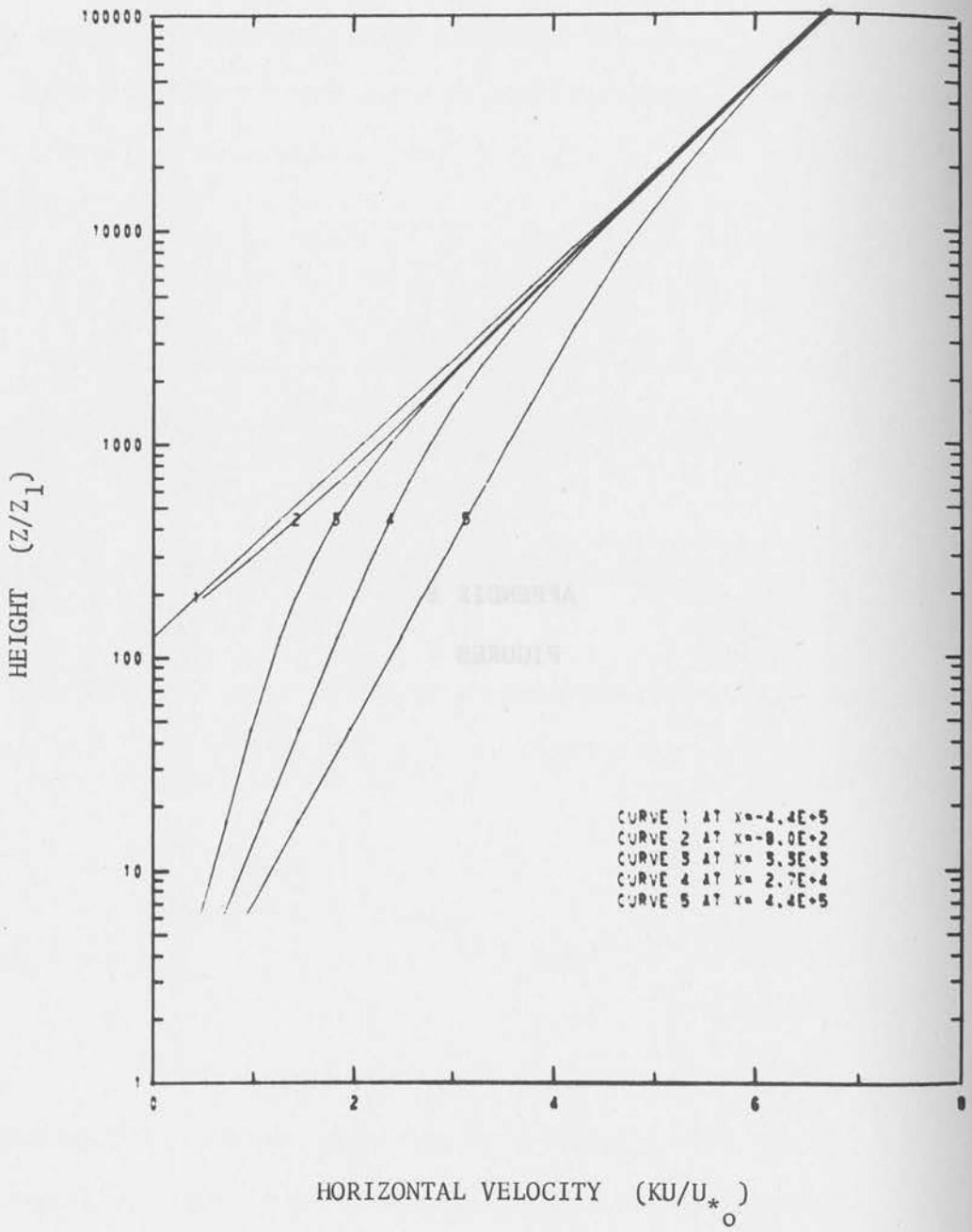

Figure 8.1-1 Calculated (pressure included) nondimensional wind profiles at various nondimensional distances (x/z_1) from the origin for a rough to smooth transition with $M \simeq 5$

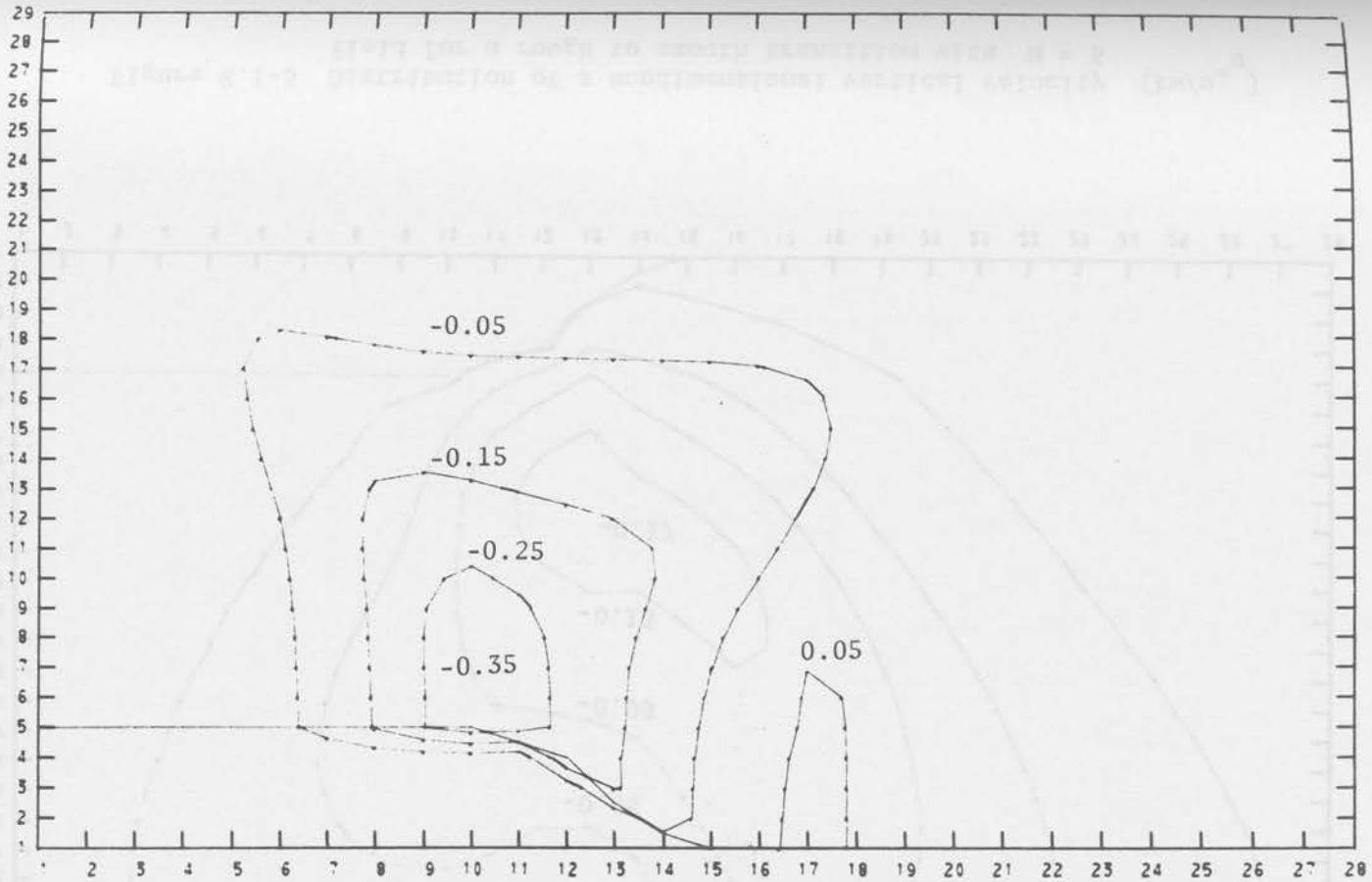

Figure 8.1-2 Distribution of a nondimensional pressure field (deviation from the hydrostatic pressure) for a rough to smooth transition sith $M \simeq 5$ $\left(\frac{k^2 P}{u_{*_o}^2}\right)$

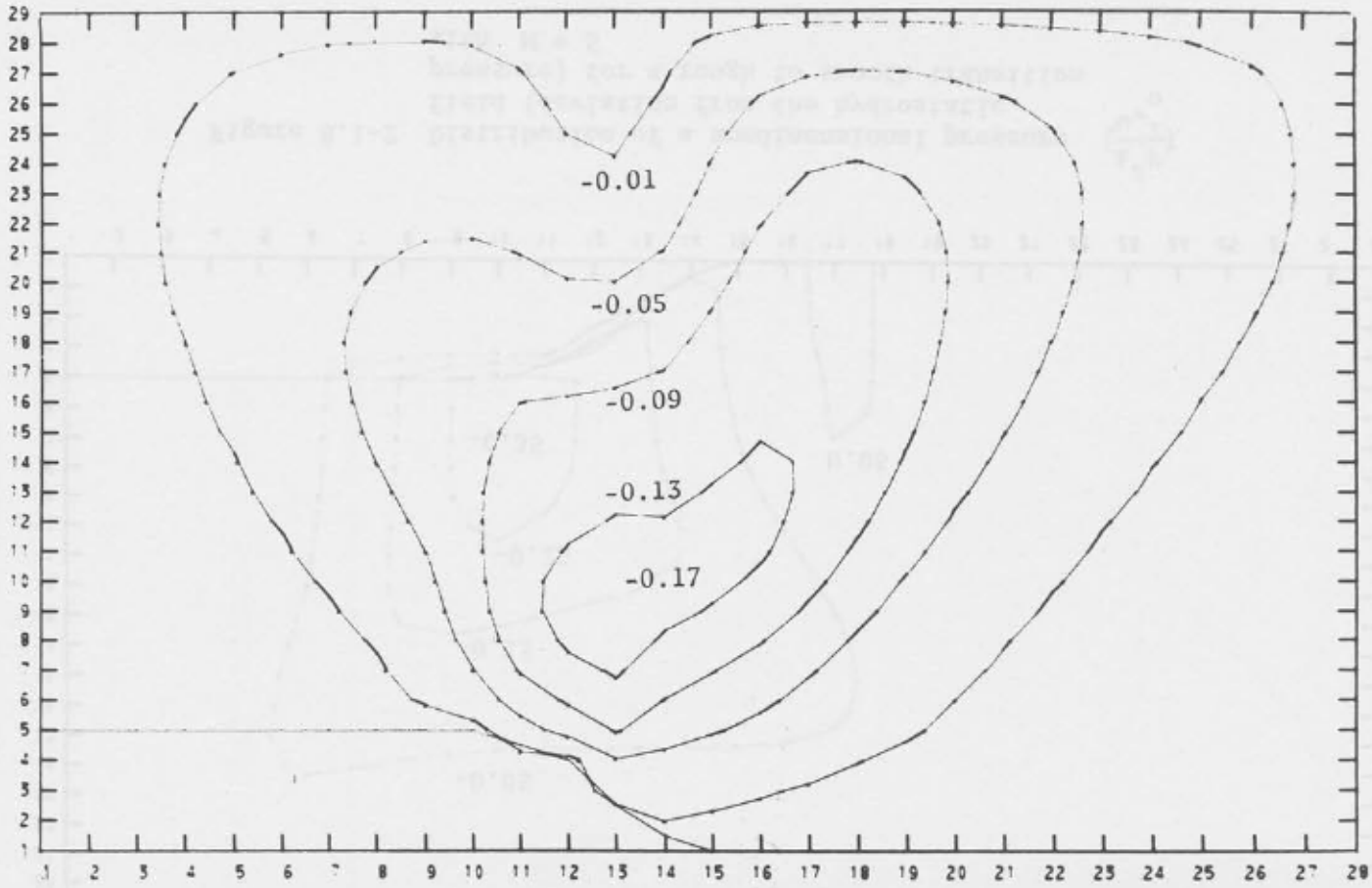

Figure 8.1-3 Distribution of a nondimensional vertical velocity (kw/u_{*_o}) field for a rough to smooth transition with $M \simeq 5$

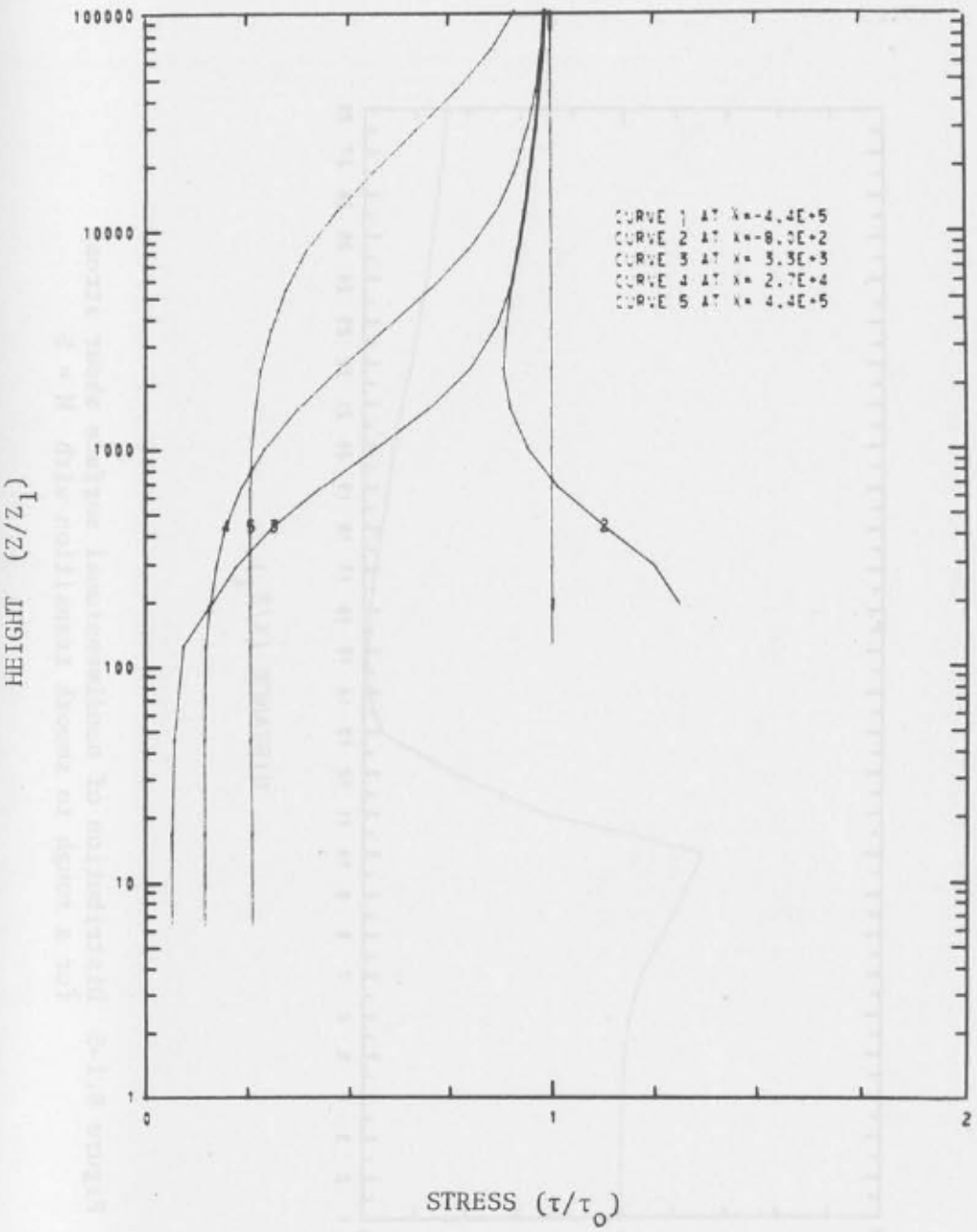

Figure 8.1-4 Nondimensional shear stress profiles for distances from the origin for a rough to smooth transition with $M \simeq 5$

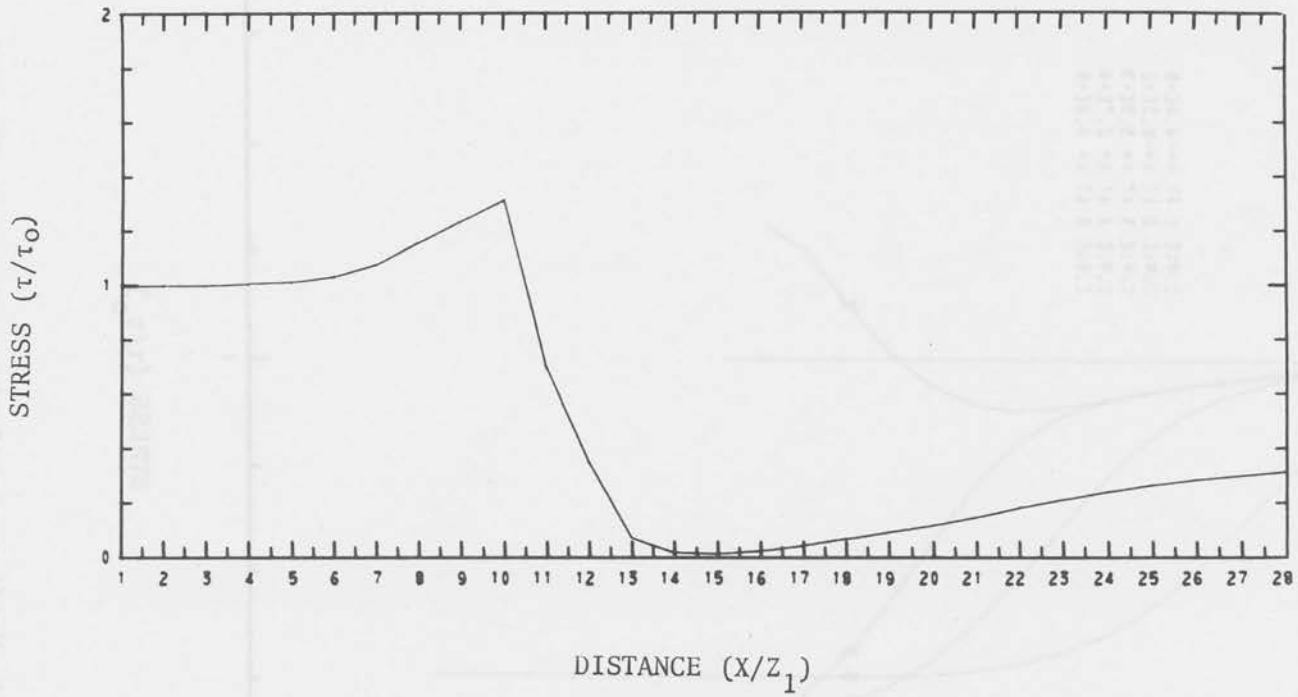

Figure 8.1-5 Distribution of nondimensional surface shear stress for a rough to smooth transition with $M \simeq 5$

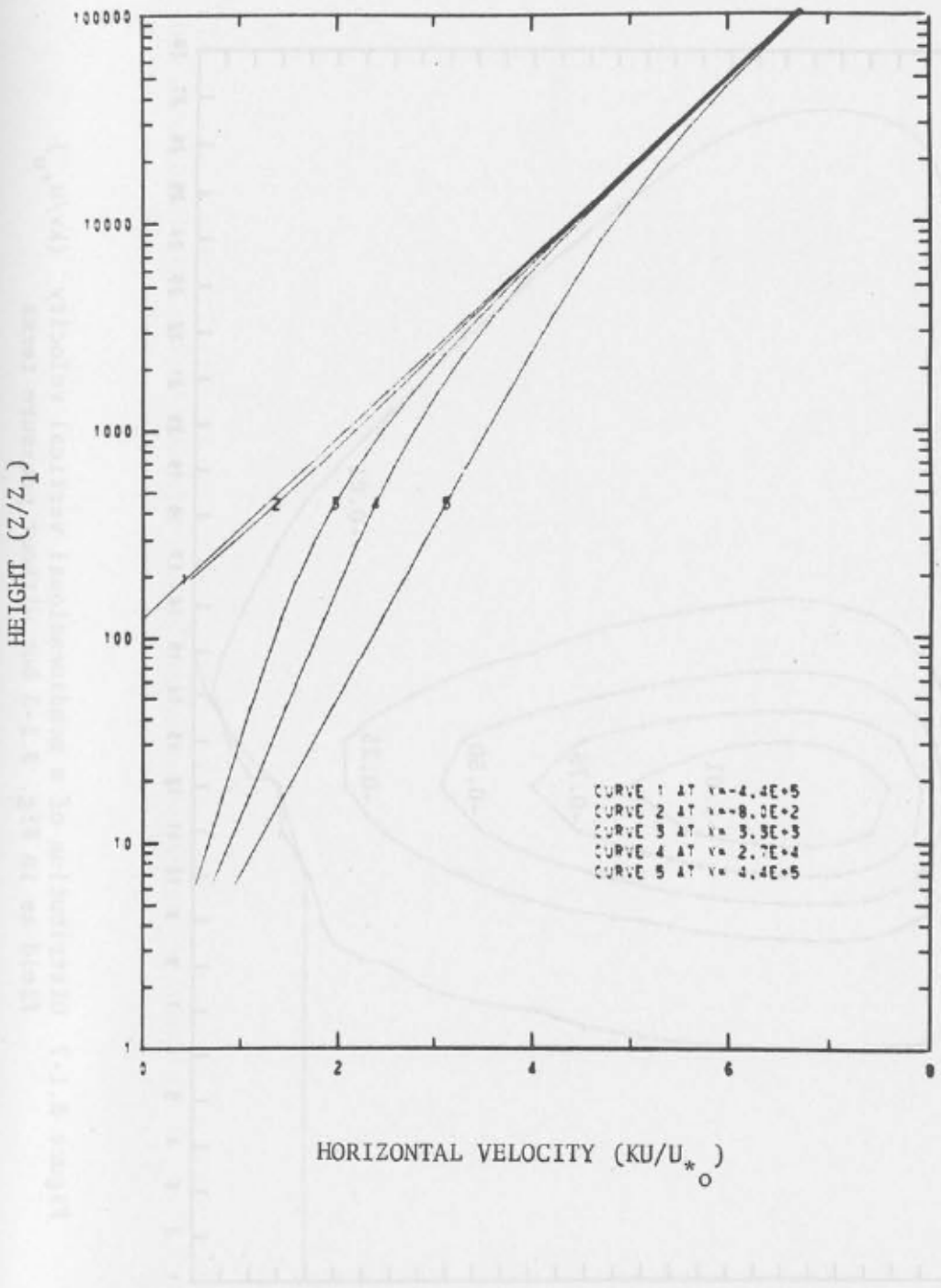

Figure 8.1-6 Calculated nondimensional velocity profiles as in Fig. 8.1-1 but without pressure terms

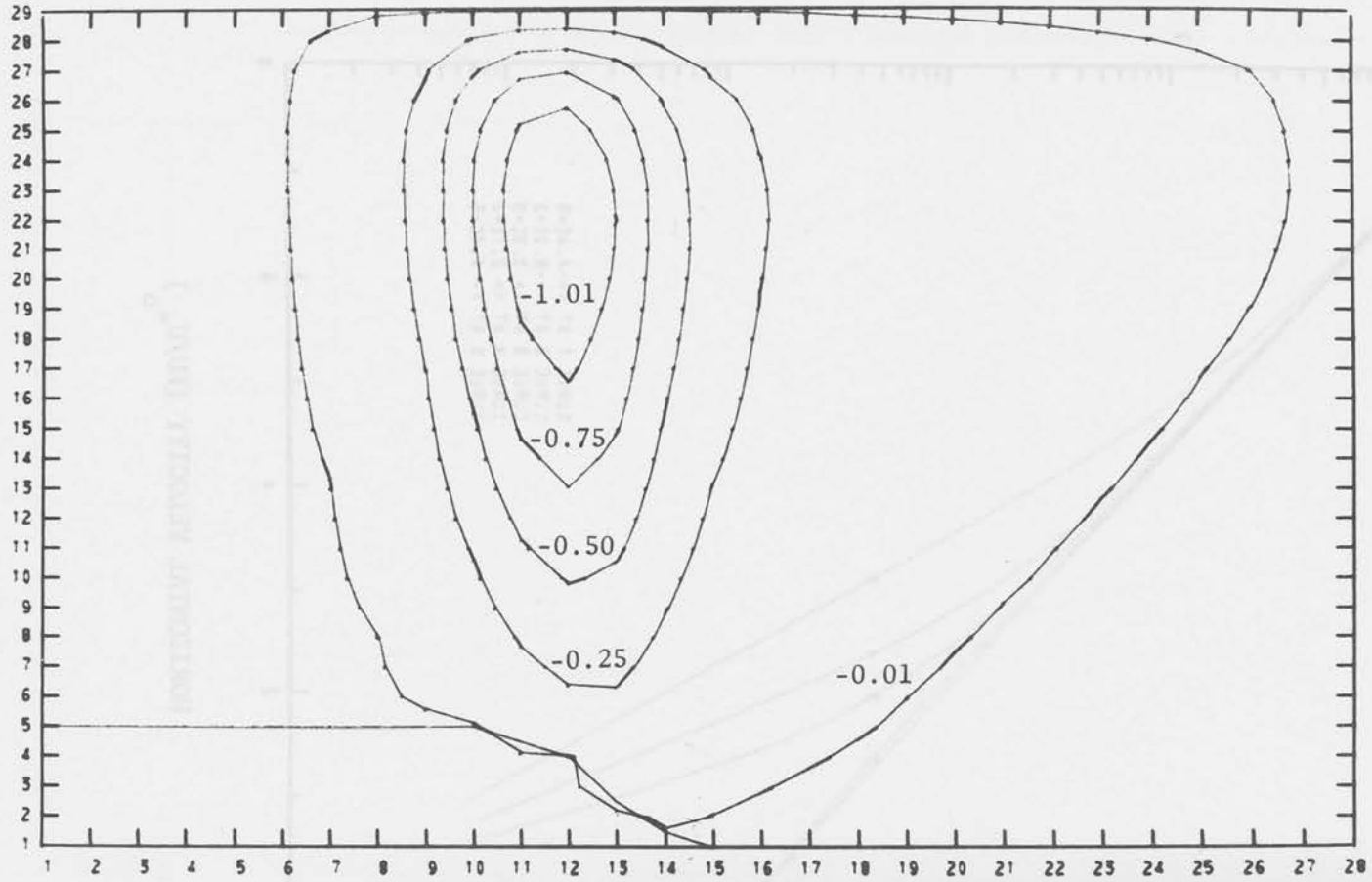

Figure 8.1-7 Distribution of a nondimensional vertical velocity (kw/u_{*_o}) field as in Fig. 8.1-3 but without pressure terms

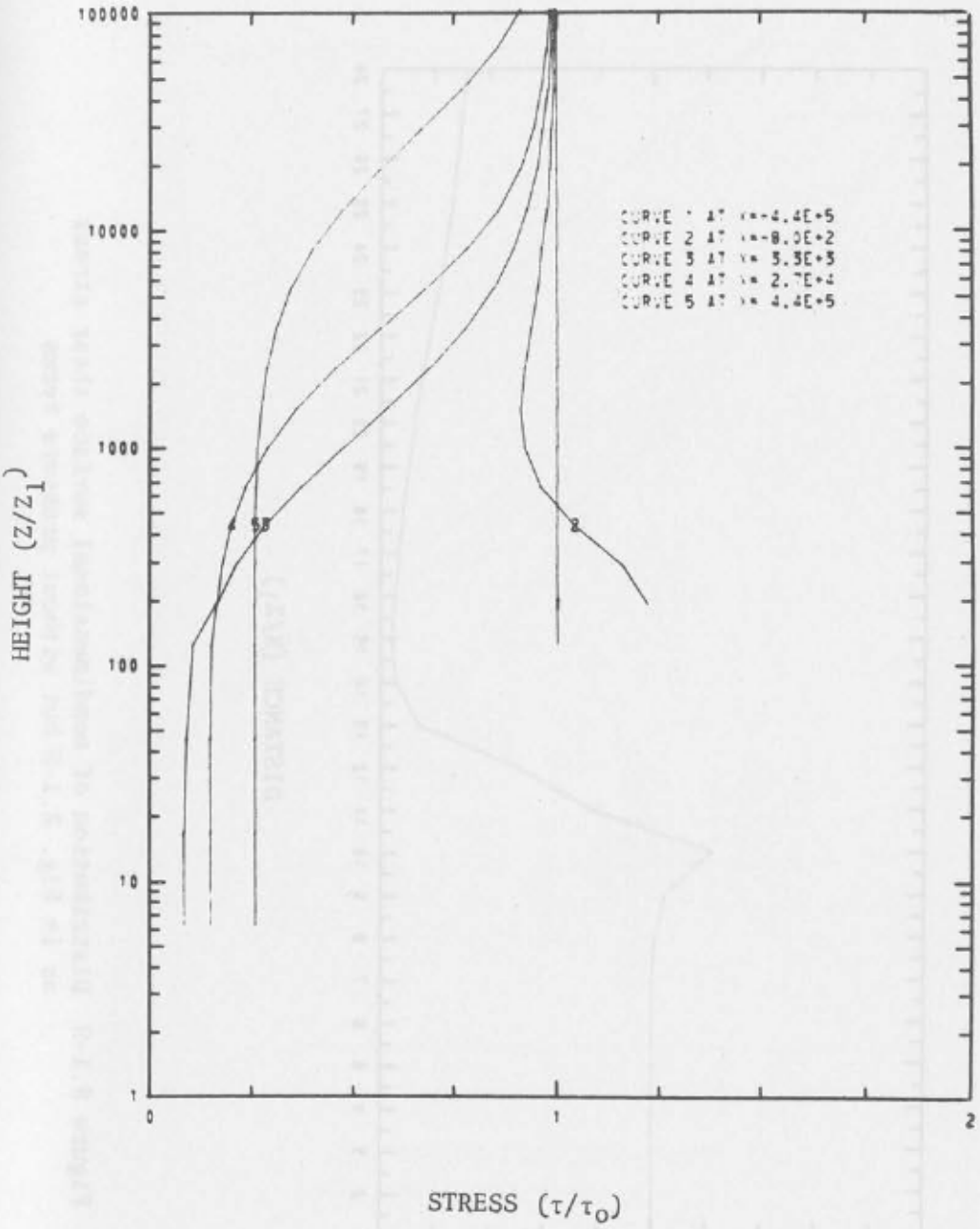

Figure 8.1-8 Nondimensional shear stress profiles as in Fig. 8.1-4 but without pressure terms

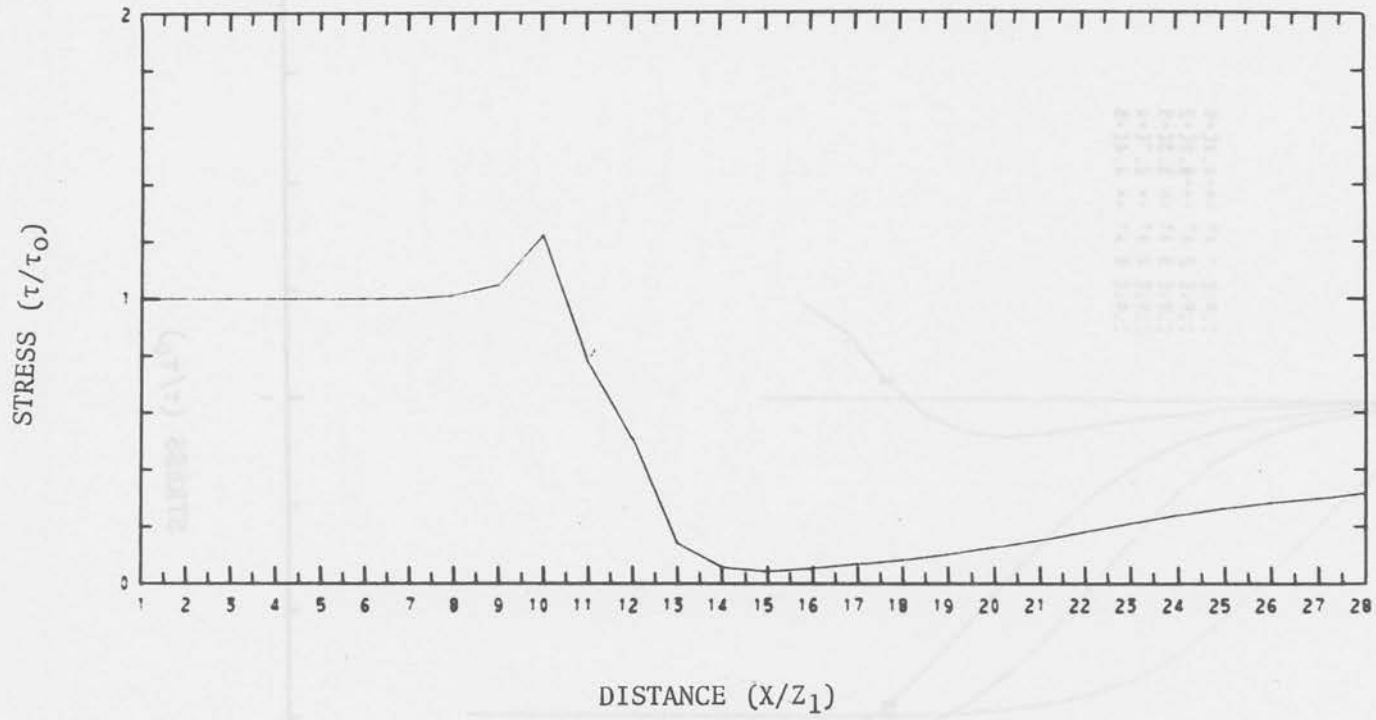

Figure 8.1-9 Distribution of nondimensional surface shear stress as in Fig. 8.1-5 but without pressure terms

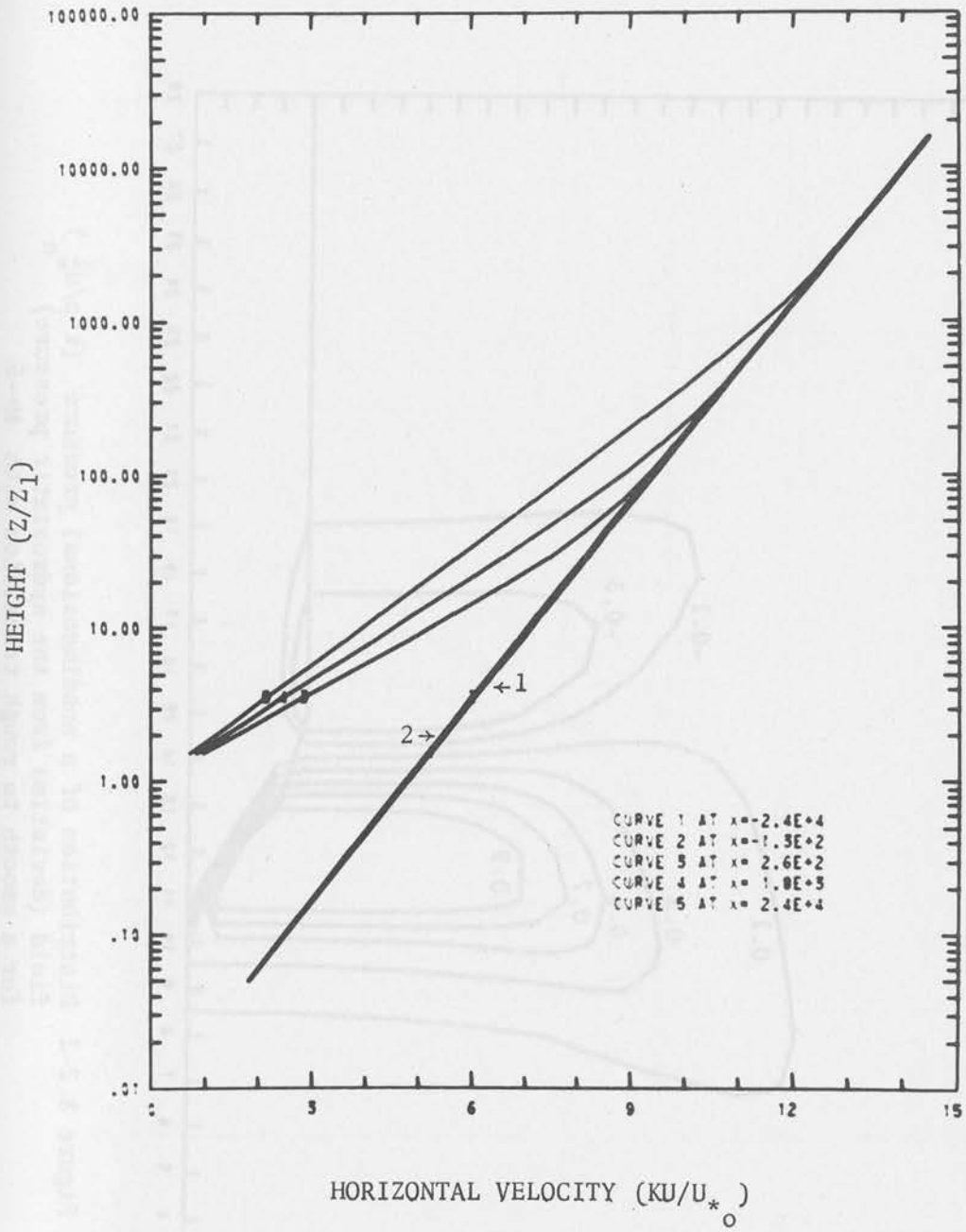

Figure 8.2-1 Nondimensional (pressure included) wind profiles at various nondimensional distances (x/z_1) from the origin for a smooth to rough transition with $M \simeq -5$ under neutral stratification

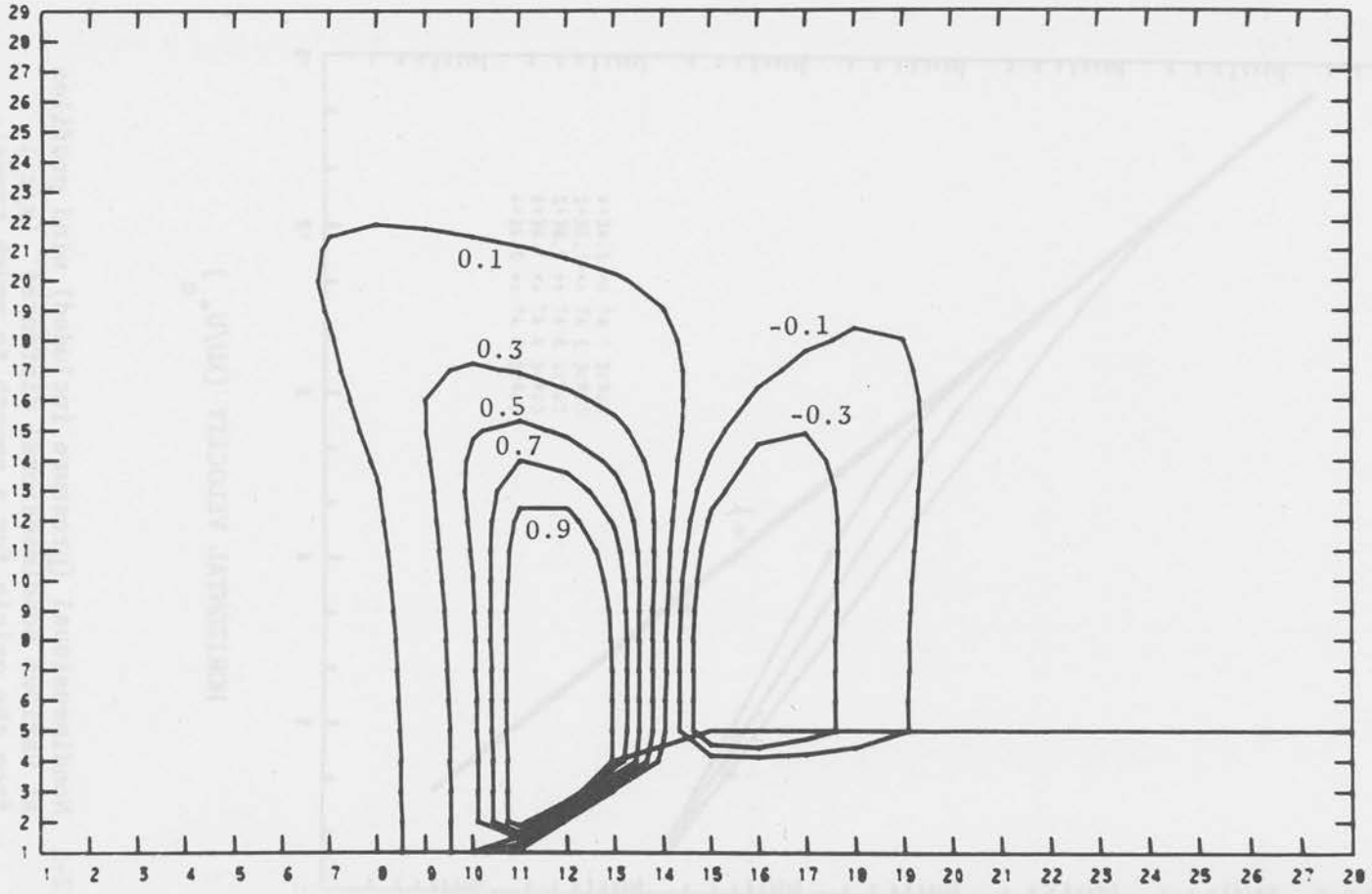

Figure 8.2-2 Distribution of a nondimensional pressure $(k^2p/u_{*_o}^2)$ field (deviation from the hydrostatic pressure) for a smooth to rough transition with $M \simeq -5$

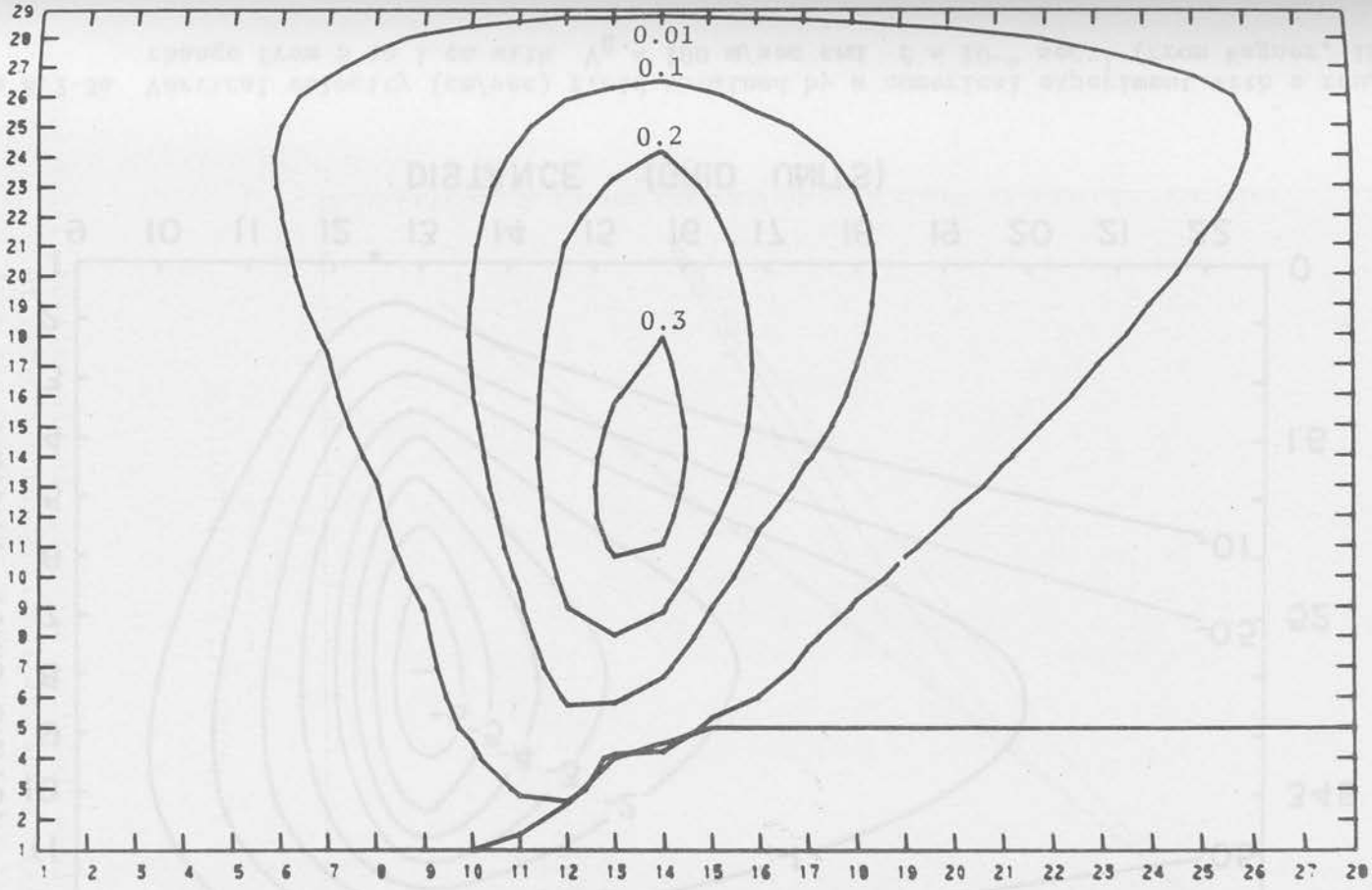

Figure 8.2-3 Distribution of a nondimensional vertical velocity (kw/u_{*_o}) field for a rough to smooth transition with M≃-5

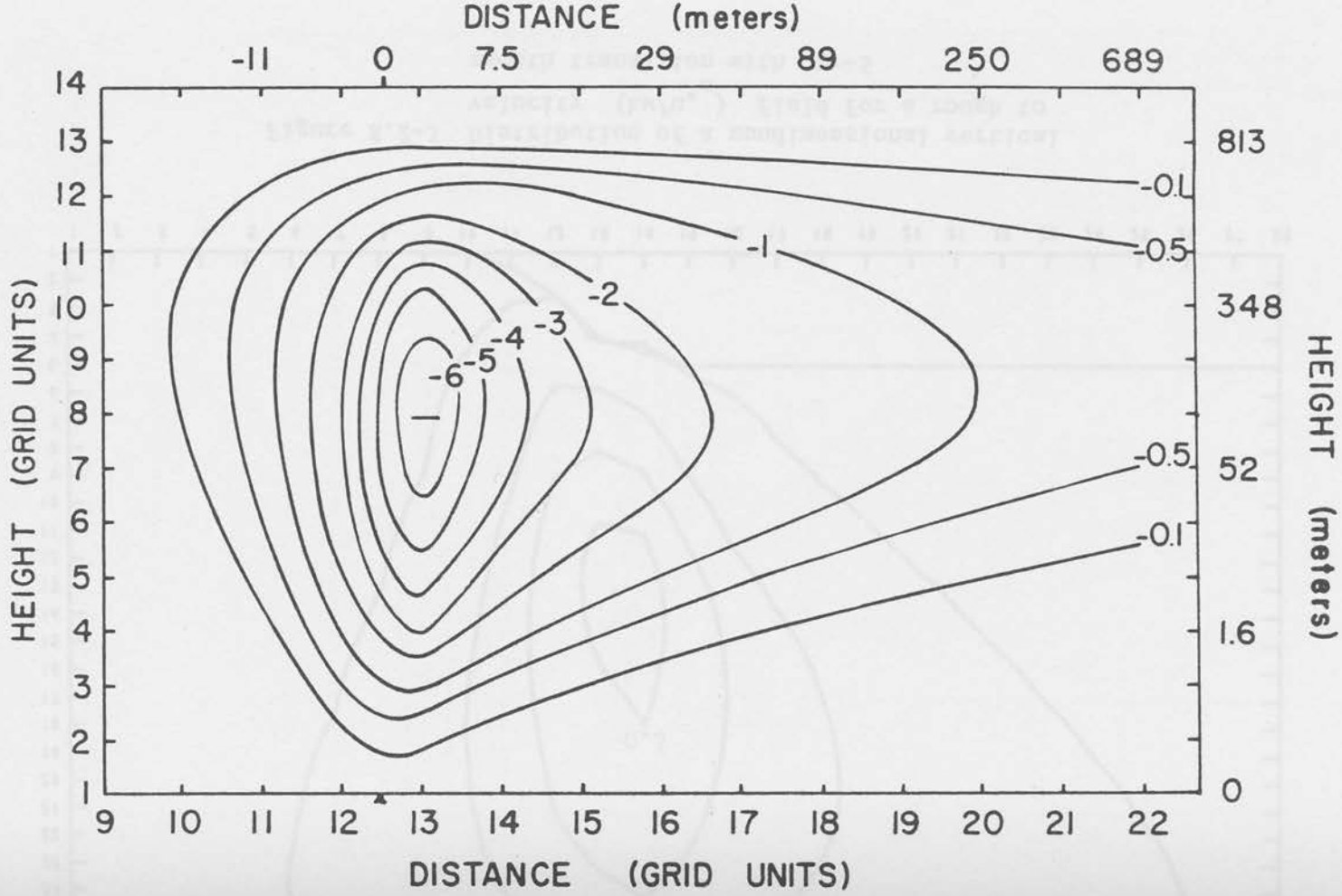

Figure 8.2-3a Vertical velocity (cm/sec) field obtained by a numerical experiment with a roughness change from 5 to 1 cm with V_g = 100 m/sec and $f = 10^{-4}$ sec^{-1} (from Wagner, 1966)

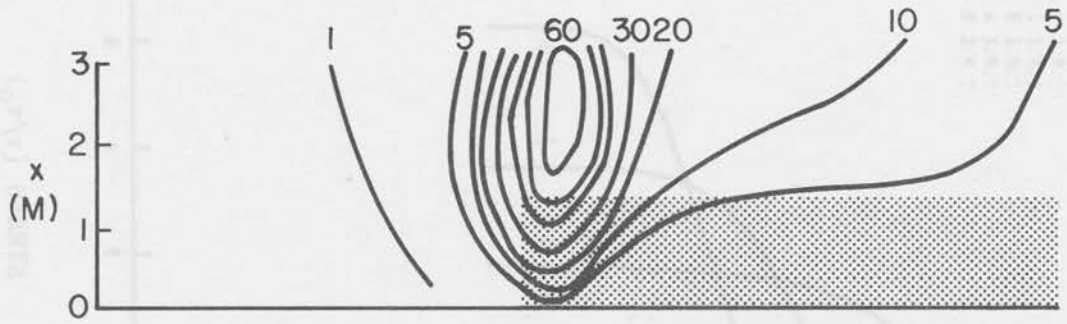

Figure 8.2-3b Vertical velocity field obtained by a Christmas tree experiment on the ice of Lake Mendota for a smooth to rough transition (from Stearns and Lettau, 1964)

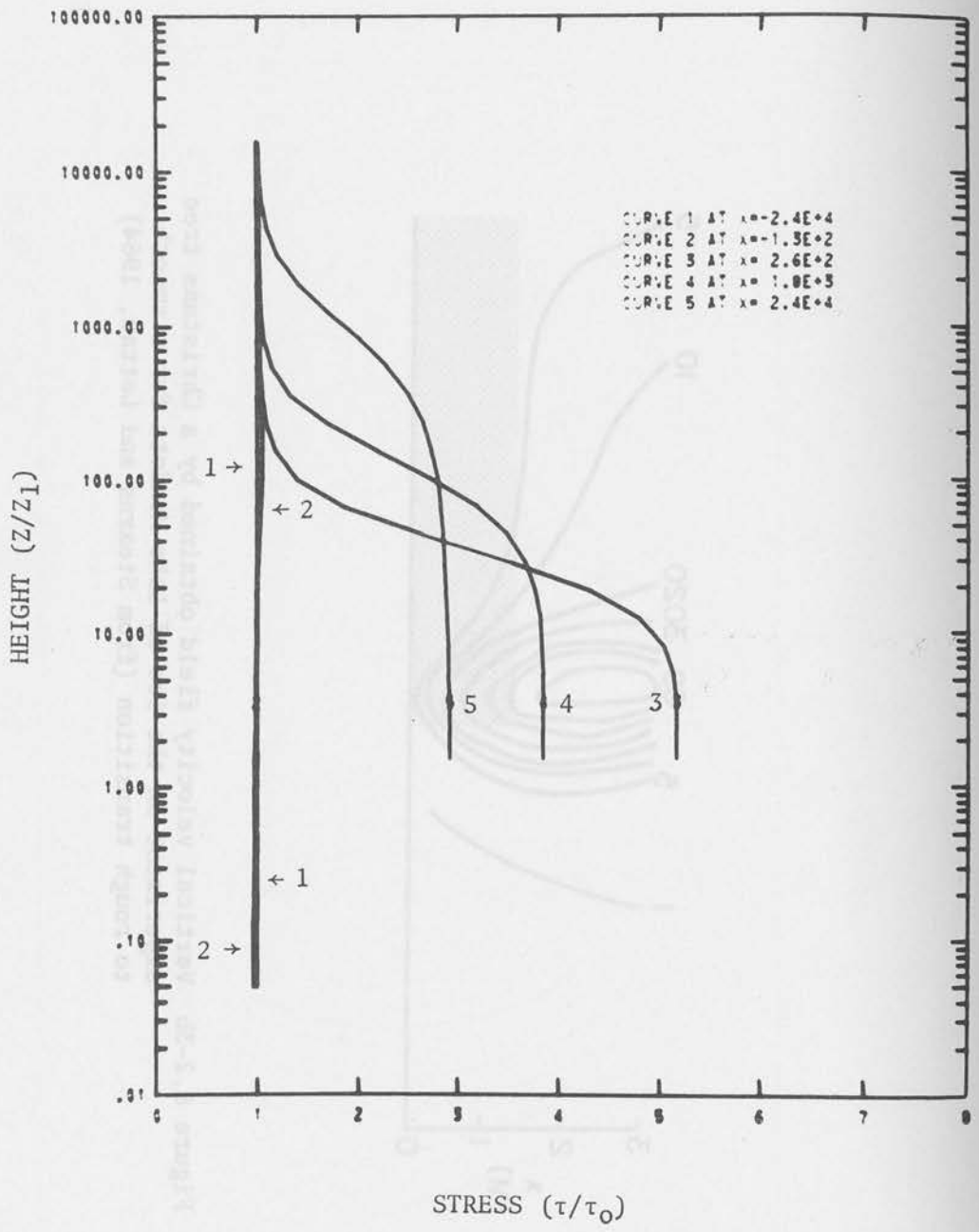

Figure 8.2-4 Nondimensional shear stress profiles for various nondimensional distances (x/z_1) from the origin for a smooth to rough transition with $M \simeq -5$

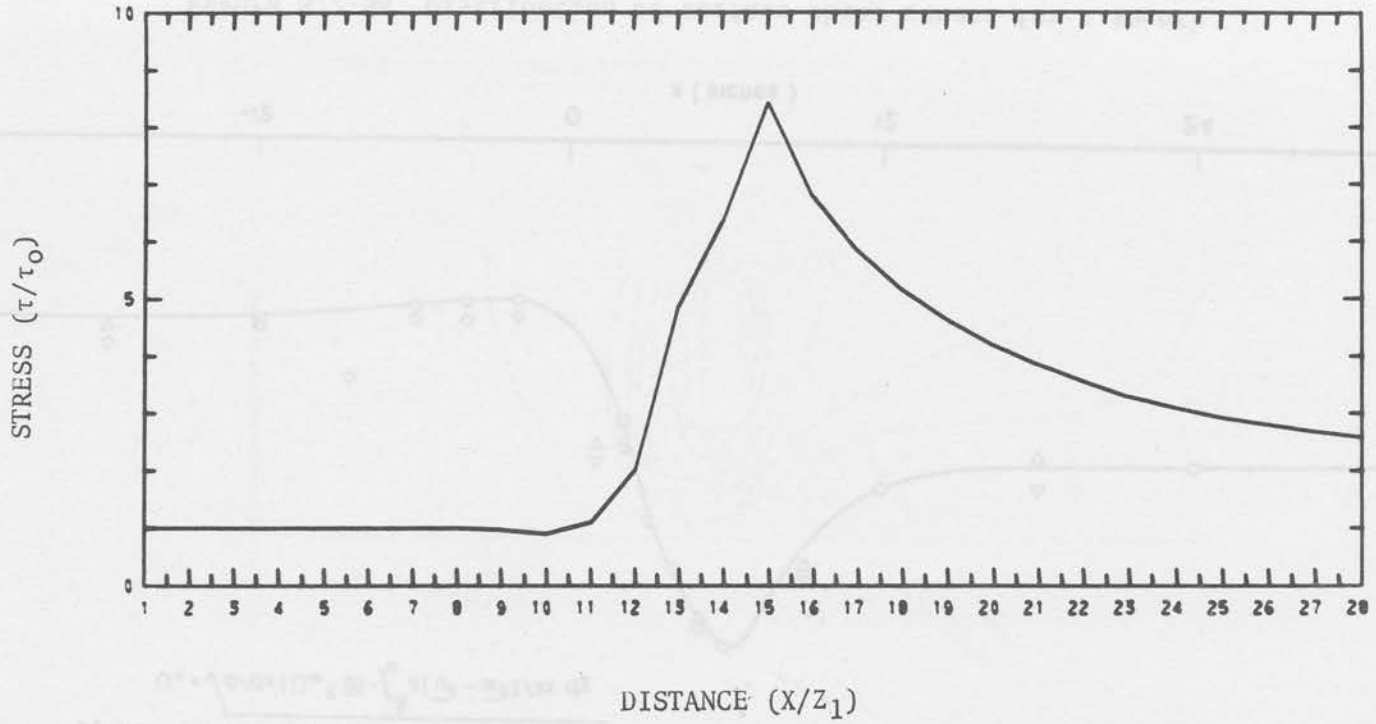

Figure 8.2-5 Distribution of nondimensional surface shear stress for a smooth to rough transition with M≃-5

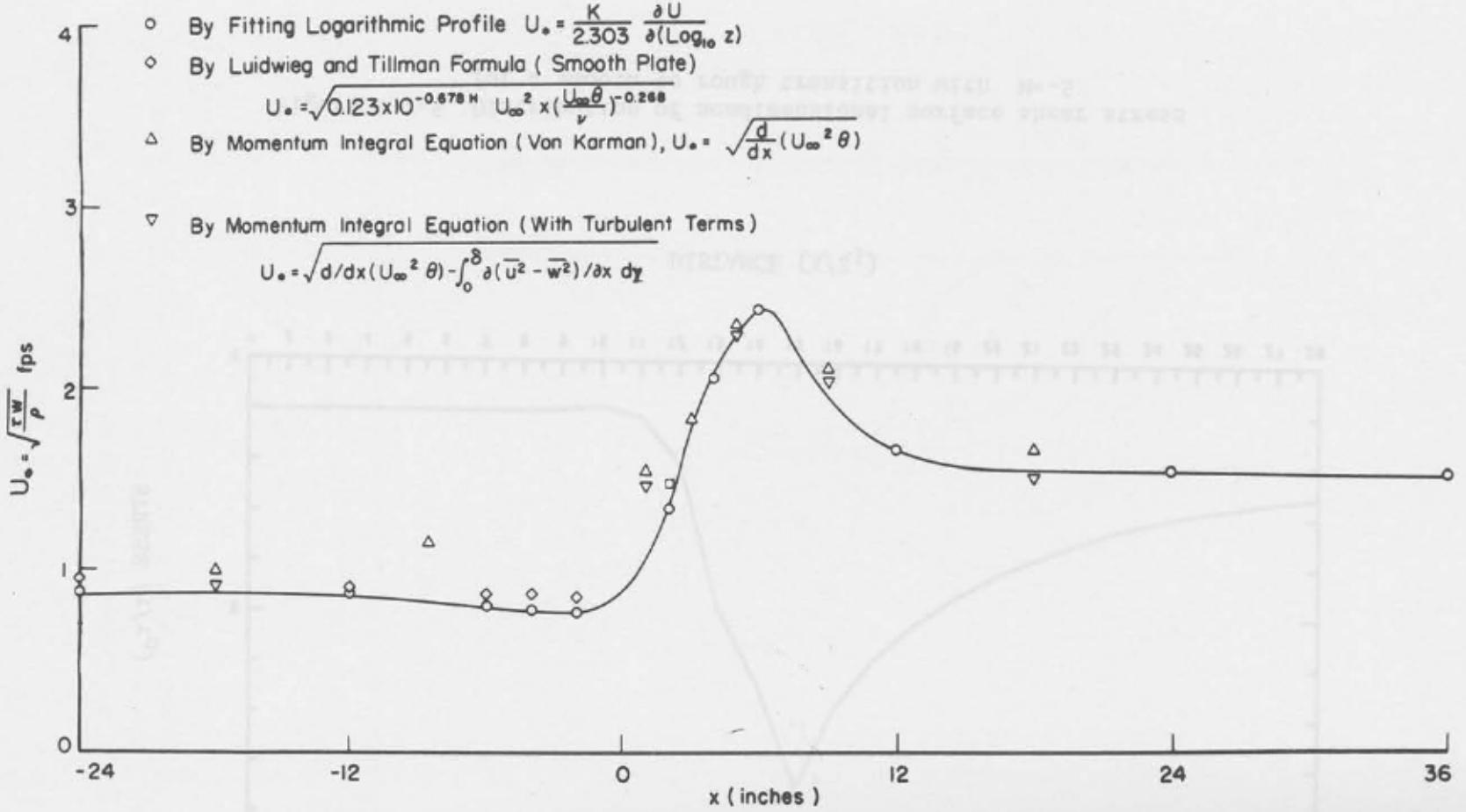

Figure 8.2-5a Distribution of surface shear stress for a smooth to rough transition (from Yeh and Nickerson, 1970)

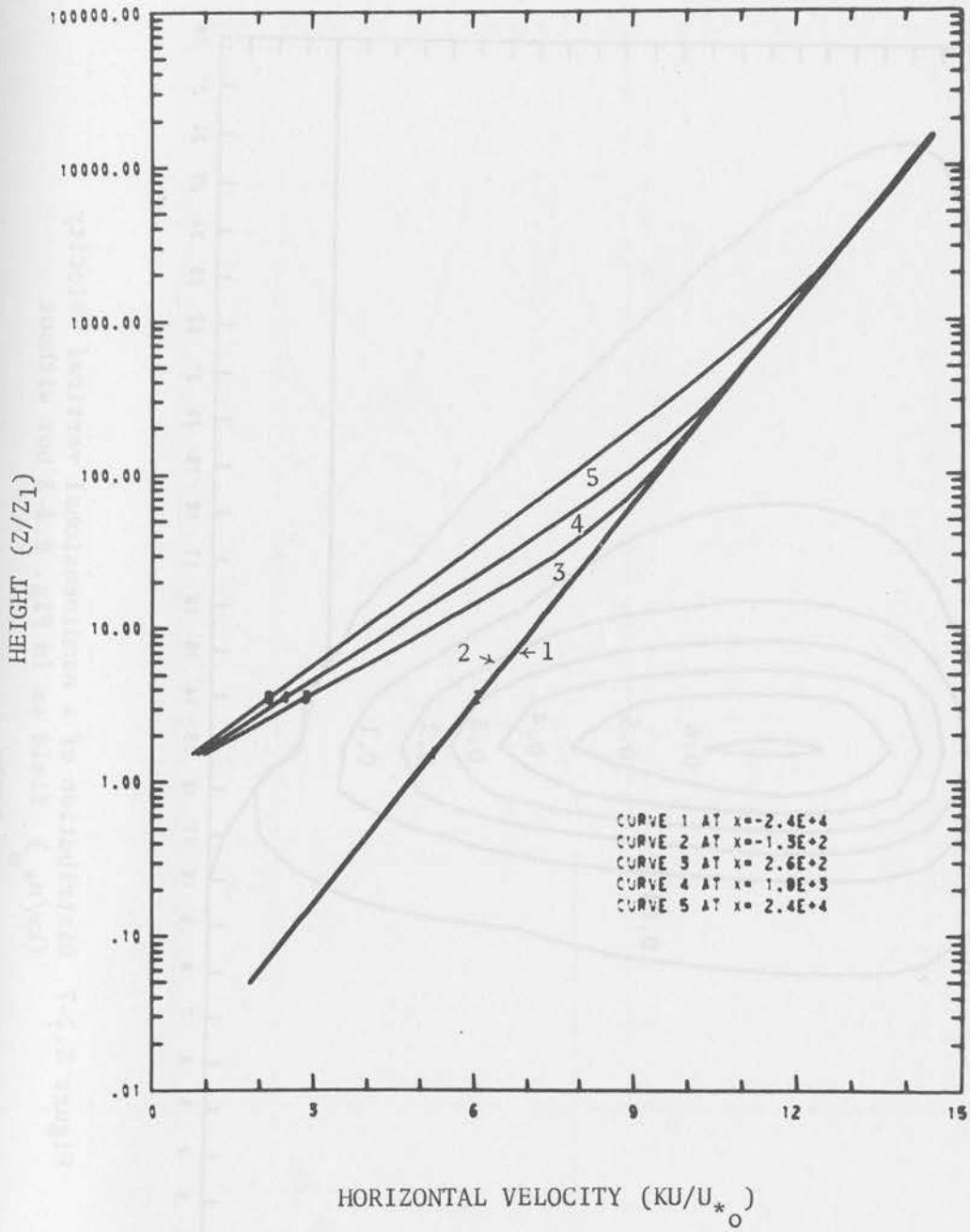

Figure 8.2-6 Nondimensional wind profiles as in Fig. 8.2-1 but without pressures

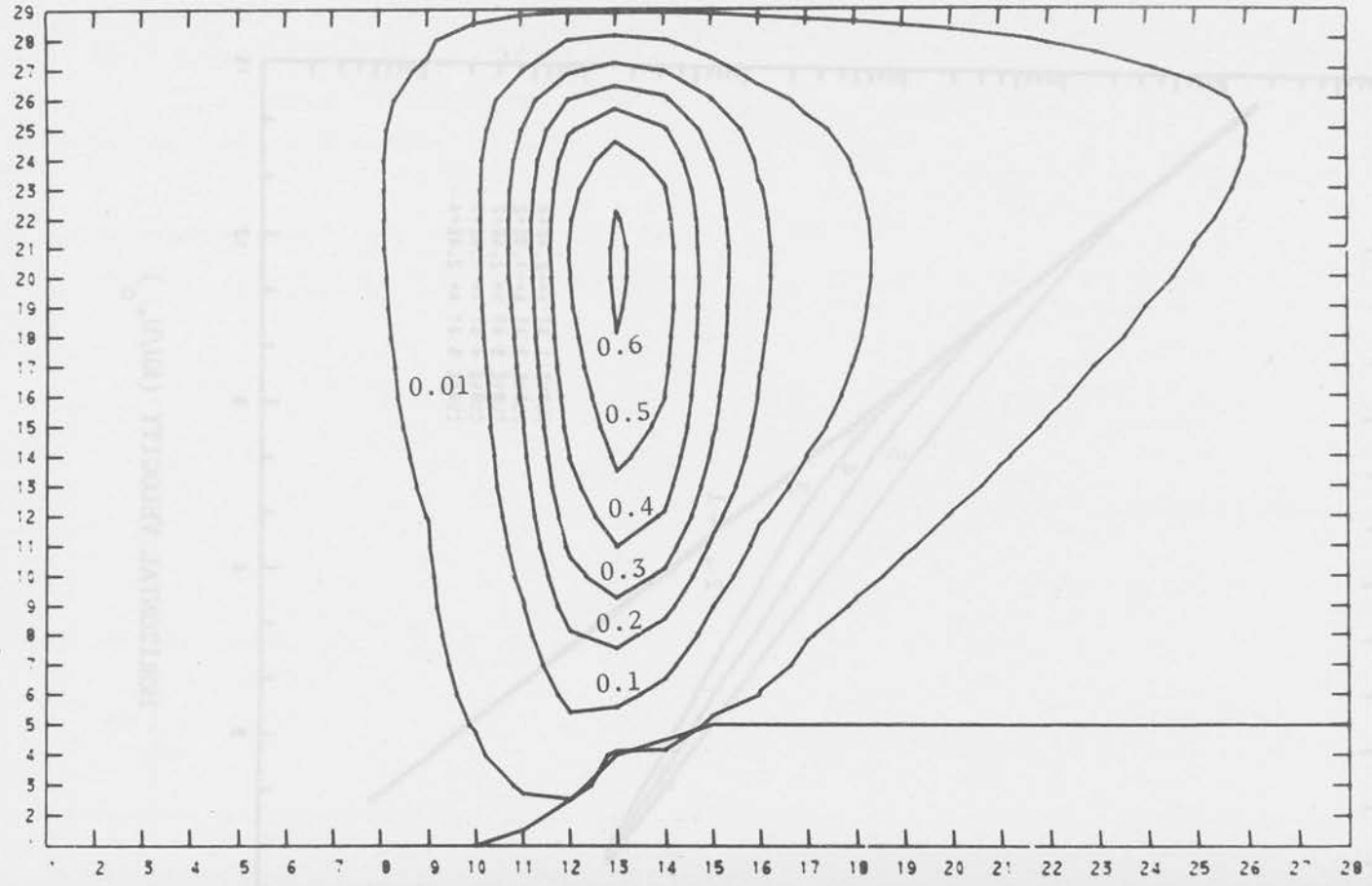

Figure 8.2-7 Distribution of a nondimensional vertical velocity (kw/u_{*_o}) field as in Fig. 8.2-3 but without pressure terms

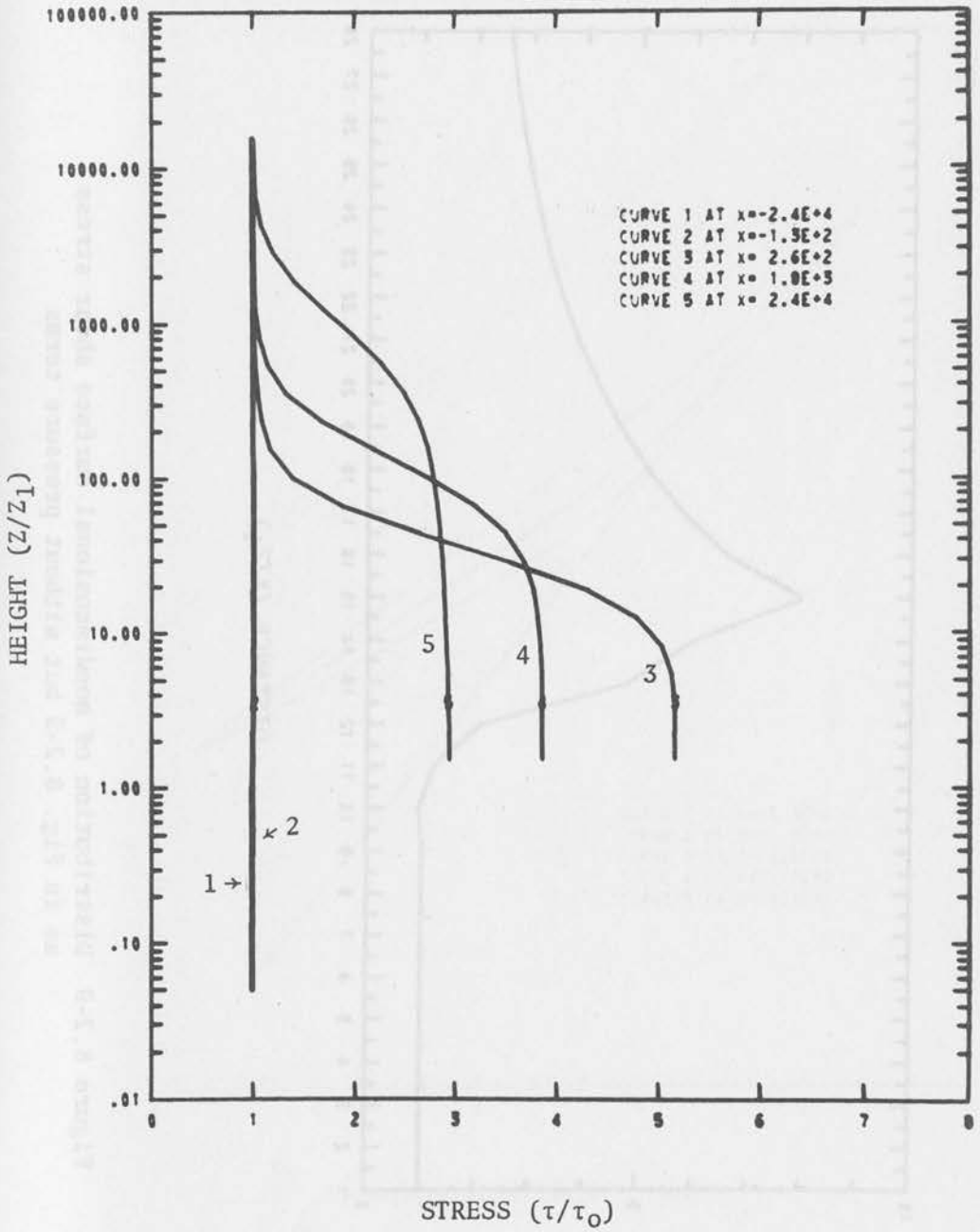

Figure 8.2-8 Nondimensional shear stress profiles as in Fig. 8.2-4 but without pressure terms

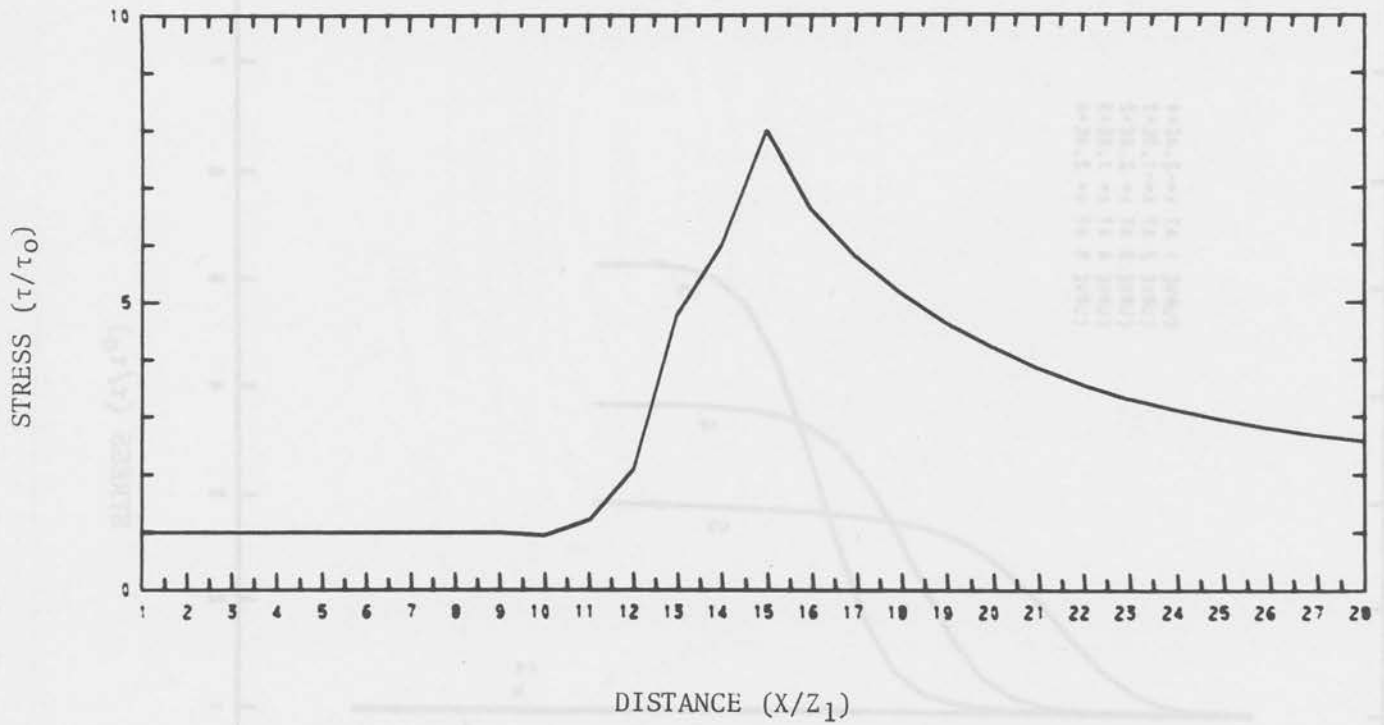

Figure 8.2-9 Distribution of nondimensional surface shear stress as in Fig. 8.2-5 but without pressure terms

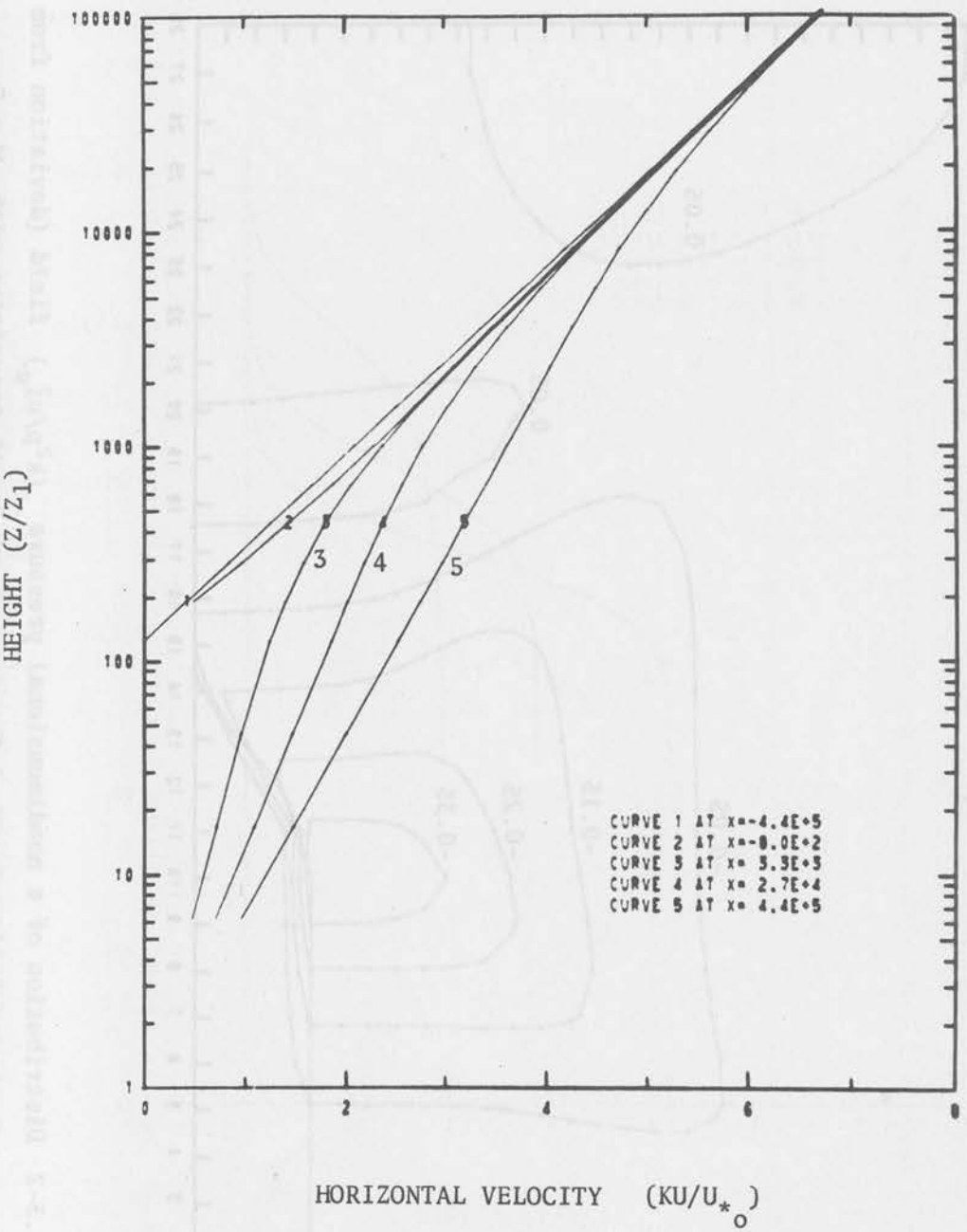

Figure 8.3-1 Nondimensional wind profiles at various distances from the origin for a rough to smooth transition with $M \simeq 5$ under unstable stratification

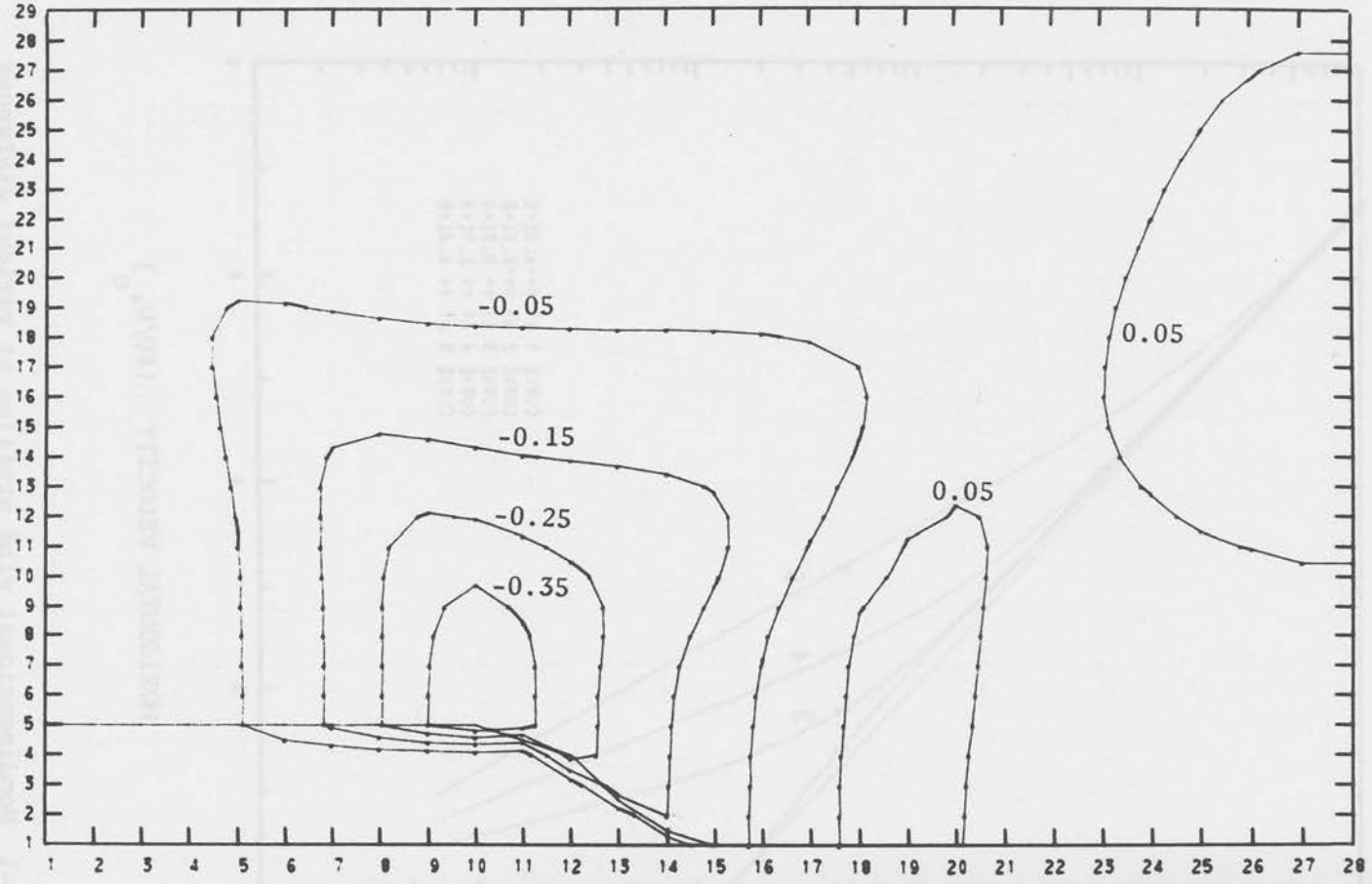

Figure 8.3-2 Distribution of a nondimensional pressure $(k^2p/u_{*_o}^2)$ field (deviation from the hydrostatic pressure) for a rough to smooth transition with $M \simeq 5$

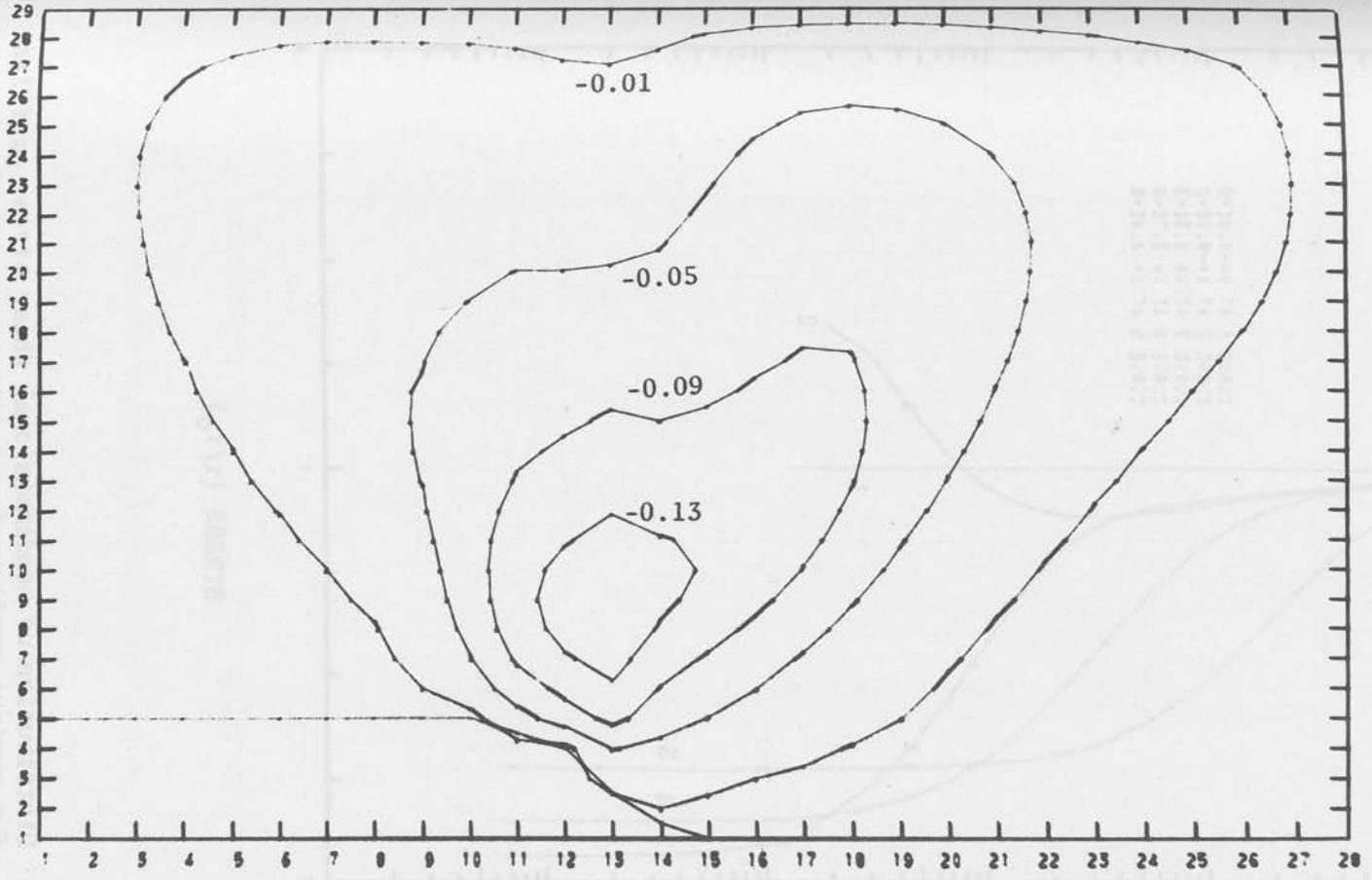

Figure 8.3-3 Distribution of a nondimensional vertical velocity (kw/u_{*_o}) field for a rough to smooth transition with $M \simeq 5$ under unstable condition

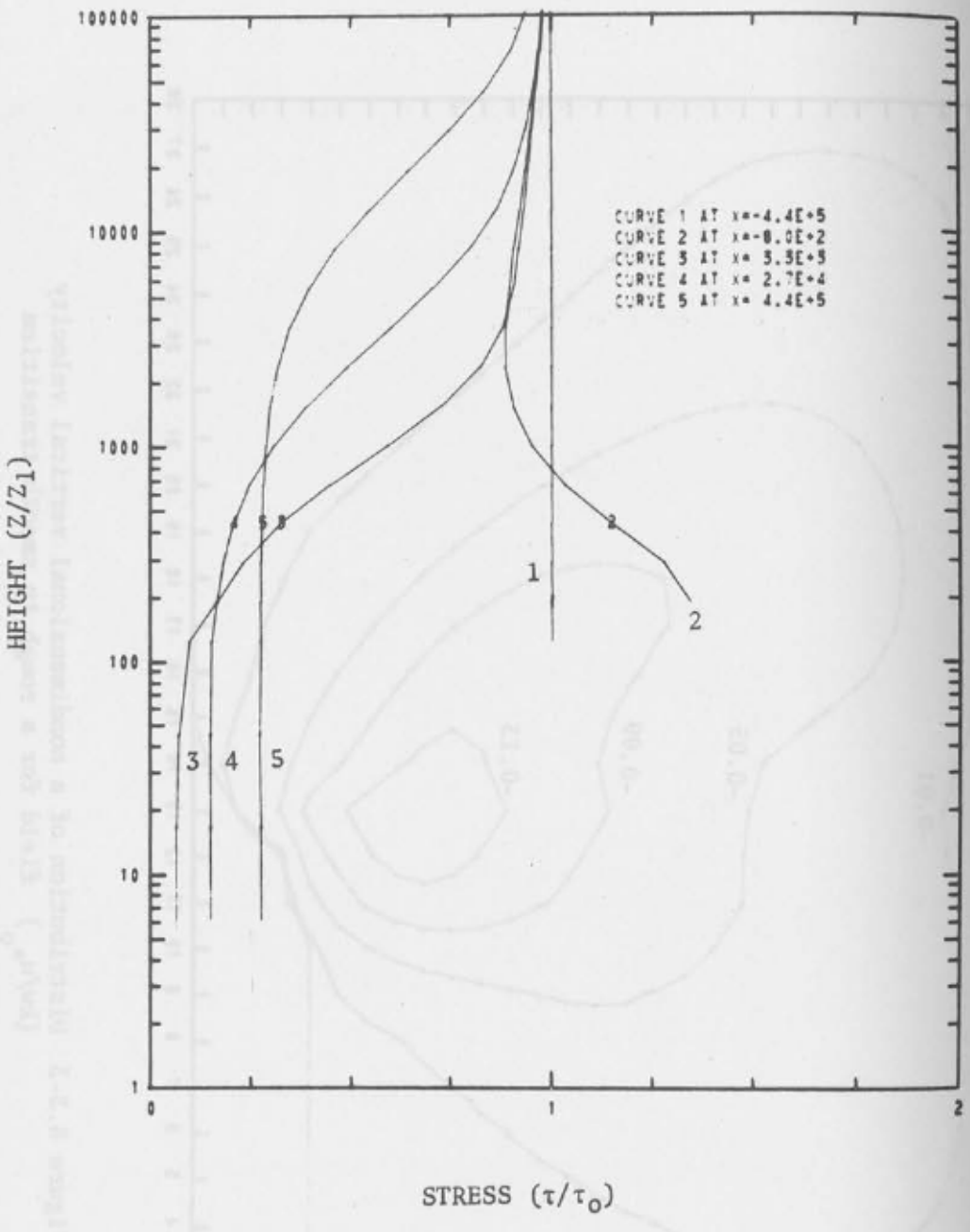

Figure 8.3-4 Distribution of nondimensional shear stress profiles for various nondimensional distances (x/z_1) from the origin for a rough to smooth transition with $M \simeq 5$ under unstable condition

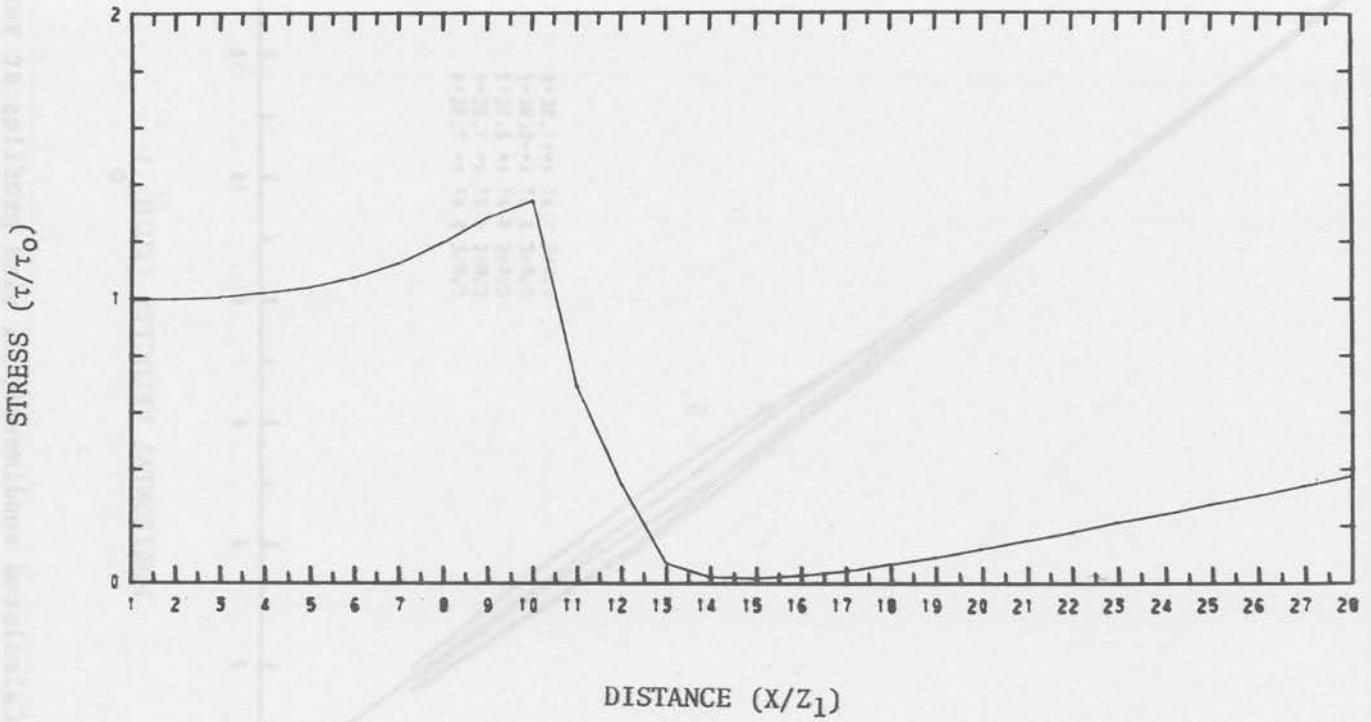

Figure 8.3-5 Distribution of nondimensional surface shear stress for a rough to smooth transition with $M \simeq 5$ under unstable condition

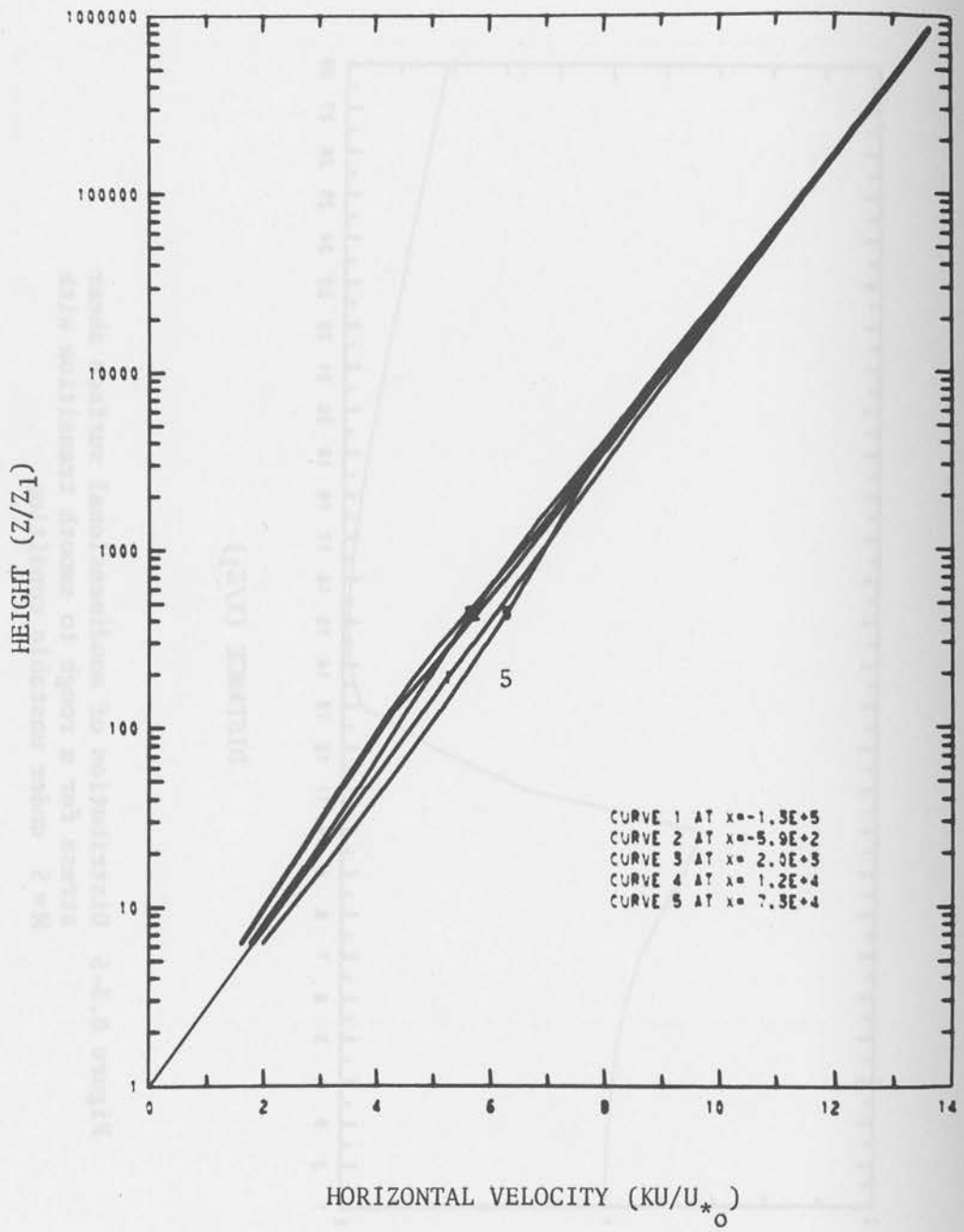

Figure 8.4-1 Calculated nondimensional wind profiles at various distances from the origin for flow moving over a constant surface roughness (M≃5) with abrupt change in surface temperature

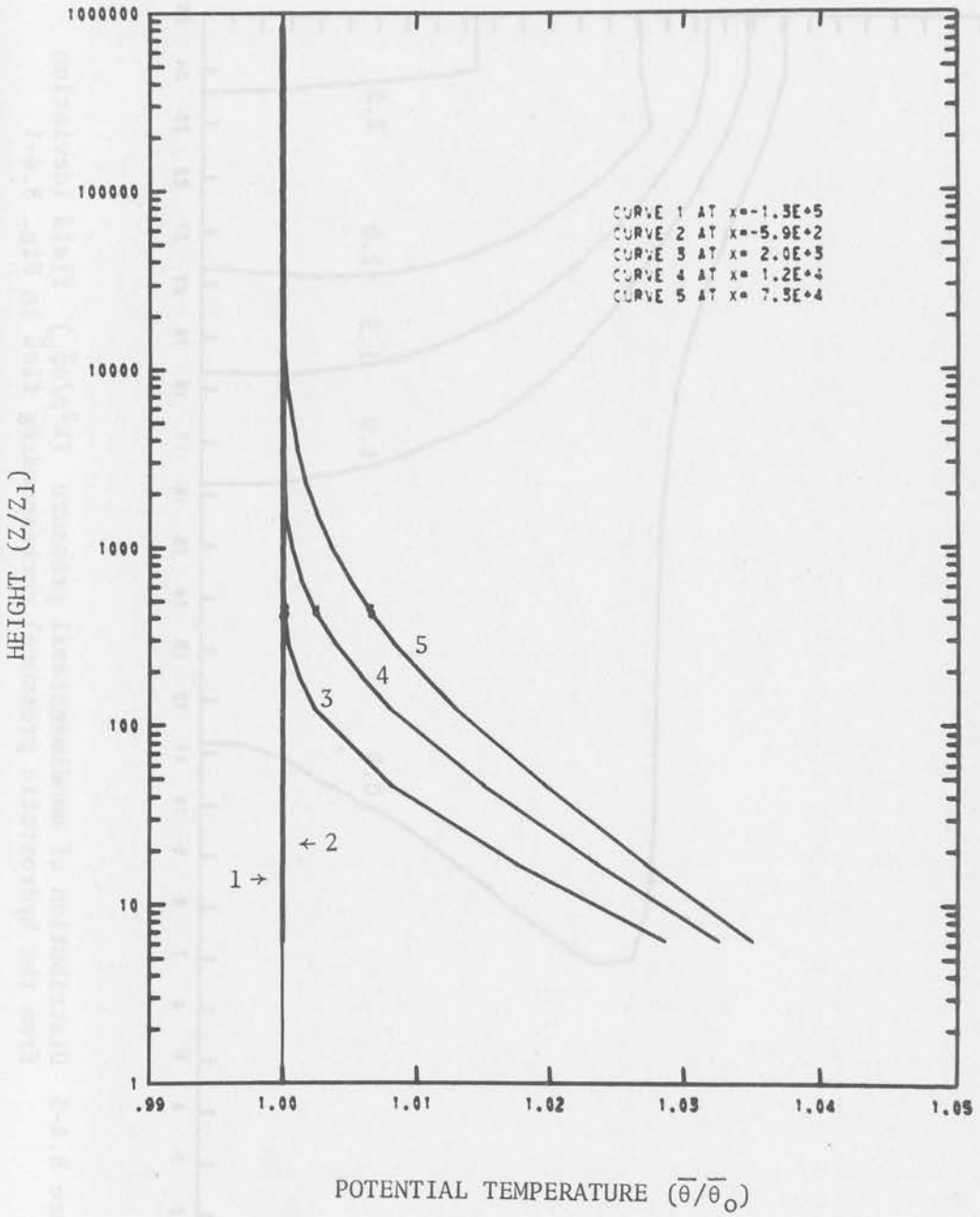

Figure 8.4-2 Nondimensional potential temperature profiles corresponding flow in Fig. 8.4-1

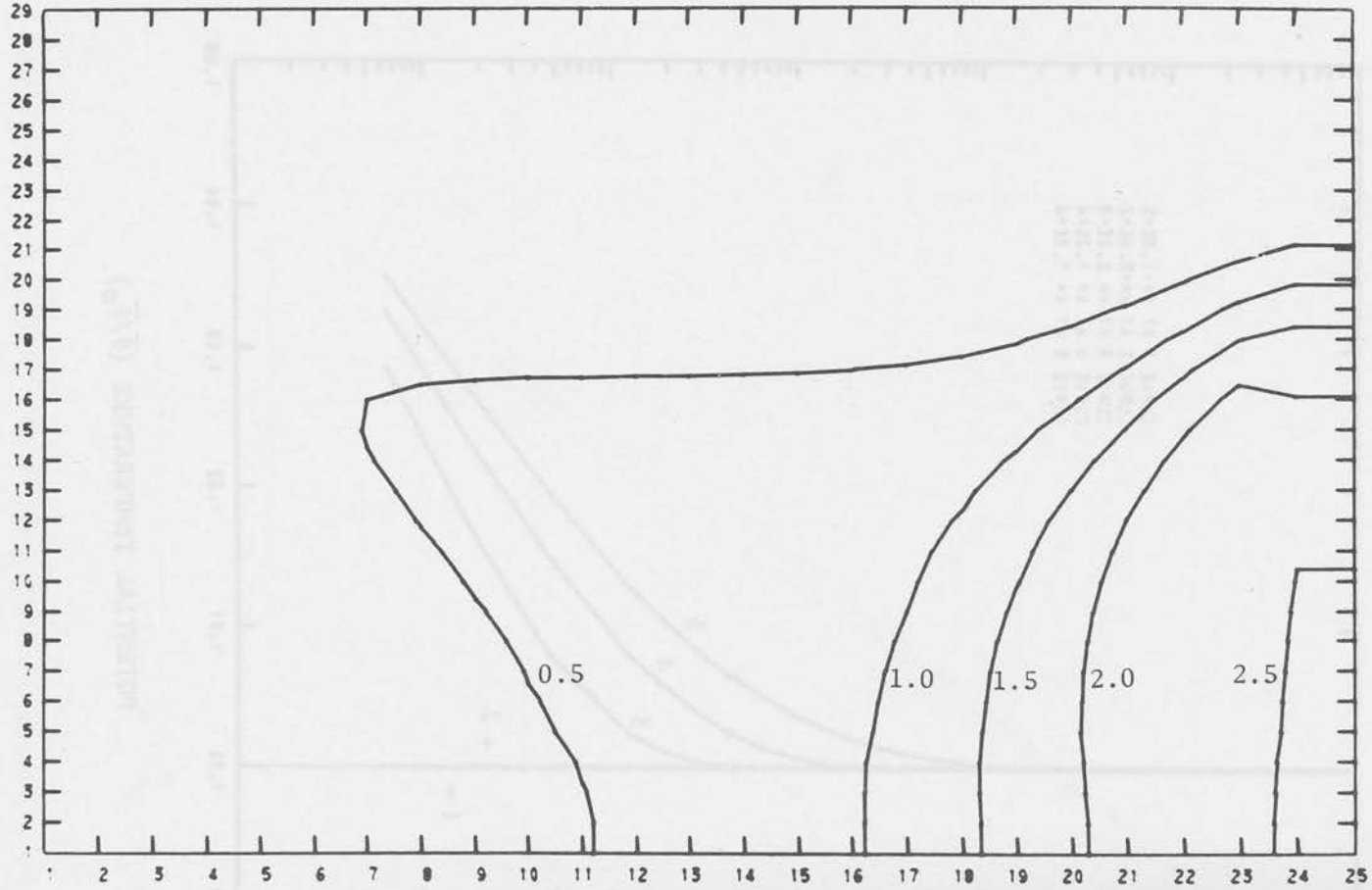

Figure 8.4-3 Distribution of nondimensional pressure $(k^2p/u_{*_o}^2)$ field (deviation from the hydrostatic pressure) corresponding flow in Fig. 8.4-1

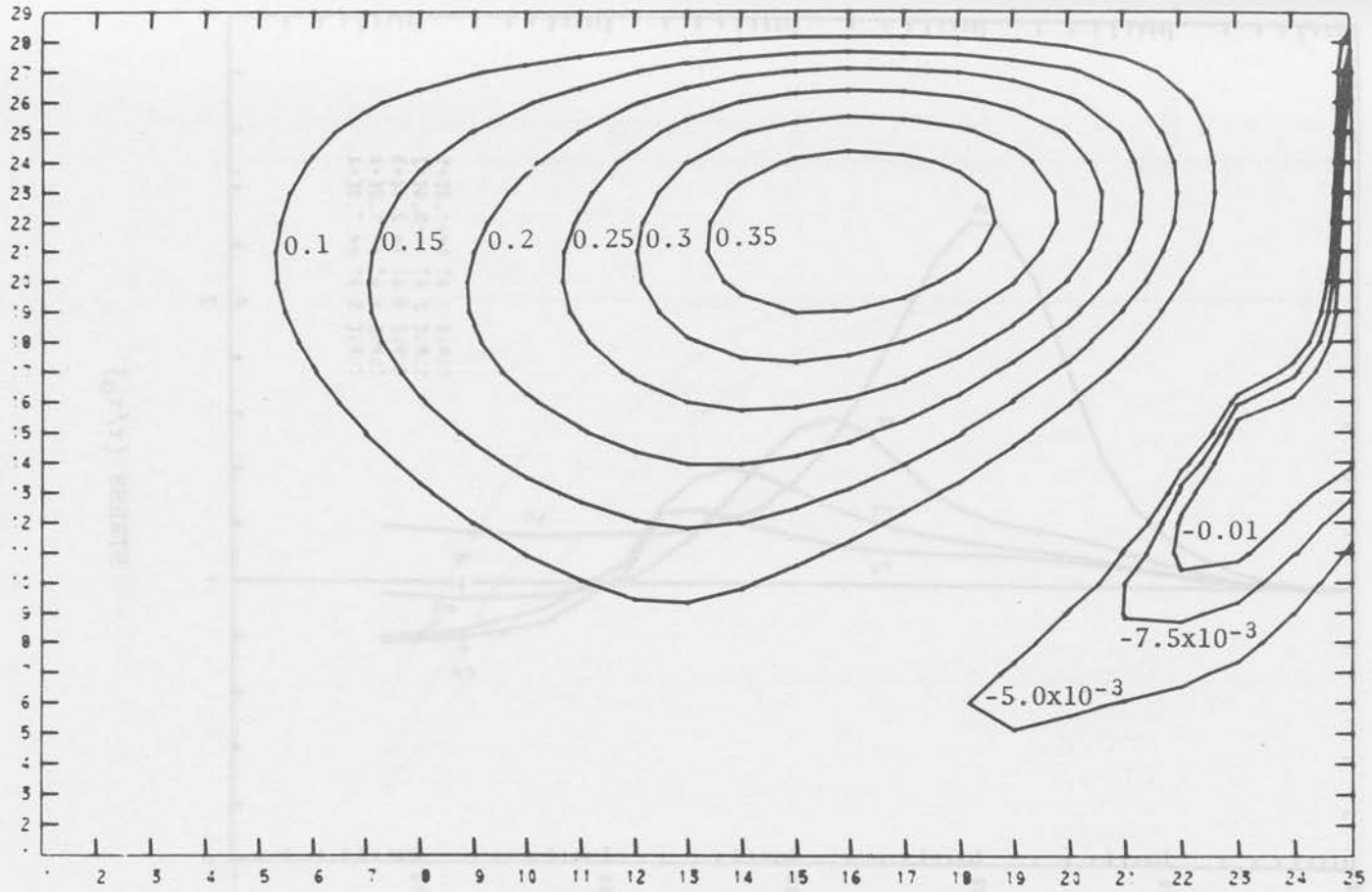

Figure 8.4-4 Distribution of a vertical velocity (kw/u_{*_o}) field corresponding flow in Fig. 8.4-1

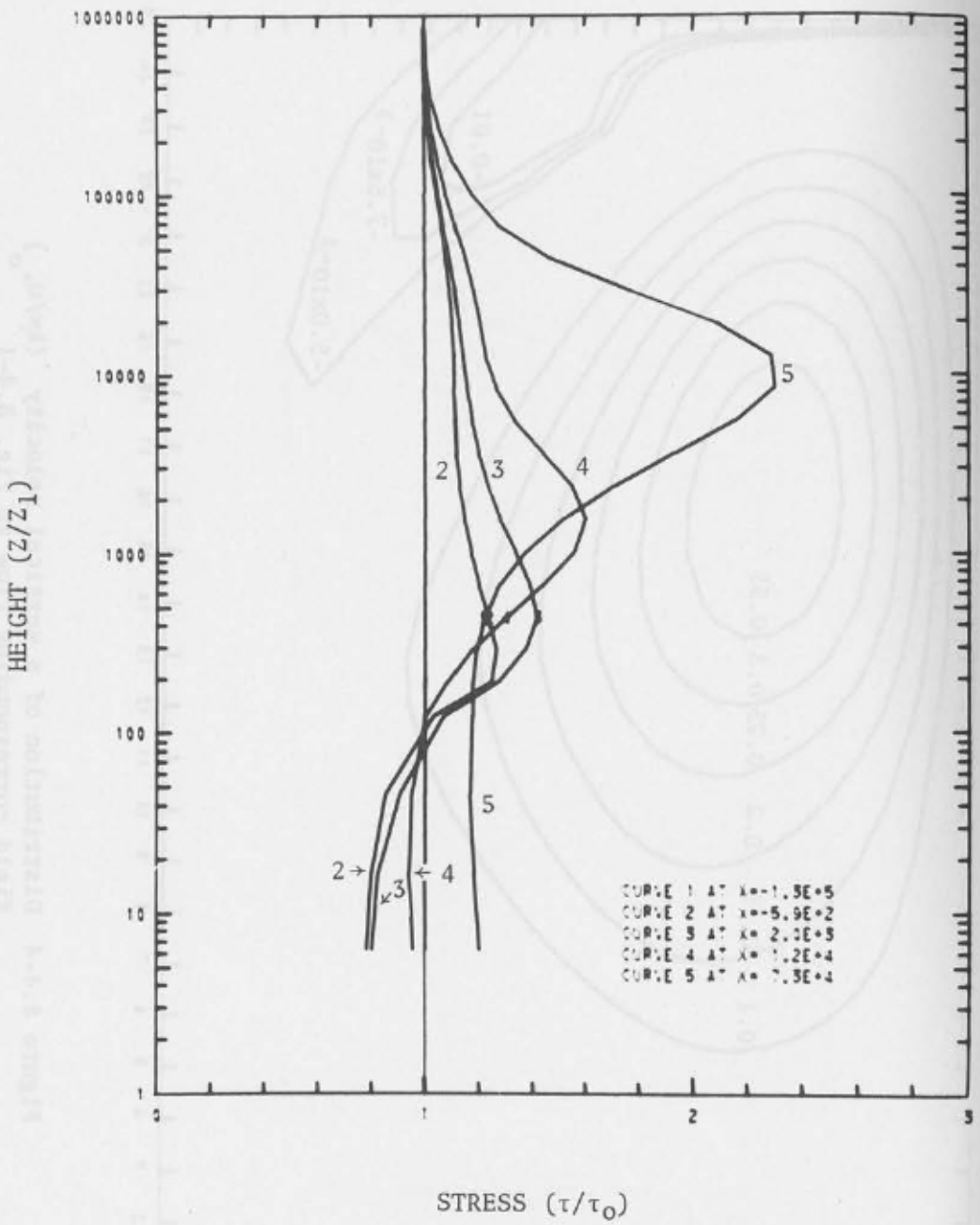

Figure 8.4-5 Nondimensional shear stress profiles corresponding flow in Fig. 8.4-1

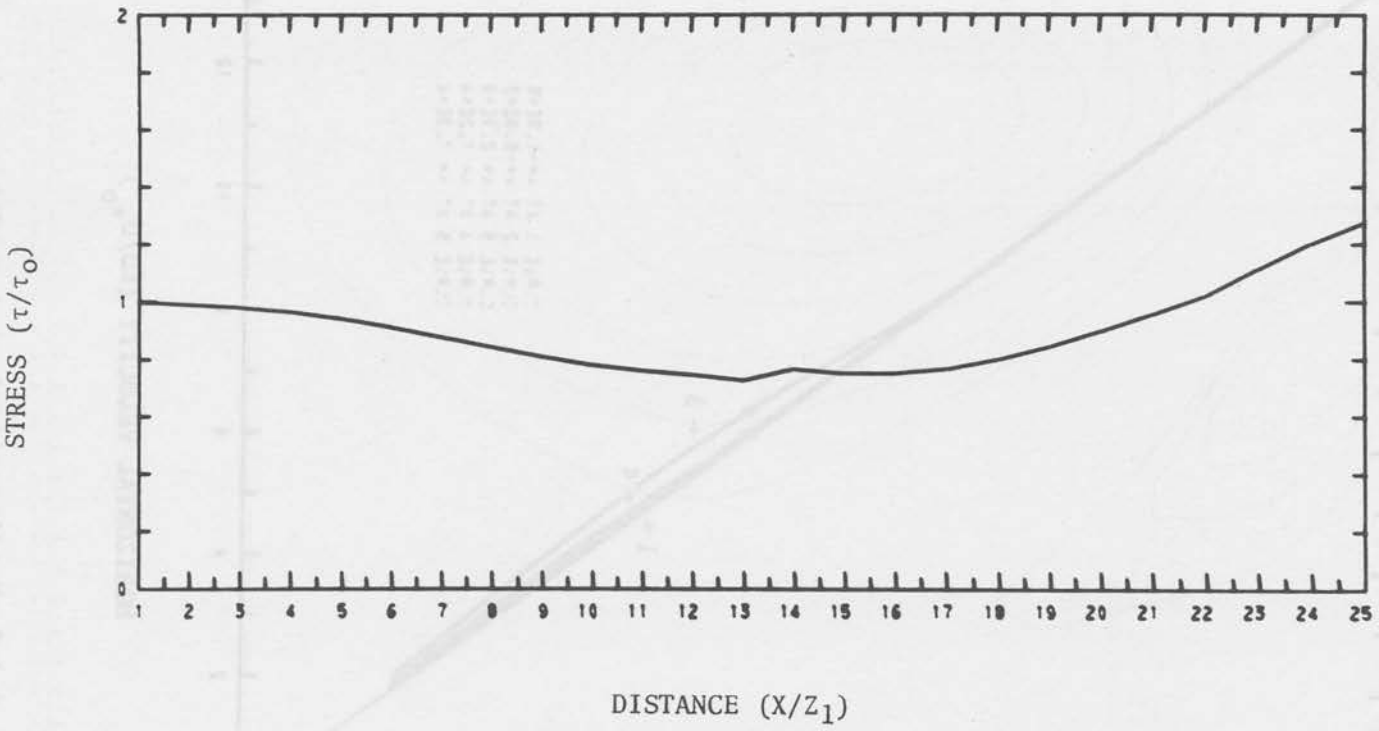

Figure 8.4-6 Distribution of nondimensional surface shear stress corresponding flow as in Fig. 8.4-1

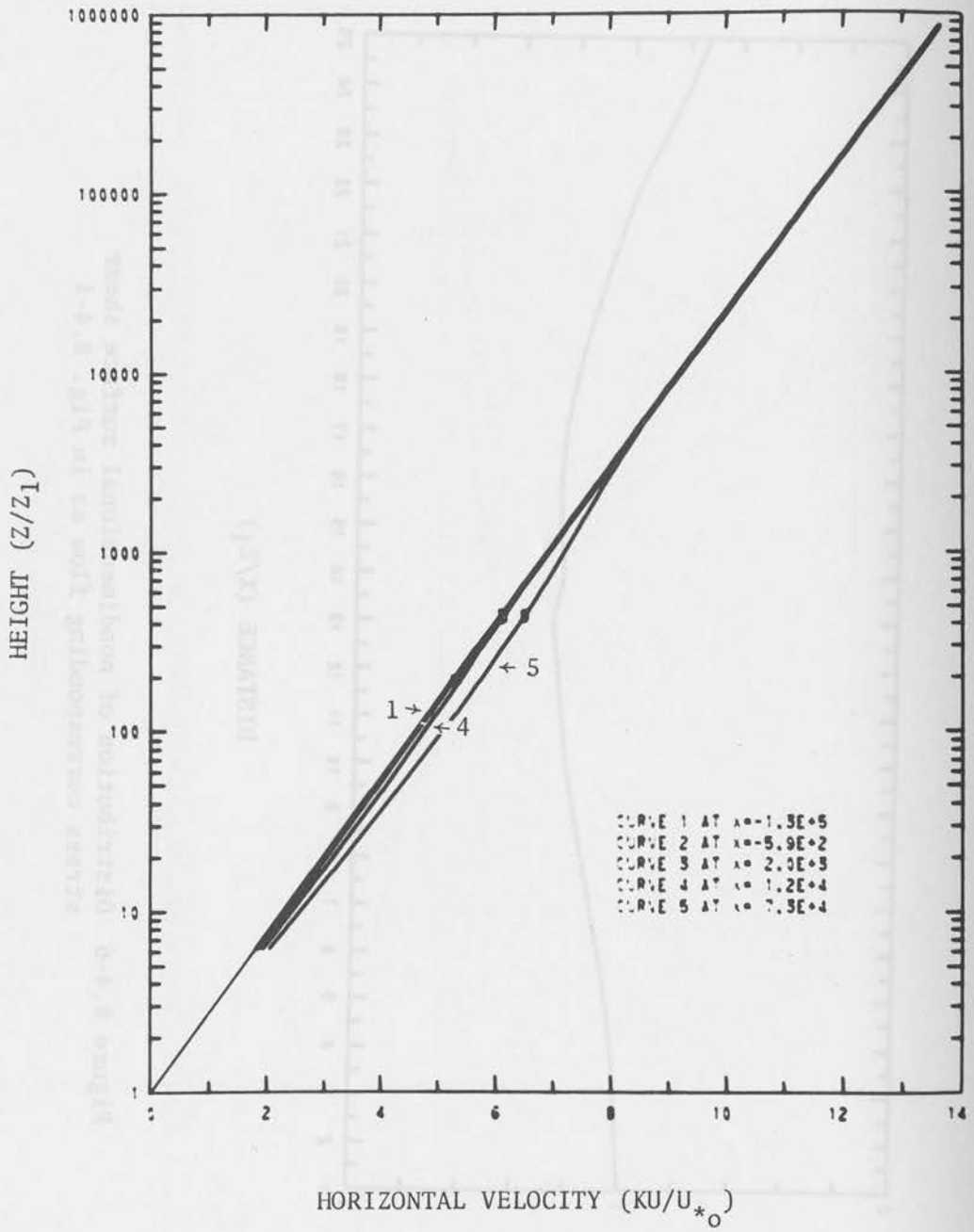

Figure 8.4-7 Nondimensional wind profiles as in Fig. 8.4-1 but without pressure terms

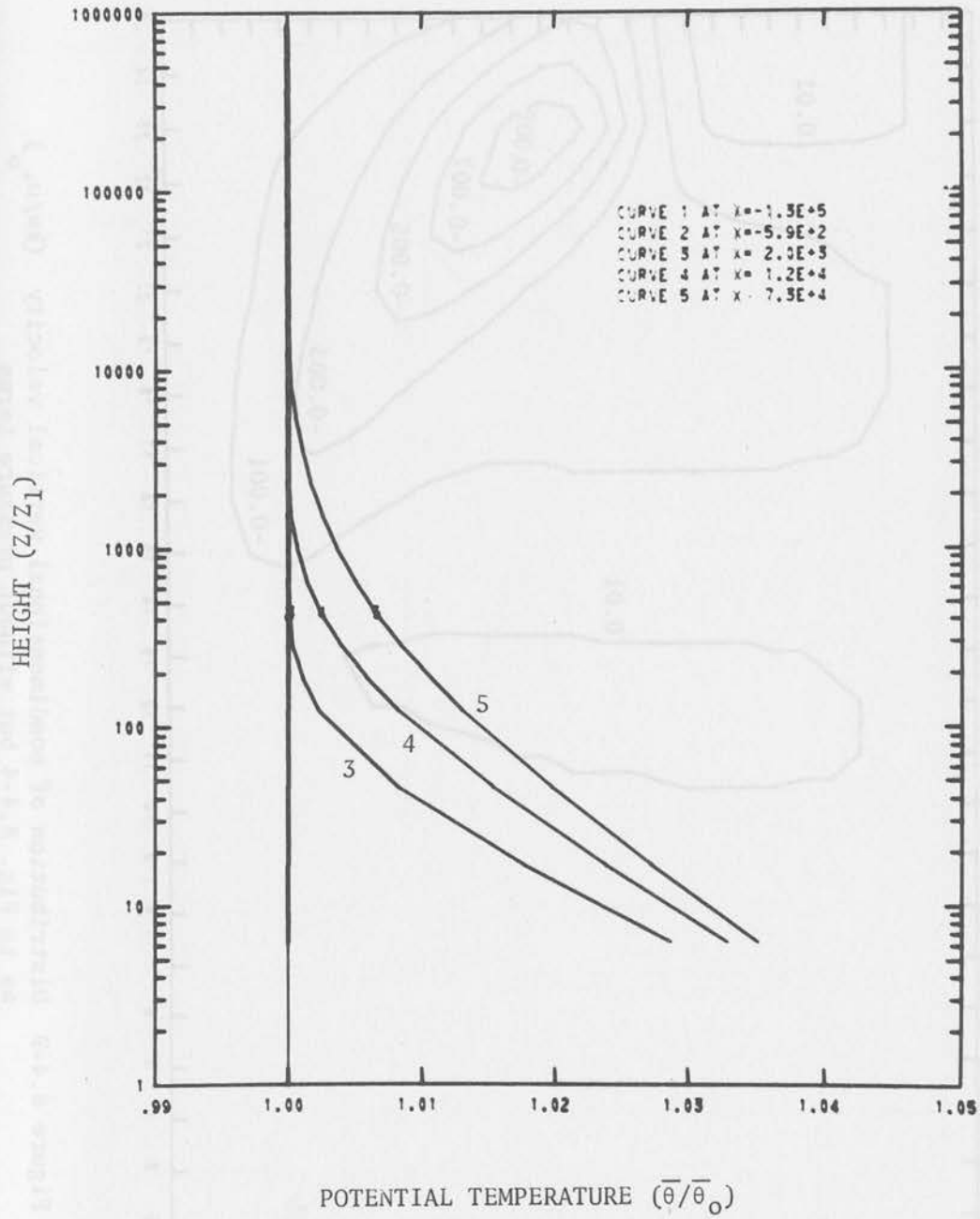

Figure 8.4-8 Nondimensional potential temperature profiles as in Fig. 8.4-2 but without pressure terms

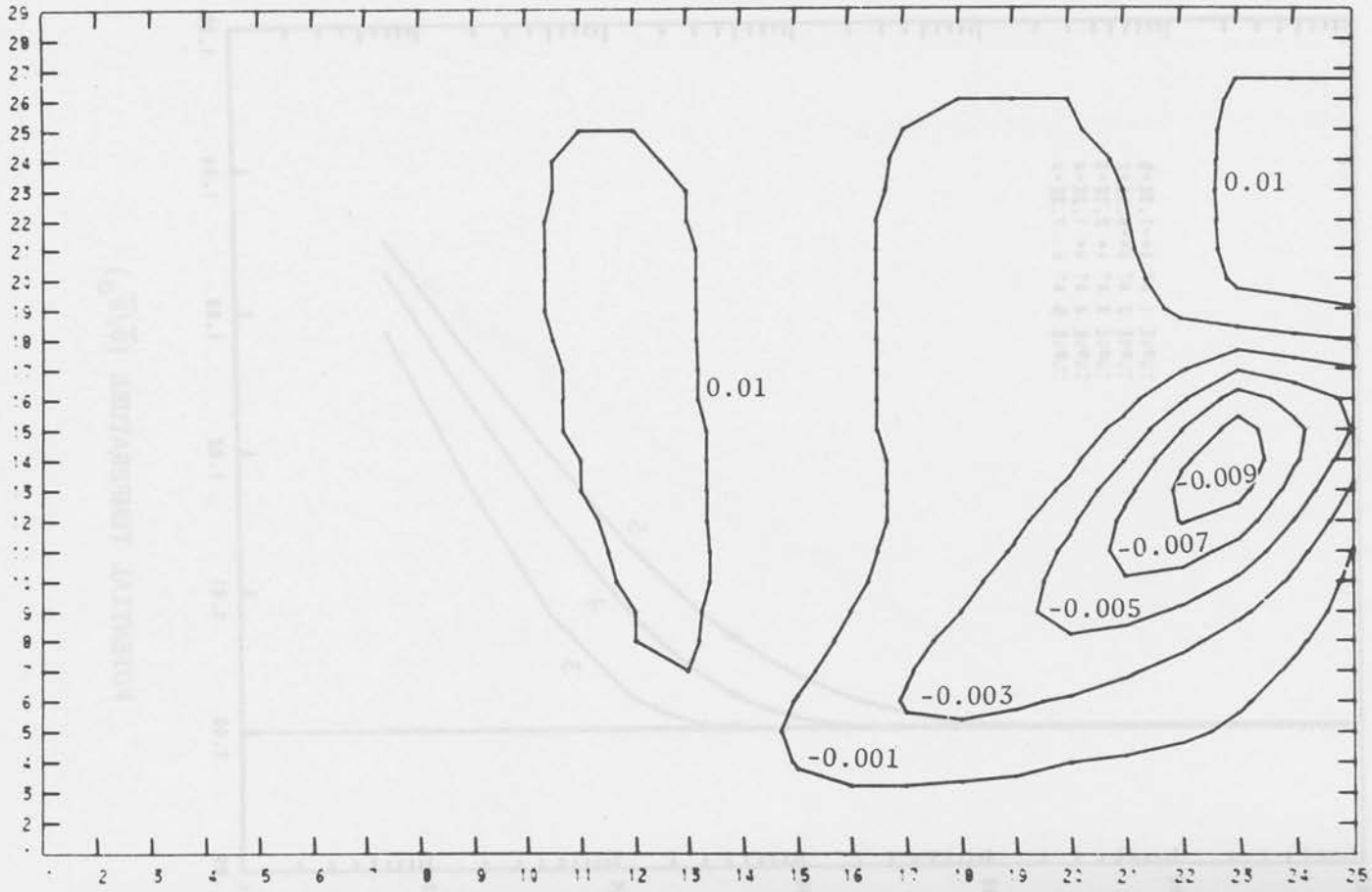

Figure 8.4-9 Distribution of nondimensional vertical velocity (kw/u_{*_o}) as in Fig. 8.4-4 but without pressure terms

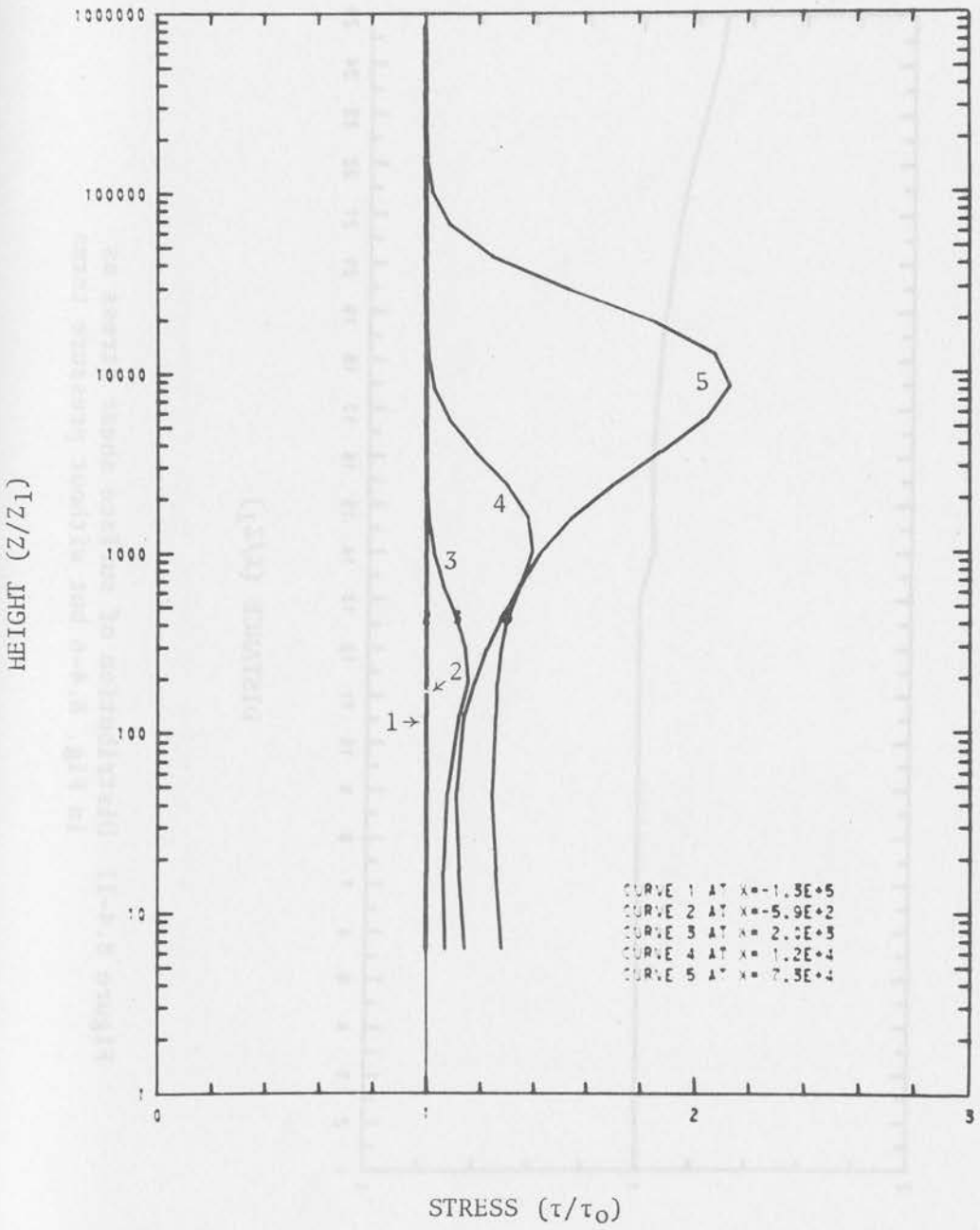

Figure 8.4-10 Nondimensional shear stress profiles as in Fig. 8.4-3 but without pressure terms

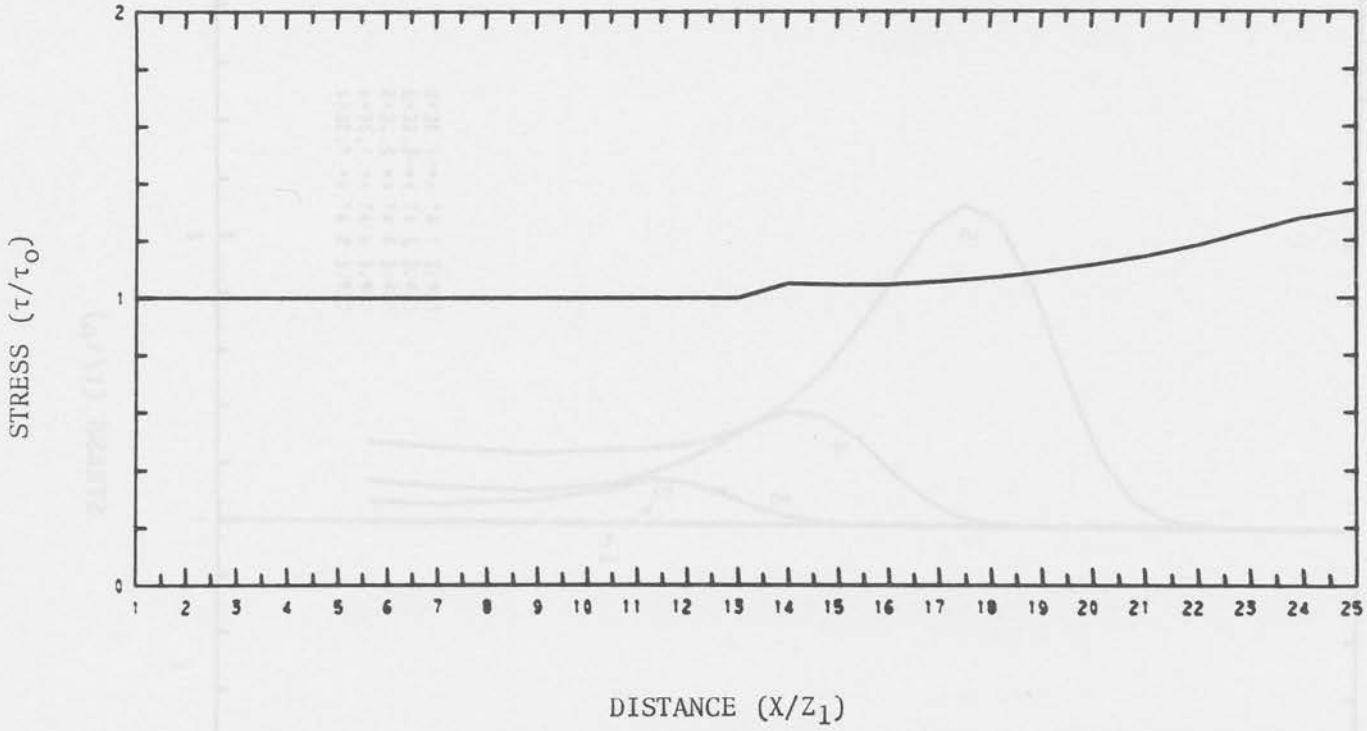

Figure 8.4-11 Distribution of surface shear stress as in Fig. 8.4-6 but without pressure terms

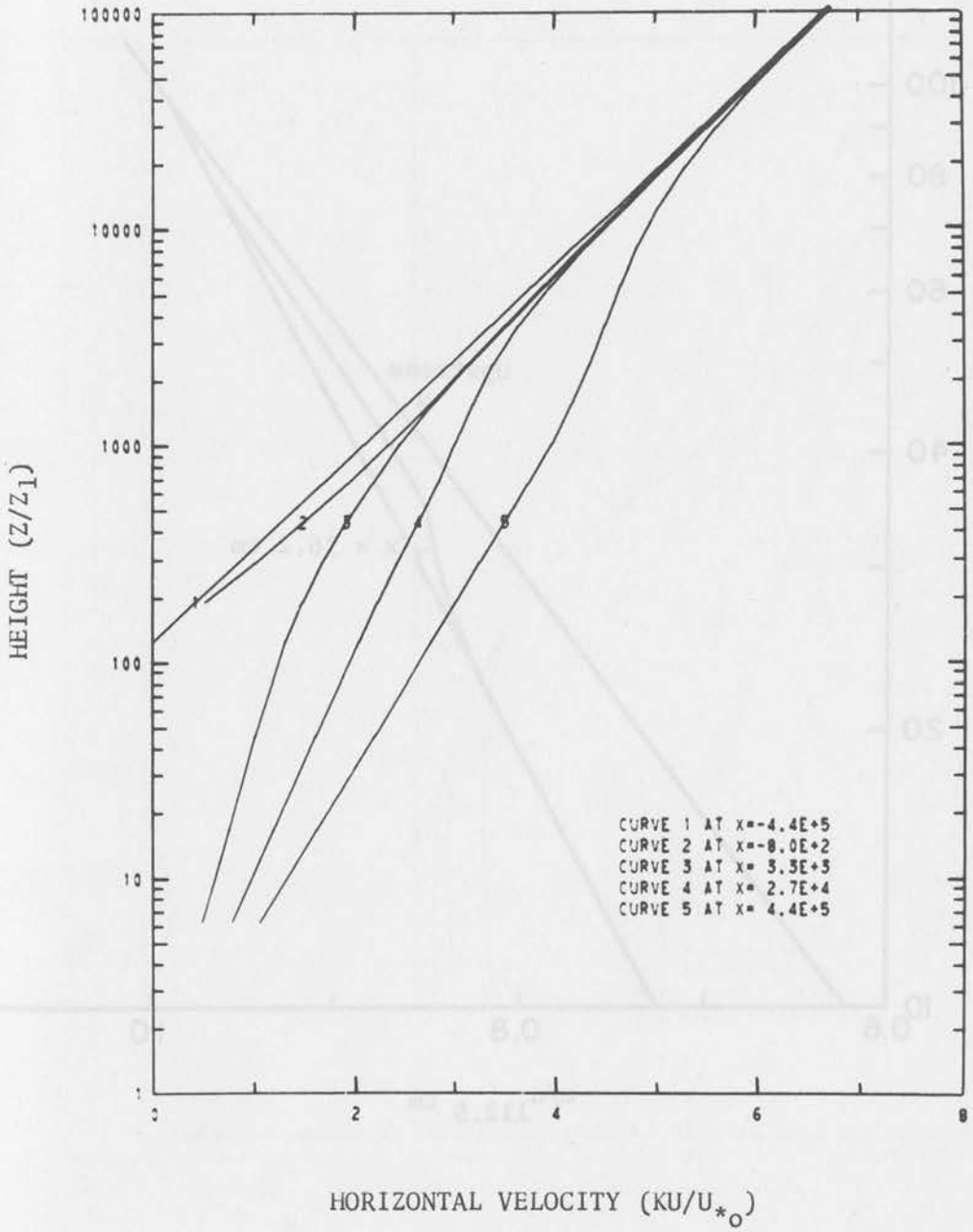

Figure 8.5-1 Nondimensional wind profiles at various nondimensional distances (x/z_1) from the origin for rough to smooth transition with $M \simeq 5$ under neutral condition

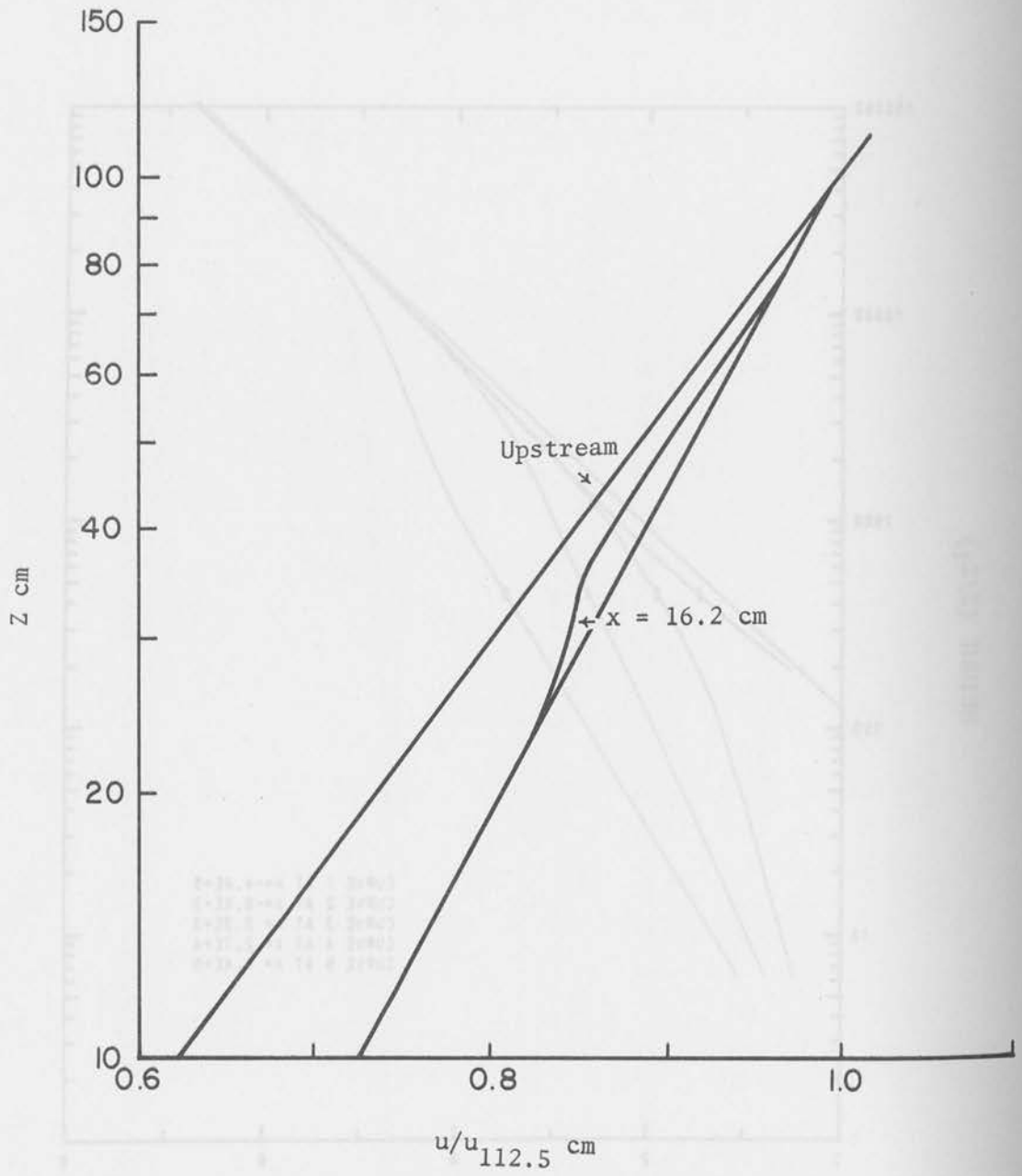

Figure 8.5-1a The inflection point shown in the wind profile at x = 16.2 cm for a rough to smooth transition (from Bradley's data, 1970)

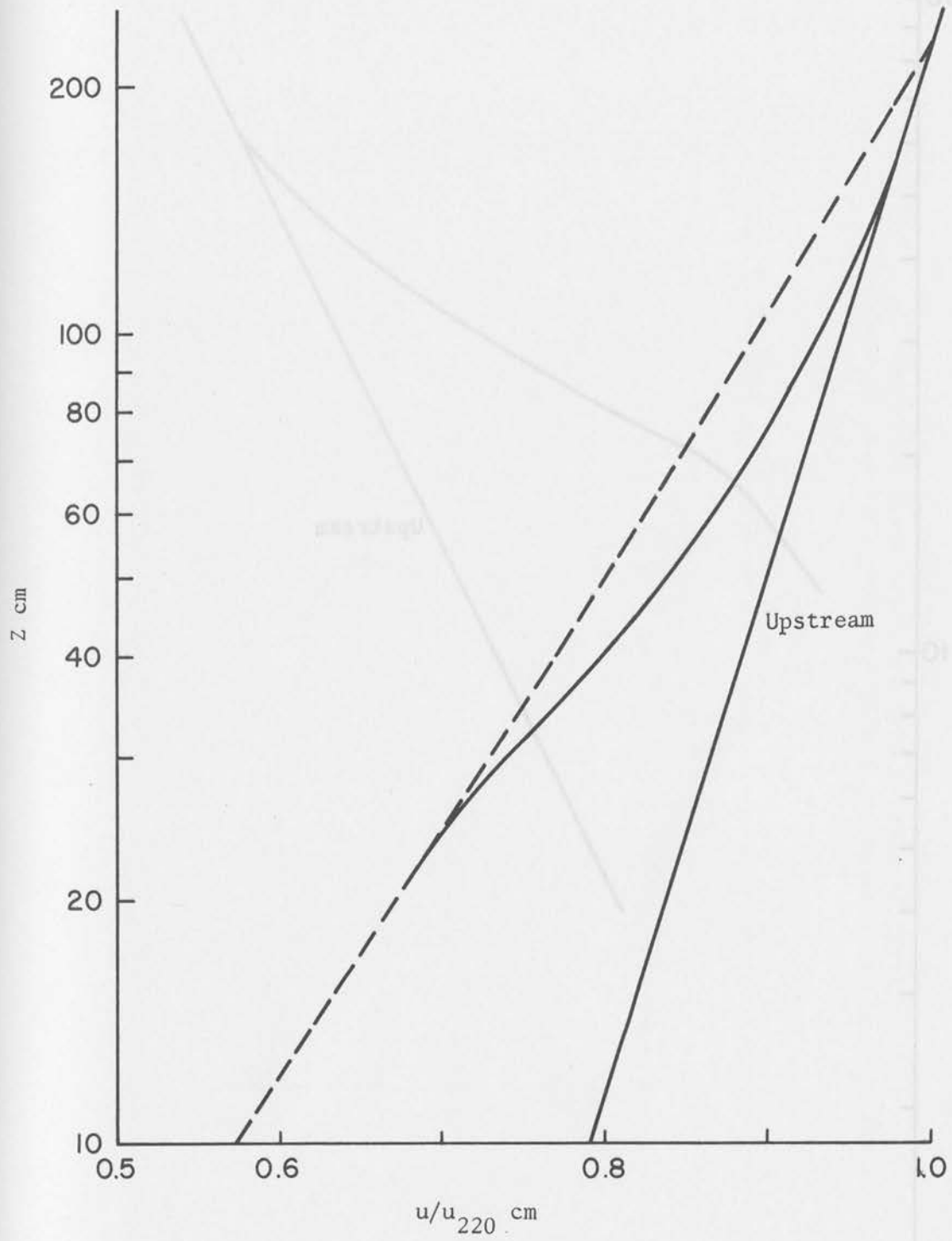

Figure 8.5-1b The inflection point shown in the wind profile at x = 16.2 cm for a smooth to rough transition (from Bradley's data, 1970)

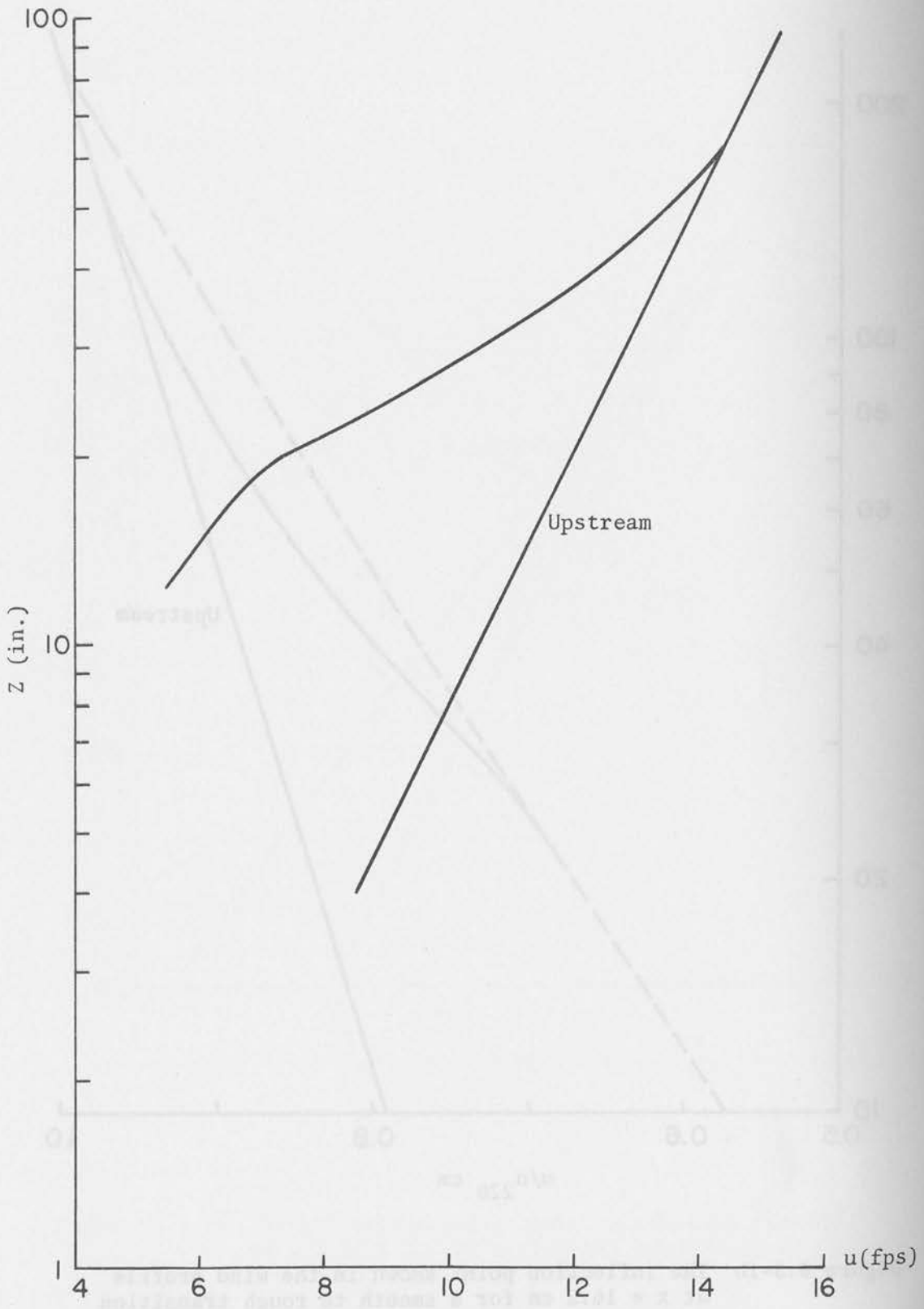

Figure 8.5-1c The inflection point shown in the wind profile for a smooth to rough transition (Yeh and Nickerson, 1970)

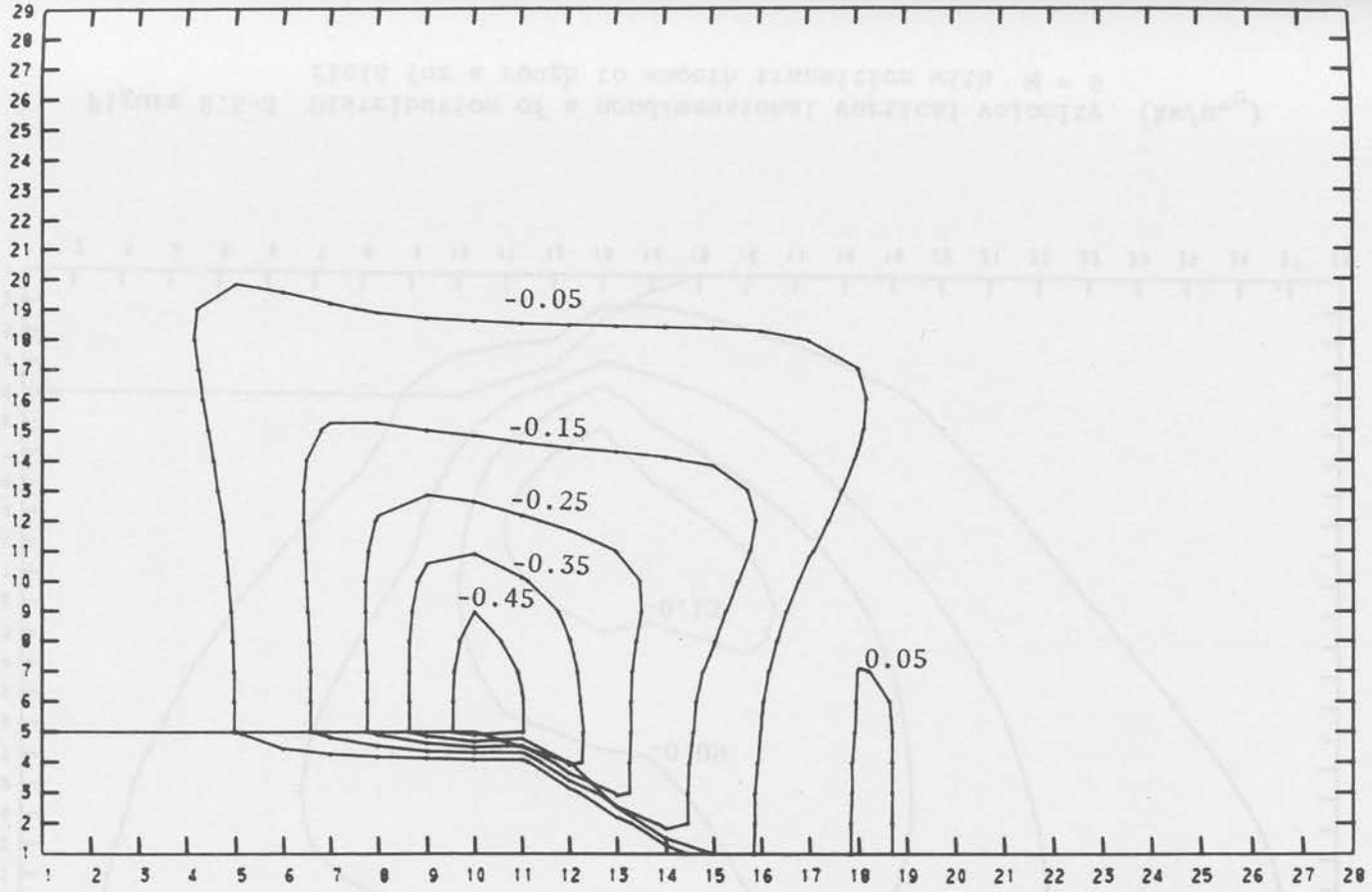

Figure 8.5-2 Distribution of a nondimensional pressure $(k^2p/u_{*_o}^2)$ field (deviation from the hydrostatic pressure) for a rough to smooth transition with $M \simeq 5$

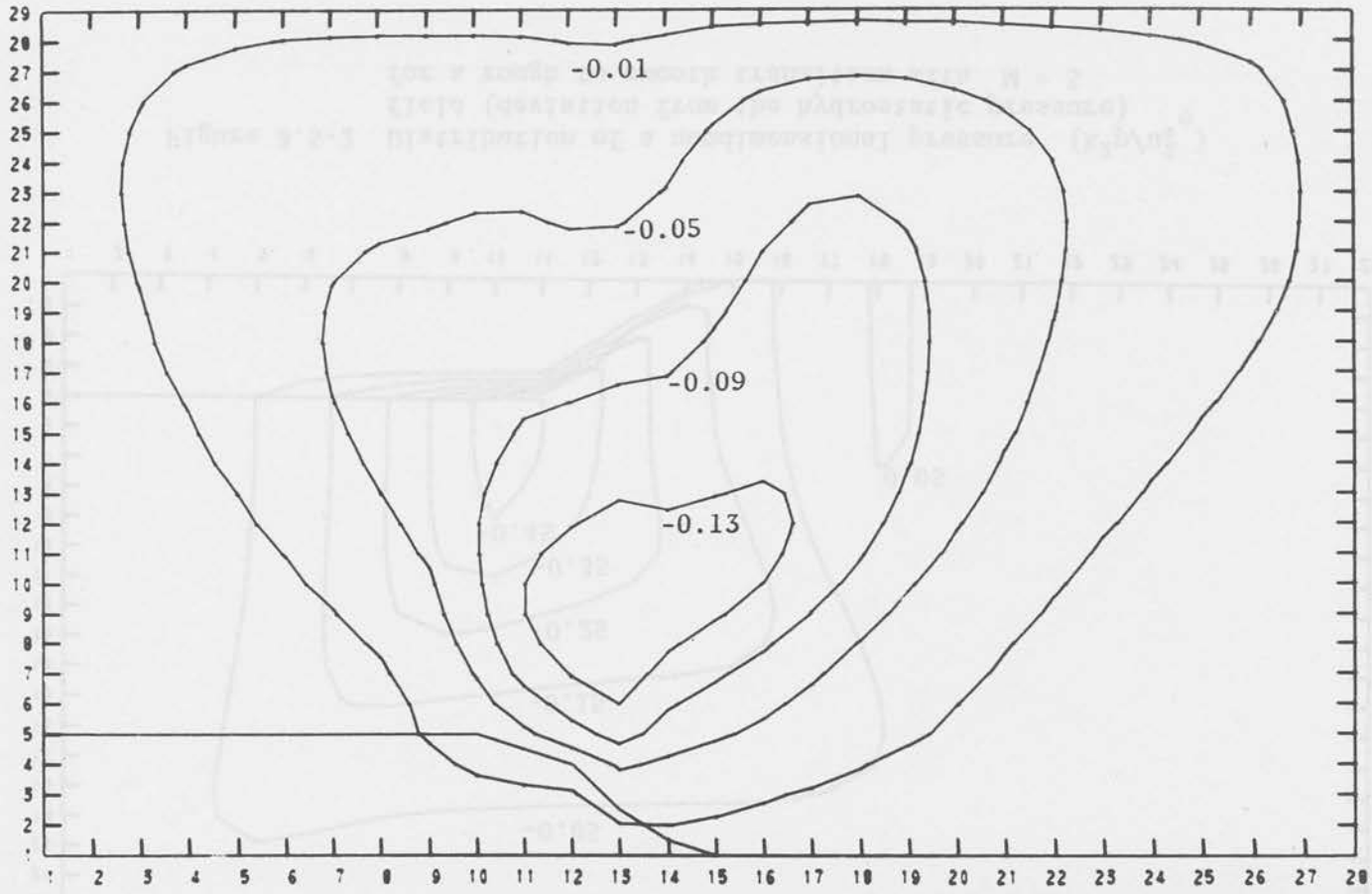

Figure 8.5-3 Distribution of a nondimensional vertical velocity (kw/u_{*_o}) field for a rough to smooth transition with $M \simeq 5$

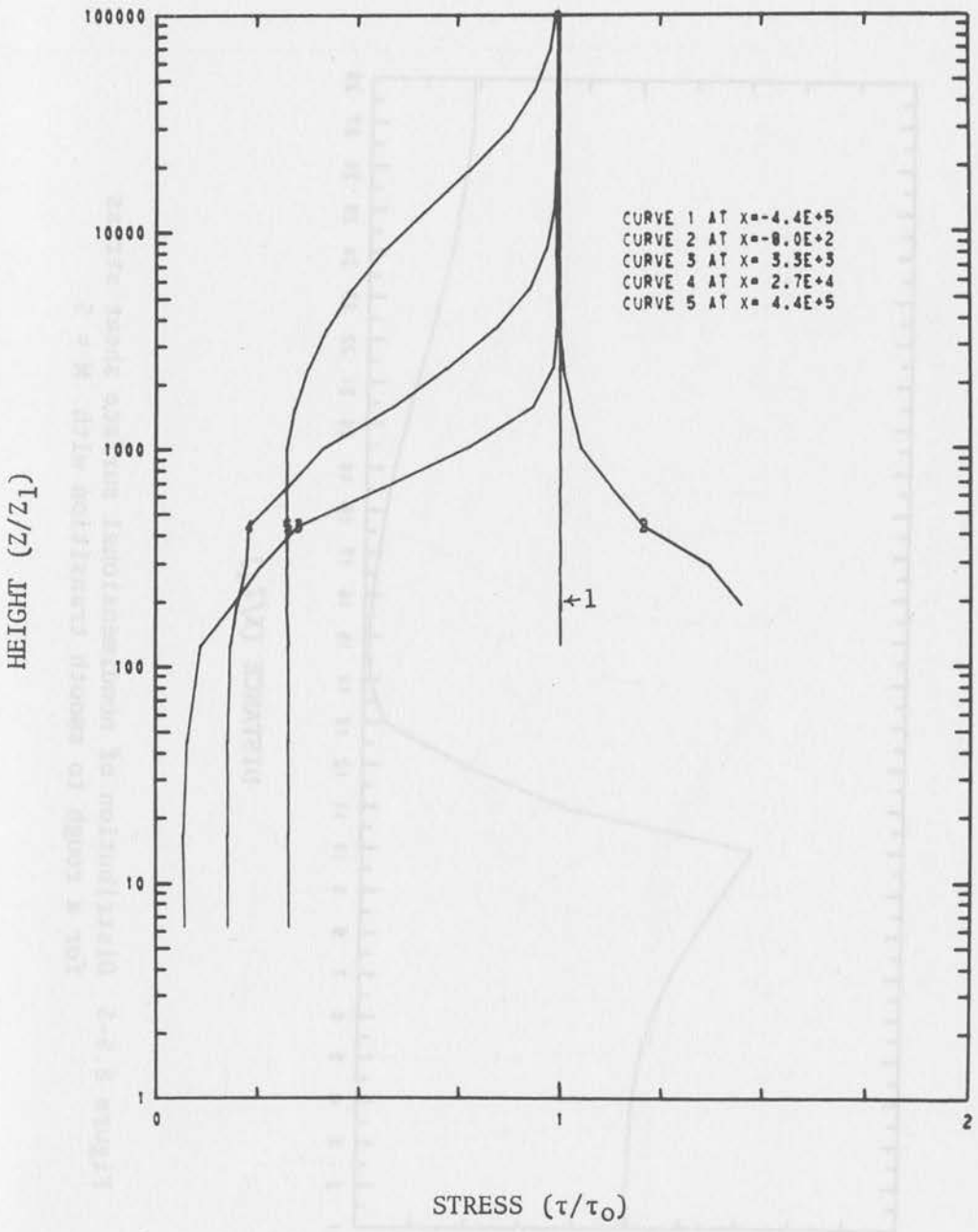

Figure 8.5-4 Nondimensional shear stress profiles for various nondimensional distances (x/z_1) from the origin for a rough to smooth transition with $M \simeq 5$

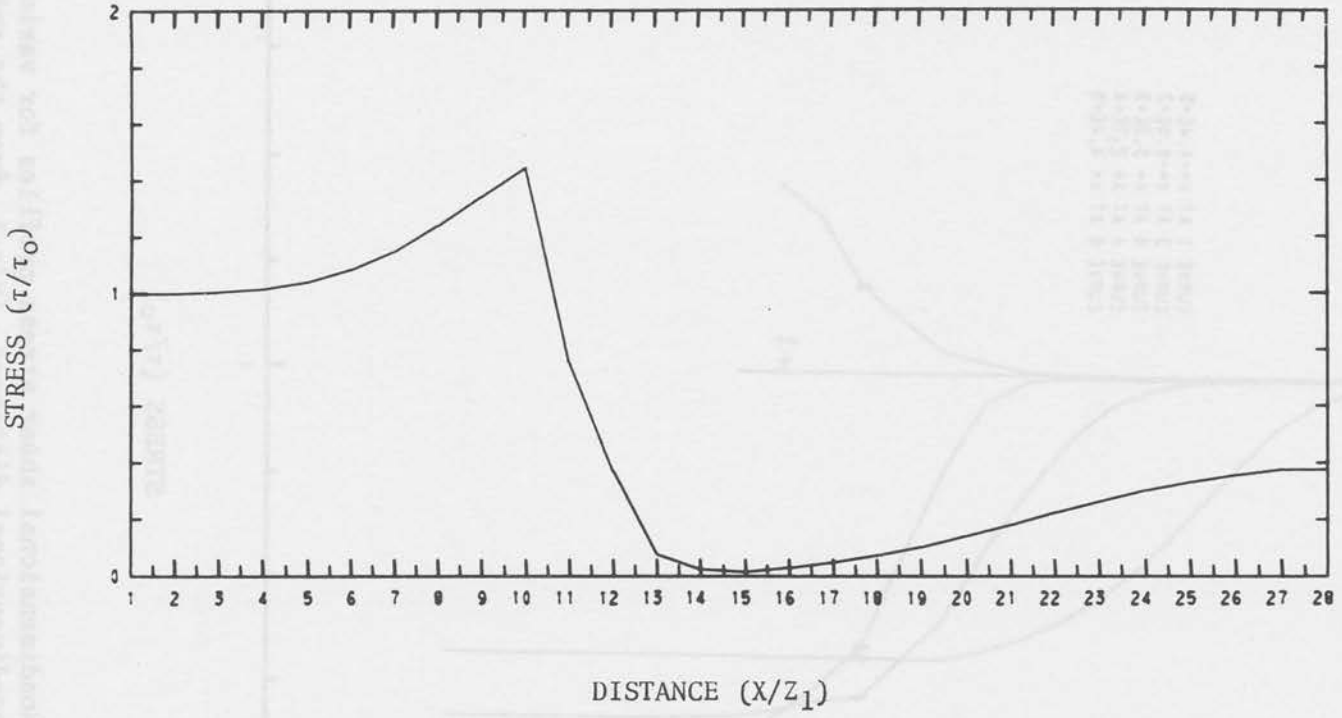

Figure 8.5-5 Distribution of nondimensional surface shear stress for a rough to smooth transition with $M \simeq 5$

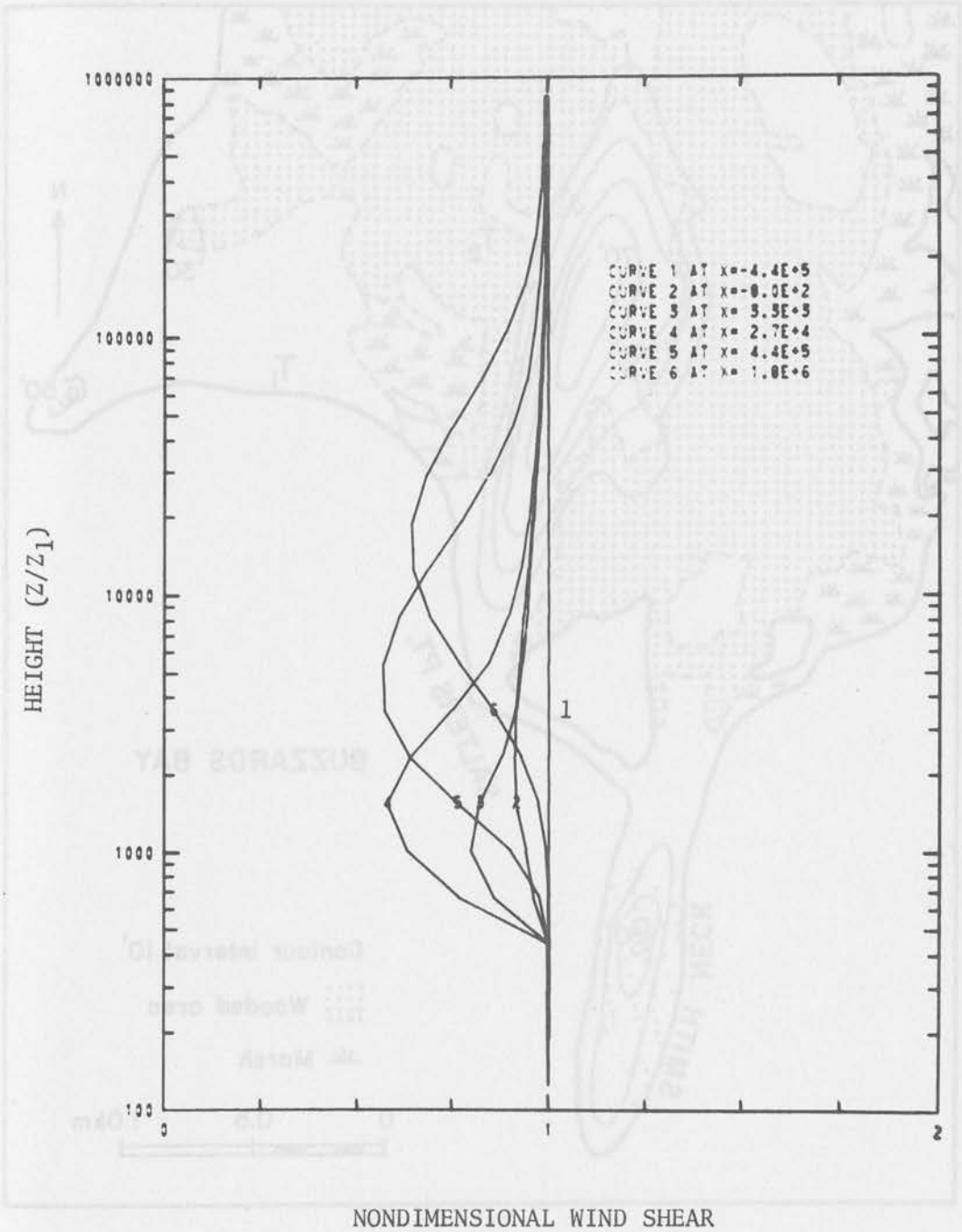

Figure 8.5-6 Nondimensional wind shears for various nondimensional distances (x/z_1) from the origin of roughness discontinuity with $M \simeq 5$. Pressure terms included

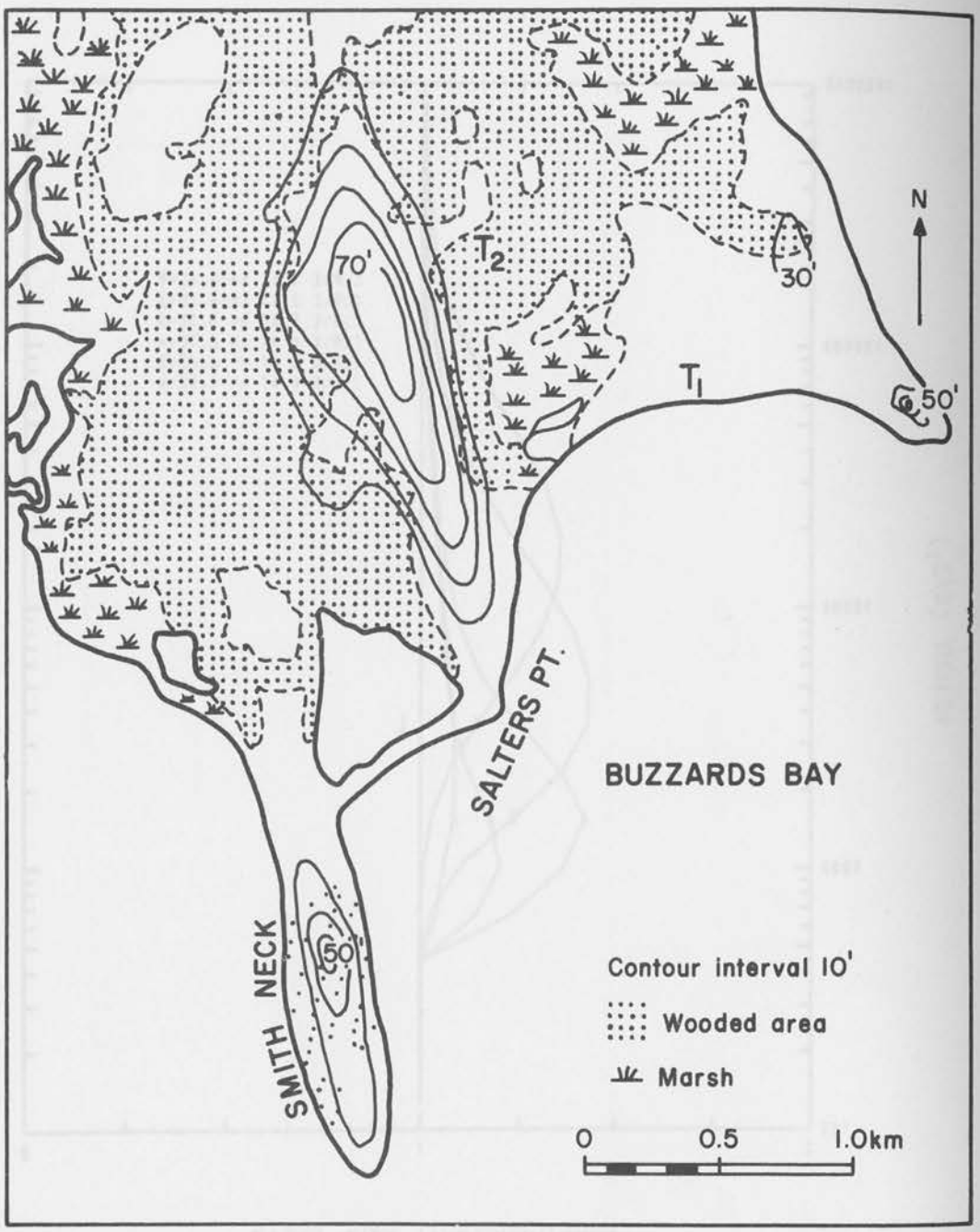

Figure 8.5-7 Topographic map of Round Hill Field Stations and the surrounding area. Tower sites denoted by T_1 and T_2 (from Cramer, 1969)

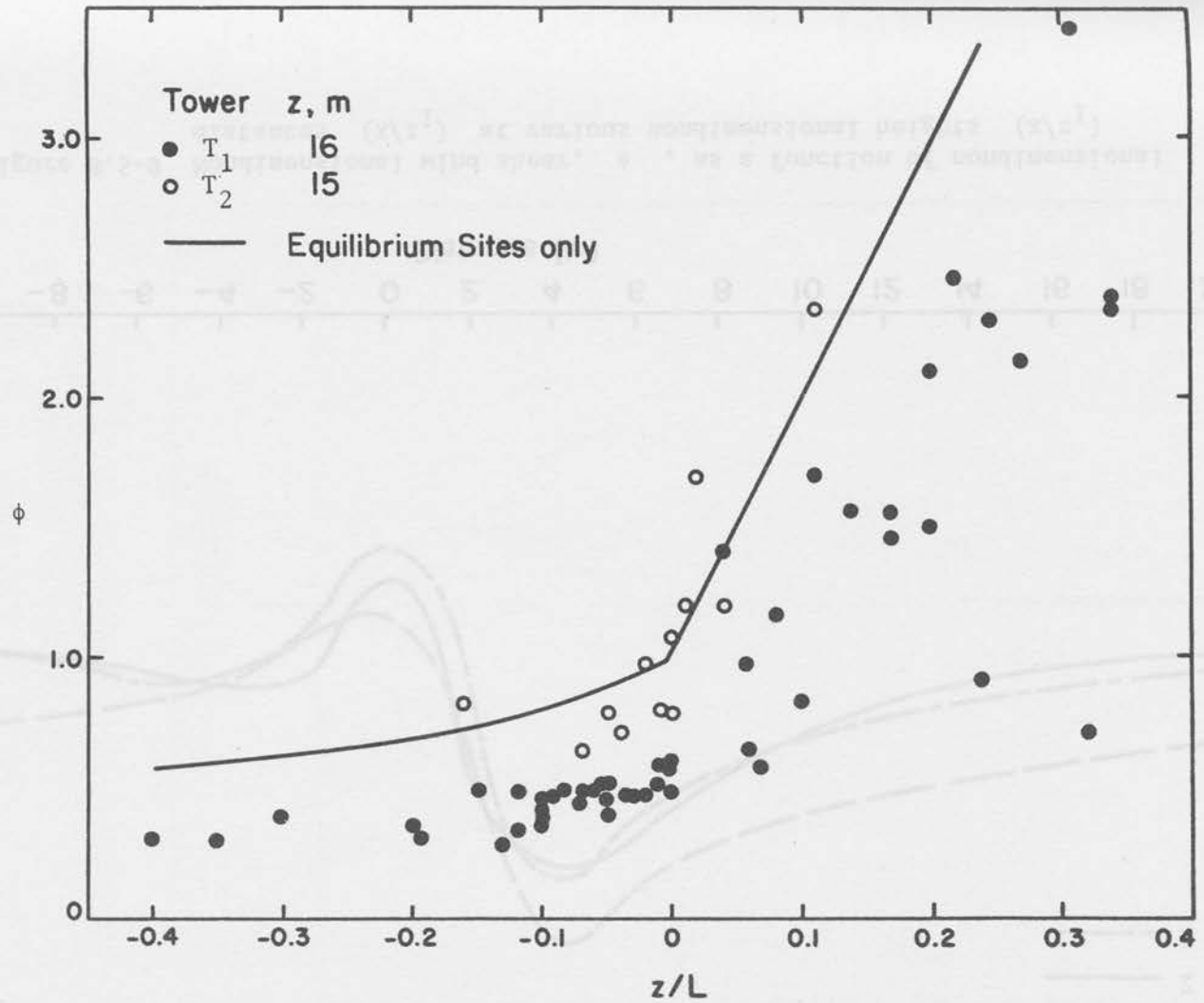

Figure 8.5-8 Nondimensional wind shear, ϕ , at South Dartmouth as a function of z/L (from Bush and Panofsky, 1968)

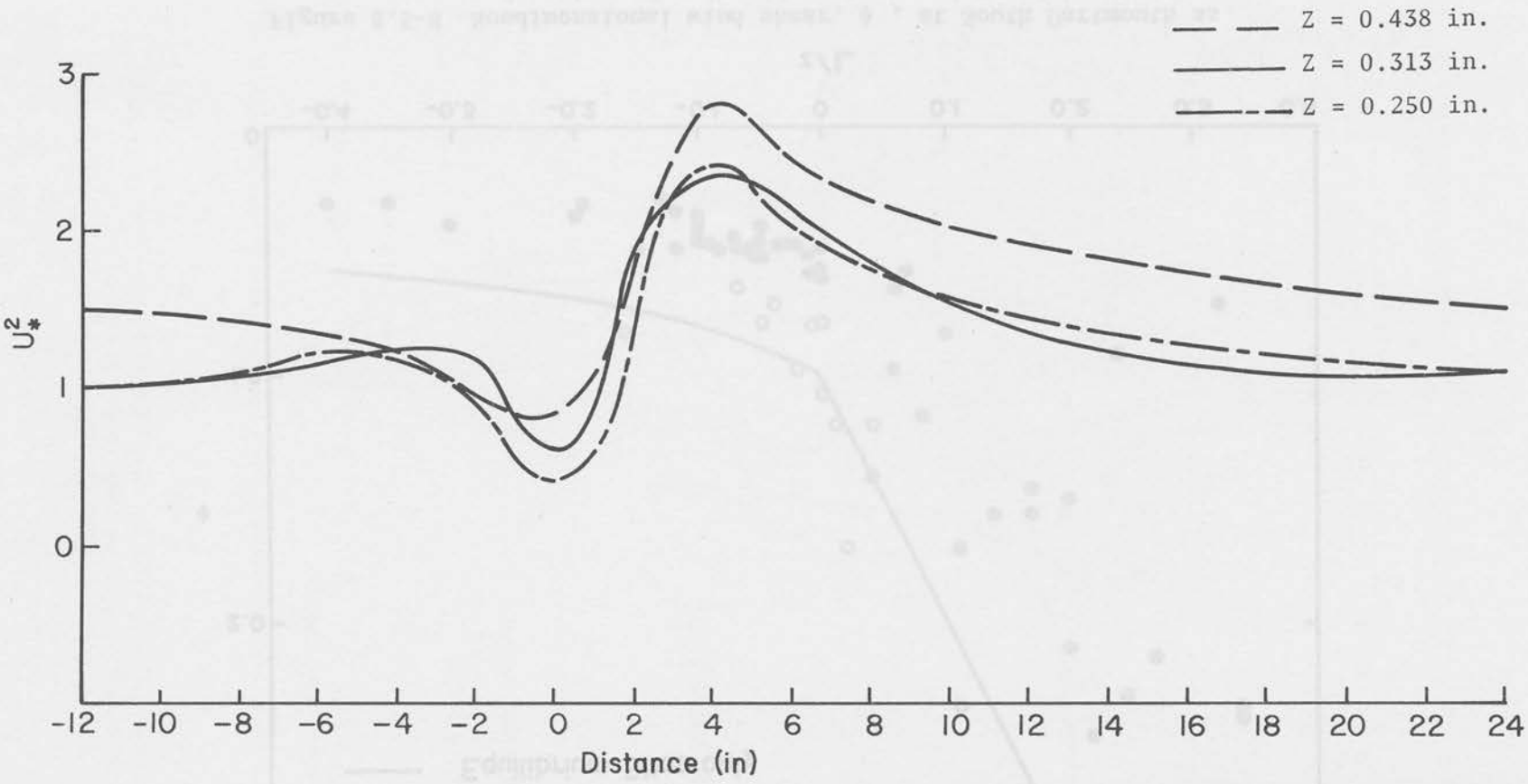

Figure 8.5-9 Nondimensional wind shear, ϕ , as a function of nondimensional distances (x/z_1) at various nondimensional heights (x/z_1)

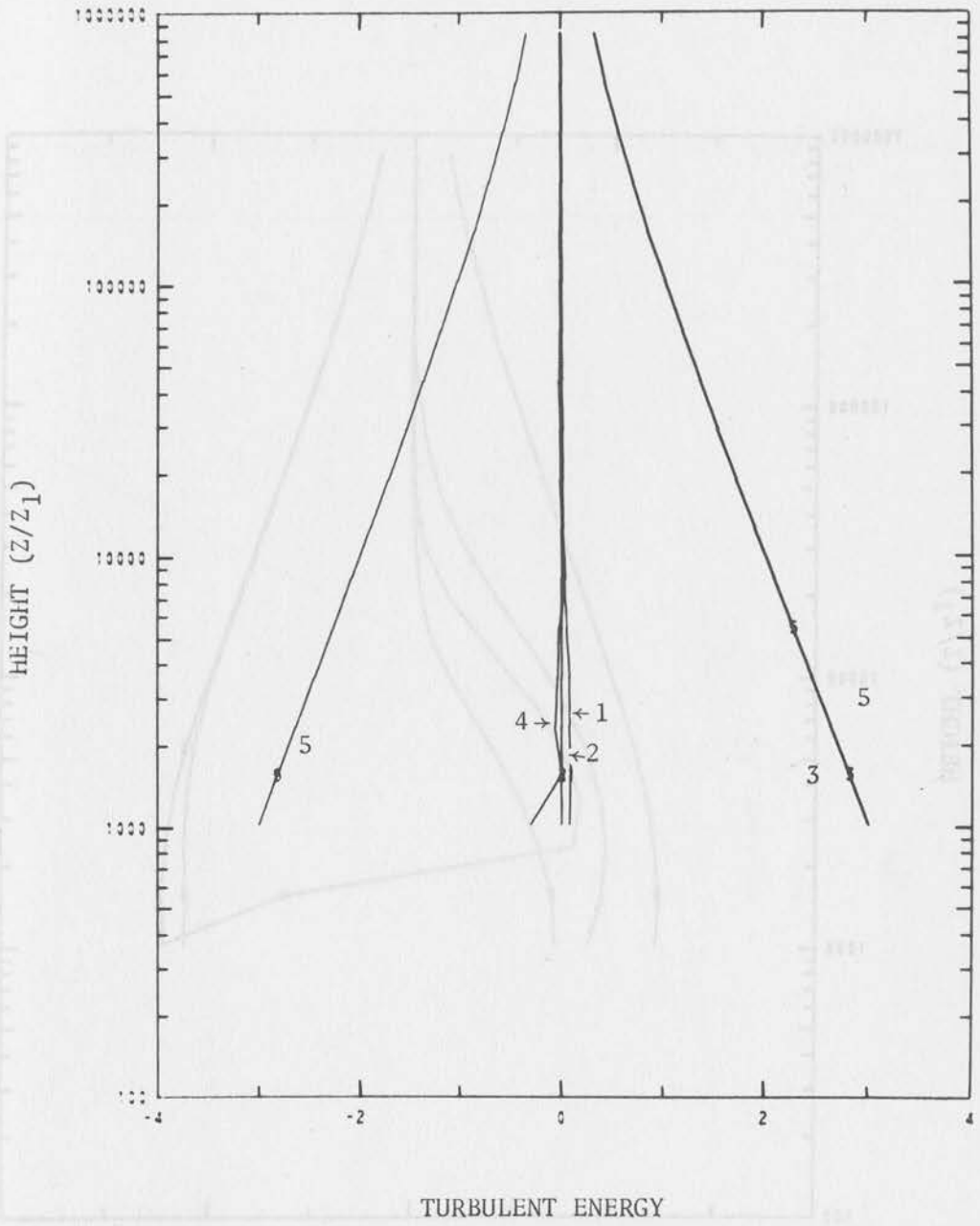

Figure 8.5-10 Terms in the turbulent energy equation at nondimensional distance $x = 2.2 \times 10^5$.
Pressure terms included.
Curve 1: Horizontal advection
Curve 2: Vertical advection
Curve 3: Production
Curve 4: Diffusion
Curve 5: Dissipation

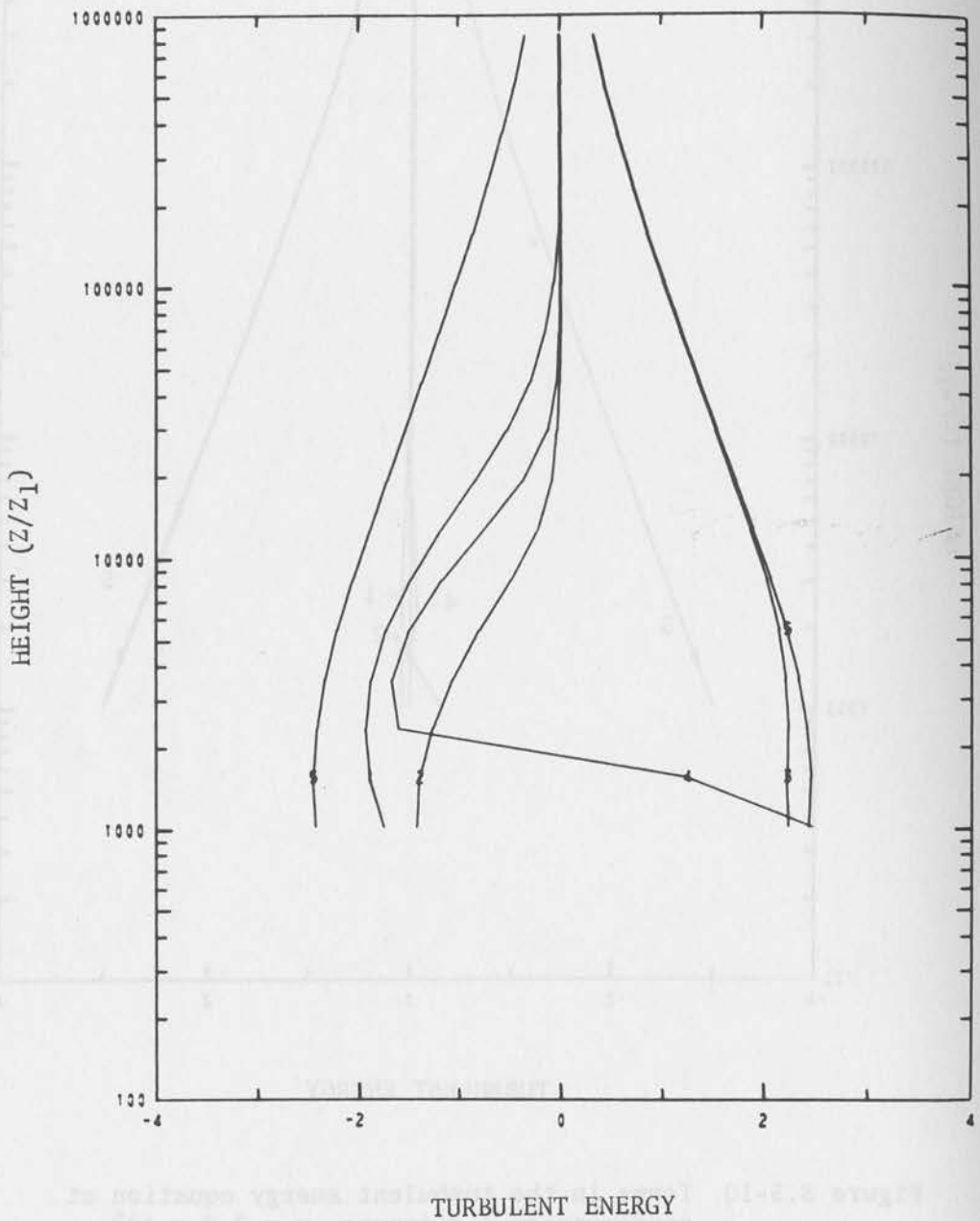

Figure 8.5-11 Terms in the turbulent energy equation at nondimensional distance $x = 2.7 \times 10^4$ as in Fig. 8.5-10

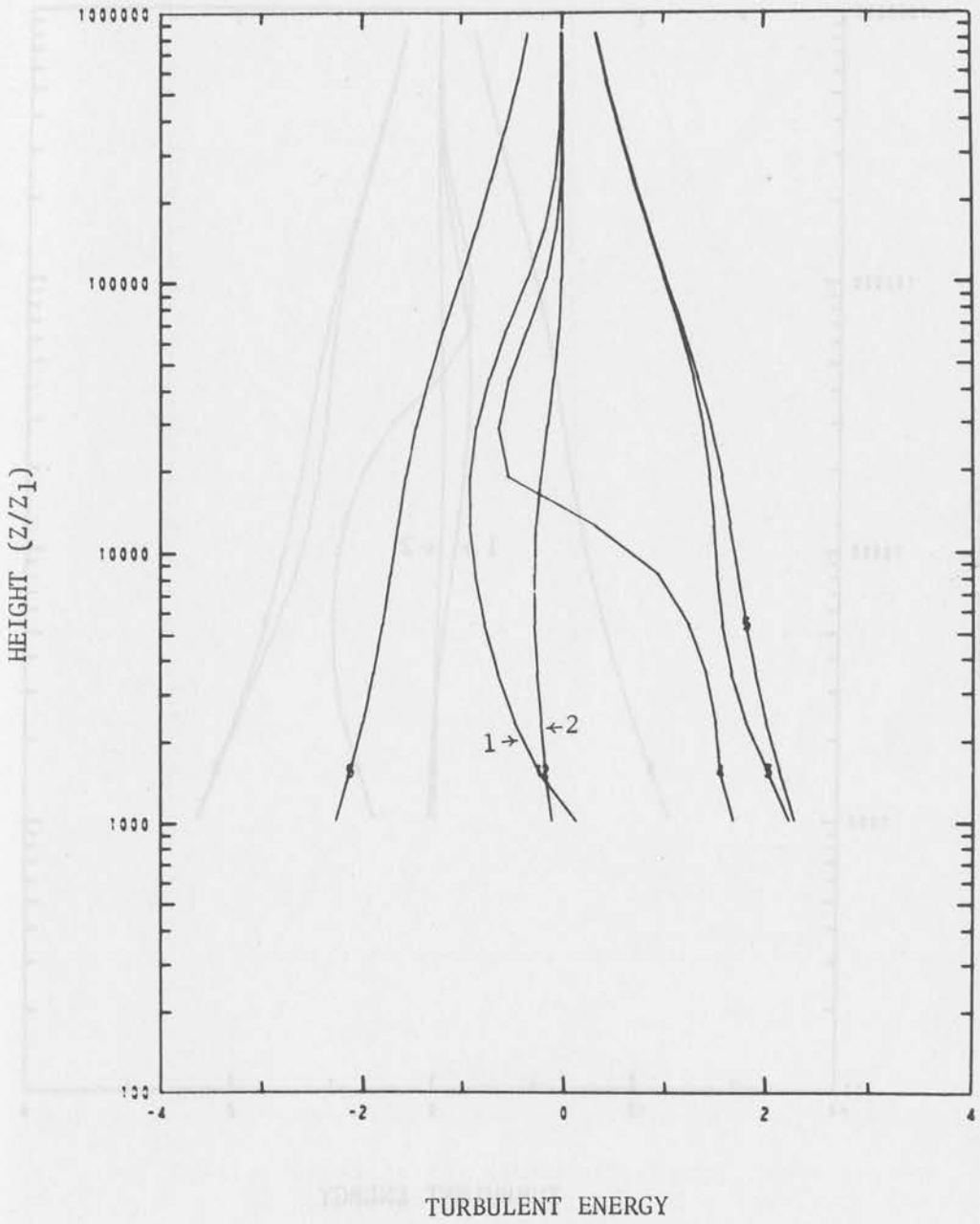

Figure 8.5-12 Terms in the turbulent energy equation at nondimensional distance $x = 4.4 \times 10^5$ as in Fig. 8.5-10

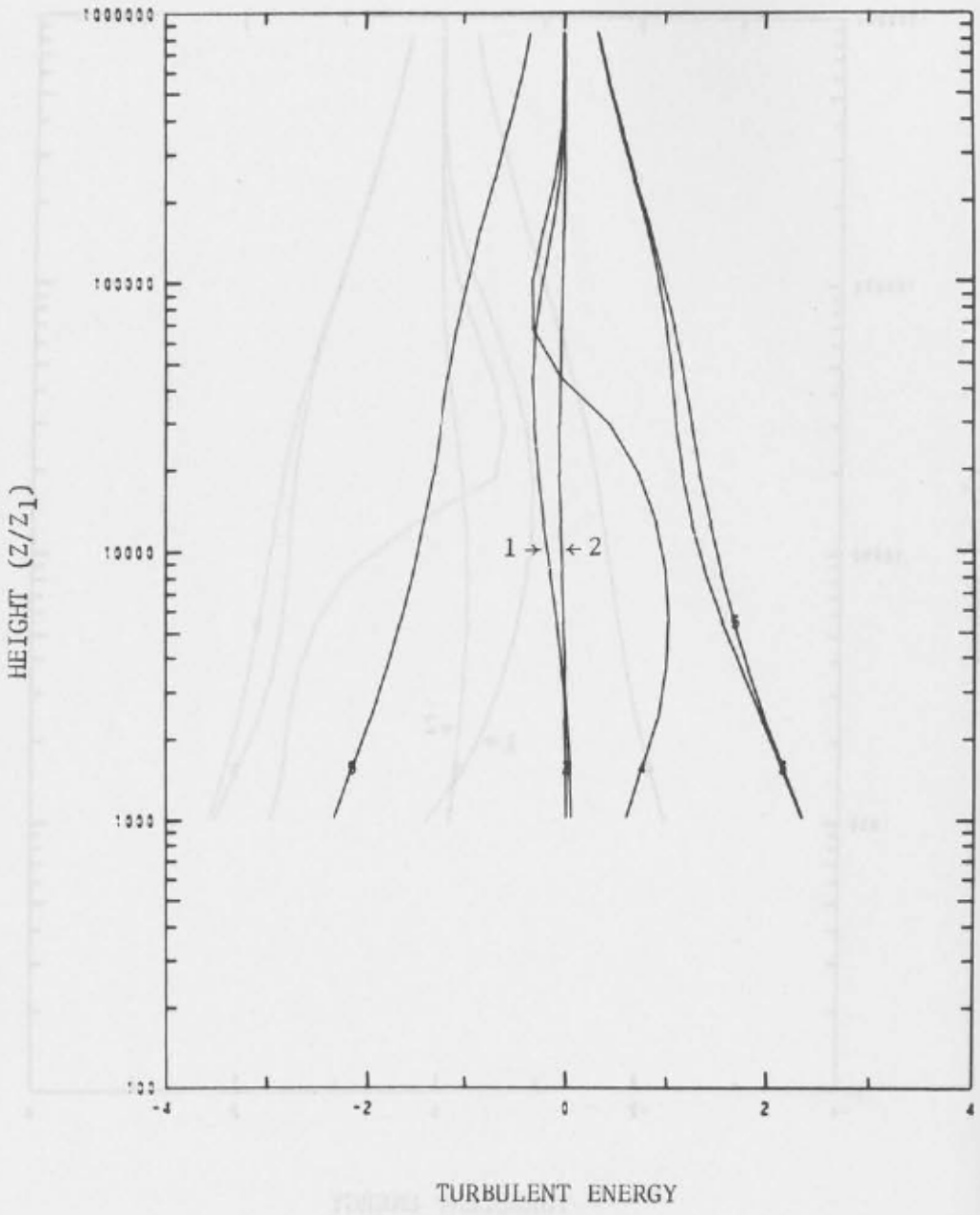

Figure 8.5-13 Terms in the turbulent energy equation at nondimensional distance $x = 1.8 \times 10^6$ as in Fig. 8.5-10

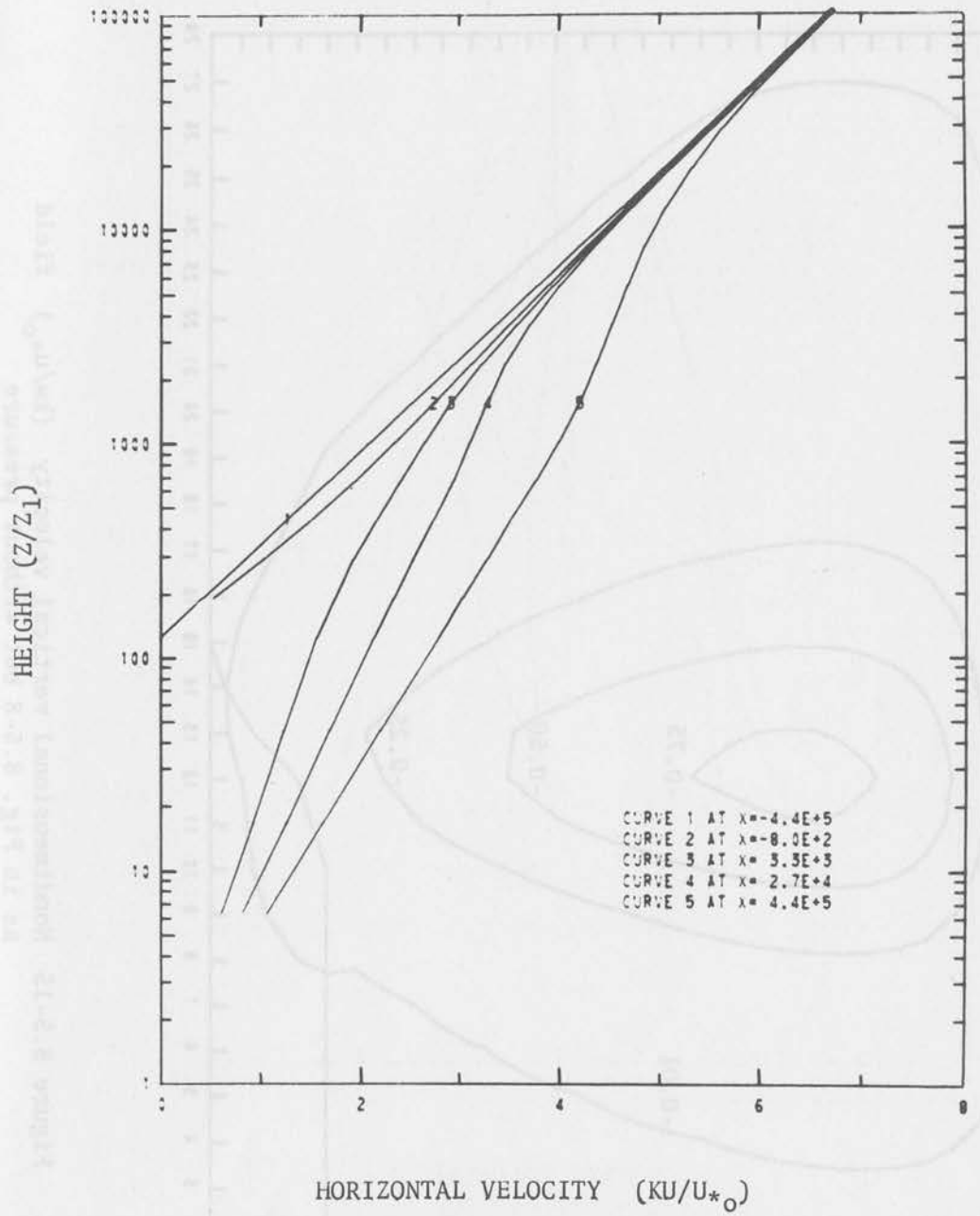

Figure 8.5-14 Nondimensional wind profiles as in Fig. 8.5-1 but without pressure

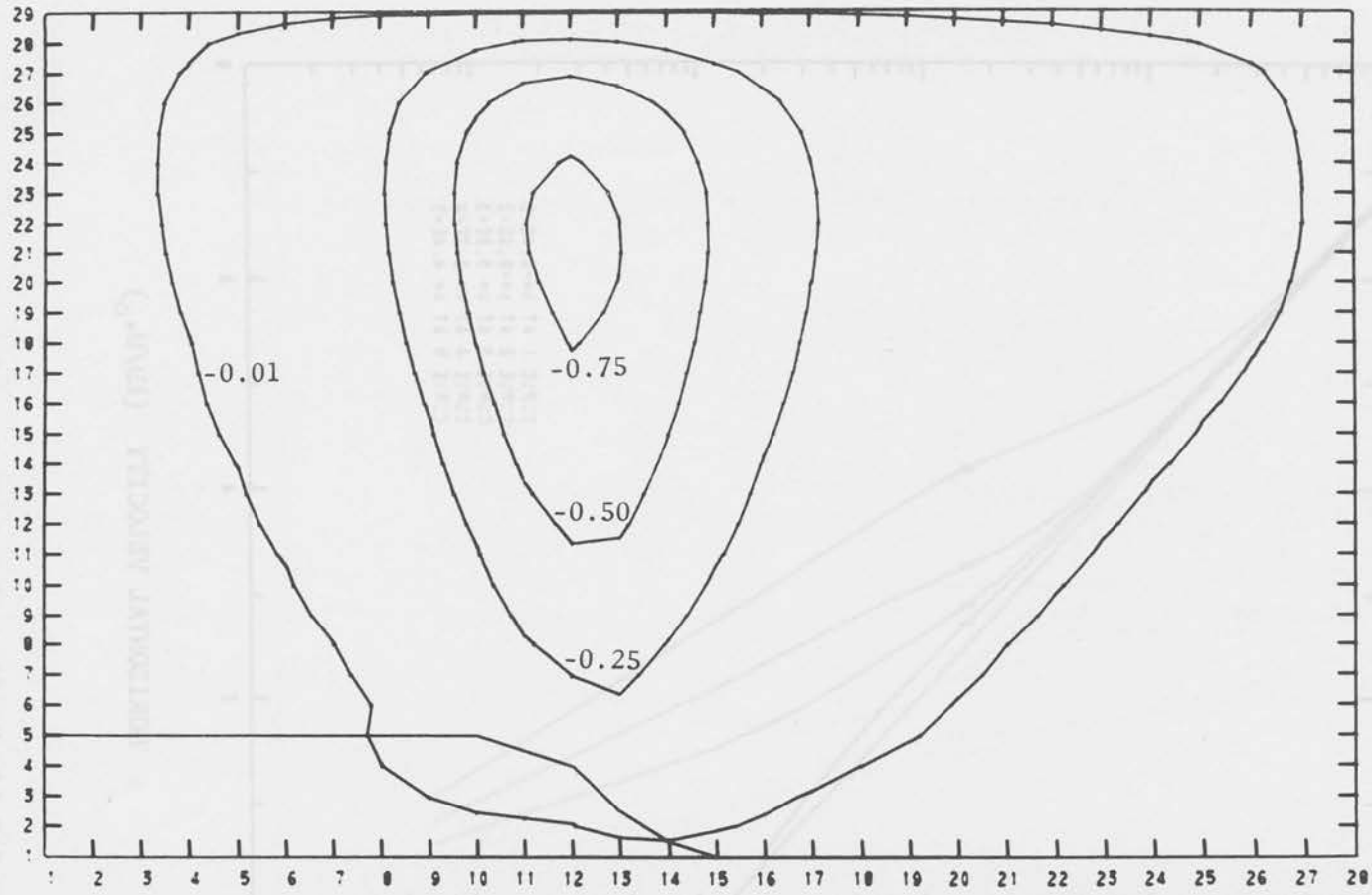

Figure 8.5-15 Nondimensional vertical velocity (kw/u_{*_o}) field as in Fig. 8.5-8 but without pressure

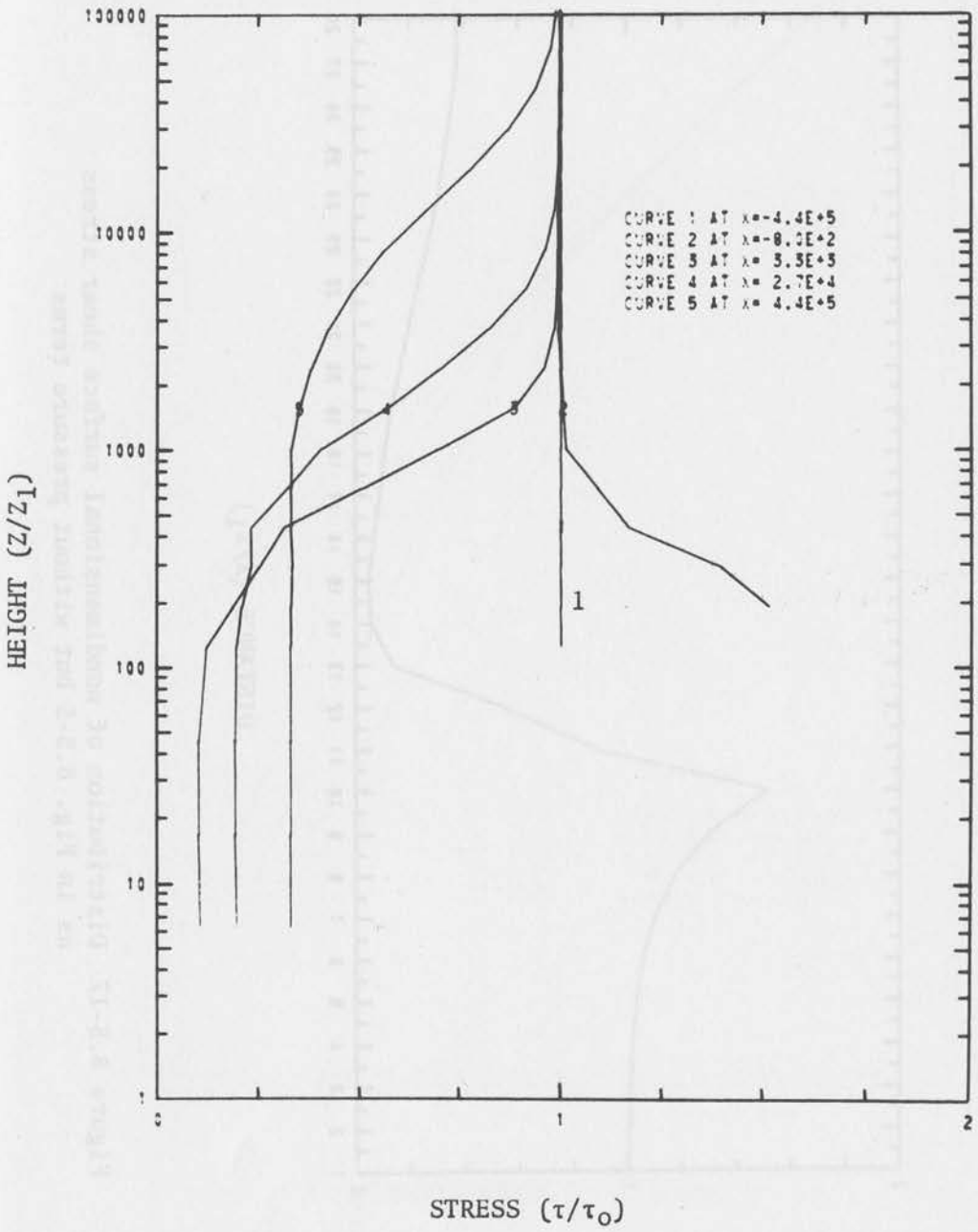

Figure 8.5-16 Nondimensional shear stress profiles as Fig. 8.5-4 but without pressure terms

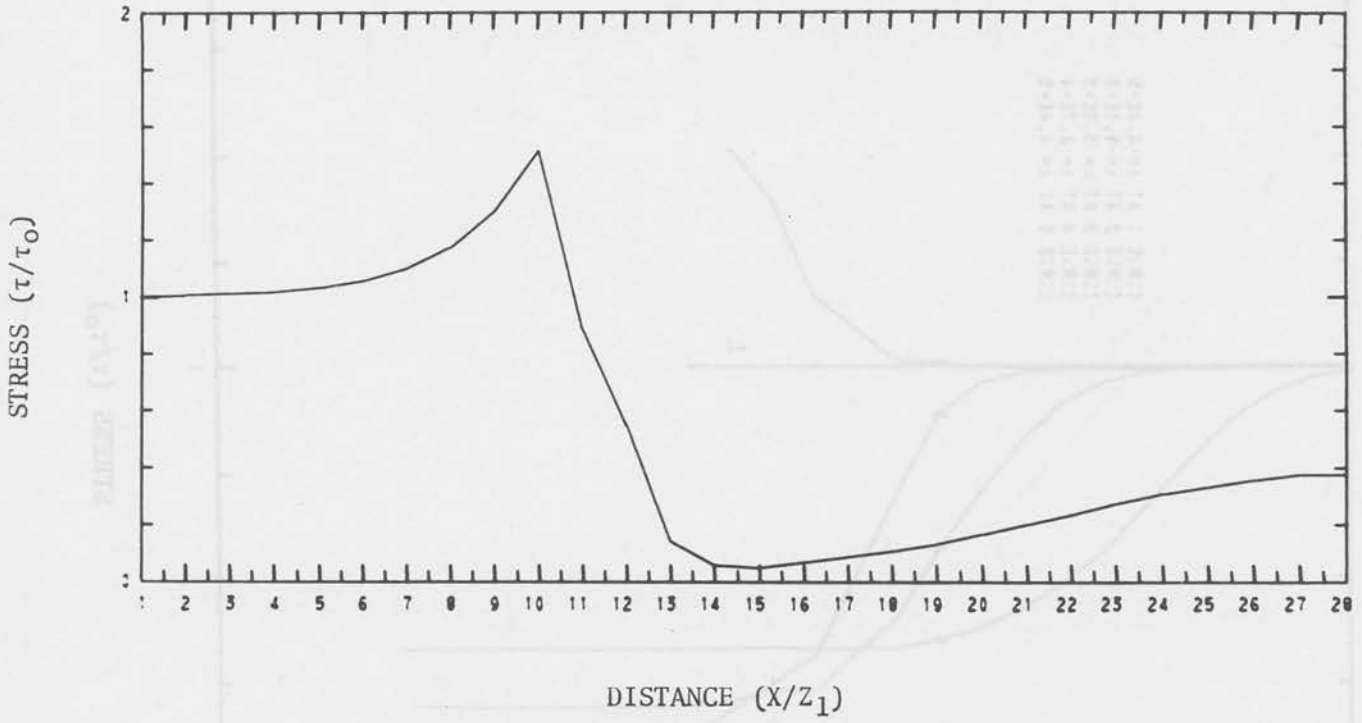

Figure 8.5-17 Distribution of nondimensional surface shear stress as in Fig. 8.5-5 but without pressure terms

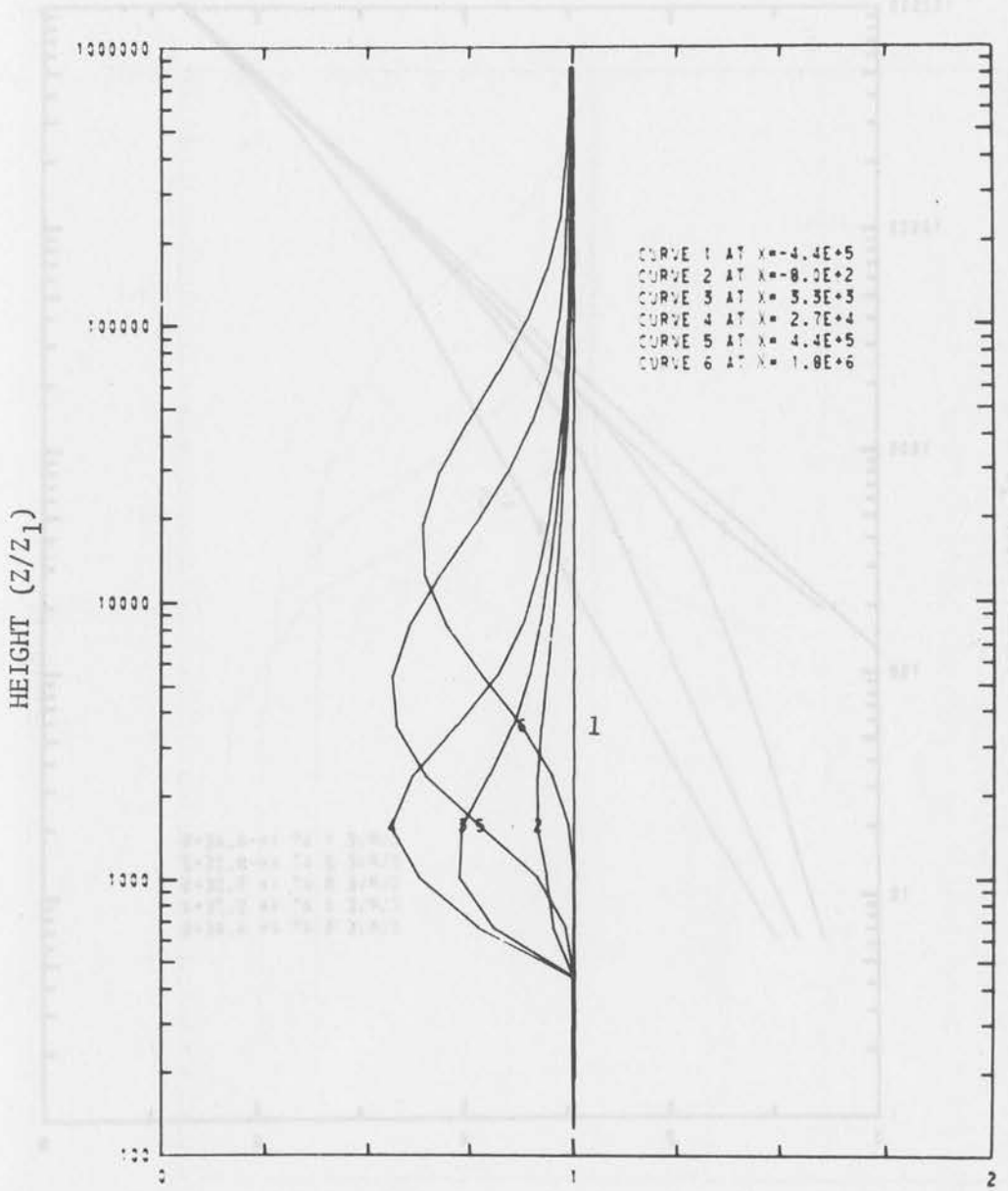

Figure 8.5-18 Nondimensional wind shear as in Fig. 8.5-6 but without pressure terms

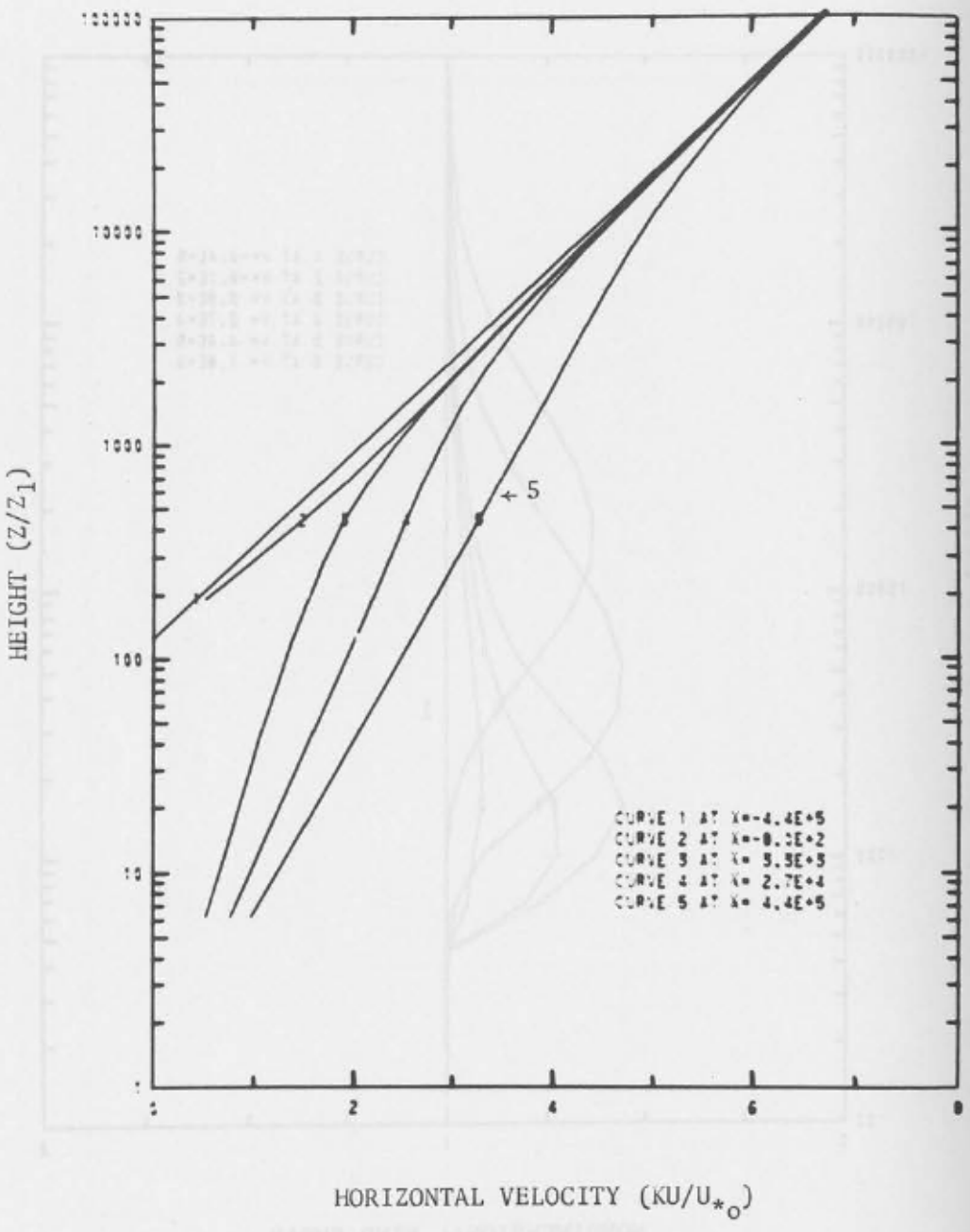

Figures 8.6-1 Distribution of nondimensional wind profiles at various nondimensional distances (x/z_1) from the origin for a rough to smooth transition with $M \simeq 5$ under neutral condition. Pressure terms included

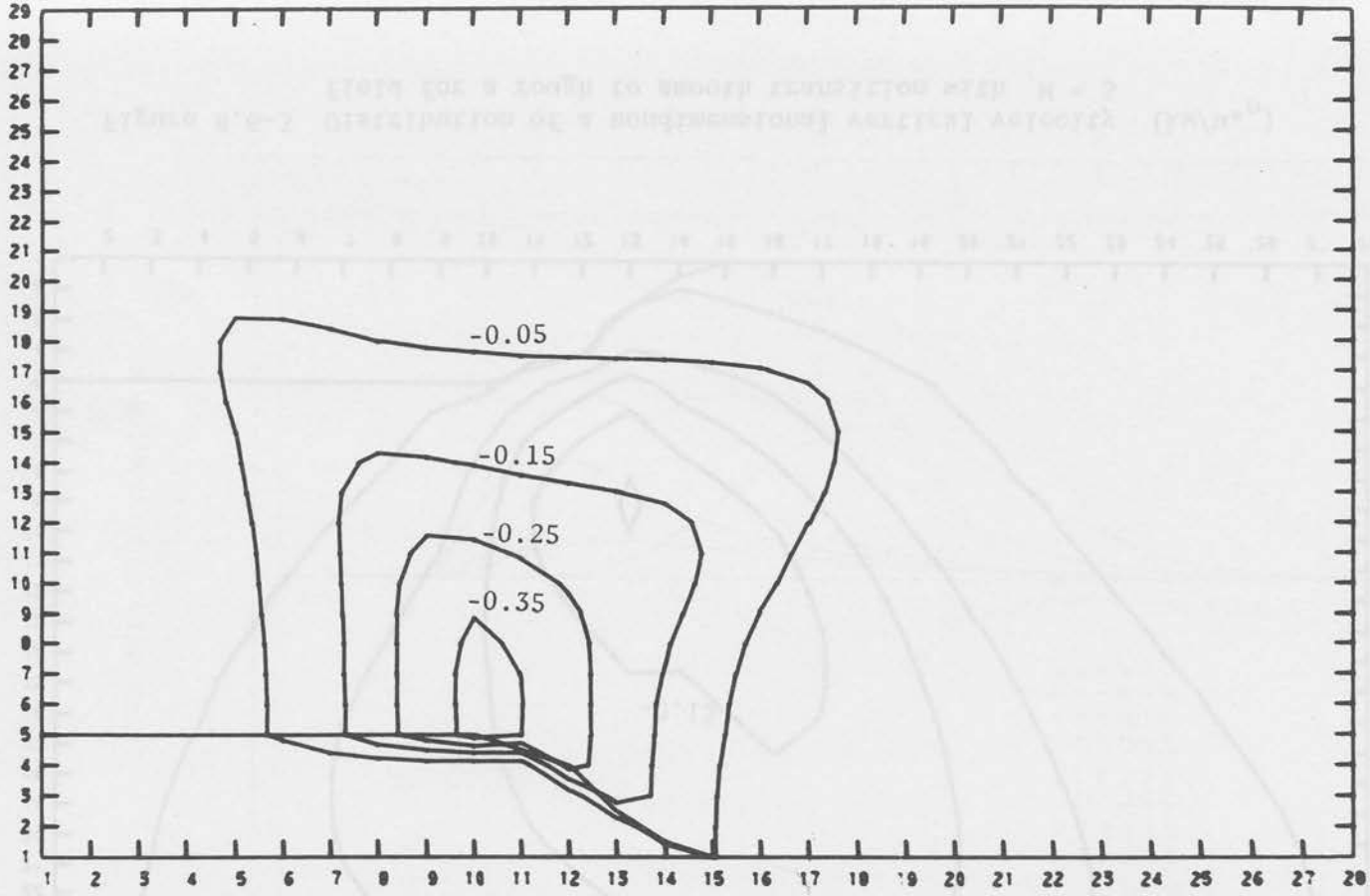

Figure 8.6-2 Distribution of a nondimensional pressure $(k^2p/u_{*_o}^2)$ field (deviation from the hydrostatic pressure) for a rough to smooth transition with $M \simeq 5$

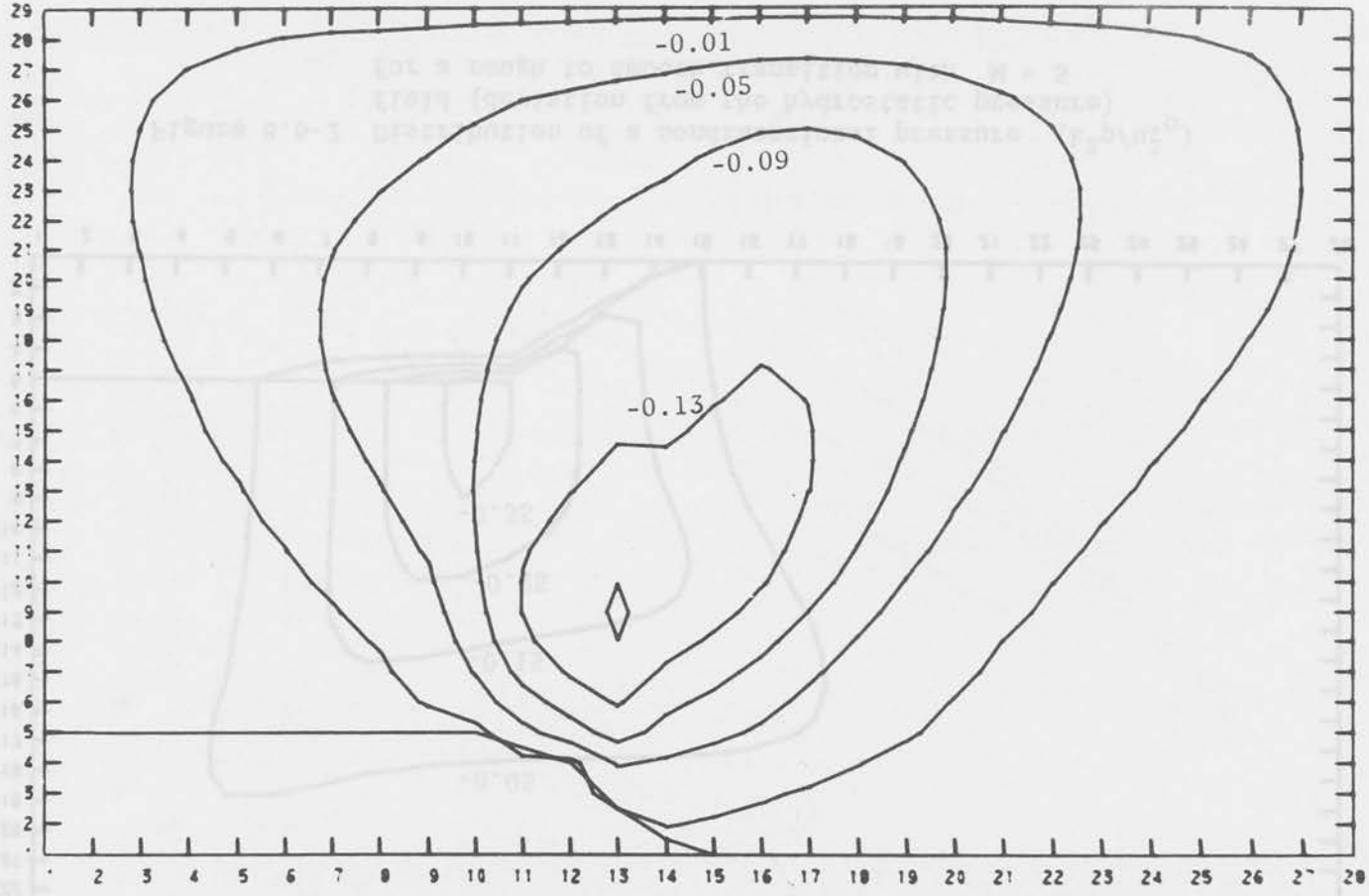

Figure 8.6-3 Distribution of a nondimensional vertical velocity (kw/u_{*_o}) field for a rough to smooth transition with $M \simeq 5$

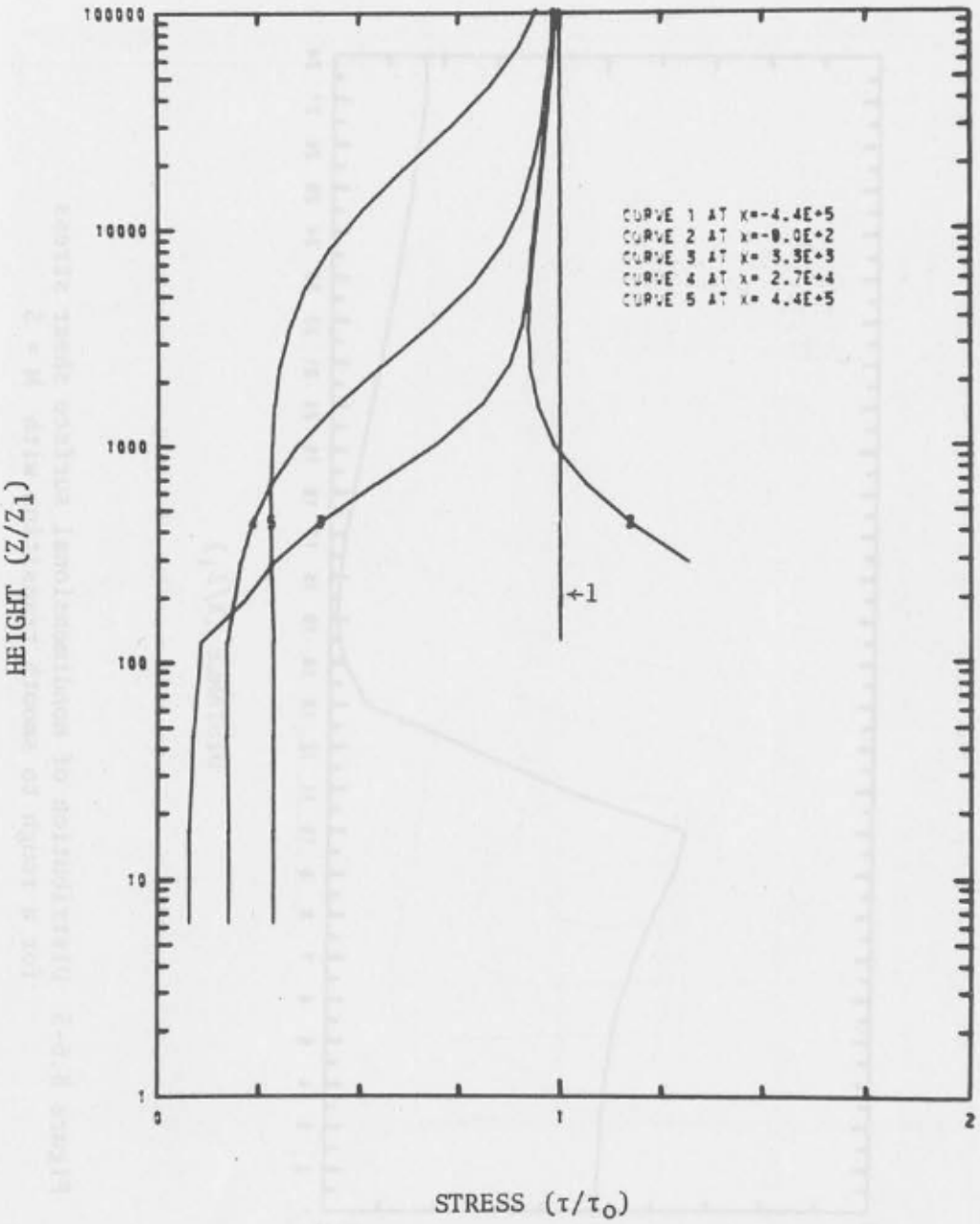

Figure 8.6-4 Nondimensional shear stress profiles for various nondimensional distances (x/z_1) from the origin for a rough to smooth transition with M≈5

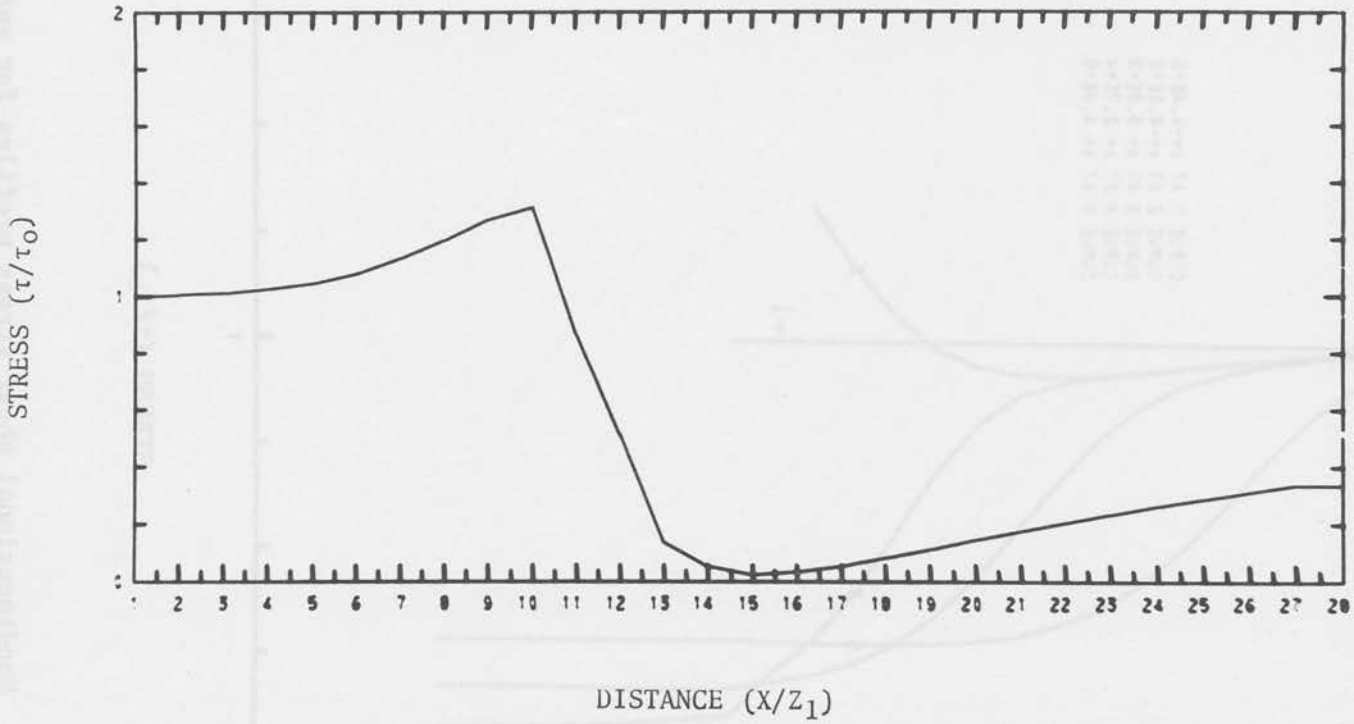

Figure 8.6-5 Distribution of nondimensional surface shear stress for a rough to smooth transition with $M \simeq 5$

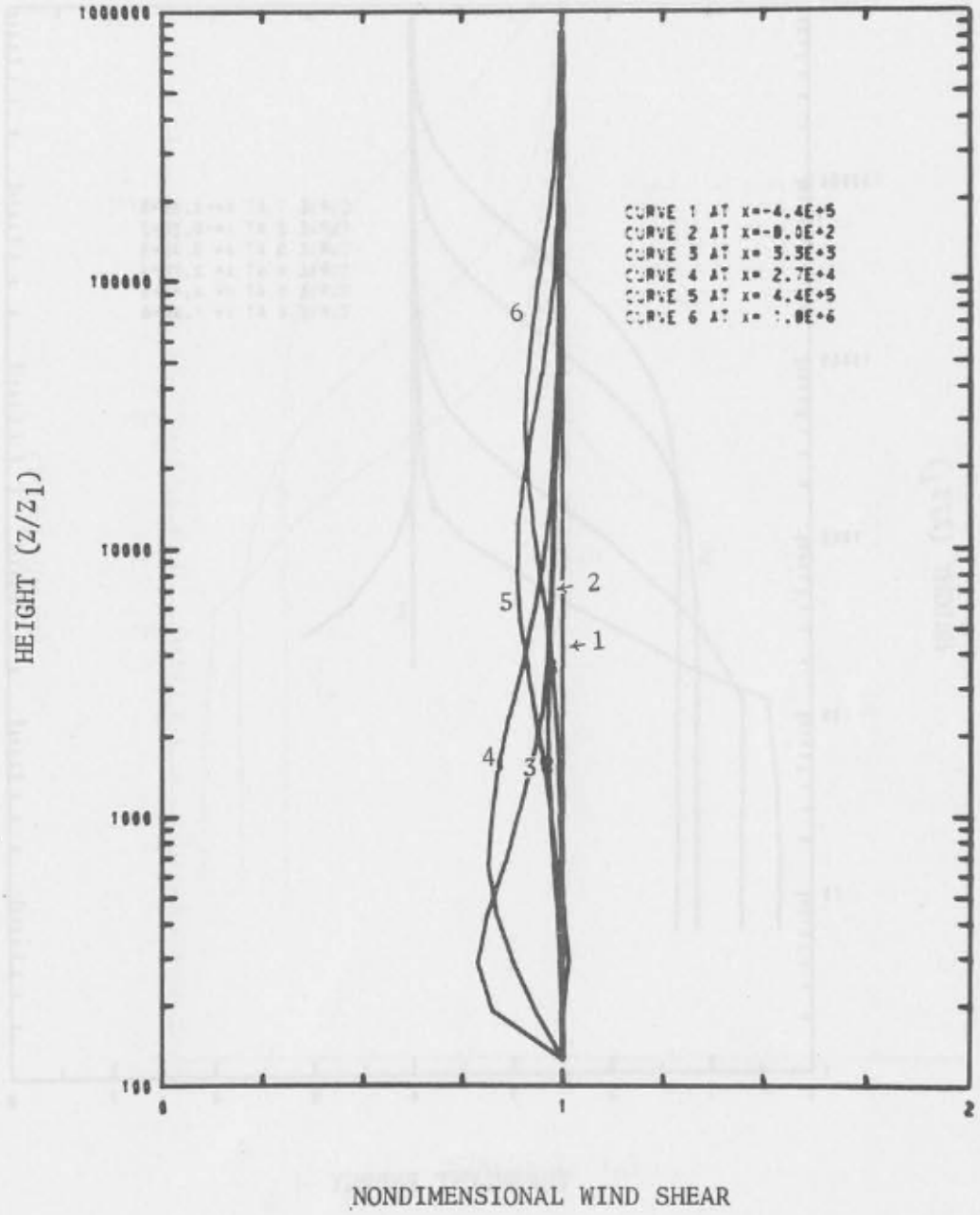

Figure 8.6-6 Nondimensional wind shear profiles for a rough to smooth transition with $M \simeq 5$

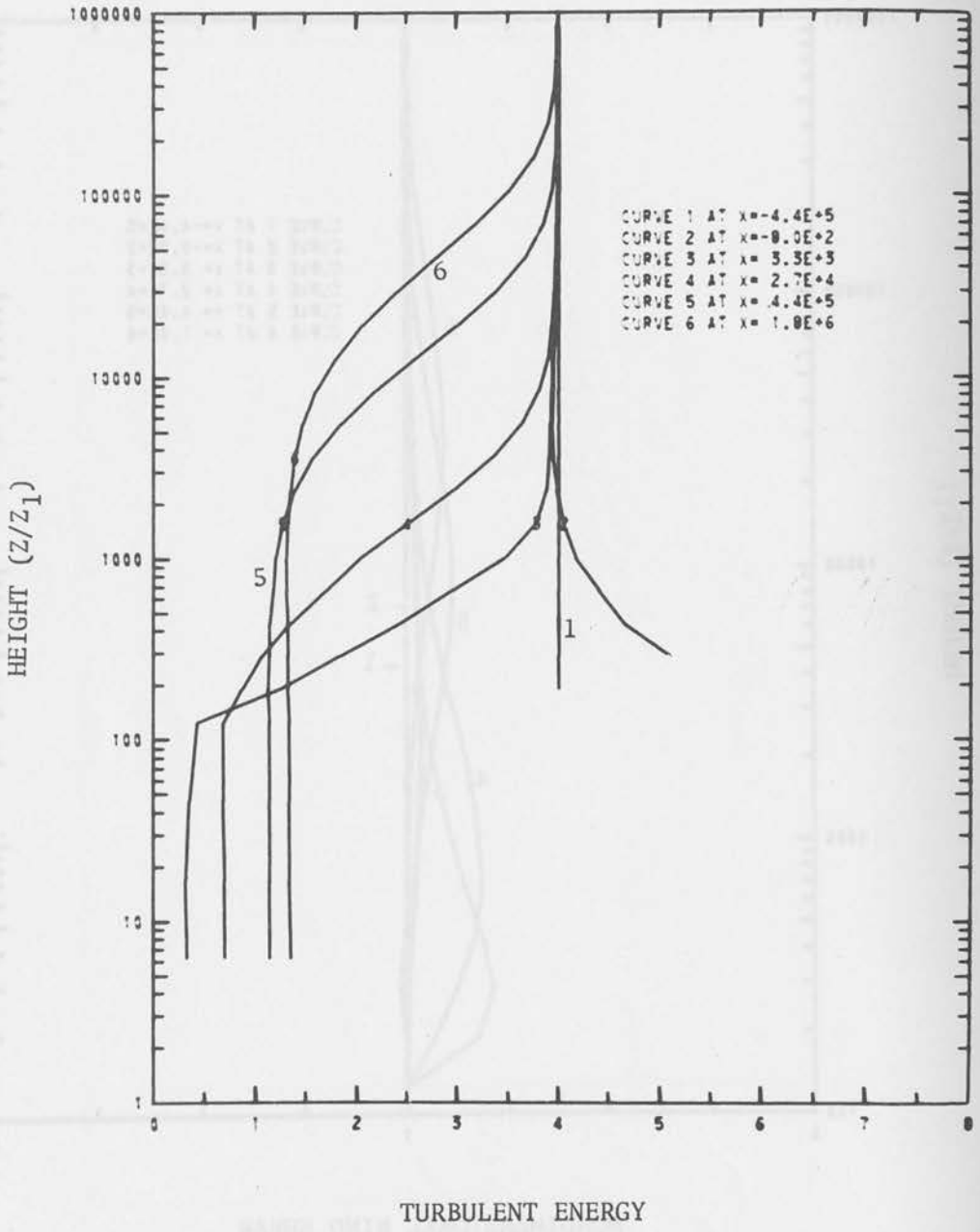

Figure 8.6-7 Nondimensional turbulent energy at various nondimensional distances (x/z_1) from the origin for a rough to smooth transition with $M \simeq 5$

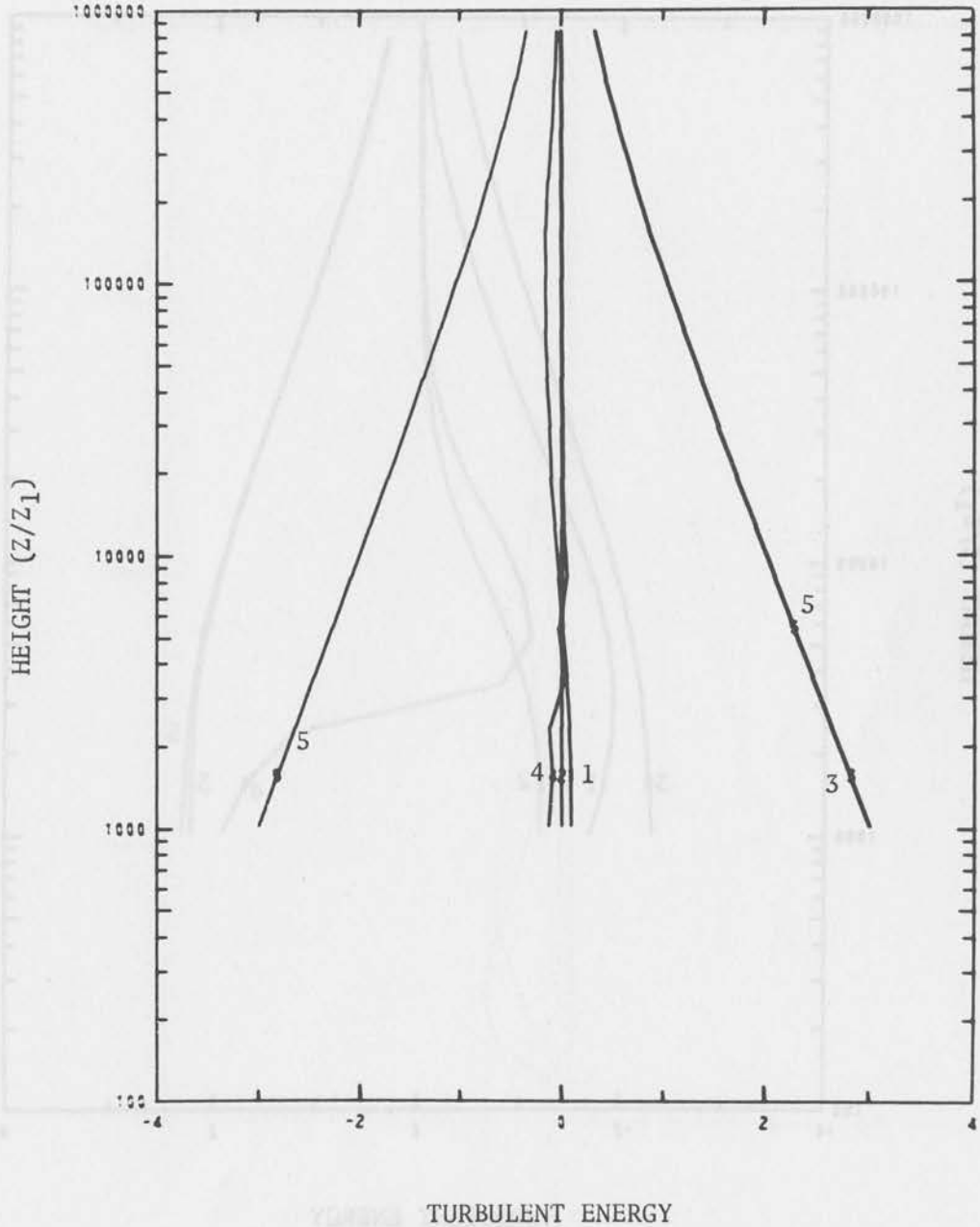

Figure 8.6-8 Terms in the turbulent energy equation at nondimensional distance $x = -2.2 \times 10^5$

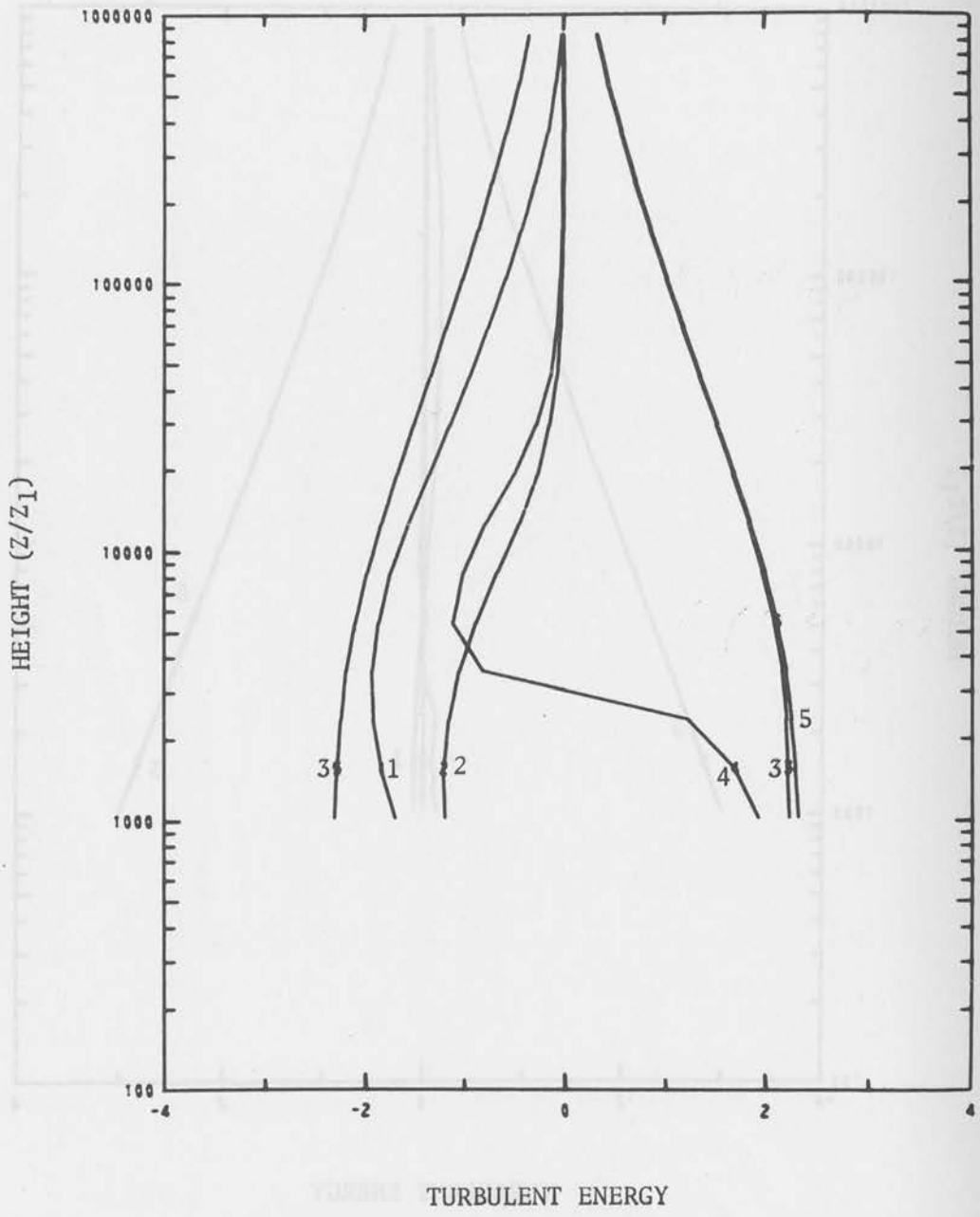

Figure 8.6-9 Terms in the turbulent energy equation at nondimensional distance $x = 2.7 \times 10^4$

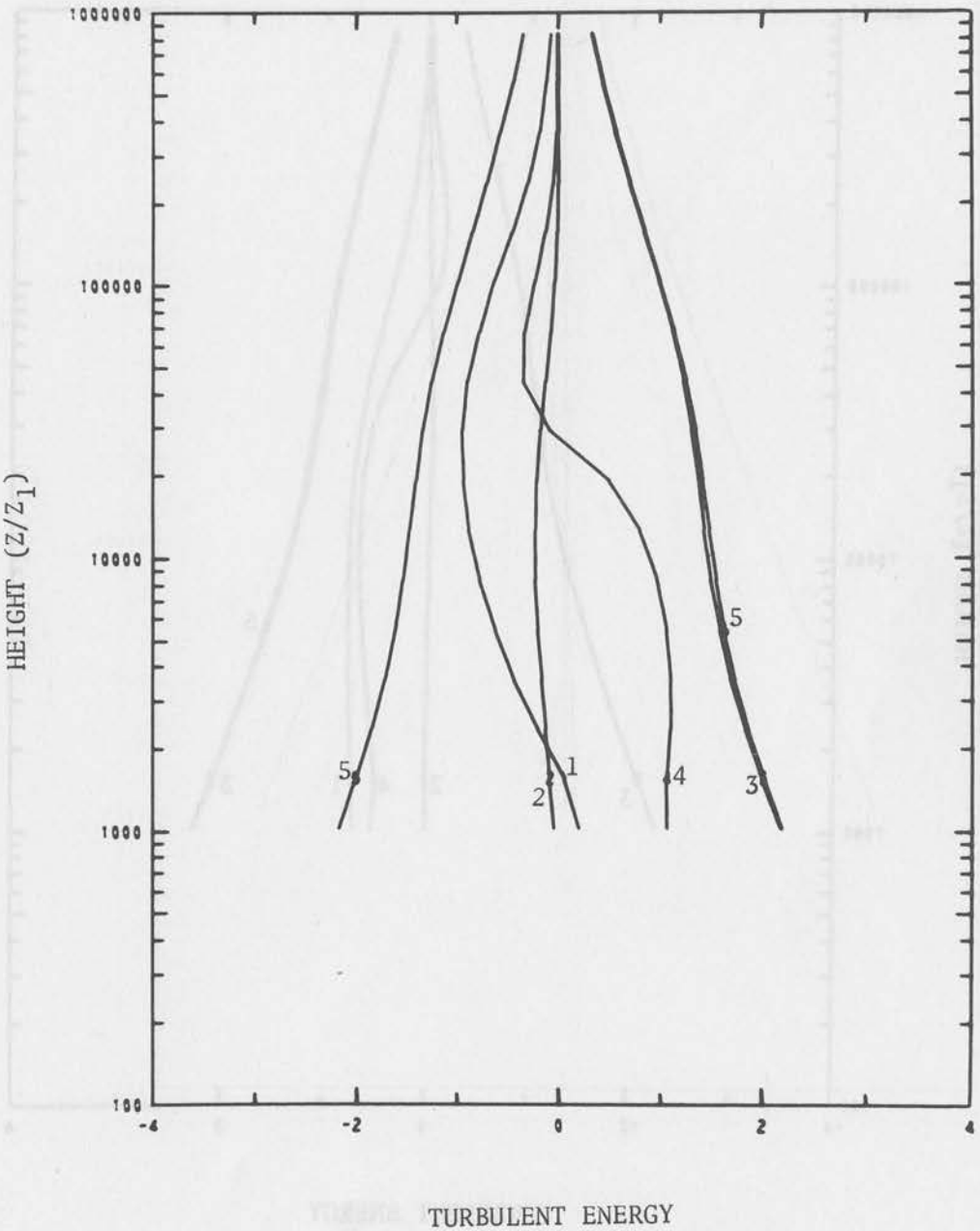

Figure 8.6-10 Terms in the turbulent energy equation at nondimensional distance $x = 4.4 \times 10^5$

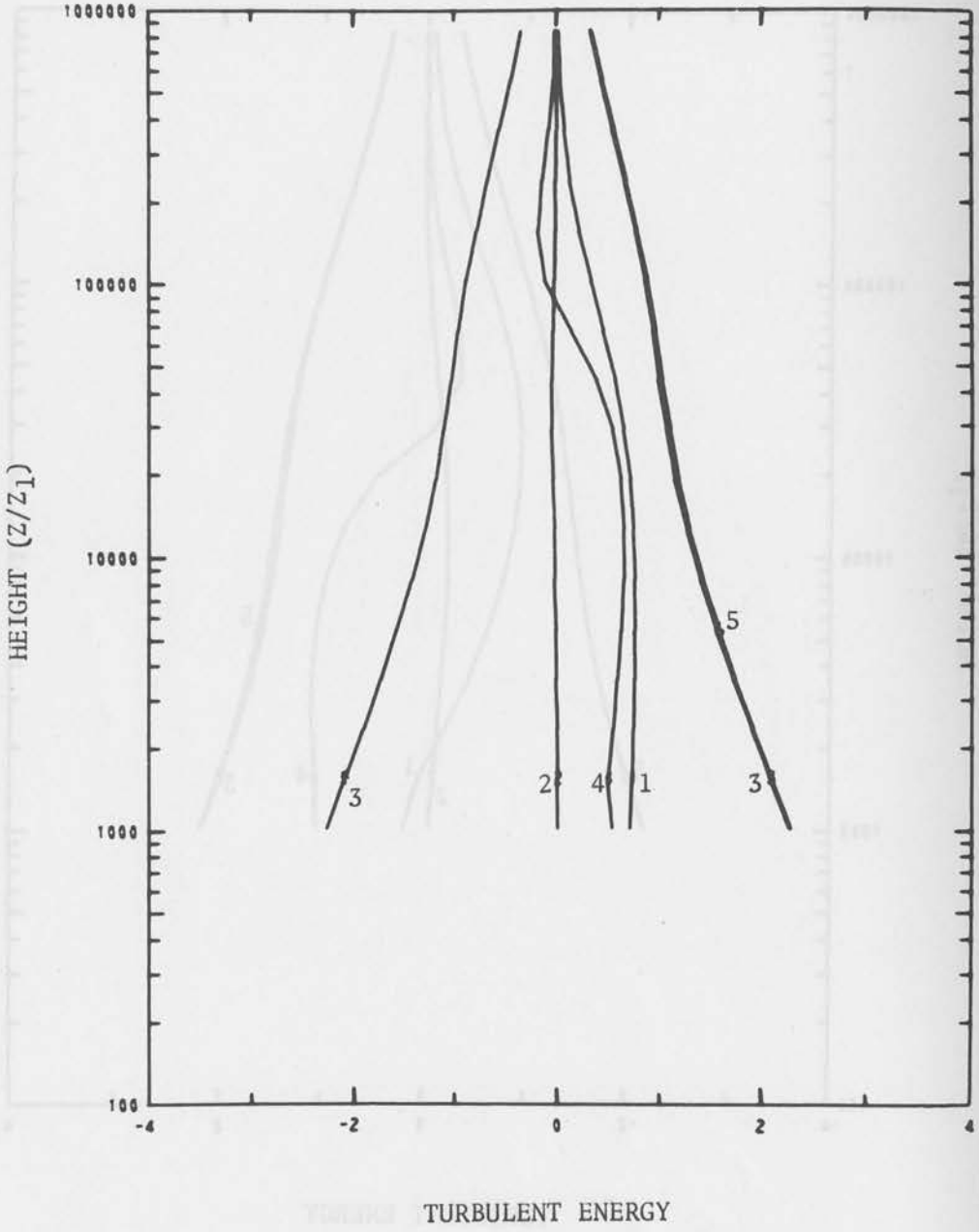

Figure 8.6-11 Terms in the turbulent energy equation at nondimensional distance $x = 1.8 \times 10^6$

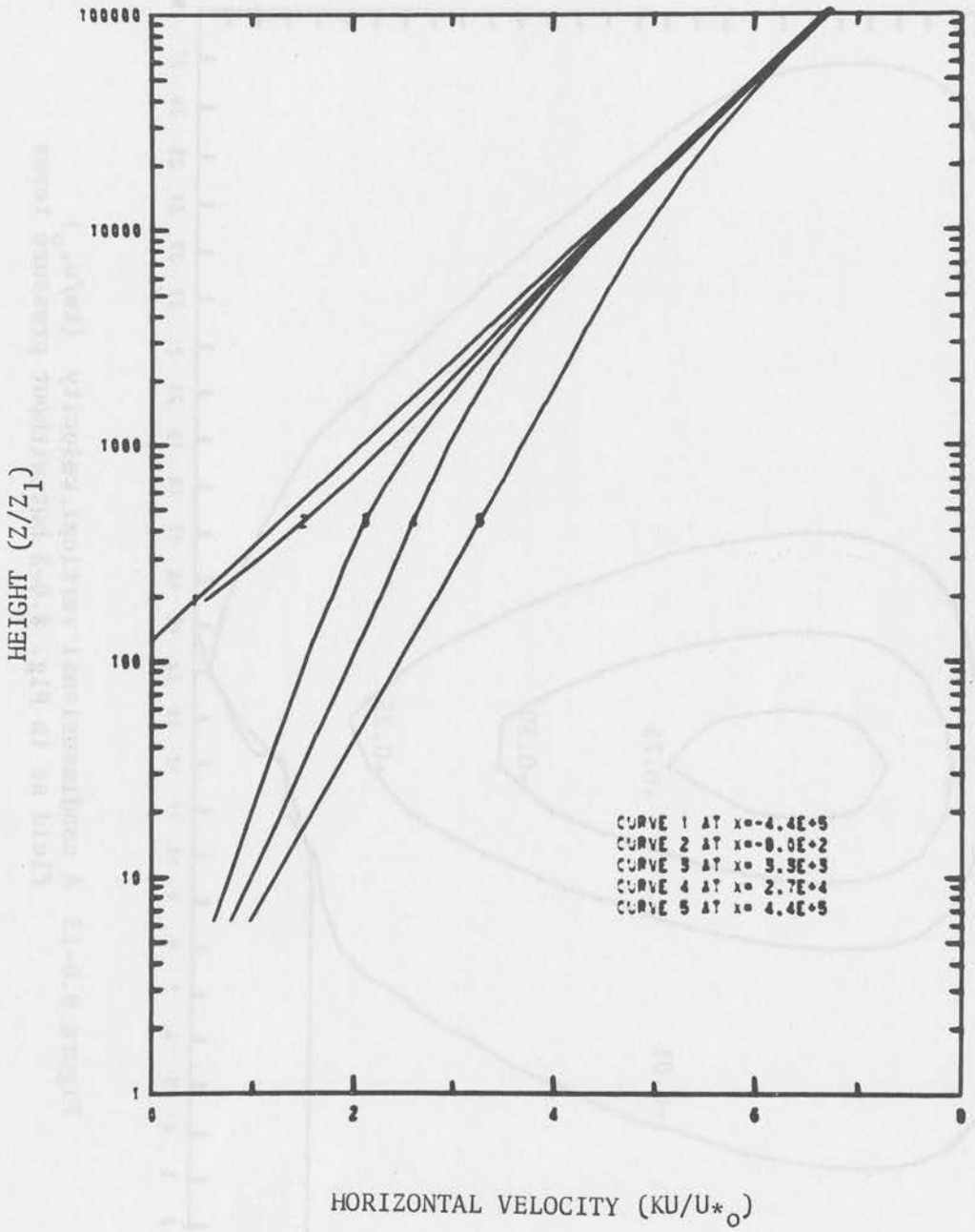

Figure 8.6-12 Nondimensional wind profiles as in Fig. 8.6-1 but without pressure terms

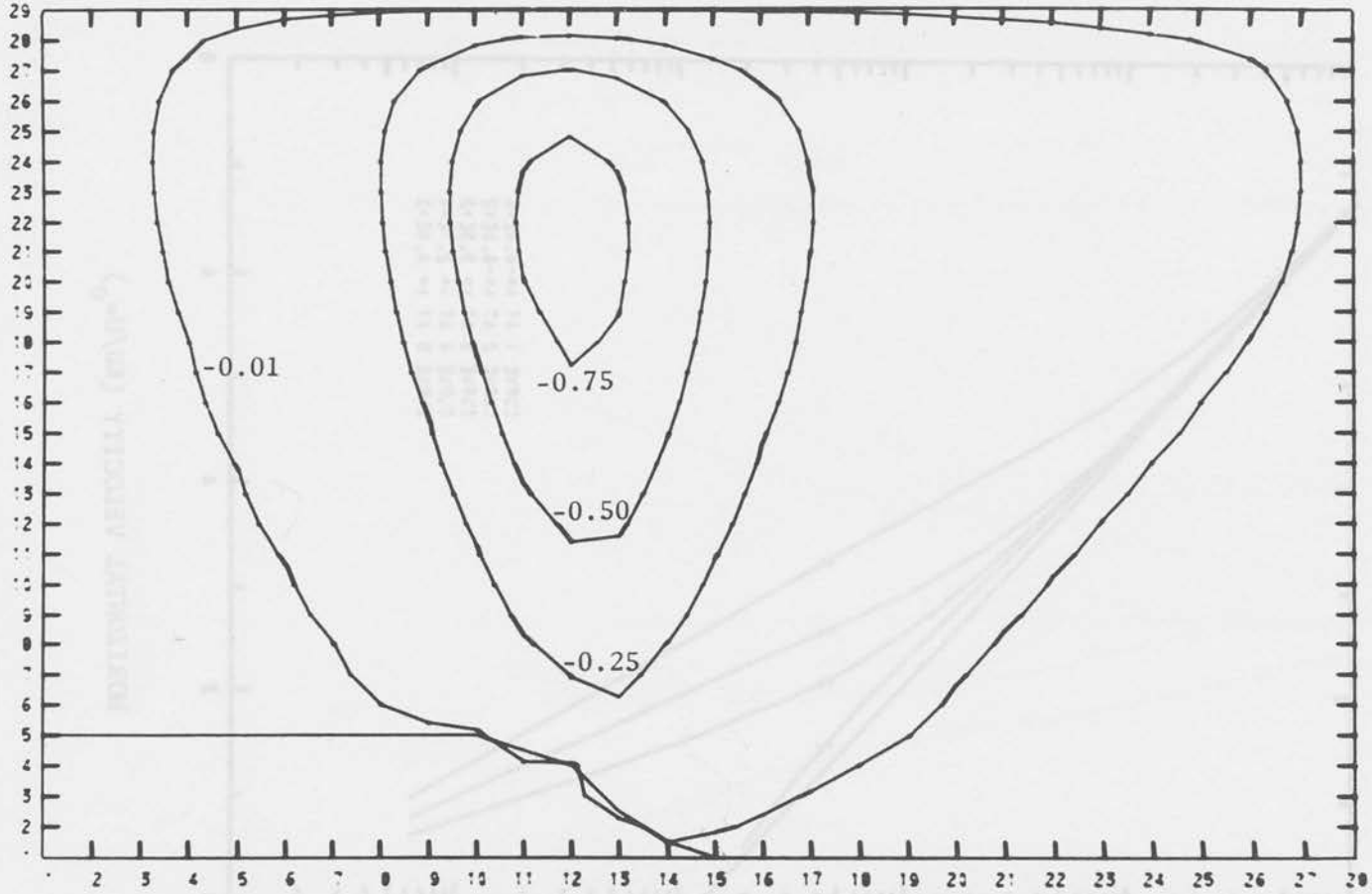

Figure 8.6-13 A nondimensional vertical velocity (kw/u_{*_o}) field as in Fig. 8.6-3 but without pressure terms

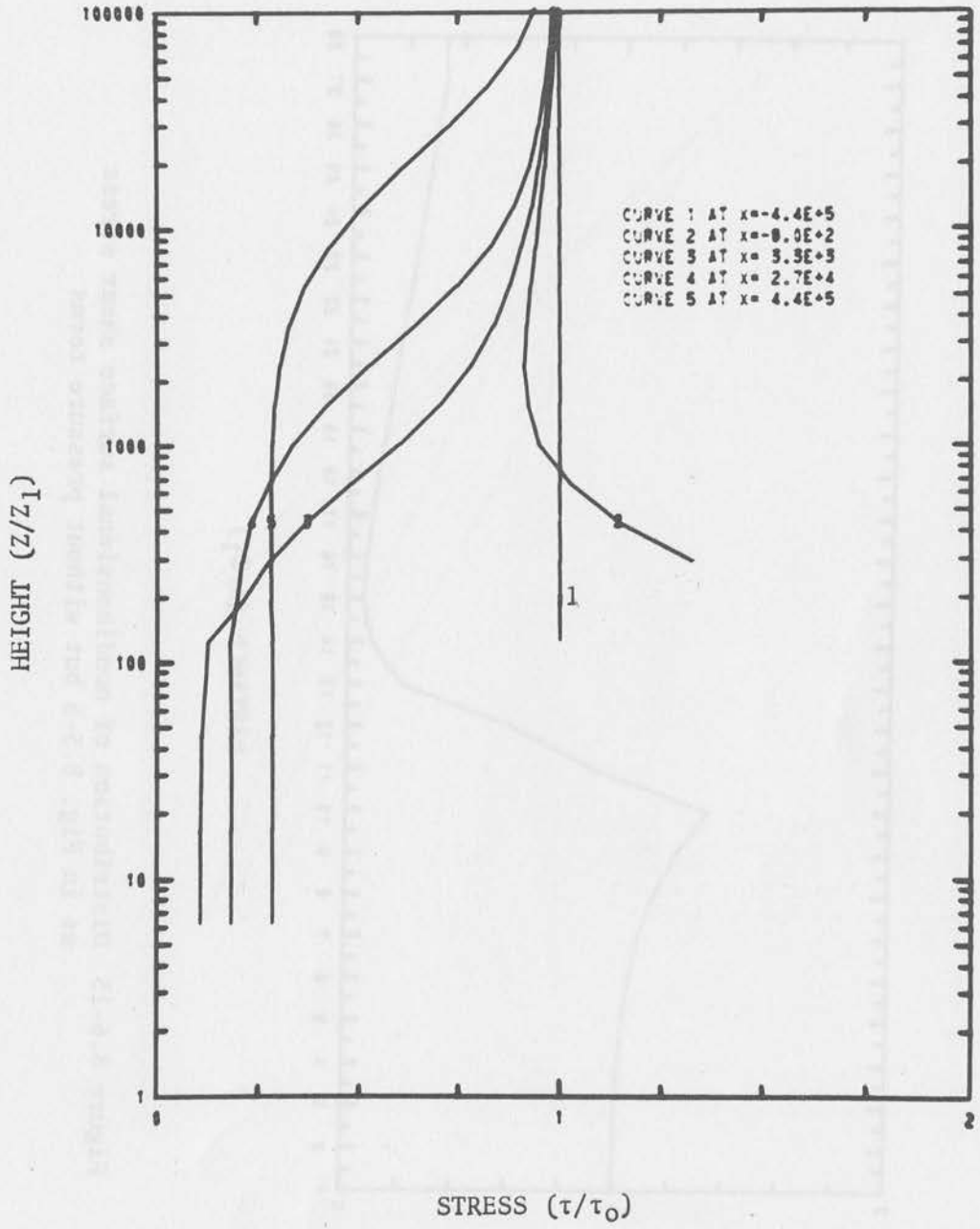

Figure 8.6-14 Nondimensional shear stress profiles as in Fig. 8.6-4 but without pressure terms

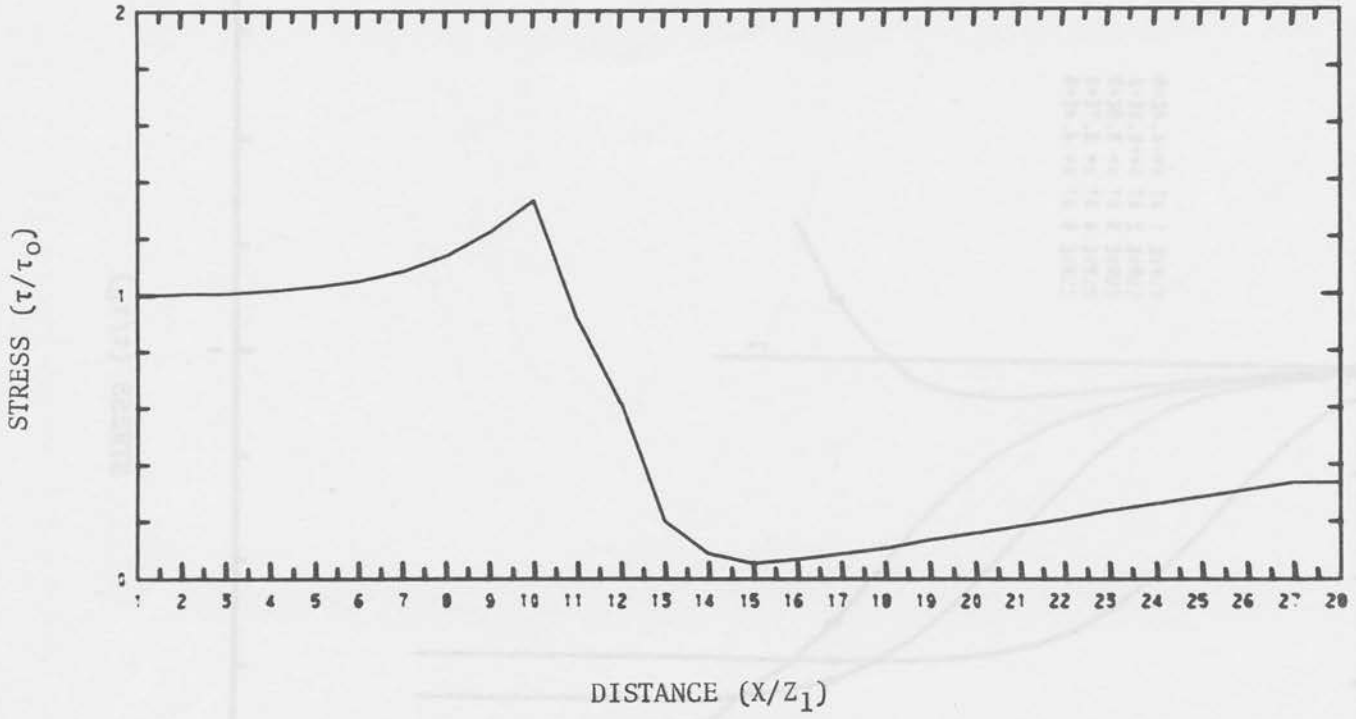

Figure 8.6-15 Distribution of nondimensional surface shear stress as in Fig. 8.5-5 but without pressure terms

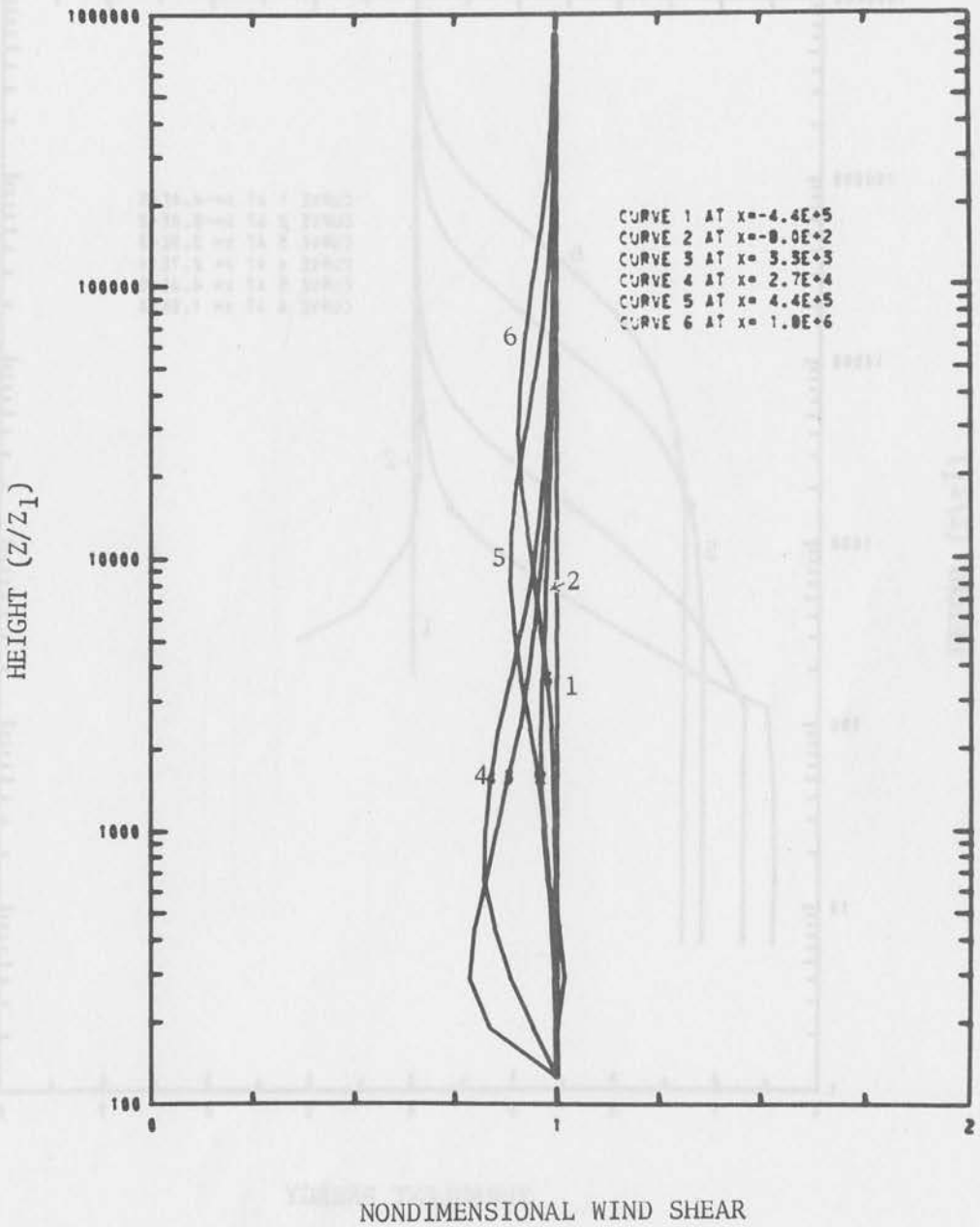

Figure 8.6-16 Nondimensional wind shear profiles as in Fig. 8.6-6 but without pressure terms

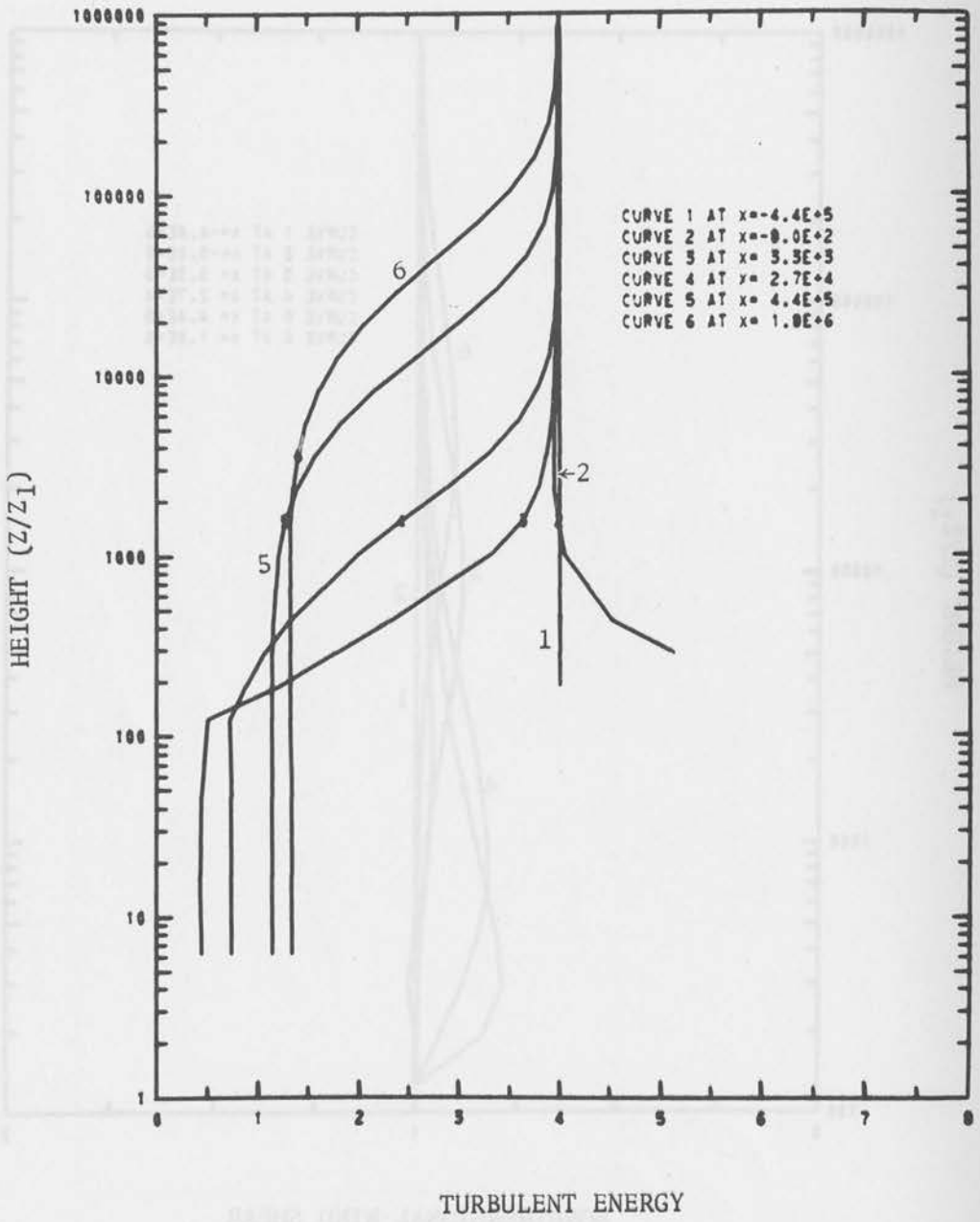

Figure 8.6-17 Nondimensional turbulent energy at various nondimensional distances (x/z_1) as in Fig. 8.6-7 but without pressure terms

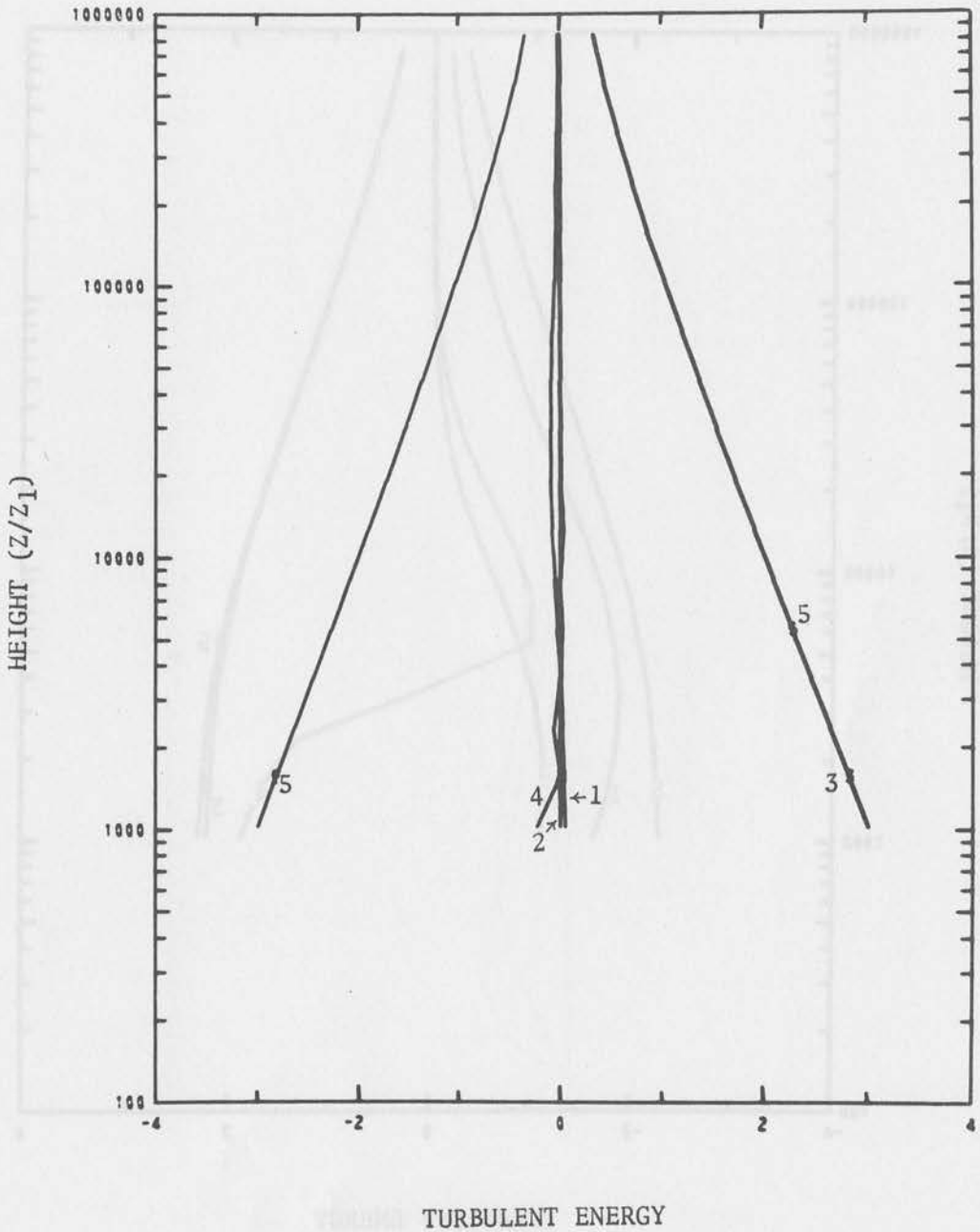

Figure 8.6-18 Terms in the turbulent energy equation at nondimensional distance $x = -2.2 \times 10^5$ as in Fig. 8.6-8 but without pressure terms

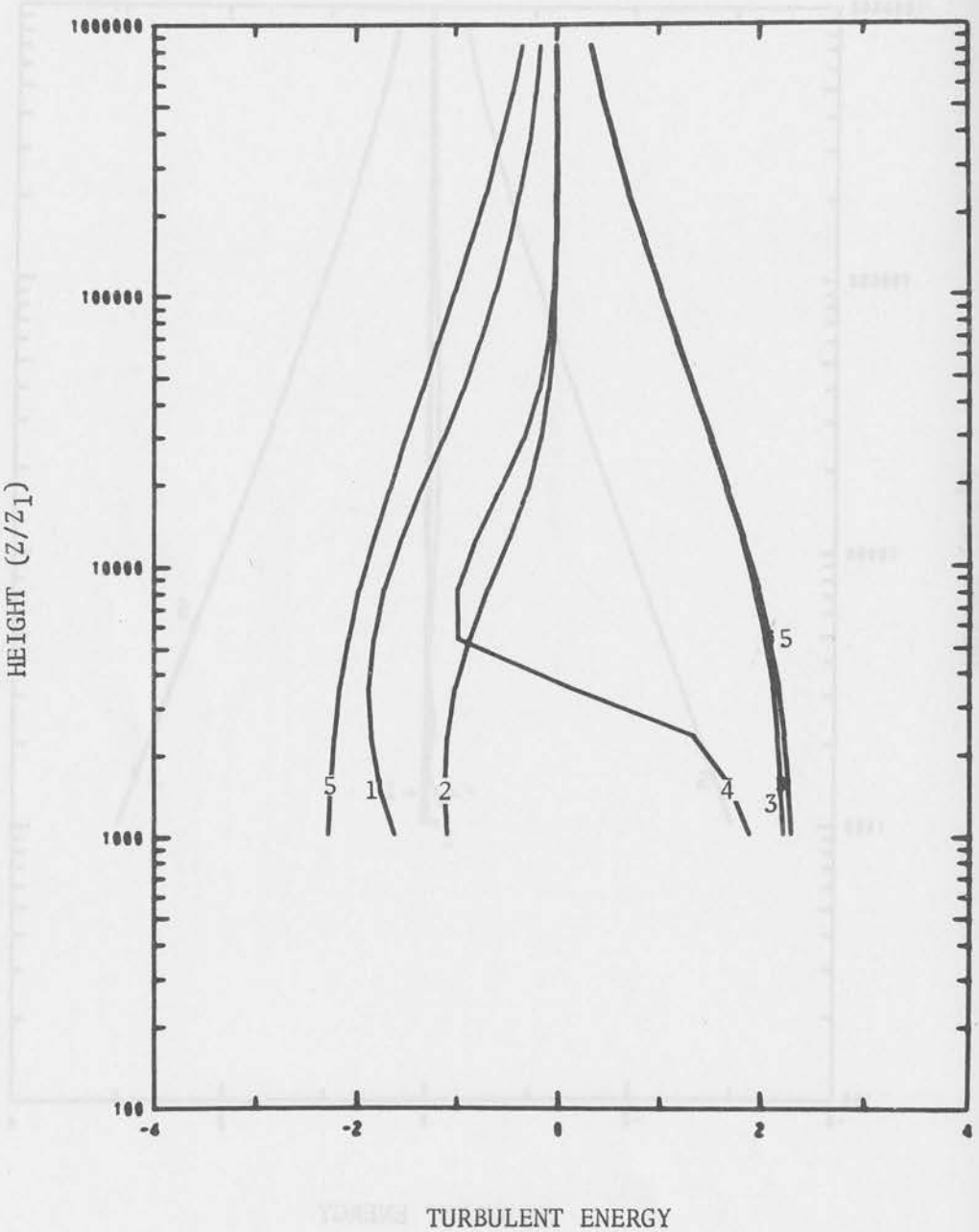

Figure 8.6-19 Terms in the turbulent energy equation at nondimensional distance $x = 2.7 \times 10^4$ as in Fig. 8.6-9 but without pressure terms

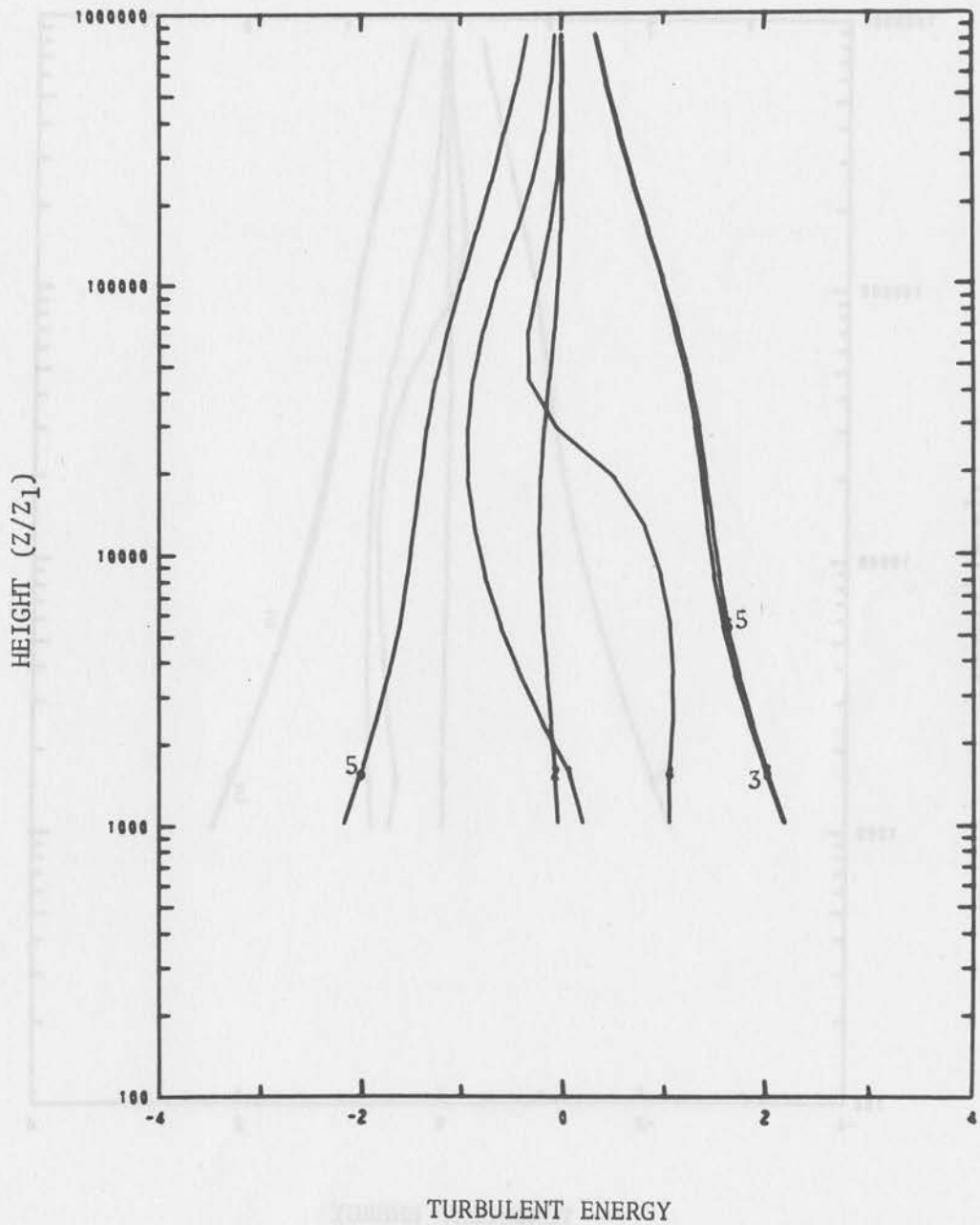

Figure 8.6-20 Terms in the turbulent energy equation at nondimensional distance $x = 4.4 \times 10^5$ as in Fig. 8.6-10 but without pressure terms

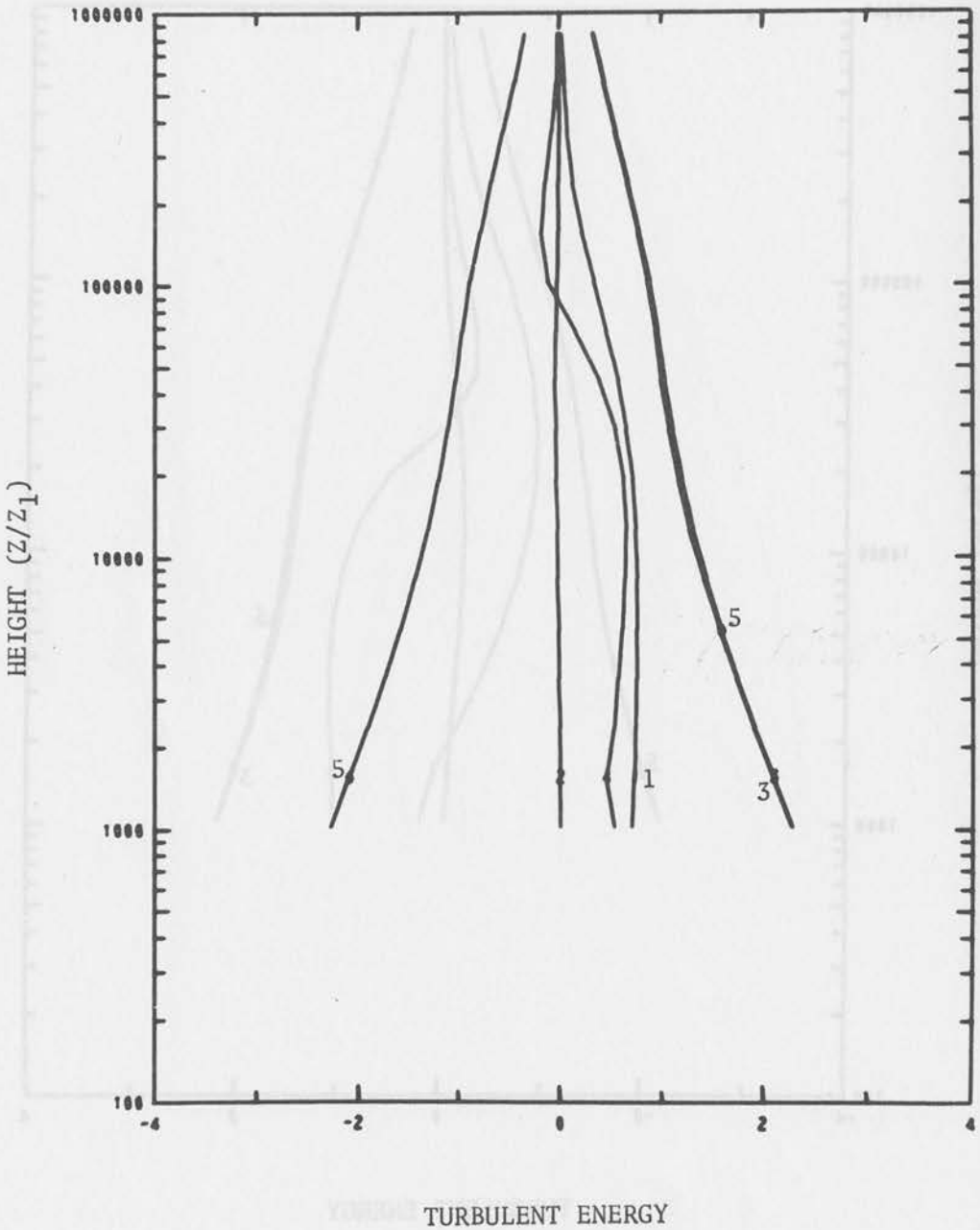

Figure 8.6-21 Terms in the turbulent energy equation at nondimensional distance $x = 1.8 \times 10^6$ as in Fig. 8.6-11 but without pressure terms

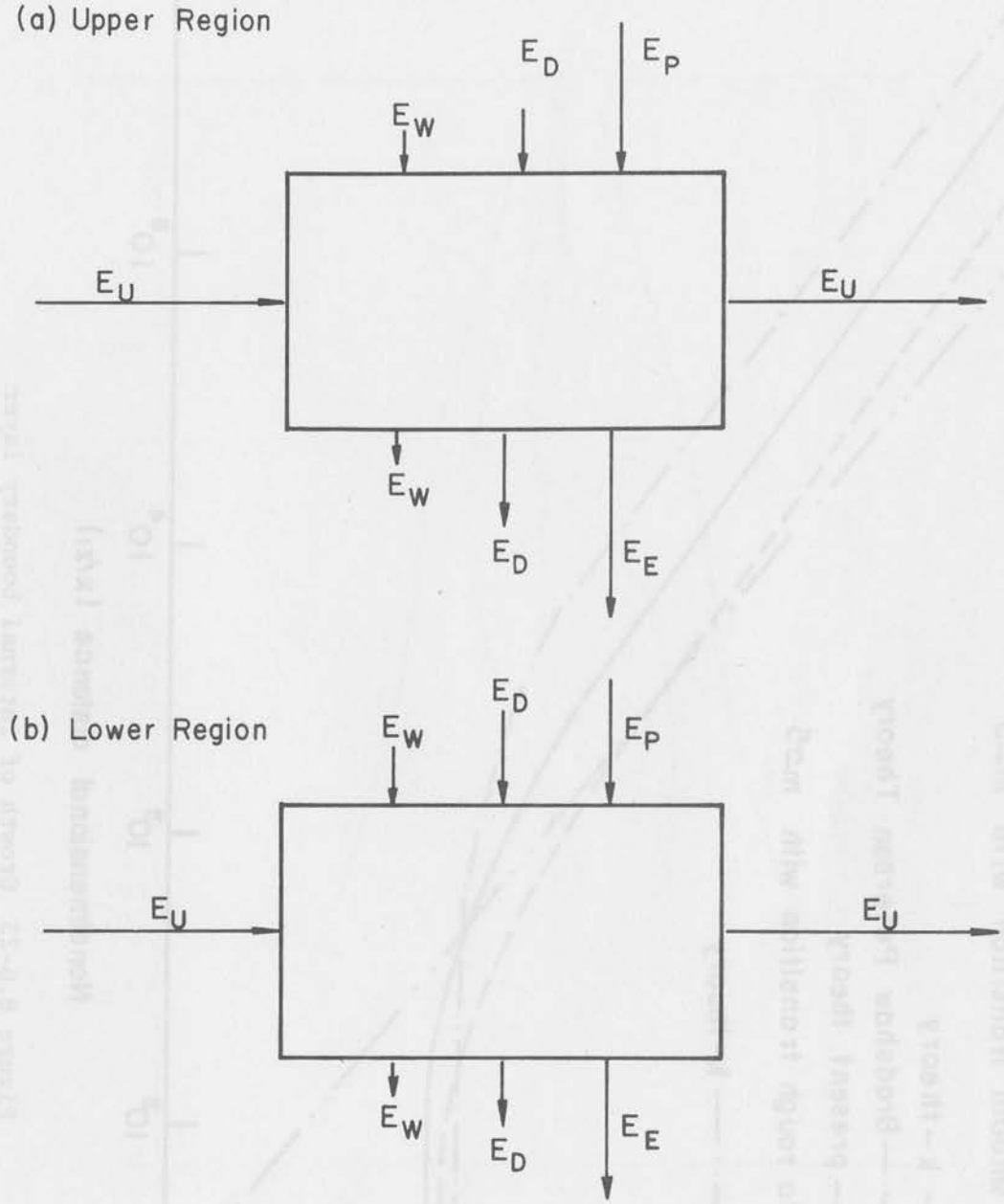

Figure 8.6-22 Mechanism of turbulent energy transfer

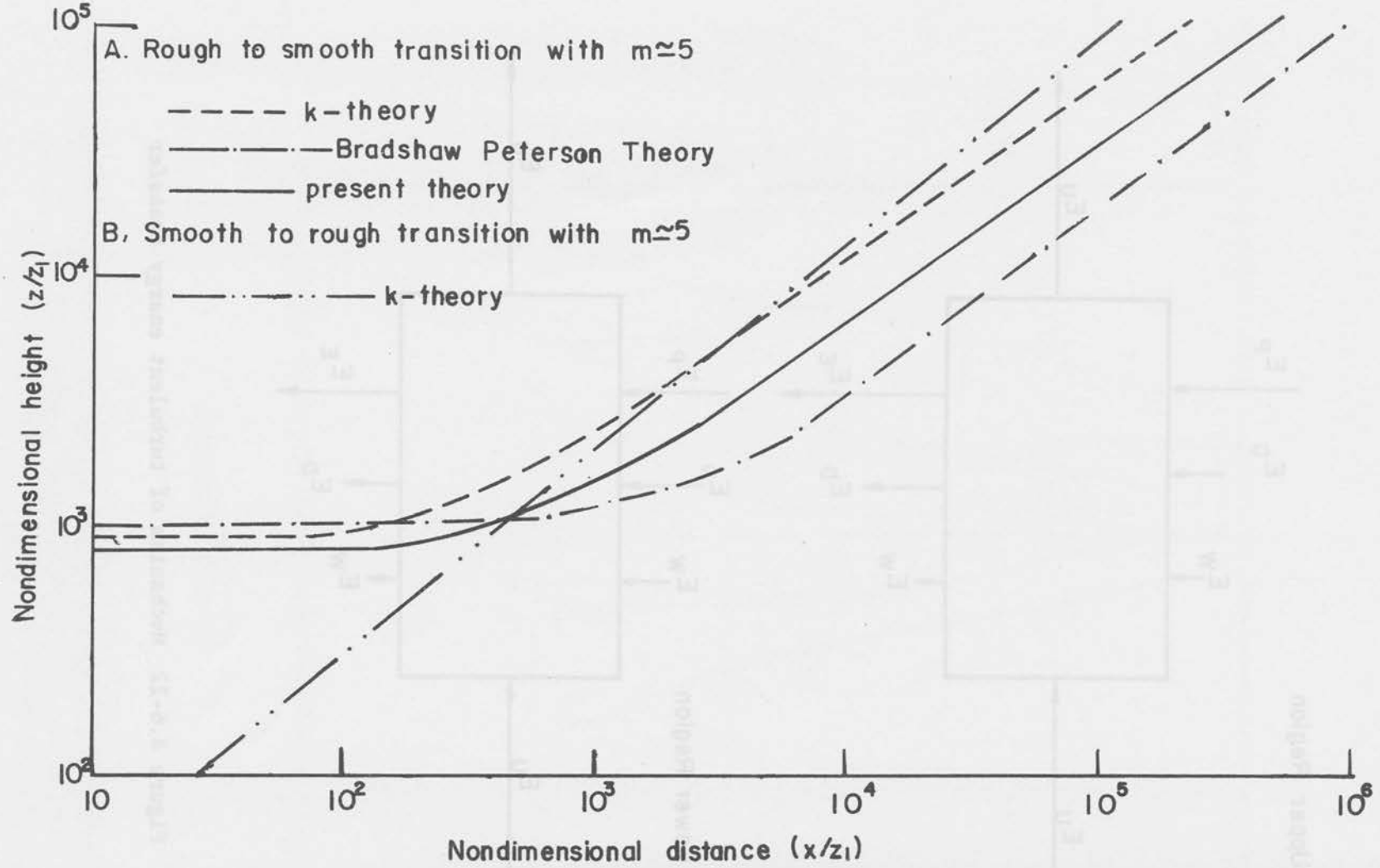

Figure 8.6-23 Growth of internal boundary layer

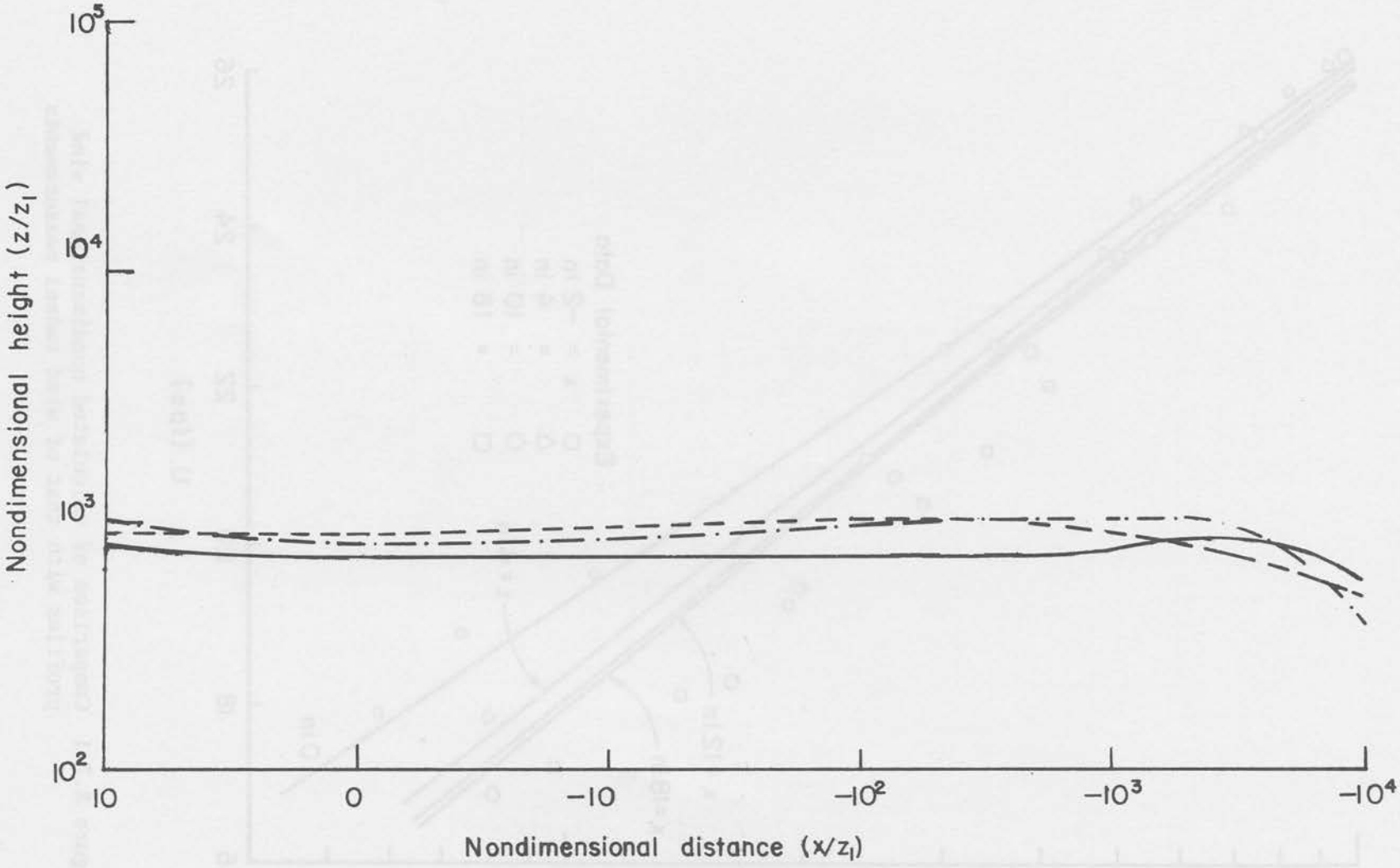

Figure 8.6-23 Continued

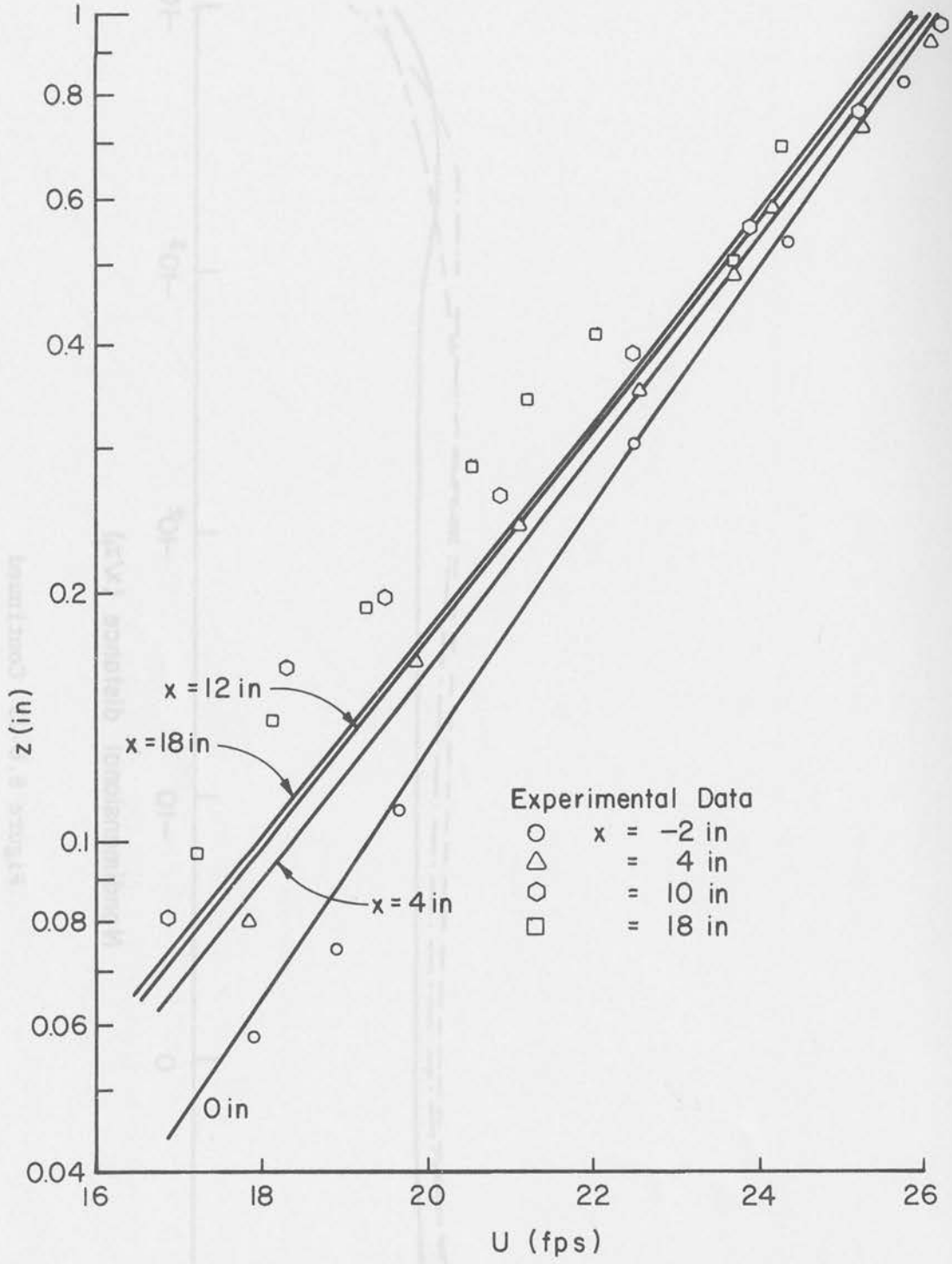

Figure 8.7-1 Comparison of calculated nondimensional wind profiles with that of wind tunnel measurements

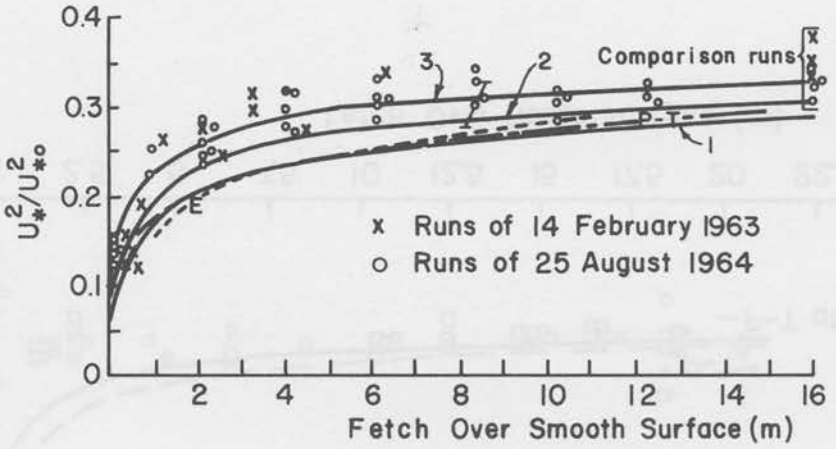

Figure 8.8-1 Variation of nondimensional surface shear stress in the downwind direction for a rough to smooth transition (M≈5). Comparison of the results obtained by the numerical model of k-theory with analytical solutions and field data. Curve 1 for nondimensional wind shear $\phi = 1$; Curves 2 and 3 for $\phi < 1$ as a function of downstream distance

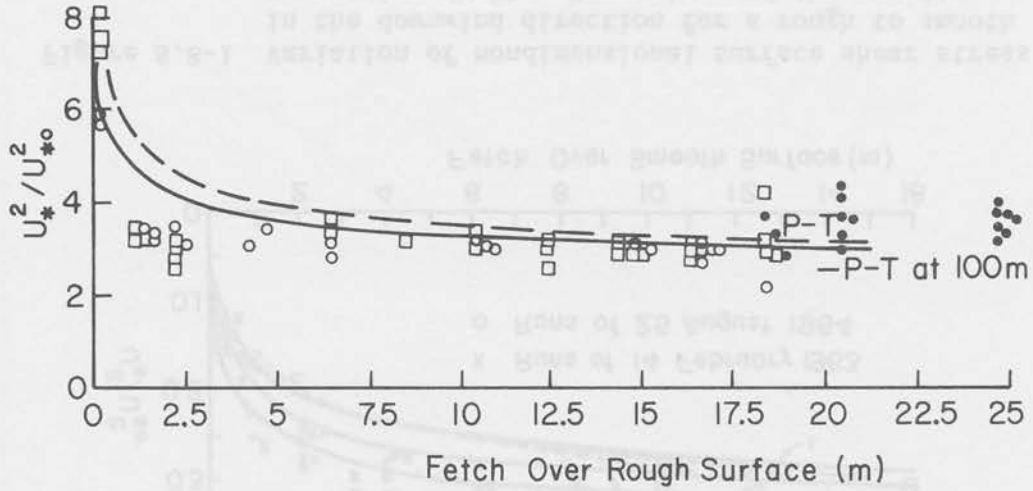

Figure 8.8-2 Variation of surface shear stress in the downwind direction for a smooth to rough transition. Comparison of the results obtained by the numerical model of k-theory with analytical solutions and field data

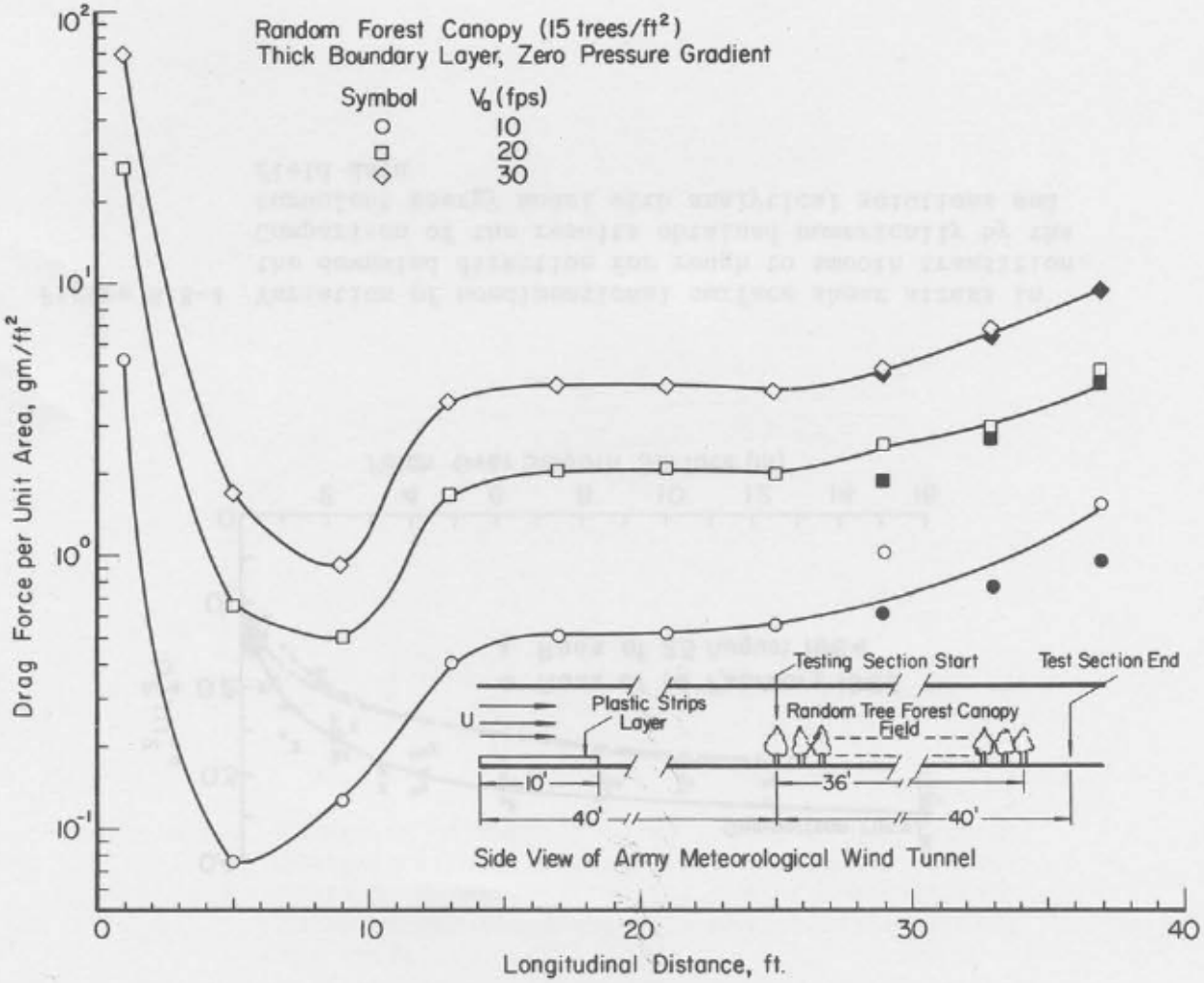

Figure 8.8-3 Shear plate drag for model forest canopy in wind tunnel experiment (from Meroney, 1969)

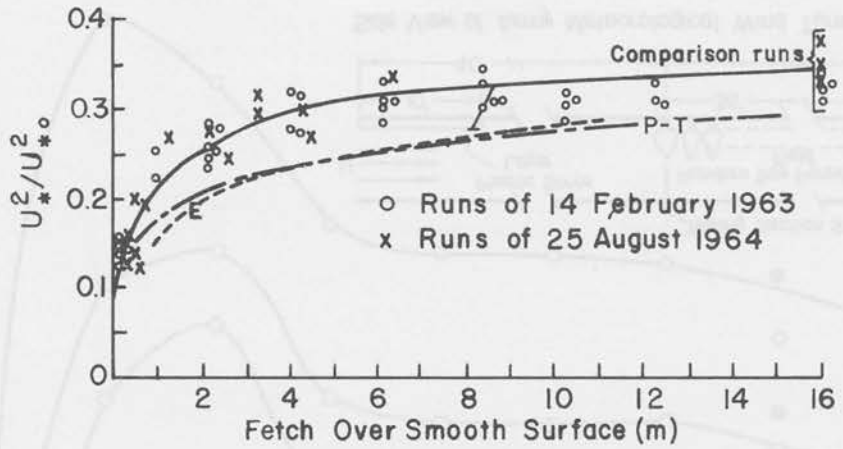

Figure 8.8-4 Variation of nondimensional surface shear stress in the downwind direction for rough to smooth transition. Comparison of the results obtained numerically by the turbulent energy model with analytical solutions and field data

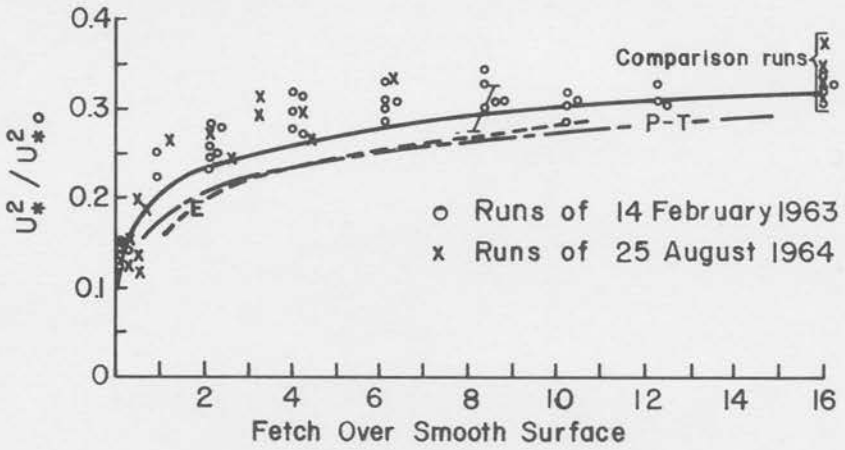

Figure 8.8-5 Variation of surface shear stress in the downwind direction for a rough to smooth transition. Comparison of the results obtained by the turbulent energy-Newtonian model with analytical solutions and field data

Unclassified
Security Classification

DOCUMENT CONTROL DATA - R & D

(Security classification of title, body of abstract and indexing annotation must be entered when the overall report is classified)

1. ORIGINATING ACTIVITY *(Corporate author)*
Fluid Dynamics & Diffusion Laboratory
College of Engineering, Colorado State University
Fort Collins, Colorado 80521

2a. REPORT SECURITY CLASSIFICATION
Unclassified

2b. GROUP

3. REPORT TITLE
Numerical Simulation of Wind, Temperature, Shear Stress and Turbulent Energy over Nonhomogeneous Terrain

4. DESCRIPTIVE NOTES *(Type of report and inclusive dates)*
Technical Report

5. AUTHOR(S) *(First name, middle initial, last name)*
Huang, Chin-hua

6. REPORT DATE	7a. TOTAL NO. OF PAGES	7b. NO. OF REFS
March 1972	276	108

8a. CONTRACT OR GRANT NO.	9a. ORIGINATOR'S REPORT NUMBER(S)
N00014-68-A-0493	CER71-72CH-ECN23
b. PROJECT NO. NR 062-414/6-6-68(Code 438)	
c.	9b. OTHER REPORT NO(S) *(Any other numbers that may be assigned this report)*
d.	THEMIS TECHNICAL REPORT NO. 12

10. DISTRIBUTION STATEMENT
Distribution of this report is unlimited

11. SUPPLEMENTARY NOTES	12. SPONSORING MILITARY ACTIVITY
	Office of Naval Research U. S. Department of Defense Washington, D.C.

13. ABSTRACT

Airflow in the atmospheric surface layer over nonhomogeneous surfaces with discontinuities in surface roughness and temperature is investigated by numerical techniques. A computational scheme is developed for solving the steady state two-dimensional boundary layer equations. Several theorems of convergence are proved. A successful numerical test, which has been compared to the exact solution, is achieved. Some iterative schemes, which have already enjoyed considerable success without theoretical support are here shown to be convergent.

The variations in pressure and buoyancy force associated with changes in surface roughness have been neglected by previous investigators whose work is included in the present study. The numerical results of velocity and shear stress are compared with wind tunnel and field data. The roughness and temperature discontinuities are shown to have an effect on the upstream as well as the downstream flow conditions.

Significant variations in the horizontal velocity, vertical velocity and shear stress profiles near the roughness discontinuity occurred between those cases neglecting and those retaining the pressure terms in the governing equations. The predicted physical quantities for diabatic conditions also show significant differences in those two cases; thus, the pressure terms should be retained in the governing equations.

DD FORM 1 NOV 68 1473

Unclassified
Security Classification

14 KEY WORDS	LINK A		LINK B		LINK C	
	ROLE	WT	ROLE	WT	ROLE	WT
Roughness Discontinuity						
Temperature Discontinuity						
Atmospheric Boundary Layer						
Mean Velocity						
Shear Stress						
Numerical Modeling						
Turbulent Energy						

April 1971

DISTRIBUTION LIST FOR UNCLASSIFIED
TECHNICAL REPORTS ISSUED UNDER
CONTRACT N00014-68-A TASK 000-414
0493-0001

Defense Documentation Center
Cameron Station
Alexandria, Virginia 22314 (12)

Technical Library
Naval Ship Research and Development Laboratory
Annapolis, Maryland 21402

Professor Bruce Johnson
Engineering Department
Naval Academy
Annapolis, Maryland 21402

Library
Naval Academy
Annapolis, Maryland 21402

Professor W.R. Debler
Department of Engineering Mechanics
University of Michigan
Ann Arbor, Michigan 48108

Professor W.P. Graebel
Department of Engineering Mechanics
University of Michigan
College of Engineering
Ann Arbor, Michigan 48108

Professor Finn C. Michelsen
Naval Architecture and Marine Engineering
445 West Engineering Building
University of Michigan
Ann Arbor, Michigan 48108

Dr. Francis Ogilvie
Department of Naval Architecture and Marine Engineering
University of Michigan
Ann Arbor, Michigan 48108

Professor W.W. Willmarth
Department of Aerospace Engineering
University of Michigan
Ann Arbor, Michigan 48108

Dr. S.A. Piacsek
Argonne National Laboratory
Applied Mathematics Division
9700 S. Cass Avenue
Argonne, Illinois 60439

AFOSR (REM)
1400 Wilson Boulevard
Arlington, Virginia 22204

Professor S. Corrsin
Mechanics Department
The Johns Hopkins University
Baltimore, Maryland 20910

Professor L.S.G. Kovasznay
The Johns Hopkins University
Baltimore, Maryland 20910

Professor O.M. Phillips
The Johns Hopkins University
Baltimore, Maryland 20910

Librarian
Department of Naval Architecture
University of California
Berkeley, California 94720

Professor Israel Cornet
Department of Mechanical Engineering
University of California
Berkeley, California 94720

Professor M. Holt
Division of Aeronautical Sciences
University of California
Berkeley, California 94720

Professor E.V. Laitone
Department of Mechanical Engineering
University of California
Berkeley, California 94720

Professor P. Lieber
Department of Mechanical Engineering
University of California
Institute of Engineering Research
Berkeley, California 94720

Professor J.R. Paulling
Department of Naval Architecture
University of California
Berkeley, California 94720

Professor J.V. Wehausen
Department of Naval Architecture
University of California
Berkeley, California 94720

Professor E.R. van Driest
Virginia Polytechnic Institute and University
Department of Aerospace Engineering
Blacksburg, Virginia 24061

Commander
Boston Naval Shipyard
Boston, Massachusetts 02129

Director
Office of Naval Research Branch Office
495 Summer Street
Boston, Massachusetts 02210

Commander
Puget Sound Naval Shipyard
Bremerton, Washington 98314

Professor J.J. Foody
Chairman, Engineering Department
State University of New York
Maritime College
Bronx, New York 10465

Dr. Alfred Ritter
Assistant Head, Applied Mechanics Department
Cornell Aeronautical Laboratory, Inc.
Buffalo, New York 14221

Dr. J.W. Morris
Manager, Material Sciences Section
Advanced Materials Research
Bell Aerospace Company
P.O. Box 1
Buffalo, New York 14240

Professor G.H. Carrier
Department of Engineering and Applied Physics
Harvard University
Cambridge, Massachusetts 02138

Commanding Officer
NROTC Naval Administrative Unit
Massachusetts Institute of Technology
Cambridge, Massachusetts 02139

Professor M.A. Abkowitz
Department of Naval Architecture and Marine Engineering
Massachusetts Institute of Technology
Cambridge, Massachusetts 02139

Professor A.T. Ippen
Department of Civil Engineering
Massachusetts Institute of Technology
Cambridge, Massachusetts 02139

Professor L.N. Howard
Department of Mathematics
Massachusetts Institute of Technology
Cambridge, Massachusetts 02139

Professor E.W. Merrill
Department of Mathematics
Massachusetts Institute of Technology
Cambridge, Massachusetts 02139

Professor E. Mollo-Christensen
Room 54-1722
Massachusetts Institute of Technology
Cambridge, Massachusetts 02139

Professor N. Newman
Department of Naval Architecture and Marine Engineering
Massachusetts Institute of Technology
Cambridge, Massachusetts 02139

Professor A.H. Shapiro
Department of Mechanical Engineering
Massachusetts Institute of Technology
Cambridge, Massachusetts 02139

Commander
Charleston Naval Shipyard
U.S. Naval Base
Charleston, South Carolina 29408

A.R. Kuhlthau, Director
Research Laboratories for the Engineering Sciences
Thorton Hall, University of Virginia
Charlottesville, Virginia 22903

Director
Office of Naval Research Branch Office
536 South Clark Street
Chicago, Illinois 60605

Library
Naval Weapons Center
China Lake, California 93555

Professor J.M. Burgers
Institute of Fluid Dynamics and Applied Mathematics
University of Maryland
College Park, Maryland 20742

Professor Pai
Institute for Fluid Dynamics and Applied Mathematics
University of Maryland
College Park, Maryland 20740

Acquisition Director
NASA Scientific & Technical Information
P.O. Box 33
College Park, Maryland 20740

Technical Library
Naval Weapons Laboratory
Dahlgren, Virginia 22448

Computation & Analyses Laboratory
Naval Weapons Laboratory
Dahlgren, Virginia 22448

Dr. C.S. Wells, Jr.
Manager - Fluid Mechanics
Advanced Technology Center, Inc.
P.O. Box 6144
Dallas, Texas 75222

Dr. R.H. Kraichnan
Dublin, New Hampshire 03444

Commanding Officer
Army Research Office
Box CM, Duke Station
Durham, North Carolina 27706

Professor A. Charnes
The Technological Institute
Northwestern University
Evanston, Illinois 60201

Dr. Martin H. Bloom
Polytechnic Institute of Brooklyn
Graduate Center, Dept. of Aerospace
Engineering and Applied Mechanics
Farmingdale, New York 11735

Technical Documents Center
Building 315
U.S. Army Mobility Equipment
Research and Development Center
Fort Belvoir, Virginia 22060

Professor J.E. Cermak
College of Engineering
Colorado State University
Ft. Collins, Colorado 80521

Technical Library
Webb Institute of Naval Architecture
Glen Cove, Long Island, New York 11542

Professor E.V. Lewis
Webb Institute of Naval Architecture
Glen Cove, Long Island, New York 11542

Dr. B.N. Pridmore Brown
Northrop Corporation
NORAIR-Div.
Hawthorne, California 90250

Dr. J.P. Breslin
Stevens Institute of Technology
Davidson Laboratory
Hoboken, New Jersey 07030

Dr. D. Savitsky
Stevens Institute of Technology
Davidson Laboratory
Hoboken, New Jersey 07030

Mr. C.H. Henry
Stevens Institute of Technology
Davidson Laboratory
Hoboken, New Jersey 07030

Dr. J.P. Craven
University of Hawaii
1801 University Avenue
Honolulu, Hawaii 96822

Professor E.L. Resler
Graduate School of Aeronautical Engineering
Cornell University
Ithaca, New York 14851

Professor John Miles
c/o I.G.P.P.
University of California, San Diego
La Jolla, California 92038

Director
Scrippe Institution of Oceanography
University of California
La Jolla, California 92037

Professor A. Ellis
University of California, San Diego
Department of Aerospace & Mechanical Engineering
La Jolla, California 92037

Dr. B. Sternlicht
Mechanical Technology Incorporated
968 Albany-Shaker Road
Latham, New York 12110

Dr. Coda Pan
Mechanical Technology Incorporated
968 Albany-Shaker Road
Latham, New York 12110

Mr. P. Eisenberg, President
Hydronautics, Inc.
Pindell School Road
Howard County
Laurel, Maryland 20810

Mr. M.P. Tulin
Hydronautics, Inc.
Pindell School Road
Howard County
Laurel, Maryland 20810

Mr. Alfonso Alcedan L.,Director
Laboratorio Nacional De Hydraulics
Antigui Cameno A. Ancon
Casilla Jostal 682
Lima, Peru

Commander
Long Beach Naval Shipyard
Long Beach, California 90802

Professor John Laufer
Department of Aerospace Engineering
University Park
Los Angeles, California 90007

Professor J.M. Killen
St. Anthony Falls Hydraulic Lab.
University of Minnesota
Minneapolis, Minnesota 55414

Lorenz G. Straub Library
St. Anthony Falls Hydraulic Lab.
Mississippi River at 3rd Avenue S.E.
Minneapolis, Minnesota 55414

Professor J. Ripkin
St. Anthony Falls Hydraulic Lab.
University of Minnesota
Minneapolis, Minnesota 55414

Dr. W. Silberman
St. Anthony Falls Hydraulic Lab.
Mississippi River at 3rd Avenue S.E.
Minneapolis, Minnesota 55414

Superintendent
Naval Postgraduate School
Library Code 0212
Monterey, California 93940

Professor A.B. Metzner
University of Delaware
Newark, New Jersey 19711

Technical Library
Naval Underwater Systems Center
Newport, Rhode Island 02840

Professor Dudley D. Fuller
Department of Mechanical Engineering
Columbia University
New York, New York 10027

Professor V. Castelli
Department of Mechanical Engineering
Columbia University
New York, New York 10027

Professor H. Elrod
Department of Mechanical Engineering
Columbia University
New York, New York 10027

Professor J.J. Stoker
Institute of Mathematical Sciences
New York University
251 Mercer Street
New York, New York 10003

Society of Naval Architects and Marine Engineering
74 Trinity Place
New York, New York 10006

Engineering Societies Library
345 East 47th Street
New York, New York 10017

Office of Naval Research
New York Area Office
207 W. 24th Street
New York, New York 10011

Miss O.M. Leach, Librarian
National Research Council
Aeronautical Library
Montreal Road
Ottawa 7, Canada

Technical Library
Naval Ship Research and Development Center
Panama City, Florida 32401

Technical Library
Naval Undersea R & D Center
Pasadena Laboratory
3202 E. Foothill Boulevard
Pasadena, California 91107

Dr. Andrew Fabula
Naval Undersea Research & Development Center
Pasadena Laboratory
3202 E. Foothill Boulevard
Pasadena, California 91107

Dr. J.W. Hoyt
Naval Undersea R & D Center
Pasadena Laboratory
3202 E. Foothill Boulevard
Pasadena, California 91107

Professor A. Acosta
Department of Mechanical Engineering
California Institute of Technology
Pasadena, California 91109

Professor H. Liepmann
Department of Aeronautics
California Institute of Technology
Pasadena, California 91109

Professor M.S. Plesset
Engineering Division
California Institute of Technology
Pasadena, California 91109

Professor A. Roshko
California Institute of Technology
Pasadena, California 91109

Professor T.Y. Wu
Department of Engineering
California Institute of Technology
Pasadena, California 91109

Director
Office of Naval Research Branch Office
1030 E. Green Street
Pasadena, California 91101

Naval Ship Engineering Center
Philadelphia Division
Technical Library
Philadelphia, Pennsylvania 19112

Technical Library
Philadelphia Naval Shipyard
Philadelphia, Pennsylvania 19112

Professor R.C. Mac Camy
Department of Mathematics
Carnegie Institute of Technology
Pittsburgh, Pennsylvania 15213

Dr. Paul Kaplan
Oceanics, Inc.
Plainview, Long Island, New York 11803

Technical Library
Naval Missile Center
Point Mugu, California 93441

Technical Library
Naval Civil Engineering Laboratory
Port Hueneme, California 93041

Commander
Portsmouth Naval Shipyard
Portsmouth, New Hampshire 03801

Commander
Norfolk Naval Shipyard
Portsmouth, Virginia 23709

Professor F.E. Bisshopp
Division of Engineering
Brown University
Providence, Rhode Island 02912

Dr. William A. Gross, Vice President
Ampex Corporation
401 Broadway
Redwood City, California 94063

Dr. H.N. Abramson
Southwest Research Institute
8500 Culebra Road
San Antonio, Texas 78228

Editor
Applied Mechanics Review
Southwest Research Institute
8500 Culebra Road
San Antonio, Texas 78206

Office of Naval Research
San Francisco Area Office
50 Fell Street
San Francisco, California 94102

Library
Pearl Harbor Naval Shipyard
Box 400
FPO San Francisco, California 96610

Technical Library
Hunters Point Naval Shipyard
San Francisco, California 94135

Librarian
Naval Ordnance Laboratory
White Oak
Silver Spring, Maryland 20910

Fenton Kennedy Document Library
The Johns Hopkins University
Applied Physics Laboratory
8621 Georgia Avenue
Silver Spring, Maryland 20910

Professor E.Y. Hsu
Department of Civil Engineering
Stanford University
Stanford, California 94305

Dr. Byrne Perry
Department of Civil Engineering
Stanford University
Stanford, California 94305

Dr. R.L. Street
Department of Civil Engineering
Stanford University
Stanford, California 94305

Professor Milton Van Dyke
Department of Aeronautical Engineering
Stanford University
Stanford, California 94305

Professor R.C. Di Prima
Department of Mathematics
Rensselaer Polytechnic Institute
Troy, New York 12180

Professor J. Lumley
Ordnance Research Laboratory
Pennsylvania State University
University Park, Pennsylvania 16801

Dr. M. Sevik
Ordnance Research Laboratory
Pennsylvania State University
University Park, Pennsylvania 16801

Dr. J.M. Robertson
Department of Theoretical and Applied Mechanics
University of Illinois
Urbana, Illinois 61803

Technical Library
Mare Island Naval Shipyard
Vallejo, California 94592

Code 438
Office of Naval Research
Department of the Navy
Arlington, Virginia 22217 (3)

Code 461
Office of Naval Research
Department of the Navy
Arlington, Virginia 22217

Code 463
Office of Naval Research
Department of the Navy
Arlington, Virginia 22217

Code 472
Office of Naval Research
Department of the Navy
Arlington, Virginia 22217

Code 468
Office of Naval Research
Department of the Navy
Arlington, Virginia 22217

Code 473
Office of Naval Research
Department of the Navy
Arlington, Virginia 22217

Code 481
Office of Naval Research
Department of the Navy
Arlington, Virginia 22217

Code 2627
Naval Research Laboratory
Washington, D.C. 20390 (6)

Library, Code 2620 (ONRL)
Naval Research Laboratory
Washington, D.C. 20390 (6)

Code 6170
Naval Research Laboratory
Washington, D.C. 20390

Code 4000
Director of Research
Naval Research Laboratory
Washington, D.C. 20390

Code 8030 (Maury Center)
Naval Research Laboratory
Washington, D.C. 20390

Code 8040
Naval Research Laboratory
Washington, D.C. 20390

Code 031
Naval Ship Systems Command
Washington, D.C. 20390

Code 0341
Naval Ship Systems Command
Washington, D.C. 20390

Code 03412B (L. Benen)
Naval Ship Systems Command
Washington, D.C. 20390

Code 03412 (J. Schuler)
Naval Ship Systems Command
Washington, D.C. 20390

Code 2052
Naval Ship Systems Command
Washington, D. C. 20390

Code 6034
Naval Ship Engineering Center
Center Building
Prince George's Center
Hyattsville, Maryland 20782

Code 6110
Naval Ship Engineering Center
Center Building
Prince George's Center
Hyattsville, Maryland 20782

Code 6113
Naval Ship Engineering Center
Center Building
Prince George's Center
Hyattsville, Maryland 20782

Code 6114
Naval Ship Engineering Center
Center Building
Prince George's Center
Hyattsville, Maryland 20782

Code 6120E
Naval Ship Engineering Center
Center Building
Prince George's Center
Hyattsville, Maryland 20782

Code 6136
Naval Ship Engineering Center
Center Building
Prince George's Center
Hyattsville, Maryland 20782

Dr. A. Powell
Code 01
Naval Ship Research and Development Center
Washington, D.C. 20034

Mr. W.M. Ellsworth
Code 0H50
Naval Ship Research and Development Center
Washington, D.C. 20034

Central Library
Code L42
Naval Ship Research and Development Center
Washington, D.C. 20034

Dr. W.E. Cummins
Code 500
Naval Ship Research and Development Center
Washington, D.C. 20034

Mr. S.F. Crump
Code 513
Naval Ship Research and Development Center
Washington, D.C. 20034

Mr. R. Wermter
Code 520
Naval Ship Research and Development Center
Washington, D.C. 20034

Dr. P. Pien
Code 521
Naval Ship Research and Development Center
Washington, D.C. 20034

Dr. W.B. Morgan
Code 540
Naval Ship Research and Development Center
Washington, D.C. 20034

Mr. P. Granville
Code 541
Naval Ship Research and Development Center
Washington, D.C. 20034

Mr. J.B. Hadler
Code 560
Naval Ship Research and Development Center
Washington, D.C. 20034

Dr. H.R. Chaplin
Code 600
Naval Ship Research and Development Center
Washington, D.C. 20034

Mr. G.H. Gleissner
Code 800
Naval Ship Research and Development Center
Washington, D.C. 20034

Dr. M. Strasberg
Code 901
Naval Ship Research and Development Center
Washington, D.C. 20034

Mr. J. McCarthy
Code 552
Naval Ship Research and Development Center
Washington, D.C. 20034

Code 03
Naval Air Systems Command
Washington, D.C. 20360

AIR 5301
Naval Air Systems Command
Department of the Navy
Washington, D.C. 20360

Code ORD 03
Naval Ordnance Systems Command
Washington, D.C. 20360

Code ORD 035
Naval Ordnance Systems Command
Washington, D.C. 20360

Code ORD 05413
Naval Ordnance Systems Command
Washington, D.C. 20360

Code ORD 9132
Naval Ordnance Systems Command
Washington, D.C. 20360

Oceanographer of the Navy
Washington, D.C. 20390

Commander
Naval Oceanographic Office
Washington, D.C. 20390

Chief Scientist (CNM PM-1)
Strategic Systems Project Office
Department of the Navy
Washington, D.C. 20360

Technical Division (CNM PM 11-20)
Deep Submergence Systems Project Office
Department of the Navy
Washington, D.C. 20360

Dr. A.L. Slafkosky
Scientific Advisor
Commandant of the Marine Corps (Code AX)
Washington, D.C. 20380

Librarian Station 5-2
Coast Guard Headquarters
NASSIF Building
400 7th Street, S.W.
Washington, D.C. 20591

Office of Research and Development
Maritime Administration
441 G. Street, N.W.
Washington, D.C. 20235

Division of Ship Design
Maritime Administration
441 G. Street, N.W.
Washington, D.C. 20235

National Science Foundation
Engineering Division
1800 G. Street, N.W.
Washington, D.C. 20550

Dr. G. Kulin
National Bureau of Standards
Washington, D.C. 20234

Science & Technology Division
Library of Congress
Washington, D.C. 20540

Chief of Research & Development
Office of Chief of Staff
Department of the Army
The Pentagon, Washington, D.C. 20310

Professor A. Thiruvengadam
Department of Mechanical Engineering
The Catholic University of America
Washington, D.C. 20017

Professor G. Birkhoff
Department of Mathematics
Harvard University
Cambridge, Massachusetts 02138

AIR 604
Naval Air Systems Command
Department of the Navy
Washington, D.C. 20360

Dr. A.S. Iberall, President
General Technical Services, Inc.
451 Penn Street
Yeadon, Pennsylvania 19050

Professor J.F. Kennedy, Director
Iowa Institute of Hydraulic Research
State University of Iowa
Iowa City, Iowa 52240

Professor L. Landweber
Iowa Institute of Hydraulic Research
State University of Iowa
Iowa City, Iowa 52240

Dr. Lee Segel
Department of Mathematics
Rensselaer Polytechnic Institute
Troy, New York 12180

Code 6101E
Naval Ship Engineering Center
Center Building
Prince George's Center
Hyattsville, Maryland 20782